

# THE EVALUATION OF WHOLE-ROCK AND PARTIAL LEACH GEOCHEMICAL EXPLORATION TECHNIQUES APPLIED TO THE EXPLORATION FOR TANZANITE DEPOSITS – MERELANI, NORTH-EASTERN TANZANIA

By

Robert N. Hansen

This thesis presented in partial fulfillment of the requirements for the degree of Master of Science at the University of Stellenbosch



December 2007

Study Leaders:

Dr. R. Scheepers, Prof. G. Stevens

### **Declaration**

I the undersigned declare that the work contained in this thesis is my own original work and has not previously in its entirety or in part been submitted at any university for a degree.

**Signature**

**Date**

---

Robert Neill Hansen

## Abstract

The aim of the study is to ascertain whether geochemical exploration techniques can be used in the search for tanzanite deposits in the Merelani area, NE Tanzania. Previous studies have successfully demonstrated a partial extraction method (*in situ* soil leaching) in identifying prospective ultramafic bodies at the Rockland ruby mine in the Mangare area, Kenya, thereby demonstrating the usefulness of geochemical methods in gemstone exploration. In this study, a partial extraction as well as a whole-rock geochemical method was used to determine the applicability of these methods in prospecting for tanzanite mineralisation using different sampling media, such as soil, stream sediment and calcrete. It is possible that this geochemical approach may not be as effective as physical methods such as the separation and examination of heavy mineral suites. However, its viability needs to be evaluated due to the potential efficiency and relative logistic ease of the method. In essence the scientific method employed is to compare overburden (soils, stream sediments and calcrete) chemistry with known underlying geology, the latter having been established via diamond core drilling. A positive correlation would allow the prediction of overburden covered tanzanite mineralisation.

Soil samples were collected from a trench dug perpendicular to regional lithological strike over both barren and tanzanite-bearing horizons. XRF trace element data for the soils was compared to the chemistry of the underlying lithologies. ICP-AE data derived from 1 molar HCL soil leachate (12 hour leach) and soil XRF data, from the same samples, was compared, using a mass balance index, to discern any hydromorphic dispersion of selected trace elements and to evaluate the leachate as a viable alternative to XRF analysis. In general, a good correlation exists between the soil and rock trace element data profiles over the length of the section. However, Ti- and Zr-normalised mass balance calculations show some down-hill drift, but this does not disrupt the overall pattern. The ICP-AE acid leach data show that hydromorphic dispersion is low, that the trace elements of interest (V, Cr, Ni and Cu) are hosted within non-soluble phases. Consequently, the leach technique is not a viable alternative to XRF analysis of the soils. XRF analysis of the soils was shown to be potentially useful in identifying new areas of mineralisation as the soils overlying a graphitic calc-silicate schist, that always occurs adjacent to the tanzanite mineralisation in the Merelani area, was found to be easily identifiable based on anomalous concentrations of V.

An exploration concession was chosen for stream sediment sampling on the basis of the presence of large streams, of a few tsavorite mines indicating high prospectivity for tanzanite, and because of a variation in geology on the property. Tanzanite and tsavorite are cogenetic in the known tanzanite deposits. In this case the aim was to investigate the possible occurrence of tanzanite-like geochemical anomalies (i.e. the anomalous V observed in the soil chemistry investigation) could be detected in the vicinity of the tsavorite mines. Tsavorite, the gem variety of grossular garnet, also contains high concentrations of V. The samples were analysed by XRF whole-rock methods for trace element content. The data shows a number of clear positive V anomalies in the study area. The data also shows that each of the existing or abandoned mines in the area is marked by a positive V anomaly. This section of the study also demonstrated a relatively low degree of stream sediment dispersion of the trace elements of interest – most likely a function of the semi-arid climate. The fine fraction (<90 $\mu\text{m}$ ), however was shown to be mobilised to a relatively larger degree than the coarse (180 $\mu\text{m}$  – 300 $\mu\text{m}$ ) and medium (90 $\mu\text{m}$  - 180 $\mu\text{m}$ ) fractions. As is predictable from the leachate analysis, factor analysis of the data shows that the trace elements are dominated by heavy mineral geochemistry and that a study in heavy mineral exploration might provide a cheaper and more viable option to those explored in this study.

Calcrete samples were taken from an abandoned, 10m deep mine shaft, which was sunk through the calcrete to reach the tanzanite deposit. The shaft was sampled from the bottom, closest to the tanzanite mineralisation, to the surface to investigate the association between trace element geochemistry and proximity to the deposit. There was no vertical association between the trace element geochemistry of the calcrete and proximity to the tanzanite deposit. There was also no clear indication in the geochemistry of the calcrete of the existence of the tanzanite deposit beneath it. This further indicates the immobility of the elements of interest in this environment.

This study has demonstrated that properly constrained soil and stream sediment geochemical studies may be of use in tanzanite exploration. However, it must be stressed that this is only the case if the geochemical signature of the lithological package associated with the mineralisation is unique and well known.

## Opsomming

Die doel van hierdie studie is om te bepaal of geochemiese eksplorasietegniese vir die soek na tanzaniet afsettings in die Merelani area, noord-oos Tanzanië, gebruik kan word. Vorige studies het gewys dat 'n gedeeltelike ekstraksie metode (*in situ* grond looging) gebruik kon word om prospektiewe ultramafiese liggame by the Rockland rubyn myn in die Mangare area, Kenia te identifiseer. Hierby is gedemonstreer dat geochemiese eksplorasiemetodes suksesvol in edelsteen eksplorasietoegemas kan word. In hierdie studie is 'n gedeeltelike ekstraksie en heel-rots geochemiese metodes gebruik om die toepaslikheid van hierdie metodes op tanzaniet eksplorasietoets. Verskillende geologiese materiale is gemonster, naamlik grond, stroom sedimente en kalkkreet. Dit is moontlik dat hierdie geochemiese benadering nie so effektief soos fisiese metodes soos swaar mineraal skeidings mag wees nie. Dit is nogtans belangrik om die toepaslikheid van hierdie metodes op tanzaniet eksplorasietoets, as gevolg van die potensiële effektiwiteit en relatiewe logistiese gemak van die metodes. Die essensie van die wetenskaplike metodiek wat in hierdie studie gebruik is, is om die geochemie van die grond, stroom sedimente en kalkkreet te vergelyk met die geochemie van die onderliggende geologie wat deur middel van diamant boorwerk vasgestel is. 'n Positiewe korrelasie sou dan dui op 'n bedekte tanzaniet afsetting.

Grond monsters is van 'n sloot geneem wat loodreg op die strekking van die tanzaniet gemineraliseerde en ongemineraliseerde horisonne gegrawe is. XRF spoor element data van die gronde is vergelyk met die chemie van die onderliggende gesteentes. IGP-AE data wat bekom is deur die monsters met 1 molaar HCl te loog (12 uur looging) is vergelyk met XRF data van dieselfde monsters deur middel van 'n massa balans indeks om te bepaal of daar enige hidromorfiese dispersie van sekere spoor elemente is en om die toepaslikheid van looging as 'n alternatief tot die heel-rots metode te bepaal. In die algemeen is daar 'n goeie korrelasie tussen die grond en rots spoor element data profiele oor die lengte van die seksie. Alhoewel, Ti- en Zr-genormaliseerde massa balans data profiele wys dat daar 'n mate van afwaartse beweging van grond na die voet van die heuwel is, maar dat hierdie 'n breuk in die algemene patroon vorm nie. Die IGP-AE data dui daarop dat die hidromorfiese verspreiding van spoor elemente laag is en dat die spoor elemente wat van belang is (V, Cr, Ni en Cu) in nie-oplosbare fases gesetel is. Gevolglik is die loogings metode nie 'n toepaslike alternatief tot die heel-rots XRF metode op gronde nie. XRF analyses op die gronde het gewys dat die XRF metode moontlik nuttig kan wees

om nuwe areas van tanzanite mineralisasie aan te dui, omdat die gronde wat 'n grafietiese kalk-silikaat skis oorlê, wat altyd langs die tanzaniet draende horisonne voorkom, is op grond van anomale konsentrasies van V geïdentifiseer.

'n Eksplorasië konsessie is op die basis van die teenwoordigheid van groot strome, 'n paar tsavoriet myne wat aanduidend is van hoë prospektiwiteit vir tanzaniet is en as gevolg van 'n variasie in geologie in die area vir stroom sediment monsterring gekies. Tanzaniet en tsavoriet is kogeneties in bekende tanzaniet afsettings. In hierdie geval was die doel om te ondersoek of tanzanietagtige anomalieë (nl. die anomale konsentrasies van V wat in die ondersoek van die grond chemie opgemerk is) in die omgewing van die tsavoriet myne geïdentifiseer kan word. Tsavoriet, die edelsteen variëteit van grossulaar granaat, bevat hoë konsentrasies V. Die monsters is deur middel van die XRF heel-rots metode vir spoor elemente geanaliseer. Die data dui op 'n paar monsters met hoë V konsentrasies in die ondersoek area. Hierdie studie het ook gedui op 'n lae stroom sediment verspreiding van die spoor elemente van belang, heel waarskynlik is dit 'n funksie van die semi-ariëde klimaat. Die fyn fraksie (< 90µm) blyk tot 'n groter mate as die growwer (90µm tot 180µm en 180µm - 300µm) fraksies gemobiliseer te word. Soos voorspel kan word deur die loogings analise het faktor analise gewys dat die spoor elemente deur swaar mineraal geochemie gedomineer word en dat 'n studie op swaar minerale moontlik 'n goedkoper en meer toepaslike eksplorasie metode is as die wat in hierdie studie ondersoek is.

Kalkreet monsters is van 'n ongebruikte, 10m diep myn skag wat deur die kalkreet gesink is om by die tanzaniet gemineraliseerde horison uit te kom geneem. Monsters is van die bodem van die skag, naaste aan die tanzaniet mineralisasie, tot die oppervlak geneem om die assosiasie tussen die spoor element geochemie en afstand van die tanzaniet mineralisasie te ondersoek. Geen vertikale assosiasie tussen spoor element geochemie en die nabyheid tot die tanzaniet afsetting kon vasgestel word nie. Daar was geen duidelike aanduiding in die geochemie van die kalkreet op die onderliggende tanzanite afsetting nie. Hierdie is 'n verdere aanduiding op die nie-mobiele toestand van spoor elemente in hierdie omgewing.

Hierdie studie het suksesvol gedemonstreer dat goed gedefinieerde grond en stroom sediment geochemiese studies moontlik in geochemiese eksplorasië vir tanzaniet bruikbaar kan wees. Dit is belangrik om in gedagte te hou dat dit slegs die geval is as die

geochemie van die litologiese pakket wat met die mineralisasie geassosieer is uniek en goed bekend is.

## **Acknowledgements**

Thank you first of all to Reyno Scheepers for initiating the project and allowing me the opportunity for exposure in Africa. I would also like to thank Prof. Gary Stevens at the University of Stellenbosch for taking over the reigns of this logistically challenging project, for his time and invaluable advice. Thank you to the external examiners, Prof. Rozendaal and Dr. Okujeni for their valuable comments and suggestions. Lastly I would like to thank Rhondie and my family for their unwavering support in seeing the thesis to completion.



# Contents

Page

**Abstract**

**Opsomming**

**Acknowledgements**

**List of Figures and Tables**

<b>1. Introduction</b>	1
<b>2. Regional Geology</b>	
2.1. Tanzanian Craton	4
2.2. The East African Orogen and its Tectonic Evolution	5
2.3. Cenozoic Cover	7
<b>3. Local Geology</b>	
3.1. Dolomitic Marble	9
3.2. Garnet-Sillimanite-Biotite Gneiss	9
3.3. Kyanite-Graphite Gneiss	10
3.4. Graphite-Plagioclase Gneiss	10
3.5. Calc-Silicates	11
3.6. Graphite-Calc-Silicate Schist	13
3.7. Banded Calc-Silicate Fels	13
3.8. Superficial Deposits	14
3.9. Structural Geology	14
3.10. Trench geology and pedology	15
<b>4. Sampling and Analytical Techniques</b>	
4.1. Soil Samples	19
4.2. Stream sediment samples	21
4.3. Calcrete samples	22
4.4. Precision	22
<b>5. Analysis of Soil XRF and ICP and Published XRF Data</b>	
5.1. Introduction	25
5.2. Additional samples	25
5.3. Merelani lithology and trench soil characterisation and data description	26
5.3.1. Lithology characterisation	27
5.3.2. Soil characterisation	27
5.3.3. Comparison between lithologies and soils	29
5.3.4. Ti- and Zr-normalisation as a test of trace element mobility	32
5.3.5. Total (XRF) and partial (ICP) trace element extraction and analysis	35
5.3.6. Chemical evaluation of various size fractions	36
5.4. Correlation	38
5.4.1. Merelani lithology and trace element correlations	39
5.4.2. Merelani soil trace element correlations	45
5.5. Discussion and conclusions	46

<b>6. Stream Sediments</b>	
6.1. Introduction	49
6.2. Stream sediment characterisation	50
6.3. Factor analyses	53
6.4. Discussion and conclusions	64
<b>7. Geochemical Model</b>	
7.1. Introduction	65
7.2. Geochemical model for soils	65
7.3. Geochemical model for stream sediments	67
7.4. Discussion, final conclusions and recommendations	68
<b>8. References</b>	70
<b>Addendum Compact Disc</b>	

## List of Figures

- Figure 1 Study area
- Figure 2 Simplified map of the East African Orogen
- Figure 3 Schematic diagram of the tectonic evolution of the East African Orogen
- Figure 4 Comparison between the East African Orogen and the Himalayas
- Figure 5 Simplified geological map of the East-African rift
- Figure 6 Simplified map of the Merelani Lower Horizon lithologies
- Figure 7 Schematic of boudinaging of the JW zone
- Figure 8 Schematic of different types of boudins
- Figure 9 Map of the Merelani trench
- Figure 10 Photo of the Merelani trench
- Figure 11 Photo of Zone 1 soil zone
- Figure 12 Photo of Zone 2 soil zone
- Figure 13 Photo of Zone 3 soil zone
- Figure 14 Photo of Zone 4 soil zone
- Figure 15 Photo of Zone 6 soil zone
- Figure 16 Photo of Zone 7 soil zone
- Figure 17 Photo of Zone 8 soil zone
- Figure 18 Satellite image of stream sediment sampling points
- Figure 19 Map of the trench in plan view, additional soil sampling points and old mine shafts
- Figure 20 Flow diagram of sample collection and preparation
- Figure 21 Merelani lithological units normalised to bulk continental crust
- Figure 22 Photo of evidence of folding in the JW zone in the Merelani trench
- Figure 23 Soil zone samples normalised to bulk continental crust
- Figure 24 Trace element profiles of Merelani lithologies and soil zones over the trench
- Figure 25 Ti- and Zr-normalised percentage change profiles
- Figure 26 Spider diagrams of Ti-normalised percentage change of Merelani soil zone trace elements
- Figure 27 Spider diagrams of Zr-normalised percentage change of Merelani soil zone trace elements
- Figure 28 Scatterplots for size fraction evaluation
- Figure 29 Statistical data ranges
- Figure 30 Examples of different values of  $r$

- Figure 31 Schematic presentation of possible problems related to r
- Figure 32 Rb vs.  $K_2O$
- Figure 33 Ce vs.  $P_2O_5$
- Figure 34 Stream sediment data normalised to upper and lower continental crust
- Figure 35 Grain size evaluation of stream sediment data
- Figure 36 Providence evaluation of stream sediment data
- Figure 37 3D factor vectors
- Figure 38 Trace element medium fraction profiles over the sampled streams
- Figure 39 Trace element fine fraction profiles over the sampled streams
- Figure 40 Satellite image of anomalous V concentration in the stream sediments
- Figure 41 Fine fraction factor ratio plots
- Figure 42 Medium fraction factor ratio plots
- Figure 43 Stream sediment factor score profiles
- Figure 44 Stream sediment factor ratio profiles
- Figure 45 Satellite image of stream sediment factor plots of the fine fraction
- Figure 46 Satellite image of stream sediment factor plots of the medium fraction
- Figure 47 Satellite image of stream sediment factor ratio plots of the fine fraction
- Figure 48 Satellite image of stream sediment factor ratio plots of the medium fraction
- Figure 49 Satellite image enlargement of stream sediment sampling area
- Figure 50 Satellite image and marked structural possibilities for observed topography
- Figure 51 Schematic diagram of factors influencing landscape geochemistry
- Figure 52 Photo showing slopes influencing fluid flow
- Figure 53 Conceptual geochemical model for the soils
- Figure 54 Conceptual geochemical model for the stream sediments

### List of Tables

- Table 1 Merelani lithology names
- Table 2 Trench soil zones and the lithologies they cover
- Table 3 XRF calibration materials
- Table 4 ICP-AE detection limits
- Table 5 XRF precision calculations
- Table 6 XRF detection limits
- Table 7 Additional sample data ranges

Table 8	Correlation coefficients between Ti- and Zr-normalised percentage change values
Table 9	Ti- and Zr-normalised percentage change values
Table 10	Fine fraction percentage leachable metal
Table 11	Medium fraction percentage leachable metal
Table 12	Selected element data ranges
Table 13	Groups of mutually correlating trace elements of the Kyanite Gneiss LK4
Table 14	Groups of mutually correlating trace elements and major element oxides of the Kyanite Gneiss LK4
Table 15	Mineral phases represented by groups of mutually correlating trace elements and major element oxides for the Merelani lithologies
Table 16	Correlation matrix for Merelani lithology data set
Table 17	Published distribution coefficient of REE between apatite and fluid
Table 18	Average concentration of REE in Merelani lithologies
Table 19	EMP analyses of mineral grains
Table 20	Mineralogic hosts to trace elements in Merelani lithologies
Table 21	A-Horizon trace element correlations
Table 22	C-Horizon trace element correlations
Table 23	Stream sediment fine fraction factors (cut-off loading of 0.7000)
Table 24	Stream sediment fine fraction factors (cut-off loading of 0.5000)
Table 25	Stream sediment fine fraction correlation matrix
Table 26	Fine and medium fraction stream sediment skewness and kurtosis data
Table 27	Stream sediment fine and medium fraction factor loadings
Table 28	Stream sediment medium fraction factors (cut-off loading of 0.7000)
Table 29	Stream sediment medium fraction factors (cut-off loading of 0.5000)
Table 30	Stream sediment medium fraction correlation matrix
Table 31	Fine fraction stream sediment factor score outlying samples
Table 32	Medium fraction stream sediment factor score outlying samples

## 1. Introduction

The current tanzanite mining company, Tanzanite One, has projected a life of mine of 15 years. Additional tanzanite reserves will have to be found if the period is to be extended beyond the current estimation. This study was conducted to ascertain whether two common methods in geochemical exploration, whole-rock XRF and partial leach, can be applied in exploring for additional tanzanite deposits.

The Merelani tanzanite deposit is located in the Lelatema mountains in the Merelani region, north-eastern Tanzania. The Lelatema mountains are defined by the slopes of a large anticlinal structure rising above the relatively low-lying plains. This is the only significant topography in the immediate area. The climate is semi-arid, with heavy rain falling from March to May. The development of abundant calcrete as well as the positive weathering of the dolomite in the area attests to the aridity of the climate. Vegetation consists of mostly Acacia species intergrown almost impenetrably in the rainy season. Natural rock outcrop is limited to the limbs of the Lelatema anticlinal structure and to isolated inselbergs occurring on the flat plane between the limbs.

Tanzanite occurs in intensely boudinaged and folded units in a kyanite gneiss in a granulite facies metamorphic terrane. The deposit is confined to an area of about 7km<sup>2</sup> in the Merelani area. It has been mined on a small scale for about 30 years and on a large scale for the past 7 years. The geology of the deposit has been the subject of intense study for the last few years (Davies and Chase, 1994; Malisa, 1987; Malisa and Muhongo, 1990; Malisa and Koljonen, 1989; Olivier, 2006; Scheepers and Kisters, 2000) and is well known. Mining of the deposit is a complex process due to the intricate structure by which the tanzanite mineralisation is guided. The tanzanite mineralisation is located in low-pressure shadows within boudins and along fold hinges. Inclined shafts are sunk along the apparent to true dip of the JW-zone, which is the tanzanite mineralised horizon, to intersect the generally NE plunging fold hinges. Individual ore shoots are mined via lateral drives along the plunge of the fold hinges. Winzes and raises are developed from the main lateral drives to investigate the pressure shadow boudin structures associated with the fold hinges, in which tanzanite is also mineralised. The ore is transported to the decline shafts by means of either monorope or vacuumation systems. From the decline shafts ore is transported to the surface by means of a skip and track system.

The lithologic package in which the tanzanite deposit is hosted is covered by an overburden layer of variable thickness consisting of either calcrete and/or soil. The possibility therefore exists that geochemical exploration methods employing these different overburden types can provide relatively cheap and logistically simple methods of finding additional tanzanite deposits.

Levitski and Sims (1997) raised the possibility that gemstone deposits can be sought via geochemical exploration techniques, due to the fact that a gemstone is coloured by a specific chromophoric trace element. They tested the method of diffusion extraction (MDI) at the Rockland ruby mine in south-east Kenya. By using the method they were able to successfully pinpoint the positions of covered ultramafic bodies which are closely related to the ruby mineralisation in the area. The principles used in the Rockland study were used to conceptualise a study to test the applicability of geochemical exploration techniques in tanzanite exploration.

Tanzanite is a vanadiferous zoisite ( $\text{Ca}_2\text{Al}_2\text{O}.\text{AlOH}[\text{Si}_2\text{O}_7][\text{SiO}_4]$ ) which contains up to 3300ppm vanadium (~0,5wt%  $\text{V}_2\text{O}_3$ ). However, due to the “pocket”-mode of tanzanite mineralisation and the subsequently low ore to wall-rock ratio, vanadium dilution is expected to occur during the process of soil formation when rock particles containing high V concentrations are mixed with particles containing low V concentrations. This is in addition to the probable low trace element dispersion in the soils and stream sediments, because of the semi-arid climate. The challenge may therefore lie in searching for low contrast geochemical anomalies. Like the ruby deposits of the Rockland Ruby mine, tanzanite deposits are associated with a specific rock type. Thus another exploration method may be to identify geochemical patterns unique to specific rock-types, which either contain the tanzanite mineralisation or are closely associated with the mineralised host-rocks.

The geochemistry of the lithological package in which the tanzanite deposit occurs is well constrained through analysis of bore-hole and rock-chip samples (Olivier, 2006). This study will focus on the trace element geochemistry of the overburden (soil, stream sediment and calcrete) and try to relate it to the chemistry of the underlying lithologic package, which hosts the tanzanite mineralisation. Two potential methods exist which could identify potential anomalies associated with the tanzanite deposit: whole-rock

and partial extraction methods. The partial extraction method is tested due to its relative low cost as well as logistical ease with which a geochemical survey using partial extraction can be conducted. In addition the partial extraction data will also show whether the trace elements in the overburden occur in soluble or insoluble phases. The analysis of stream sediments may be useful in identifying anomalies related to tanzanite deposits not yet discovered, depending on the mode of trace element dispersion within the stream systems. Tsavorite and tanzanite are cogenetic in the mined tanzanite deposits. In addition no lithologic data exists outside the mining area. Therefore the presence of operating and abandoned tsavorite mines in an exploration concession will be used as a guide of any potential anomalies and their meaning in terms of their proximity to the mines. Abundant calcrete is found throughout the area. If the data from analysis of the calcrete can be used to identify anomalies associated with tanzanite deposits, the cost of a geochemical exploration program will be significantly reduced as these samples, occurring on the surface, are easy to collect and relatively cheap to transport.

The results of this study will heavily rest on XRF and partial extraction data. The partial extraction data represents the logistically easier data to collect, as no pre-milling and crushing of the samples is required and therefore also the cheapest. The XRF data will potentially prove to be the more accurate in anomaly identification and establishing a link between the overburden and underlying rock types. In addition to the geochemical methods explored in this study, heavy mineral separation and analysis may also prove to be a viable exploration method for additional tanzanite deposits. This study aims to show that geochemical exploration methods can be used to identify the location of the tanzanite deposit.



## **2. Regional Geology**

The study area is located in the Neo-Proterozoic, north-south trending Mozambique tectono-metamorphic belt in north-eastern Tanzania (Fig.1). Although the term “Mozambique Belt” is still frequently used, the term “East African Orogen” (EAO), proposed by Stern (1994) incorporating the Arabian-Nubian shield into the belt, is preferred. The EAO will be dealt with in more detail as it is host to the various gemstone deposits discussed in this thesis.

The geology of north-eastern Tanzania is subdivided into mainly two domains on the basis of their structural and chronostratigraphic characteristics, namely the Tanzanian Craton (ca. 2.0–3.1Ga) and the EAO (ca. 870-600Ma). The terranes are overlaid by Cenozoic cover (1.2Ma to present).

### **2.1. The Tanzanian Craton**

The Archaean Tanzanian Craton forms the central nucleus of the eastern Tanzanian continental crust. The craton has been dated by Chesley et al. (1999) at 2.5 - 2.9Ga by using Re-Os systematics from chromites obtained from mantle xenoliths in the East African Rift as well as from the craton itself. They also show that the ancient refractory lithosphere extends at least ~140km beneath the East African Rift in northern Tanzania and that extensive rift-related thinning has not yet occurred as it has been shown to have developed in Kenya (Chesley et al., 1999). Other ages for the craton also exist, such as the 2.7 - 3.1Ga ages obtained from granitoids and reported by Möller et al. (1998).

The craton has been subdivided into two contrasting domains (Maboko, 2000). The first is a central domain consisting of granite, granodiorite, felsic gneisses and migmatites associated with metamorphic supracrustal rocks. The second domain is composed of the granite-greenstone association of basic to acid volcanics, turbidites, pelites and banded iron formations intruded by granites and overlain by conglomerates, argillaceous sediments and minor volcanics. Both domains are intruded by post-orogenic granites (age ~2.6Ga) and pegmatites (age 2.5Ga). This is used by Maboko and Nakamura (1995) to infer that the craton had cooled below 300°C by ~2.5Ga.

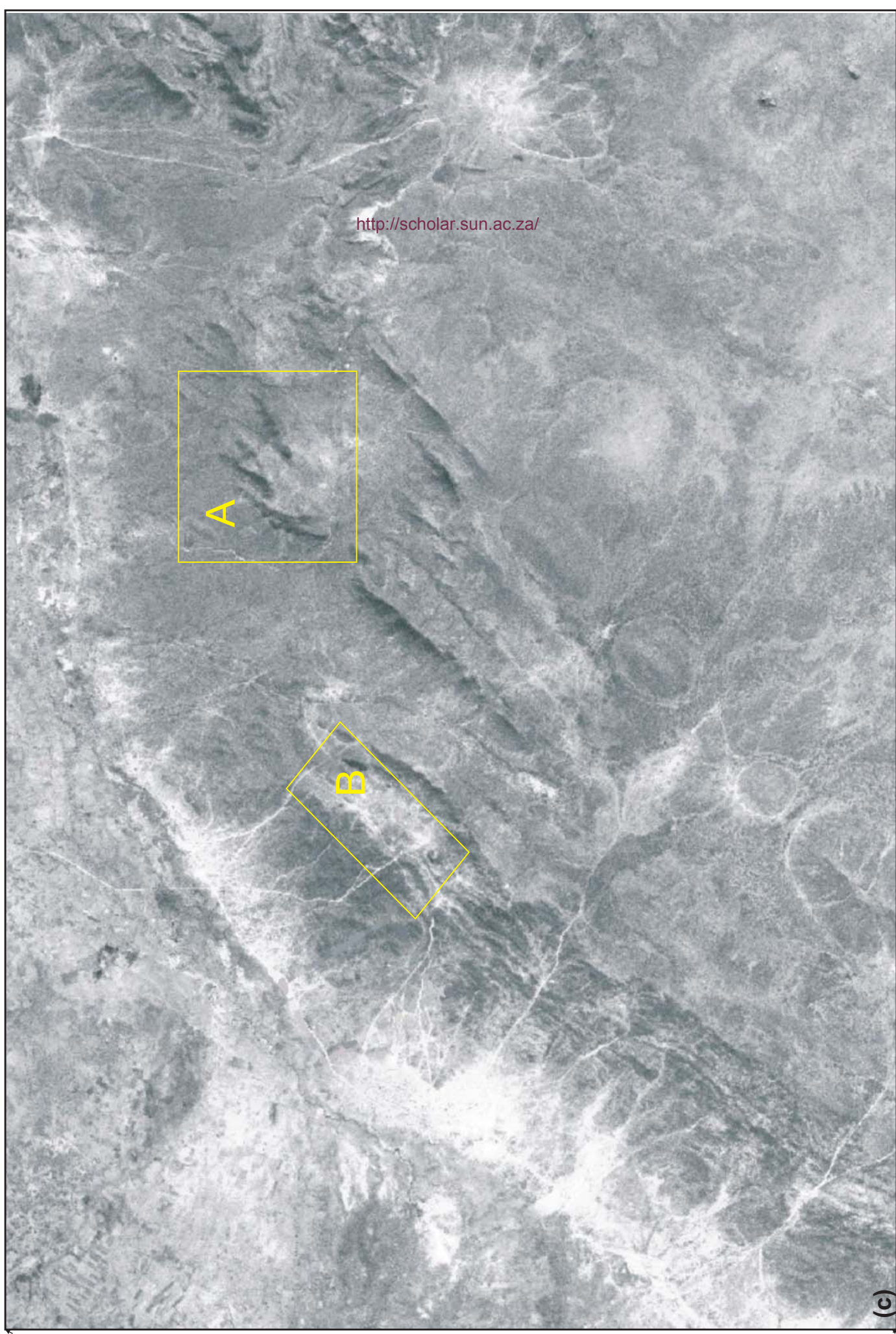
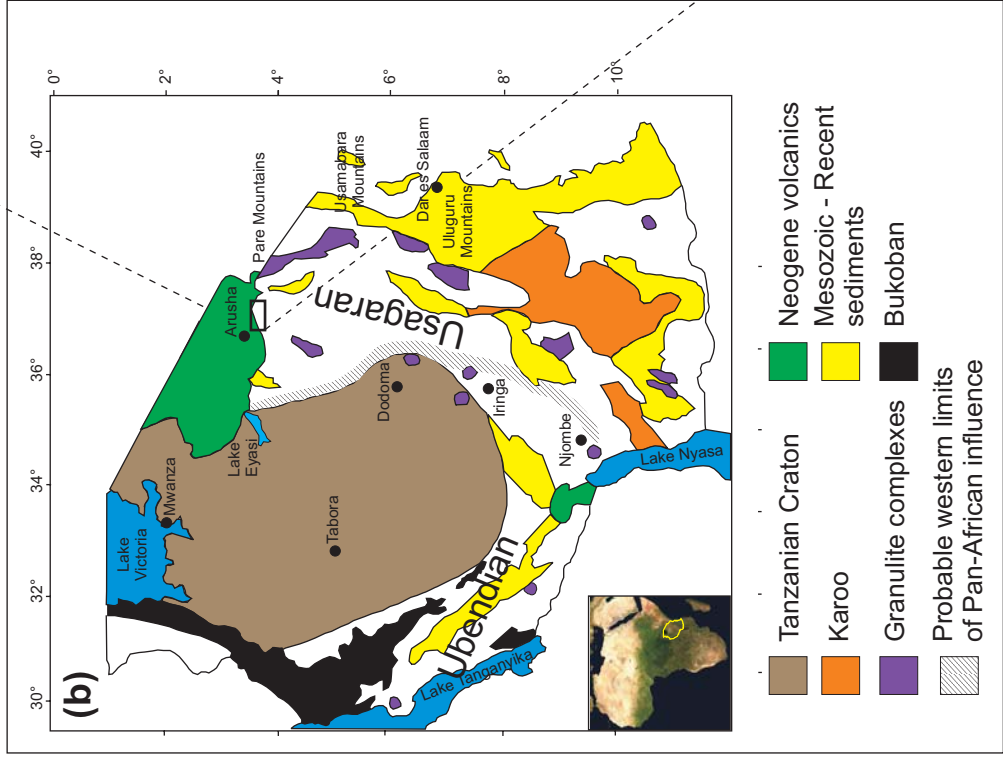
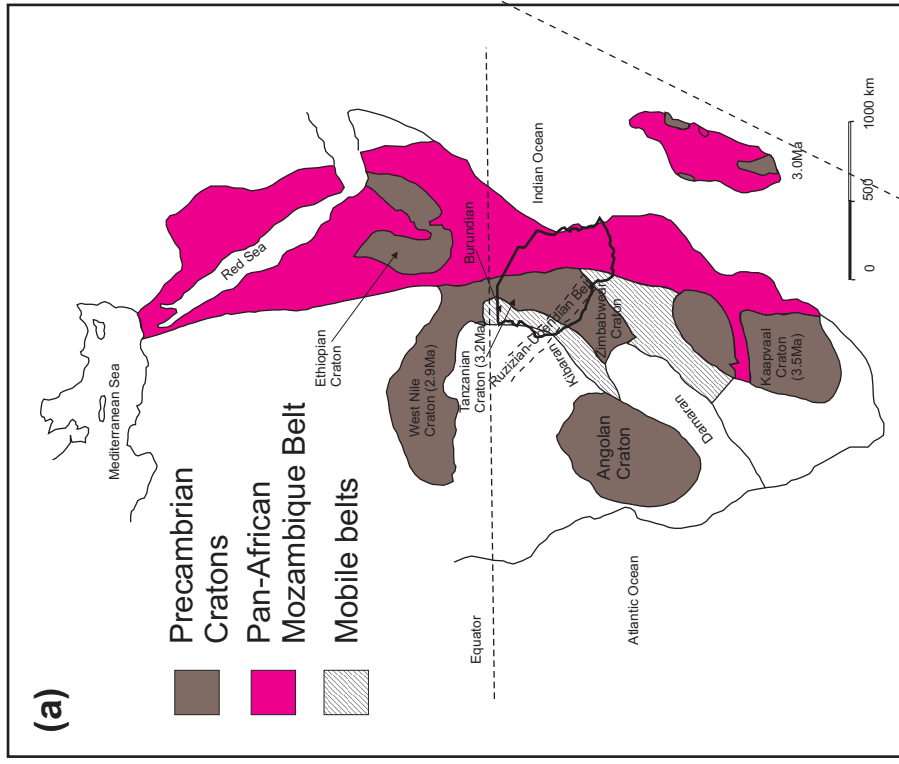


Fig.1 (a) Tanzania relative to the regional East-African Orogen as well as the continental cratons (simplified from Malisa and Muhongo, 1990). (b) The study area in relation to the regional geology of Tanzania (simplified from Malisa and Muhongo, 1990). (c) Satellite image of the northwestern limb of the Lelatema anticlinal structure showing the areas chosen for soil (yellow block A) and stream sediment sampling (yellow block B)

The Tanzanian craton is flanked in the west and south-west by high grade metamorphic rocks of the Paleo-Proterozoic Ubendian Belt (~2.0Ga) and in the east by the Usagaran rocks of similar age (Fig.1b) (Maboko, 2000). It is inferred by Möller et al. (1995) that the age of 2.0Ga represents a subduction zone, which led to the formation of the Usagaran-Ubendian belts. The east-west structural trends of these belts are truncated by the meridional trends of the EAO. It is this orogenic belt in which the various gemstone deposits are located.

## **2.2. The East African Orogen and its Tectonic Evolution**

The rocks representing the EAO in north-eastern Tanzania are mostly meta-igneous and meta-sedimentary rocks which have witnessed multiple stages of deformation and have been metamorphosed to granulite facies and subsequently retrogressed to amphibolite facies (Maboko, 2000). The granulites in north-eastern Tanzania (Fig. 1b) display pressures and temperatures which indicate that they once formed part of the middle to lower crust. Examples are the Usambara and Uluguru granulites, which both display temperatures and pressures of ~800°C and 9.5 - 11kbar and the meta-anorthosites, which occur in the same area, for which pressures and temperatures of 950 - 1100°C and 13 – 17kbar are recorded (Muhongo et al., 1999). It is generally accepted that these rocks underwent isobaric, slow cooling with three accelerated periods of cooling during the early Cretaceous, late Cretaceous and late Eocene to early Oligocene due to the episodic reactivation of high angle normal faults, inherited from the Neo-Proterozoic Pan-African orogeny (Muhongo et al., 1999; Noble et al., 1997; Maboko and Nakamura, 1995). In fact, the cooling rate was 2 - 3°C per million years, which is extremely slow and is been used to infer a collisional regime in Neo-Proterozoic times, because such slow cooling implies thermal relaxation of continental crust thicker than average (Noble et al., 1997).

The EAO is an impressive belt in terms of size, being approximately 6000km long as well as spanning a time of 350 million years in evolution (Fig.2) (Stern, 2002) rendering it comparable to modern orogenic belts, such as the Andean orogeny.

It is thought that about 1.1Ga the supercontinent Rodinia had formed (Hoffman, 1989). It is thus proposed that the history of the EAO started with a Rift-Rift-Rift (RRR) triple junction around 870Ma ago with the subsequent opening of the Mozambique Ocean

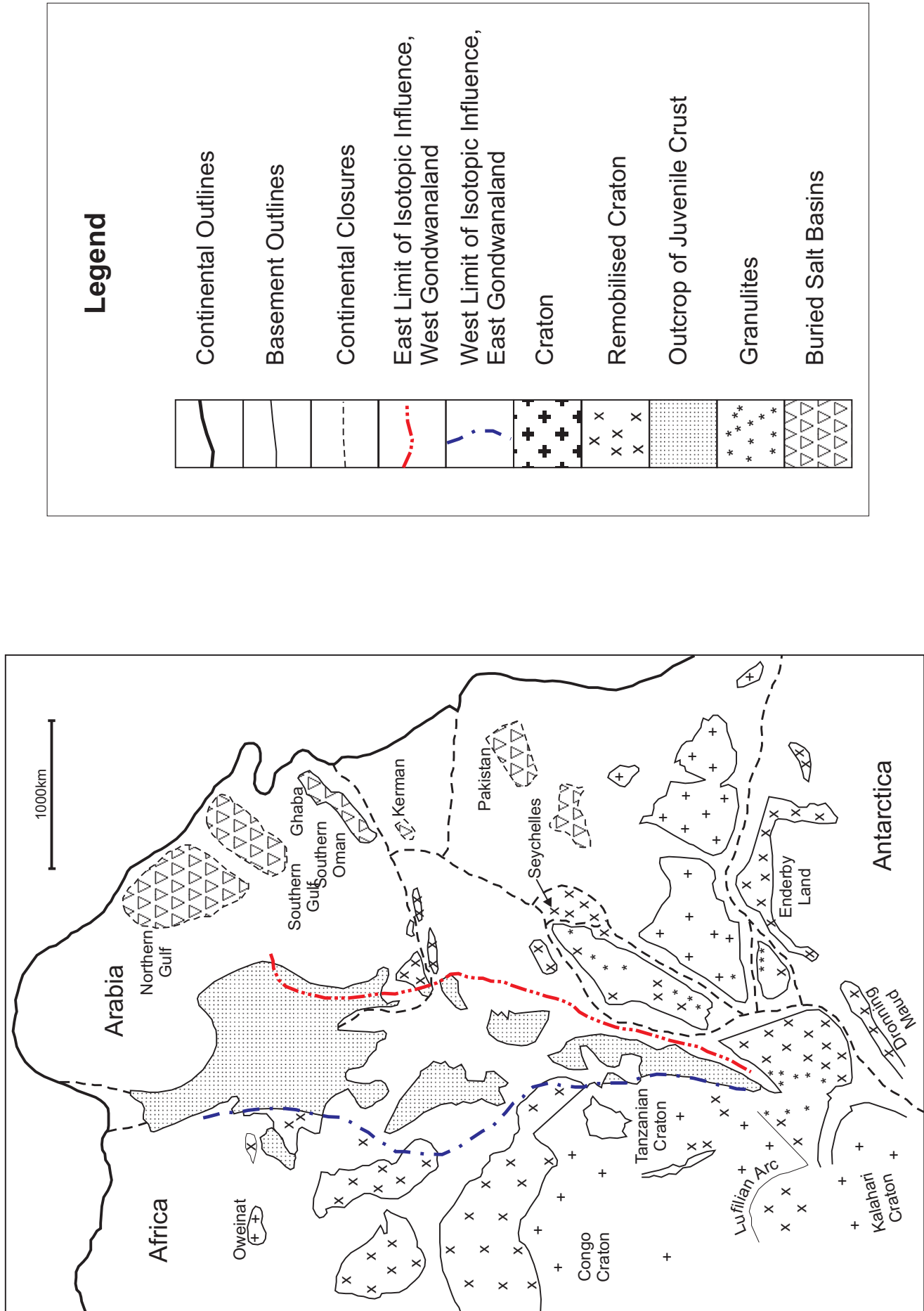


Fig.2 Tectonic map of the East African Orogen . Continental fragments are shown as configured at the end of the Precambrian (simplified from Stern 1994)

(Fig.3) (Stern, 1994 and 2002). The presence of abundant ophiolites and a significant volume of juvenile crust, as well as other evidence, suggests that this ocean was large, perhaps as large as the modern Pacific (Fig. 3) (Stern, 1994). The seafloor spreading was reversed sometime during the Neo-Proterozoic, until it completely closed around a pivot in what is now South Africa resulting in the collision between east and west Gondwanaland around 700Ma, but which could have occurred as early as 750Ma ago (Fig.3) (Stern, 1994). Collision occurred with the Tanzanian craton as the rigid indenter and with the western flank of Gondwana being the area of crustal thickening and plastic deformation (Bonavia and Chorowicz, 1992). Escape tectonics was used to infer the direction of subduction as well as the duration of the collisional event. Escape took place mainly to the north, beginning before 660Ma and ending after 610Ma, which implies that the convergence of east and west Gondwana continued for 120 to 170Ma after initial collision (Fig. 3) (Stern, 1994). The tectonic escape led to rift basins forming in north-east Africa and Arabia, which led to continental separation and the formation of a passive margin on the north flank of Gondwanaland at the end of the Precambrian (Brookfield, 1993). The East African orogenic scenario is comparable to the current collisional scenario between India and Asia (Stern, 1994) (Fig.4).

The presence of granulites in the EAO indicates the areas of greatest thickening and subsequently where the inter-continental collision was most intense. Granulites are found in southern Kenya, Tanzania, Malawi and Mozambique, marking these areas as the focus of the collision. Granulites are absent north of Central Sudan and in southern Ethiopia (Stern, 1994). There are differences of opinion among various researches about the exact age of peak metamorphism in the granulites. The Usambara granulites, for example, have been dated with ages ranging from ~605Ma to ~640Ma (Maboko et al., 2002). These discrepancies are interpreted by Maboko (2000) as the result of isotopic equilibration during cooling, thus rendering the calculated ages a minimum for peak metamorphism. Peak metamorphism, however, is generally accepted by most researchers to have occurred around 625 - 650Ma (Muhongo et al., 2001; Maboko, 2000; Malisa and Muhongo, 1990).

After the EAO orogenic event, the basement rocks in eastern Tanzania underwent a protracted history of denudation, uplift as well as post-Carboniferous extensional tectonism. The rocks of the EAO also underwent slow, isobaric cooling with three distinct rapid cooling events, which can be ascribed to the formation and reactivation of

# Tectonic Evolution of the East African Orogen 900 - 550Ma

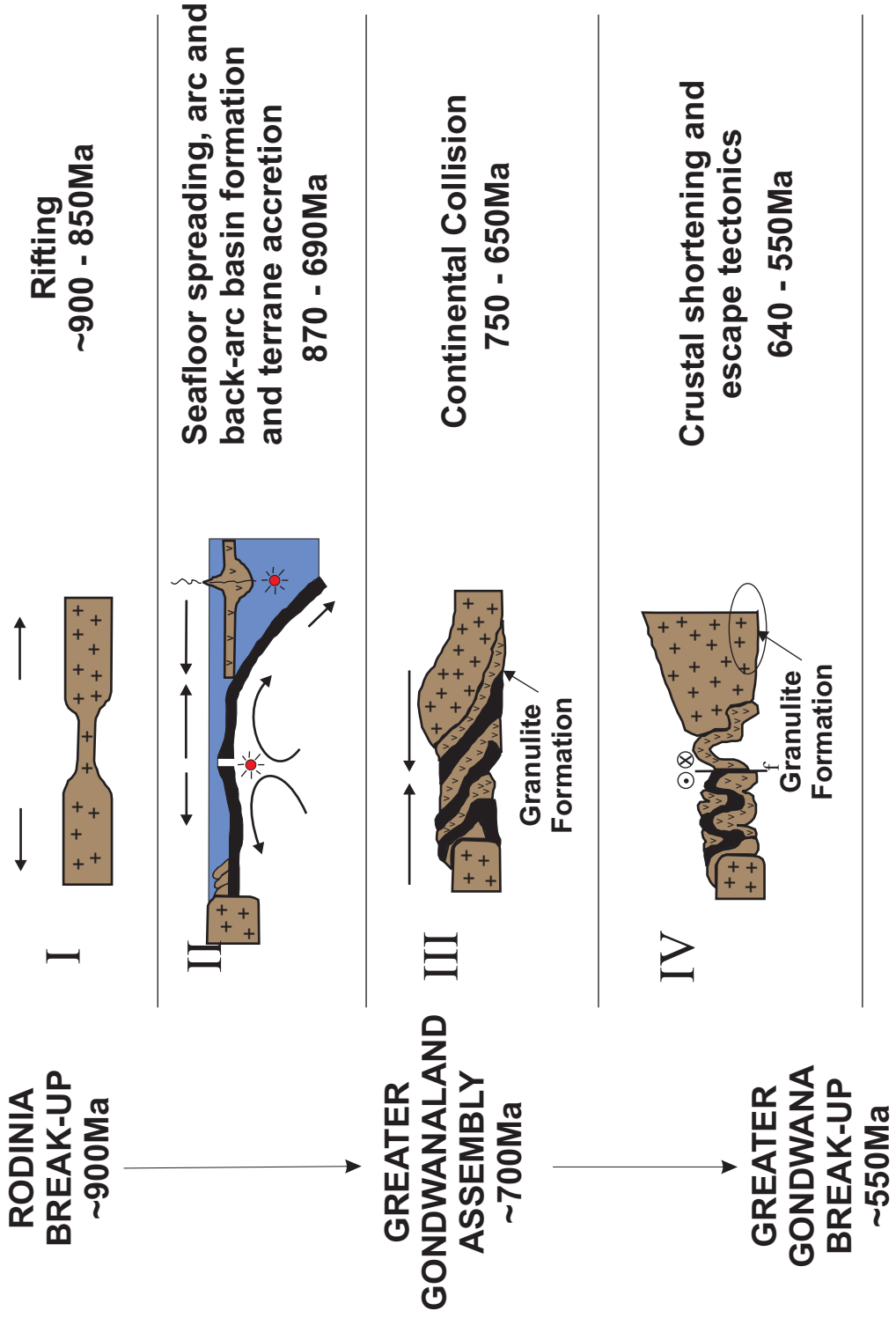


Fig.3 Two dimensional summary of the tectonic evolution of the EAO (modified from Stern 1994)

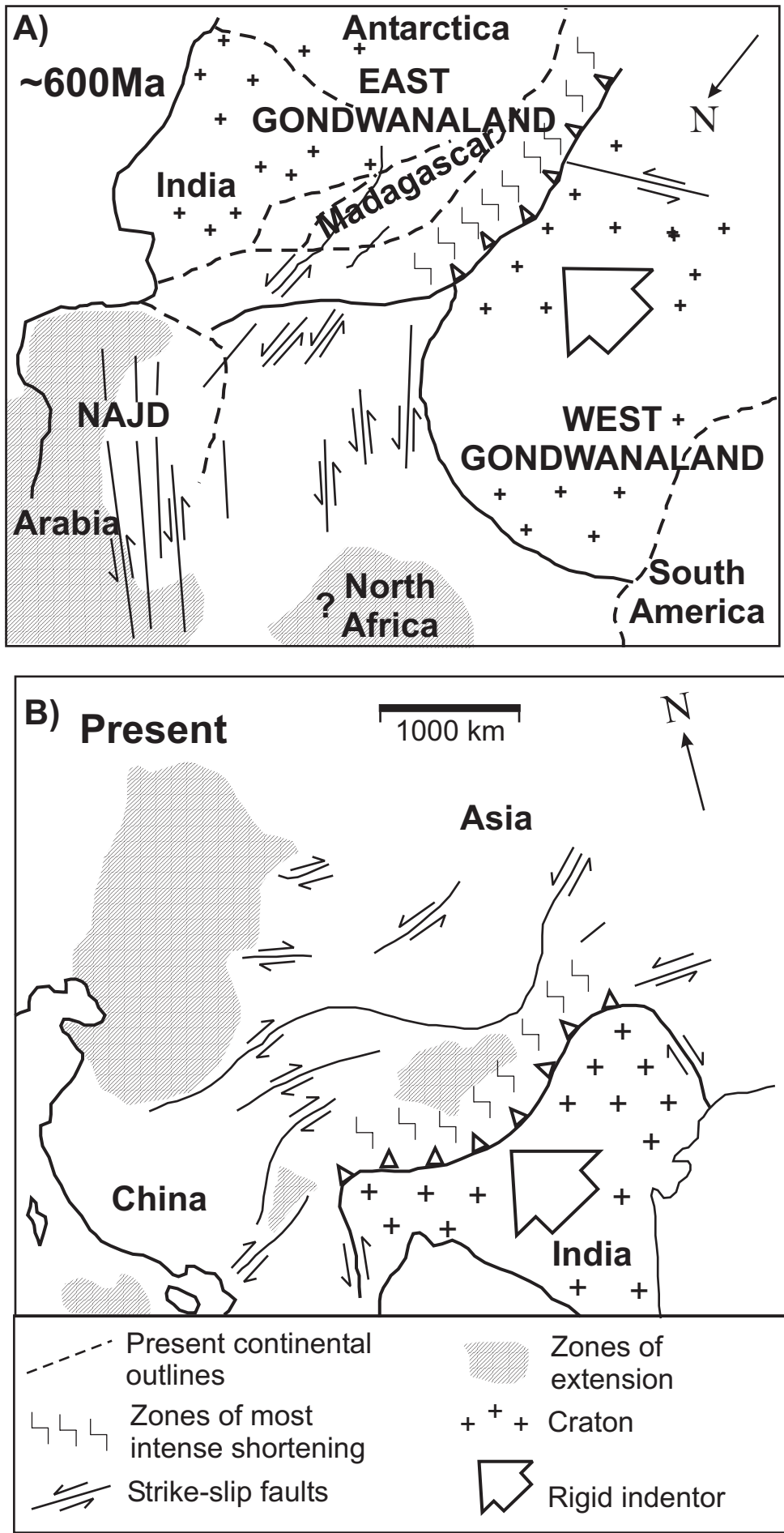


Fig.4 Comparison of continental collisions at the same scale (from Stern 1994). Both are oriented so that the rigid indenter is moving towards the upper left corner: (A) East African Orogen, ca 600Ma ago. Areas without ornamentation are juvenile or were remobilized during the Neoproterozoic. (B) Modern India-Asia collision, shown as mirror-image so that the free face and principal zone of tectonic escape are on the same side of the rigid indenter as is the case for the EAO.

high angle faults in response to intraplate stress (Noble et al., 1997). The East African Rift Valley developed in a broad region of previously block faulted and mildly extended crust during Neogene time.

### **2.3. Cenozoic Cover**

The Cenozoic cover constitutes the upper Cenozoic volcanism associated with the East African Rift and unconsolidated Quaternary sediments, which overlies the older eastern Tanzanian rocks (Dawson, 1992, 1997).

The East African Rift is a linear structure following the meridional trend of the EAO (Fig.5) (Dawson, 1997). Rifting in northern Tanzania started about 1.2Ma ago. The Neogene volcanic rocks of the northern Tanzanian province comprise two ages of volcanic activity. The first (pre-1.2Ma) age is defined by a major central group of volcanoes of the alkali-basalt-phonolite association, with basalt being the dominant lava type. The second (post-1.2Ma) volcanic group comprises mainly nephelinite-phonolite-carbonatite volcanoes. Kibo peak on Mt Kilimanjaro (45km from the study area), which belongs to the latter group of volcanoes, is regarded as active (Dawson, 1992).



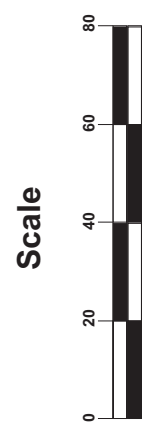
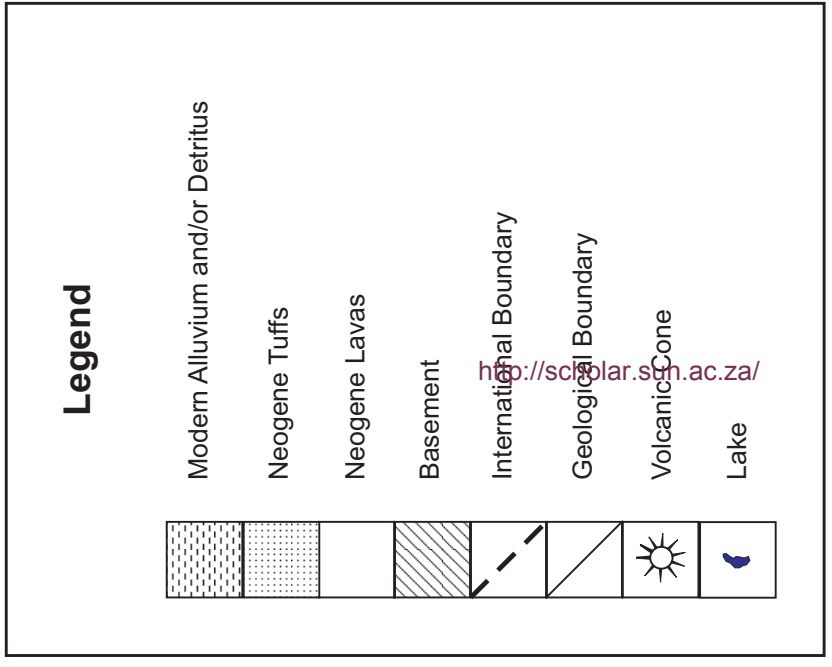
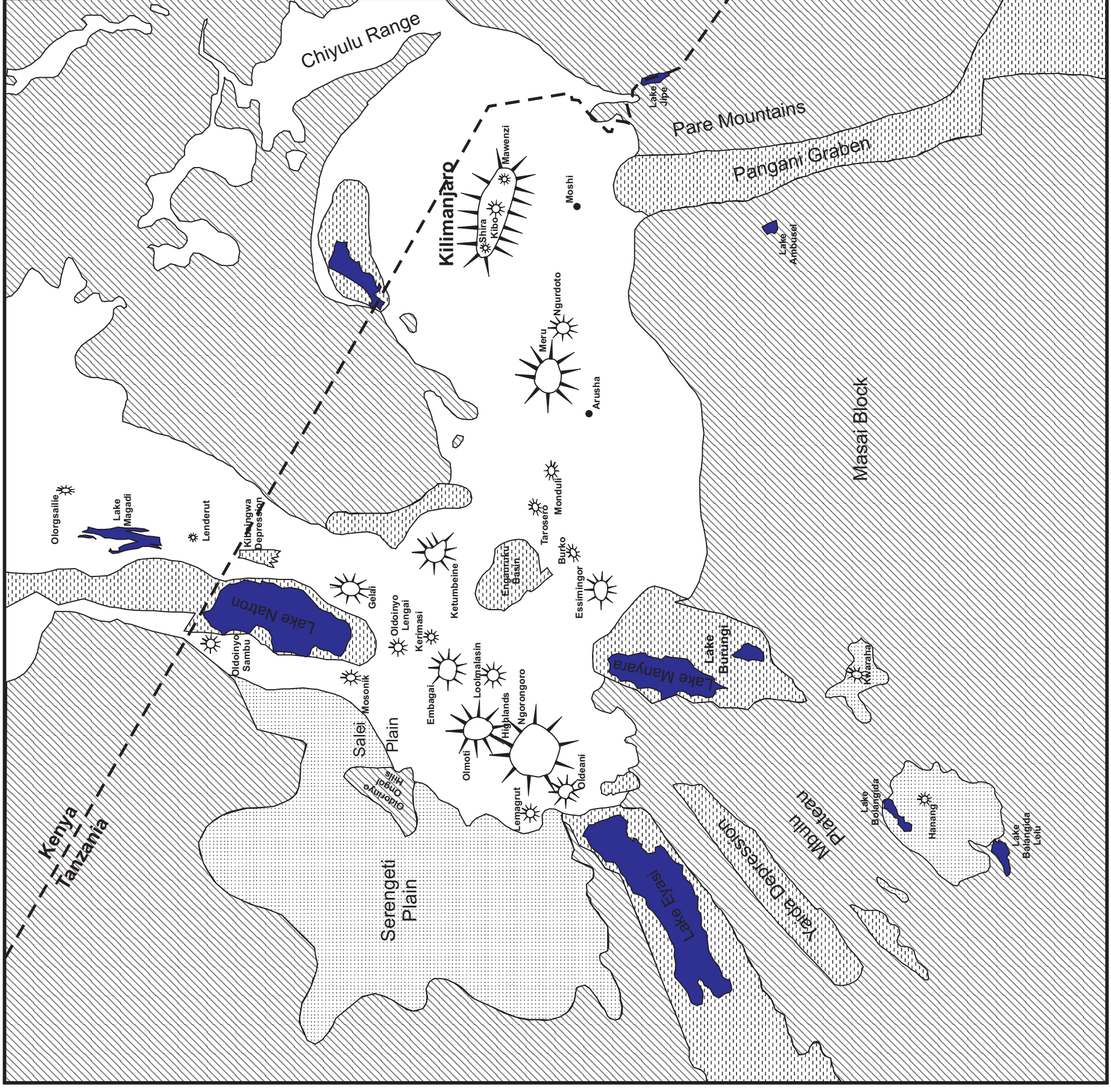


Fig.5 Distribution of Neogene tuffs and lavas. (Simplified map from Dawson, 1992)

### 3. Local Geology

The rocks of the Merelani area in Tanzania consist of a poly-metamorphosed metasedimentary sequence of upper amphibolite to granulite facies (Malisa et al., 1990; Davies et al., 1994). The Merelani area itself, specifically the area surrounding the active tanzanite mines, is situated on the northwestern limb of a large antiformal structure in northeastern Tanzania defining the Lelatema Mountains and subsequently termed the “Lelatema Anticline” (Malisa, 1987). The layers of the western limb of the anticline itself display moderate dips of 30° to 60° to the west and a general strike of 040°, with the fold hinge dipping at ~16° to the north (Malisa, 1987; Scheepers and Kisters, 2000).

The rocks of the Merelani area have been subdivided into two stratigraphic horizons, the Upper and Lower horizons. It is the lithologies of the Lower Horizon which host the tanzanite mineralisation and it is thus this horizon on which the current study is focused.

The rocks in the Merelani area were subdivided into various lithological units by Malisa (1987), but the nomenclature was deemed insufficient and was revised by Olivier (2006). His subdivisions are presented in Table 1 together with the old names as suggested by Malisa (1987). The entire Lower Horizon stratigraphic package is sandwiched between two garnet gneiss units. A dolomite unit occurs in the centre of the sedimentary package with two seemingly repetitive sub-packages occurring on either side of it (Fig.6, Fig.9). It has been suggested that the Lower Horizon represents a folded succession wrapped around the central dolomite (Rutahundurwa, Afgem geologist, pers. comm.)

A detailed description of the mode of mineralisation is beyond the scope of this study. A short description is, however, warranted for the sake of completion. The tanzanite itself is situated within an altered zone in the Kyanite Gneiss LK2 and LK1 units of the Lower Horizon sedimentary package. This altered zone is termed the Ali Jaluwatu Zone, or JWZ for short. In essence it is a plagioclase-rich schistose unit. This unit is host to intensely folded and boudinaged sub-units with the tanzanite mineralisation occurring in stress minimum zones within the boudinaged package. This boudinaged layer is subdivided into four categories:

<b>Table 1 Generalised stratigraphy and proposed new names for rocks in the Merelani area</b>	
<b>Mineralogical name (after Olivier, 2006)</b>	<b>Previous Name (after Malisa, 1987)</b>
Dolomitic Marble	Dolostone
Garnet-sillimanite-biotite gneiss (GNG1)	Garnet-silimanite gneiss
<b>Upper Horizon</b>	
Kyanite-graphite gneiss (K4)	Kyanite gneiss unit 4 (K4)
Biotite-graphite gneiss (FL2)	Flaggy graphite gneiss (FL2)
Kyanite-graphite gneiss (K3)	Kyanite gneiss unit 3 (K3)
Biotite-graphite gneiss (FL1)	Flaggy graphite gneiss (FL1)
Kyanite-graphite gneiss (K2)	Kyanite gneiss unit 2 (K2)
(MAZ)	Hydrothermally altered graphite gneiss (MAZ)
Kyanite-graphite gneiss (K1)	Kyanite gneiss unit 1 (K1)
(QF)	Quartzofeldspathic fels (QF)
<b>Lower Horizon</b>	
Garnet-sillimanite-biotite gneiss (GNG2)	Garnet-sillimanite gneiss
Kyanite-graphite gneiss (LK4)	Lower kyanite-graphite gneiss (LK4)
Graphite-plagioclase gneiss (C-Zone)	C-Zone
Kyanite-graphite gneiss (LK3)	Lower kyanite-graphite gneiss (LK3)
Graphite-calc-silicate gneiss (GCS2)	Intensely altered (LA2)
Banded Calc-silicate fels (CF2)	Metapsammite (MPS2)
Dolomitic marble (DM2)	Dolostone
Banded Calc-silicate fels (CF1)	Metapsammite (MPS1)
Graphite-calc-silicate schist	Intensely altered (LA1)
Kyanite-graphite gneiss (LK2)	Lower kyanite-graphite gneiss (LK2)
Graphite-plagioclase gneiss (JWZ)	JWZ
Kyanite-graphite gneiss (LK1)	Lower kyanite-graphite gneiss (LK1)
Garnet-sillimanite-biotite gneiss (GNG3)	Garnet-sillimanite gneiss
Dolomitic marble (DM3)	Dolostone

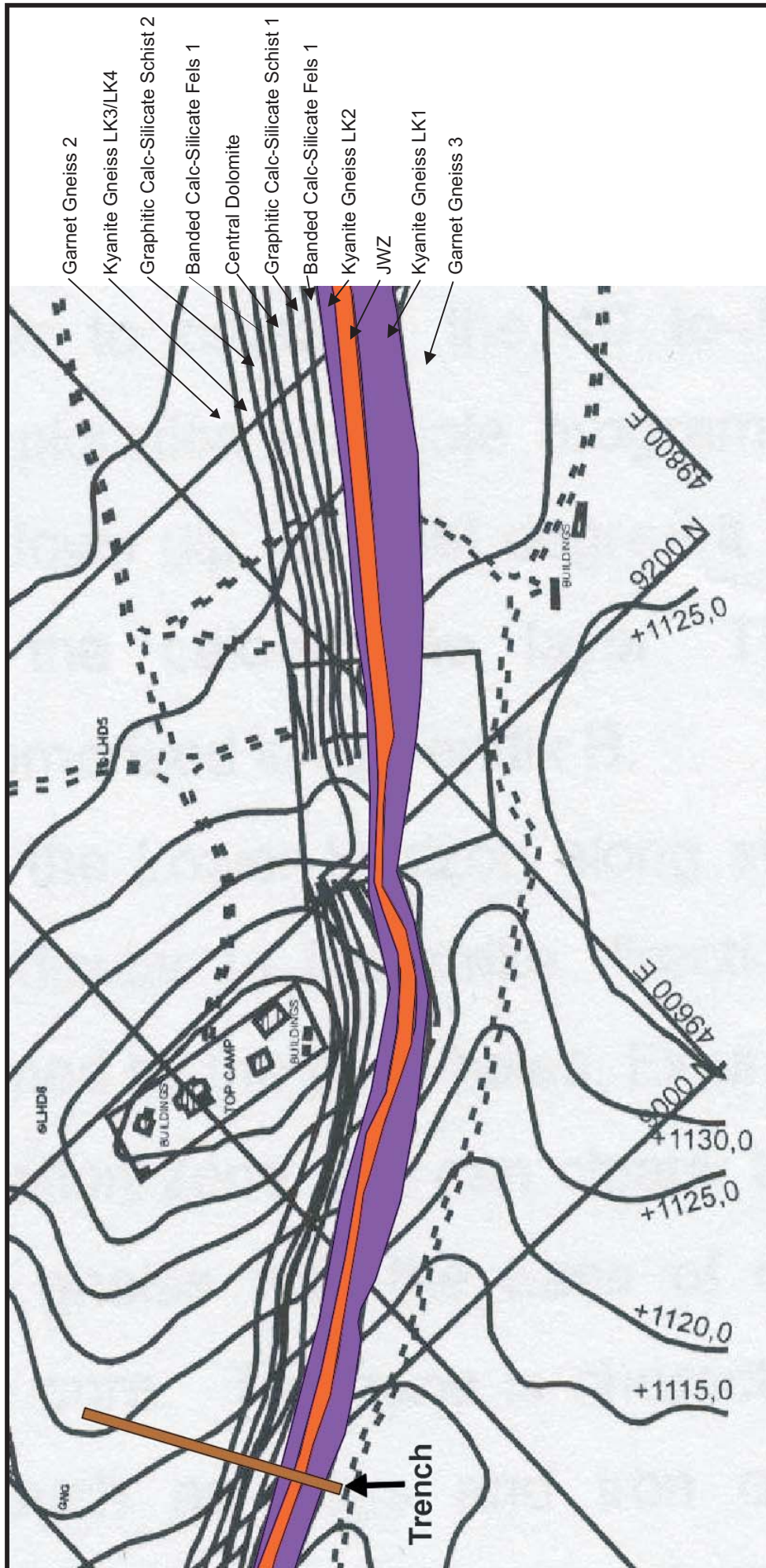


Fig.6 Geological map showing the Lower Horizon lithologies in relation to each other. The Mineralised units are highlighted with the JWZ in orange. The position for the trench dug for the soil sampling is shown in brown (simplified from Rutuhundurwa, 1995).

1. skarnoid reaction zones;
2. boudins
  - pyroxene relics within boudins;
  - calc-silicate skarn boudins and;
3. low-pressure pockets within skarn boudins

A more detailed description of the boudinaged layer is presented later on in this chapter. However, they all form part of the same altered layer, the JWZ. The kyanite gneiss units LK4 and LK3 above the central dolomite also contains an altered zone, termed the C-Zone

Fig.6 is a simplified version of the modified map of Rutahundurwa (1995). The mineralogy and petrography of the different lithological units of the Lower Horizon, the tanzanite-hosting horizon, will be discussed briefly, mainly based on the geological mapping and research by Olivier (2006).

### **3.1. Dolomitic Marble**

The Merelani lithologies are marked by dolomitic marble ridges, which flank the tanzanite deposit on the northeastern and southwestern sides. The schists and gneisses are present in a northeast-southwest trending depression. The dolomitic rocks are white in colour when pure and display shades of grey at places due to impurities of accessory minerals such as graphite, biotite and pyrite.

The dolomitic marble consists mainly of dolomite (up to 80%) and calcite (15 - 25wt%). Other mineral constituents are quartz (~5wt%), plagioclase, titanite (sphene), chlorite, pyrite, pyrrhotite, kyanite and graphite.

### **3.2. Garnet Sillimanite-Biotite Gneiss**

The garnet-sillimanite-biotite-gneiss forms the central unit between the Upper and Lower horizons. It is a medium to coarse-grained rock which displays a spotted appearance due to large, purple almandine crystals. The primary minerals are quartz, almandine, sillimanite, biotite, potash feldspar and plagioclase. The accessory

minerals are pyrite, rutile, titanite, kyanite, graphite, muscovite, zircon, hematite, ilmenite and apatite, with pyrite and rutile being the most abundant.

### **3.3. Kyanite-Graphite-Gneiss**

The kyanite-graphite gneiss has been subdivided into 5 units by Olivier (2006): Unit 1, the footwall kyanite-graphite gneiss (LK1), unit 2, the hangingwall kyanite-graphite gneiss (LK2) and units LK3 and LK4 above the central dolomite and units LK5 and LK6 in the Upper Horizon (Table 1).

The boudinaged tanzanite-bearing graphite-plagioclase gneiss (JWZ) is sandwiched between LK1 and LK2 units of the kyanite-graphite gneiss. Both the hangingwall and footwall units are locally associated with pegmatites and a characteristic hangingwall pegmatite layer is formed within unit LK2.

Units LK3 and LK4 of the kyanite-graphite gneiss are sometimes separated by a graphite-plagioclase gneiss, termed the C-Zone. Where the C-Zone is absent the units occur on top of each other and are then considered as one unit.

Units LK5 and LK6 occur above the central garnet-sillimanite-biotite gneiss and thus occur within the Upper Horizon.

The kyanite-graphite gneiss is medium grained and consists of quartz, feldspar, kyanite, graphite and variable amounts of sillimanite, mica and pyrite with pyrrhotite, sphalerite, zircon, apatite and rutile occurring as accessories. Pyrite and pyrrhotite are the main sulphide mineral phases. The feldspar occurs as separate aggregates forming feldspar-rich layers.

### **3.4. Graphite-Plagioclase Gneiss**

The graphite-plagioclase gneiss occurs as three units: the JWZ, C-Zone and D-Zone. The JWZ and C-Zone occur in the Lower Horizon, while the D-Zone occurs in the Kyanite Gneiss lithological unit in the Upper Horizon (between units LK5 and LK6). The C-Zone is sandwiched between the Kyanite Gneiss LK4 and LK3 units, while the JWZ occurs between units LK2 (hangingwall) and LK1 (footwall).

The JWZ is the most important of the graphite-plagioclase units, because it is this layer which is host to the intensely boudinaged calc-silicate layers, which host the tanzanite mineralization.

All three units consist of quartz, feldspar and graphite with mica, pyrite and titanite as the accessory mineral phases. The layers, as previously mentioned, are similar to the kyanite-graphite gneiss, but with the following most important differences:

1. Absence of aluminum silicates
2. Higher plagioclase content
3. Larger amount of alteration and oxidation (inferred from a lower rock competence and a greater concentration oxidised sulfides)
4. Higher mica content
5. Generally smaller grain size

These horizons consist mostly of quartz and plagioclase, with small amounts of diopside, tremolite, chlorite, calcite, serpentine and clay minerals which are present in localised areas of calc-silicate units.

### **3.5. Calc-Silicates**

The calc-silicate layers are intensely boudinaged and contained within the graphite-plagioclase gneiss (JWZ) unit. This horizon hosts the tanzanite mineralization and makes it the most unique layer in the world in terms of gemstone mineralization.

Where calc-silicate layers have been observed within the C-Zone, they have been developed on a small scale and it is unknown to what extent they are present over a regional scale.

The calc-silicate layers are divided into four lithological types:

- a) Skarnoid reaction zones
- b) Boudins
  - pyroxene relicts
  - calc-silicate skarn boudins

c) Low-pressure pockets within skarn boudins

a) *Skarnoid reaction zones*

These layers are isoclinally folded and wrap around and connect the calc-silicate boudins (Fig.7 and Fig.8). They are in contact with the neighboring gneisses and represent a metasomatic reaction zone between the calc-silicates and the gneisses.

The layers are highly banded, foliated and medium grained. They are of a greyish colour. The foliation is defined by the preferred crystallographic orientation of graphite and elongated quartz and zoisite grains.

The layers consist of quartz, a mixture of clay minerals from the smectite group, pyrophyllite, zoisite, graphite, pyrite, grossular and diopside with titanite and muscovite as accessories.

b) *Boudins*

- *Pyroxene relicts*

The boudins occur within the grey bands. They are situated on the fold limbs and are a few centimetres up to about 1m in length. They are dark green in colour and do not display any banding or foliation.

Diopside is the main rock-forming mineral within the relict units, with grossular garnet, quartz, pyrite and graphite occurring in minor amounts.

- *Calc-silicate skarn boudins*

These altered boudins were formed by the hydrothermal alteration of the pyroxene relict precursor.

The skarn boudins consist of diopside, quartz, graphite, pyrite, haematite, zoisite (occasionally tanzanite), grossular garnet (occasionally its gem



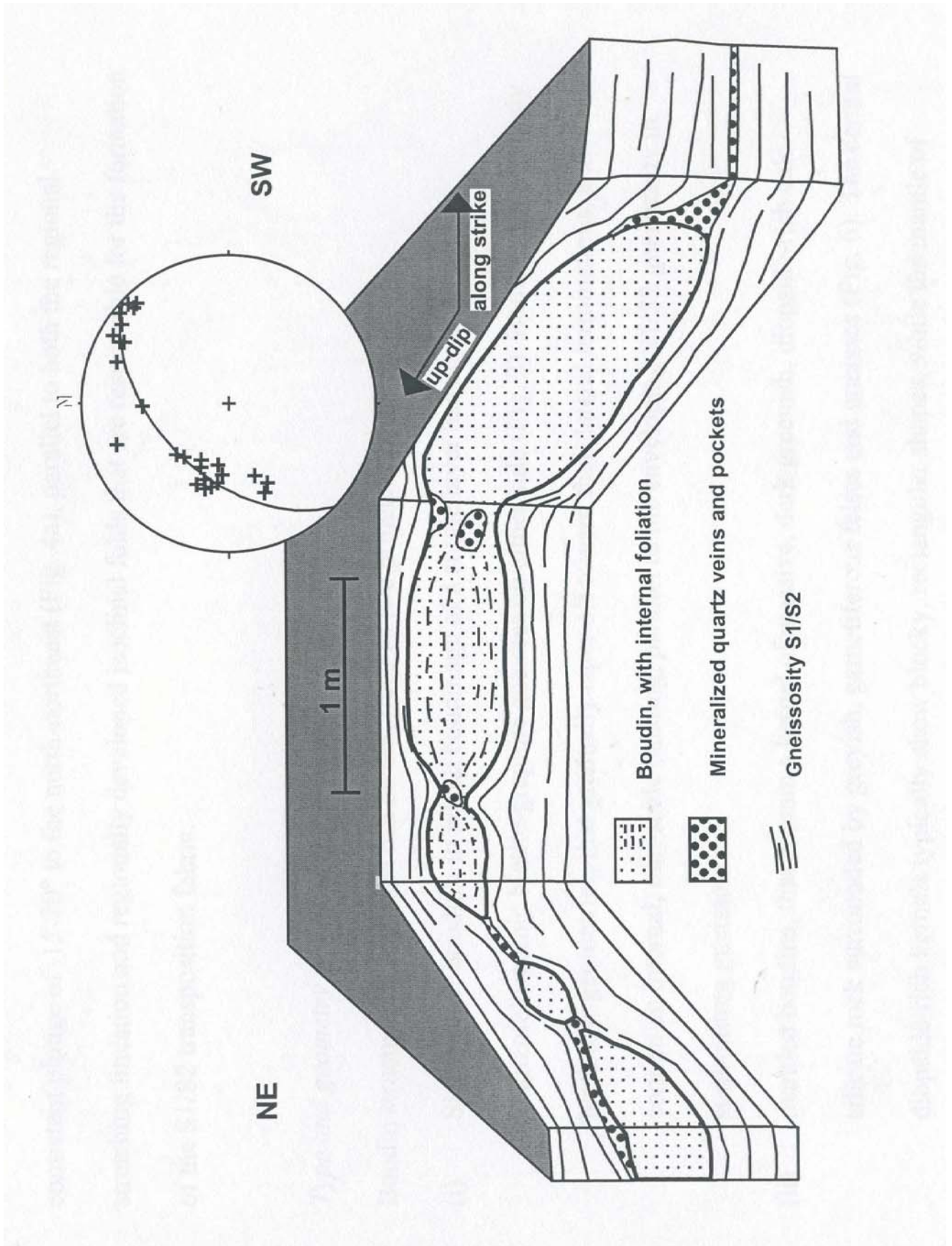


Fig.7 Showing the structure of the Boudins of the JWZ (after Schreepers and Kisters, 2000)

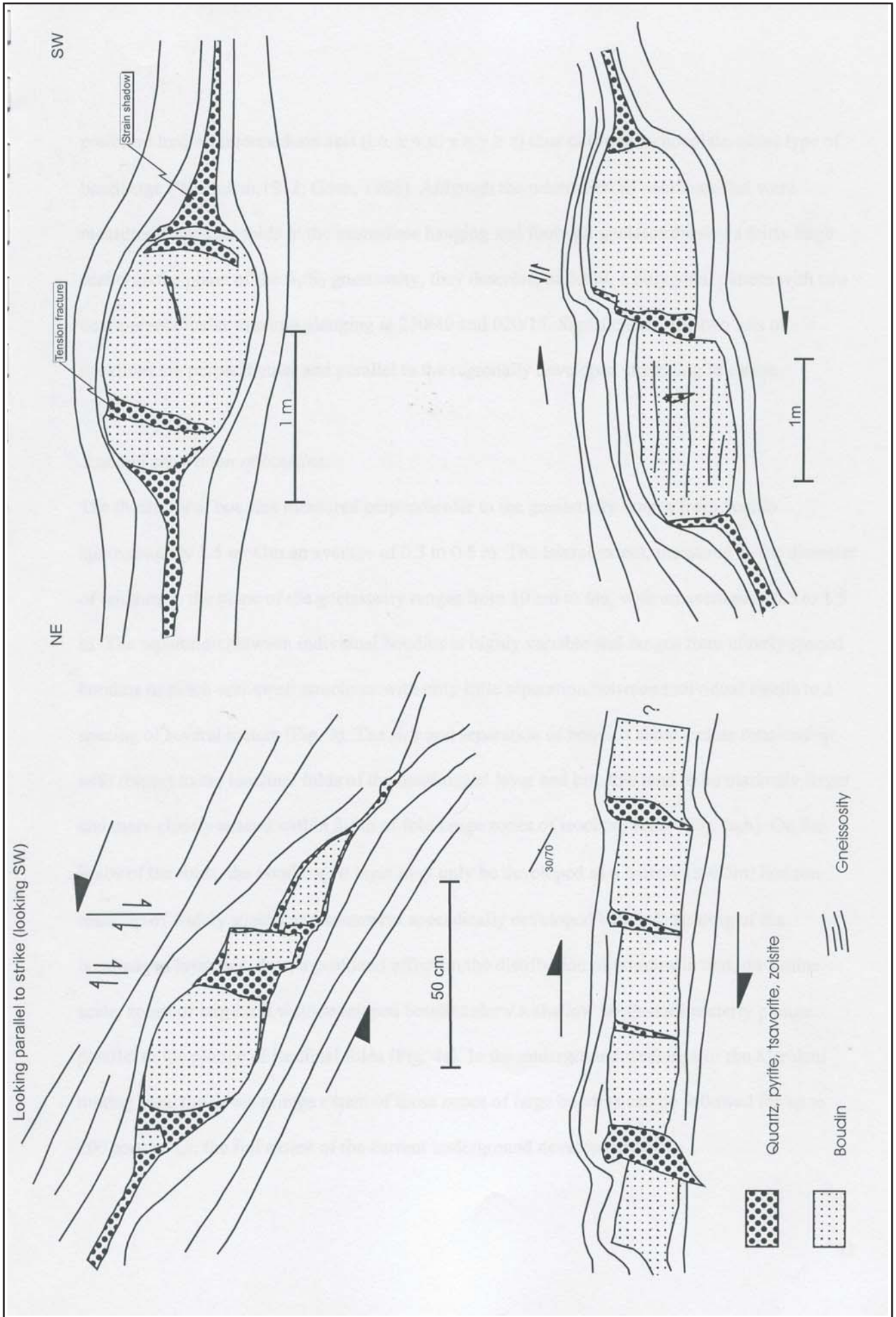


Fig.8 Schematic diagram showing the various orientations of boudins and their structure (after Scheepers and Kisters, 2000)

variant tsavorite) as well as secondary alteration minerals such as goethite, halloysite and illite.

### *c) Pockets of low pressure*

The hydrothermal boudins contain pockets of coarse-grained quartz, grossular, zoisite (predominantly tanzanite), pyrite, calcite, graphite and diopside. The pockets are situated in various types of low-pressure sites within and adjacent to the boudins, such as at boudin necks (Fig.8). These pockets are the main source of gem-quality tanzanite and tsavorite. Other minerals which also occur within these pockets are pyrite, occurring as large euhedral crystals up to about 15cm with smooth crystal faces, calcite, also as well-formed crystals and crystal aggregates, graphite, occurring as flakes and halloysite, which occurs as irregular clots and as fracture fillings in zoisite (and tanzanite).

### **3.6. Graphite-Calc-Silicate Schist**

The graphite-calc-silicate schist has the following mineral constituents: Quartz, graphite, grossular garnet, diopside, scapolite and plagioclase with pyrite, hematite, titanite, serpentine and various clay minerals being the accessory minerals, with titanite as the most abundant accessory.

The schistosity is defined by sub-parallelized graphite flakes. The rock has a greyish to silver colour due to the graphite and also displays a green spotted appearance, due to disseminated grossular crystals. The rock contains millimetre scale zones which are richer in calc-silicate minerals. These zones consist mainly of the mineral diopside, with variable amounts of quartz, graphite and feldspar.

### **3.7. Banded Calc-Silicate Fels**

The banded calc-silicate fels has been divided into two units, CF1 and CF2, both surrounding the central dolomitic marble in the Lower Horizon. Both units are medium- to coarse-grained and are light grey in colour. The fels consists of millimetre scale banding of alternating silicate and calc-silicate layers. The banding is also defined by sulphides, which are especially abundant in the transition zones between silicate and calc-silicate zones.

The silicate zone consists of microcline and quartz with minor amounts of plagioclase, muscovite, pyrrhotite, pyrite and accessory minerals, graphite, diopside and titanite.

The calc-silicate zone consists of diopside, calcite and scapolite with lesser amounts of quartz, plagioclase and microcline with pyrrhotite, pyrite, muscovite, graphite and titanite as the accessory minerals.

### **3.8. Superficial Deposits**

Quaternary unconsolidated sediments cover most of the Merelani tanzanite deposit. The south-western part of the deposit is mostly covered by thin calcareous soil, laterites and gravel, while the north-eastern part of the deposit is covered by a hard calcrete layer, increasing in thickness towards the north-east (Olivier, 2006).

### **3.9. Structural Geology**

A detailed description of the structural geology is beyond the scope of this study and only a short summary is presented here. The following is mostly based on a report on the geology of the Merelani Tanzanite deposit by Scheepers and Kisters (2000), as well as from Olivier (2006).

The Merelani tanzanite mine is situated on the north-western limb of the shallow northerly plunging large-scale open Lelatema fold. The gneissosity shows dips of between 30° and 60° to the north-west, with a strike of 040°. On outcrop scale, however, the gneissic foliation shows a much greater complexity.

The calc-silicate layers within the JWZ have been boudinaged and isoclinally folded. Two types of boudins can be distinguished:

- a) Single-layer boudins (Pyroxene boudins), in which a layer has undergone boudinaging, which are flanked on either side by the kyanite-graphite gneiss. The boudins mainly display lenticular geometries that gradually taper off towards their terminations.
- b) Mantled boudins (Hydrothermal boudins), which have been discussed previously (p10).

The tanzanite mineralization occurs in stress minimum zones such as quartz veins and pockets. These pockets occur in specific structural sites within and adjacent to boudins. Four main types of tanzanite-bearing structures can be distinguished:

- a) Type 1: Irregularly shaped to roundish pockets in central parts of boudins (Fig.7)
- b) Type 2: Wedge-shaped masses at the lateral terminations of boudins corresponding to strain-shadow positions of boudin necks (Fig.8 a-c)
- c) Type 3: Veins that transect boudins along shear fractures (Fig.8 a, c, d)
- d) Type 4: Tension fractures in the central parts or close to the lateral terminations of boudins (Fig.8d)

### **3.10. Trench Geology and Pedology**

Fig.9 is a map of a trench that was excavated perpendicularly to strike over the JWZ (Fig.6) and adjacent lithologies. The purpose thereof is to test whether geochemical anomalies and trends can be identified for the tanzanite deposit, of its host rocks or for rocks associated with the deposits by two different geochemical exploration methods. The strike of the trench is roughly NW-SE.

The trench is 128.10m long and is divided into eight soil zones, distinguished mainly on the basis of colour. The changes of soil colour around the tanzanite deposit could be locally significant in tanzanite exploration. The Merelani soil in general can be described as something between an aridisol and a molisol, based on the definitions given by Foth (1984). An aridisol would be a typical desert soil covered by desert shrubs which later give way to grasses as the moisture increases. Mollisols generally border desert regions and support grasses which produce abundant organic matter. They generally display a high soil fertility with fair to adequate rainfall. Each soil zone overlays one or more of the Lower Horizon lithologies (Table 2; Fig.9). These zones are labeled Zone 1 to Zone 8.

Foth (1984) gives the following definitions for A-, B- and C-Horizons:

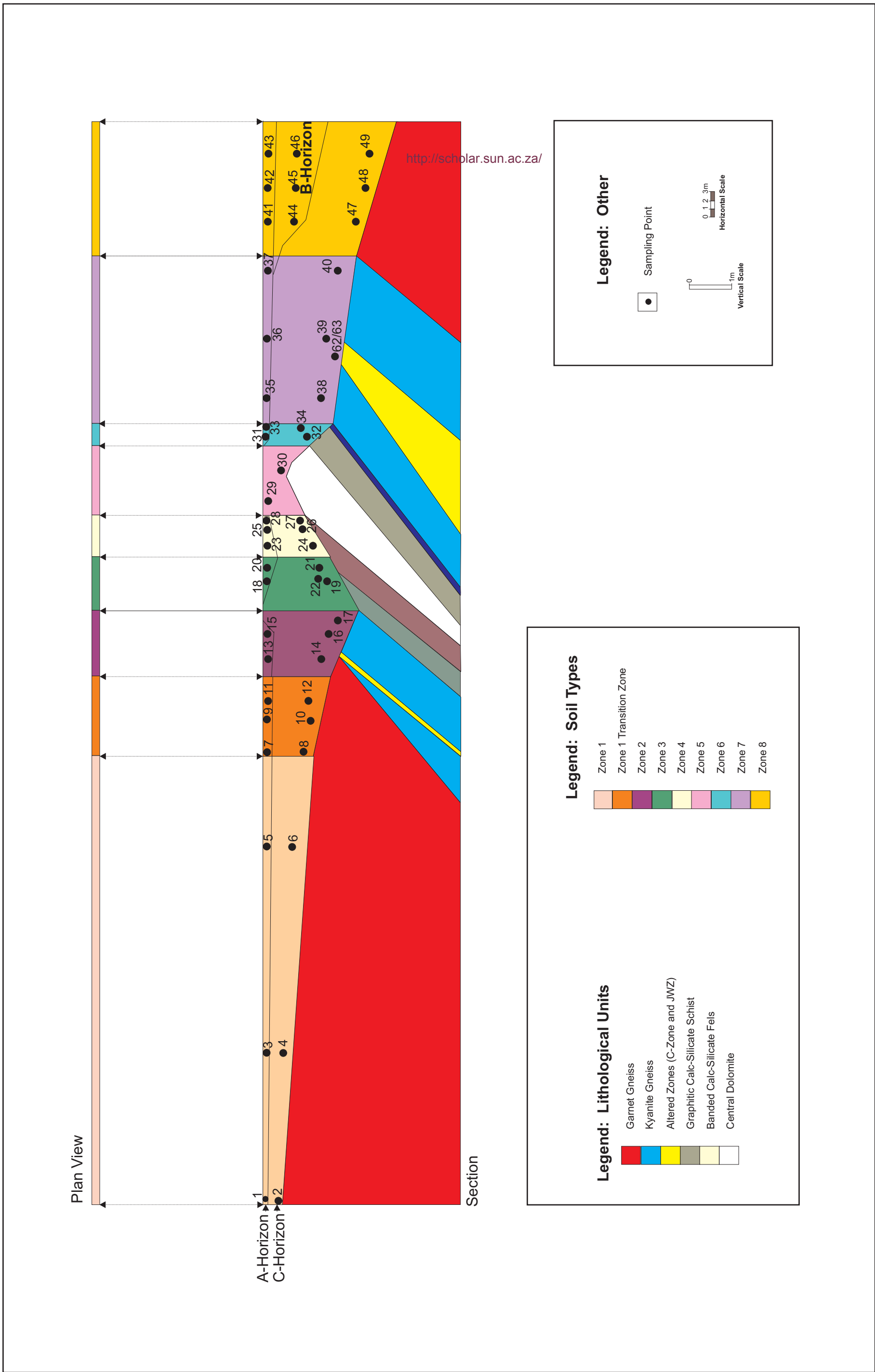


Fig.9 Map of the Merelani trench from which the soil samples were sampled (Trench position shown on Fig.6)

<b>Table.2 Table of lithologies represented by soil type</b>	
<b>Soil Type</b>	<b>Represented Lithologies</b>
Type 1	<ul style="list-style-type: none"><li>• Central Garnet-Biotite Gneiss (Dip: 55°NW)</li></ul>
Type 2	<ul style="list-style-type: none"><li>• Kyanite-Graphite Gneiss (Dip: 50°NW to 40°NW)</li><li>• C-Zone (Dip: 40°NW)</li></ul>
Type 3	<ul style="list-style-type: none"><li>• Graphite-Calc-Silicate Fels (Dip: 40°NW)</li><li>• Calc-Silicate Schist (Dip: 40°NW)</li></ul>
Type 4	<ul style="list-style-type: none"><li>• Calc-Silicate Schist (Dip: 40NW)°</li></ul>
Type 5	<ul style="list-style-type: none"><li>• Dolomitic Marble (Dip: 50°NW)</li></ul>
Type 6	<ul style="list-style-type: none"><li>• Calc-Silicate Schist (Dip: 52°NW)</li><li>• Graphite-Calc-Silicate Fels (Dip: 50°NW)</li></ul>
Type 7	<ul style="list-style-type: none"><li>• Kyanite-Graphite Gneiss (Dip: 55°NW)</li><li>• JWZ-Zone (Dip 50°NW to 40°NW)</li></ul>
Type 8	<ul style="list-style-type: none"><li>• Garnet-Biotite Gneiss (Dip: 41°NW)</li></ul>

- A: *This horizon is the first to form. It contains a high proportion of finely divided organic matter and is consequently dark in colour.*
- B: *Illuvial or residual concentration of silicate clays, sesquioxides, humus, etc., and/or development of structure if volume changes accompany changes in moisture content.*
- C: *This layer may be considered to be similar to the original appearance of the solum where there are obviously no geological nonconformities.*

Bridges (1997) corroborates these definitions with the following:

- A: *A mineral horizon formed at or near the surface, characterised by the incorporation of humified organic matter intimately associated with mineral materials.*
- B: *A subsurface mineral horizon resulting from the change in situ of soil material or the washing in of material from overlying horizons.*
- C: *An unconsolidated or weakly consolidated mineral horizon which retains evidence of rock structure and lacks the properties diagnostic of the overlying A or B horizons.*

Based on these definitions as well as comments by Hall (1998), the Merelani trench soils are divided into an A-Horizon and a C-Horizon. Only one soil zone, Zone 8, displays a B-Horizon between its A- and C-Horizons. It seems to consist of mostly transported material (Fig.10 and Fig.17), inferred from rounded grains which are slightly larger than those of the typical A-Horizons of the other soil zones in the trench. In general the soils in the trench are sand-rich. They grade from bedrock to what can best be described as a dry saprolith, due to the fact that the original lithologic textures and banding are preserved, but the material is unconsolidated, in the lower C-Horizon to a mixture of soil grains and lithic fragments in the upper C-Horizon and finally to an A-Horizon containing only soil grains.

- Zone 1:** This soil zone has a width in the trench of 52.9m (as measured from the top of the trench, i.e. as measured from the top of the hill towards the road at the bottom) (Fig.10). The colour of Zone 1 ranges from darkish red to red. A 9.5m wide "Transition Zone" (Zone 1 TZ), occurring adjacent to Zone 1, was distinguished on the basis of a





Fig. 10a



Fig. 10b

Fig.10 Photo showing the Merelani trench looking East,i.e. downhill towards the road, (a) and looking west, i.e. uphill towards the top of the trench (b). Notice how the soil colour changes from the one end to the other.

slightly browner tinge to the red colour and can be termed reddish brown (Fig.11). The A-Horizon has a thickness of 10cm while that of the C-Horizon is 30cm.

- Zone 2:* This is a greyish dark brown to light brown soil zone with red and orange patches and is 7.9m in width (measured along the strike of the trench from the end of Zone 1 and the beginning of Zone 3) (Fig.12). Here the A-Horizon reaches a thickness of 6cm, before tapering out towards the contact with Zone 3. The C-Horizon has an average thickness of 1.8m.
- Zone 3:* This soil zone is 6.4m in width and ranges in colour from a dark brown upper horizon (A-Horizon) to a dark, bluish grey lower horizon (C-Horizon) (Fig.13). The C-Horizon is mottled with patches of grey and dark purple. The A-Horizon is 15cm thick and the C-Horizon 1.6m.
- Zone 4:* The colour of this soil zone ranges from a dark brown A-Horizon to a lighter brown to light brown C-Horizon. The soil zone is distinctly lighter in colour than Zone 3 and is 5m in width (Fig.14). The A-Horizon has a thickness of 25cm and the C-Horizon a thickness of 1.45m.
- Zone 5:* This 8.2m wide soil zone is slightly lighter in colour than Zone 4 with its A-Horizon still darker brown than the C-Horizon. This zone is poorly developed over the dolomitic marble and the start of the formation of a calcrete layer can be discerned. An A-Horizon is completely absent from this soil zone. The C-Horizon has an average thickness of 1.2m.
- Zone 6:* This soil zone is 2.7m in width and has much the same colour scheme as Zone 5, although the C-Horizon is distinctly different due to the difference in terms of colour and the original rock textures and banding which have been preserved. The C-Horizon of this soil zone is light brown to light orange with a dark brown A-Horizon (Fig.15). The A-Horizon is 30cm and the C-Horizon 1.52m thick.

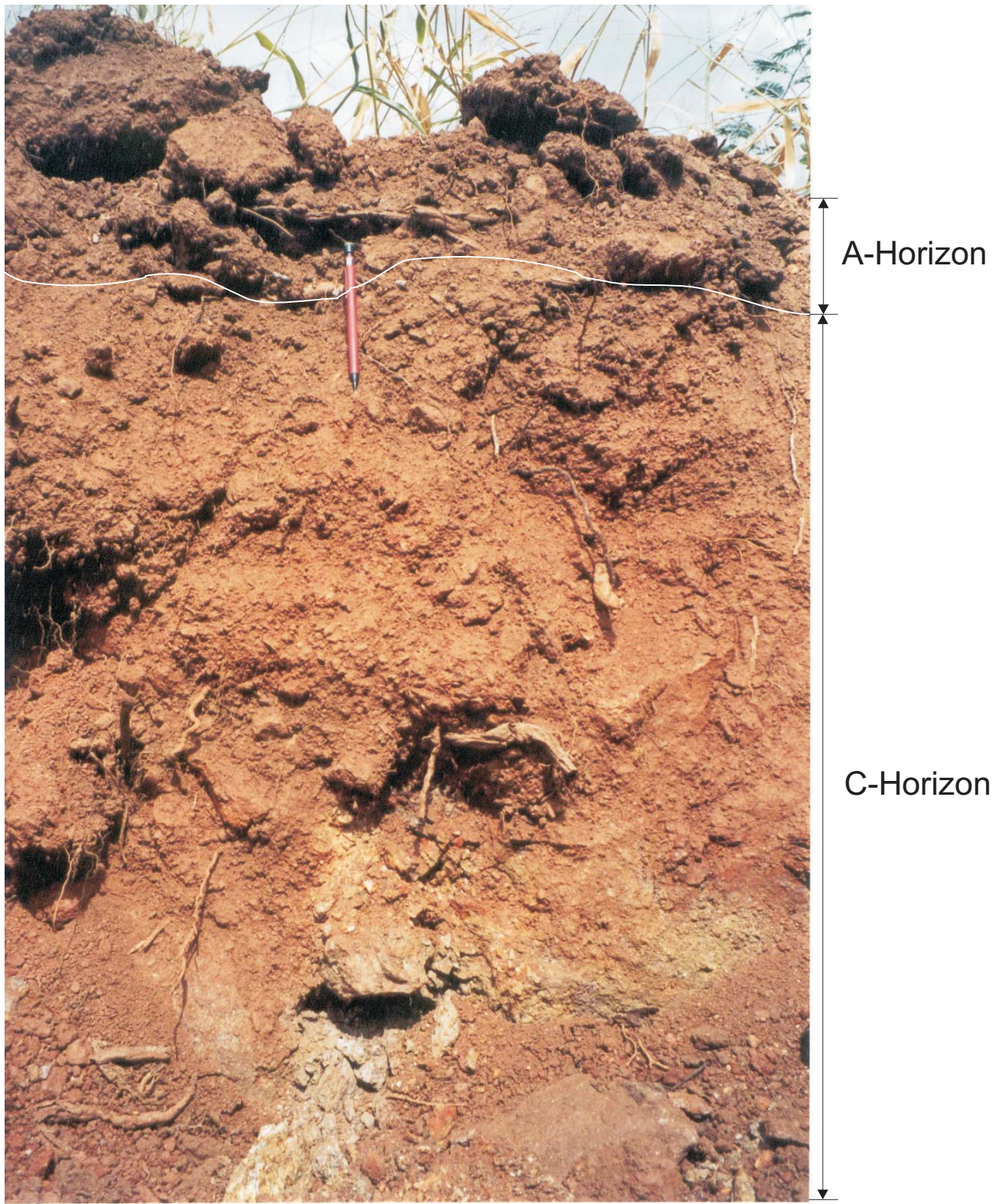


Fig.11 Type 1 Soil. Notice pen for scale (150mm).

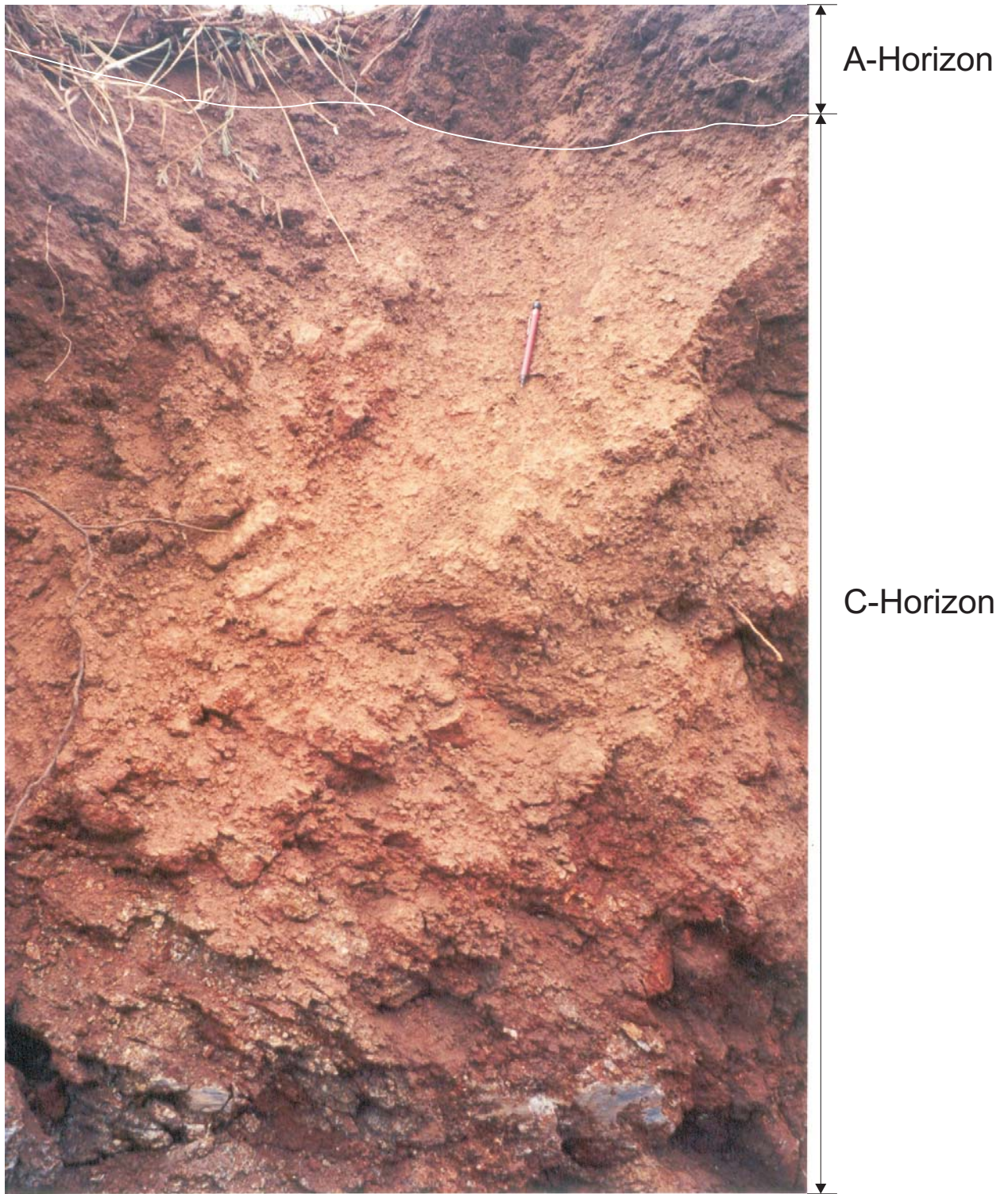


Fig.12 Soil Type 2.



Fig.13 Type 3 Soil.

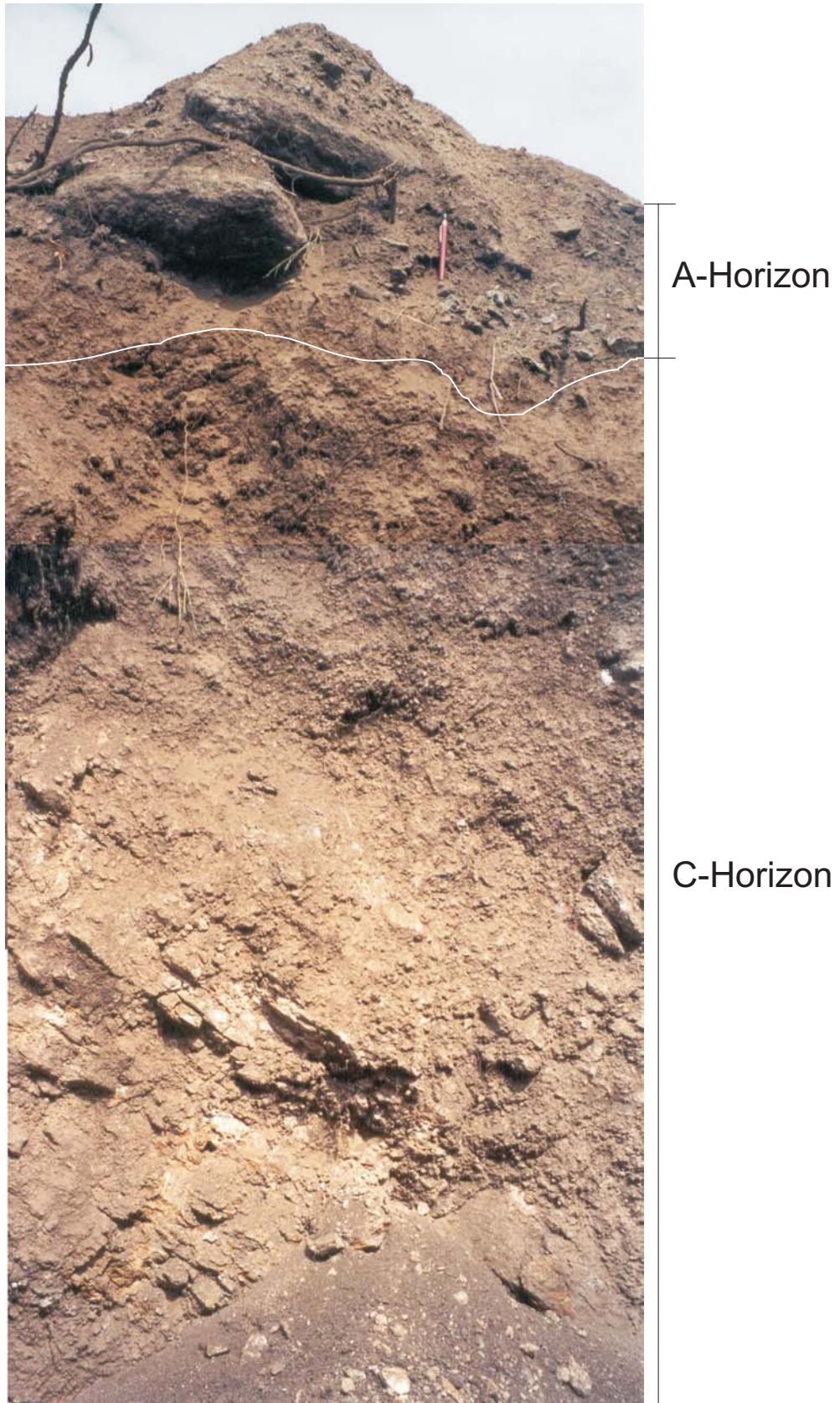


Fig.14 Soil Type 4.

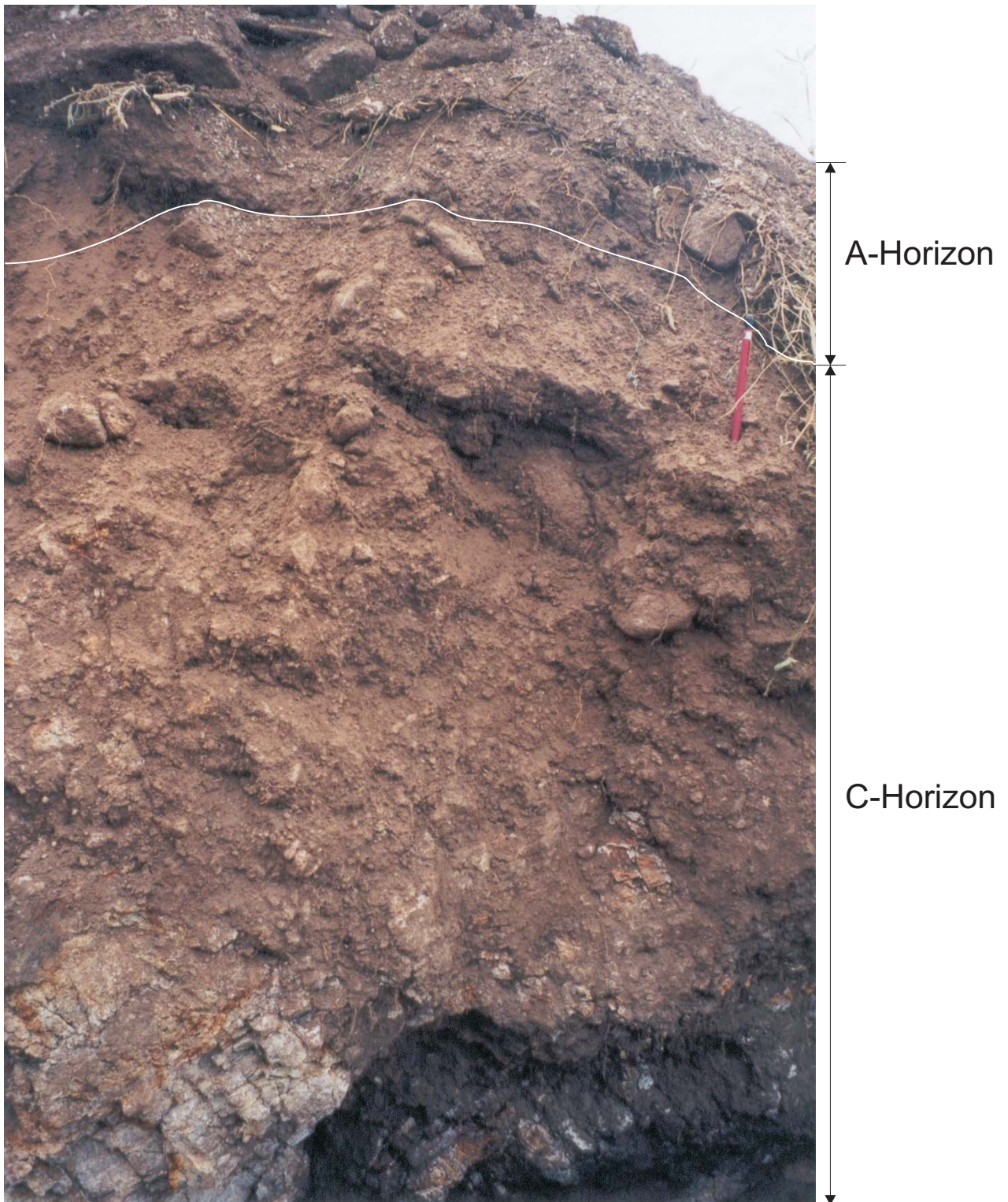


Fig.15 Soil Type 6.

*Zone 7:* The colour of the A-Horizon of this soil zone is almost identical to that of Zone 6. The colour of the C-Horizon, however, is distinctly different, being dark bluish grey to brownish grey (Fig.16). This soil zone is 19.9m in width. The A-Horizon has a thickness of 25cm and the C-Horizon of 60cm. Two additional samples of the C-Horizon were taken from the zone just above the JWZ zone. The soil zone which the additional samples represents is termed Zone-JWZ.

*Zone 8:* This soil zone starts with a dark brown A-Horizon, followed by a lighter brown B-Horizon and a light brown C-Horizon. The zone is 15.6m in width and it can be seen from Fig.9 that it reaches quite a great depth (>3m) relative to the other soil zones. The B-horizon consists of coarser material and it is thought, due to the slope downwards from the top of the road towards the south and from the top of the hill where the trench is situated towards the east, that this coarser material represents transported material rather than it being formed *situ* (Fig.17). The A-Horizon has a thickness of 20cm, the B-Horizon of 57cm and a C-Horizon of 2.43m.

The Merelani soil in general, as observed in the trench, is an immature soil. It is situated on a hill which has a slope dipping between  $\sim 5^\circ$  towards the east at the foot of the hill and  $\sim 15^\circ$  in the same direction at its steepest nearer the top. The soil zones developed over the various Lower Horizon lithologies range in total thickness from 30cm at the top of the hill to 3.2m at the foot.



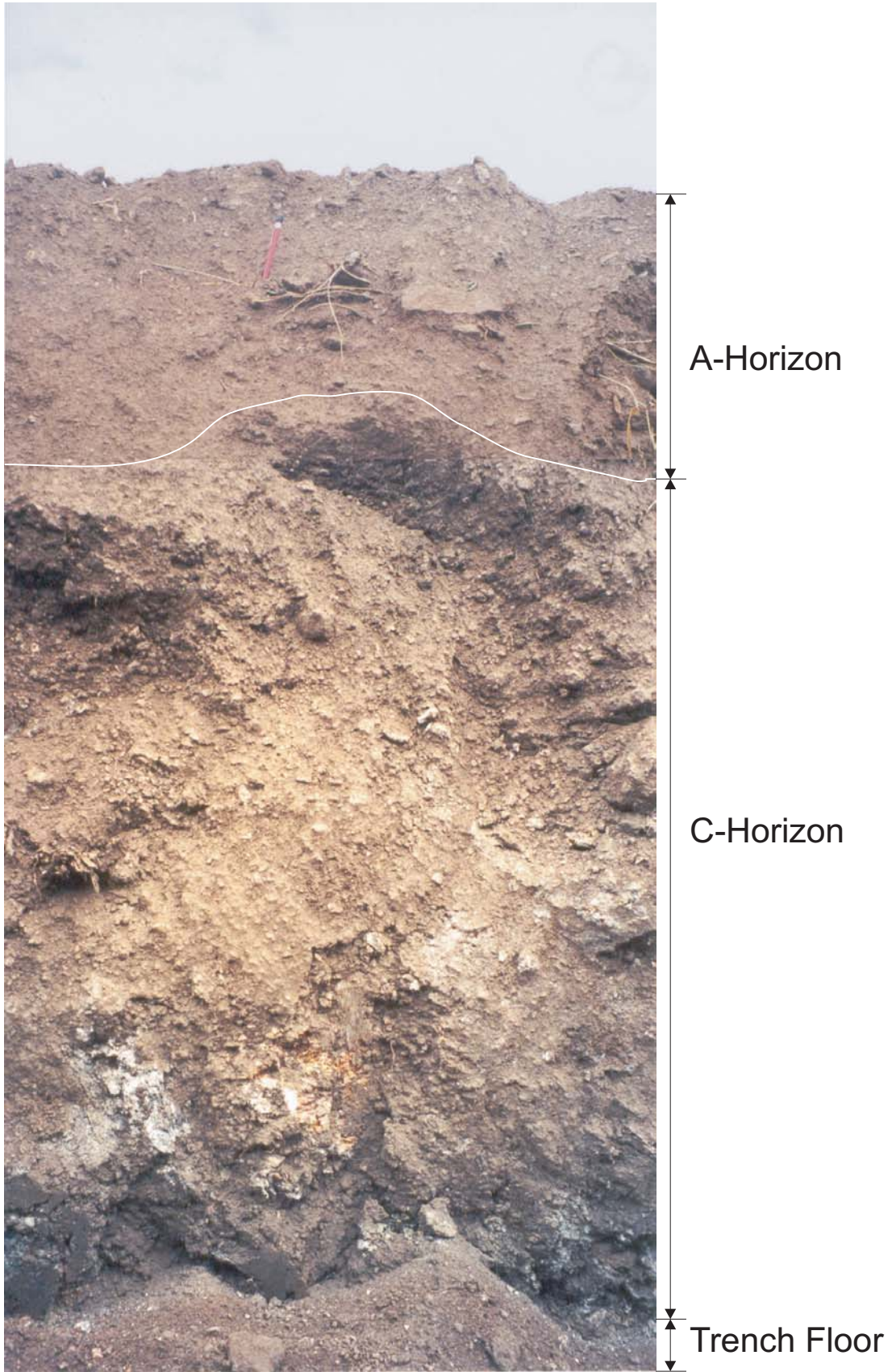


Fig.16 Soil Type 7.

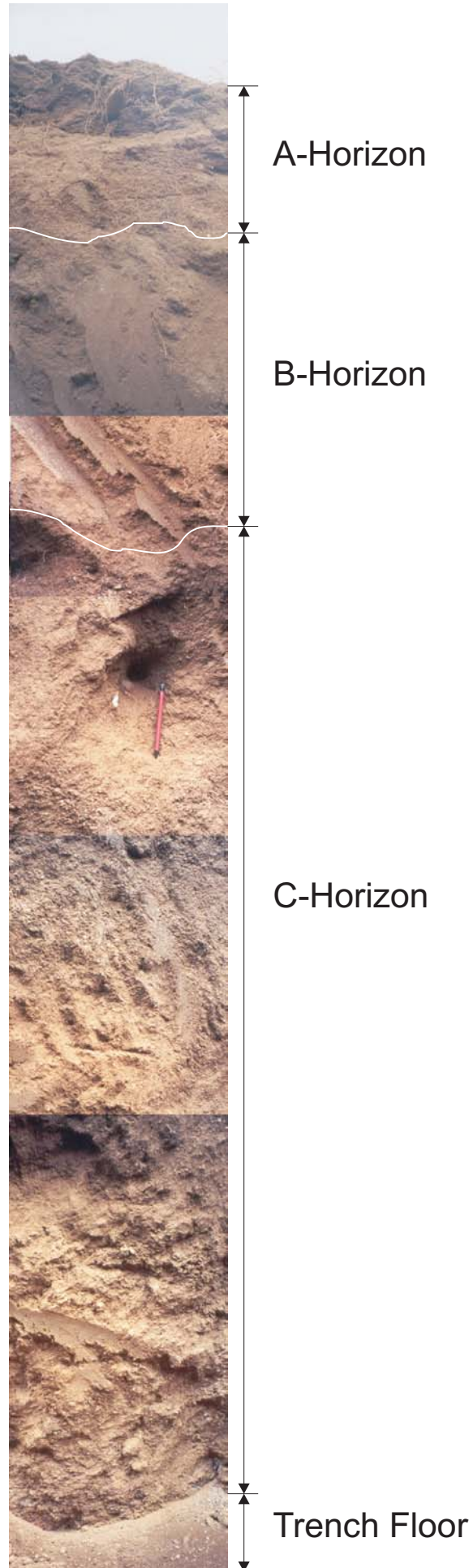


Fig.17 Soil Type 8.

## **4. Sampling and Analytical Techniques**

In order to identify whether such a unique geochemical signature exists and can be identified, various types of sample media (soil, stream sediments and calcrete) were collected and analysed. The various sample media were subjected to different analytical techniques in order to identify whether a geochemical signature exists and with what specific exploration method, if any, it can be identified. XRF whole-rock analysis was done to ascertain total chemical content of various soil and stream sediment size fractions and ICP-AE analyses were performed on the leachate of a partial extraction technique. The samples were all analysed for their trace element content, as it are these elements which act as the chromophoric elements in gemstones.

### **4.1 Soil Samples**

Soil samples were collected from a trench dug perpendicular to strike over the tanzanite mineralised as well as the barren lithologies of the Lower Horizon lithologic package (Chapter 2; Fig.9). Two to three samples of each soil horizon were collected, depending on the width of the soil profile in the trench. The purpose of the current study is to test whether geochemical exploration techniques can be used to indicate either tanzanite mineralisation or the lithologies in which the mineralisation occurs or any lithologies closely related to the tanzanite deposits. A single trench was dug for this purpose. Therefore the results of the study will have to be tested by the mining company in a comprehensive orientation study.

The Merelani trench soil zones were studied with a specific focus on soil trace-element geochemistry in order to discern which soil horizon produces optimum results in terms of anomaly-background contrast. Orientation studies are designed to glean such information from the geochemical data and apply it in an exploration program. With the eye on such future studies, if such information already available, the cost of a comprehensive orientation study will be significantly reduced. Elements concentrate in different soil environments to different degrees and it is therefore important to sample the correct soil horizon. The focus should therefore be to find the maximum anomaly-background contrast of a specific indicator element and not necessarily its maximum concentration. It is also imperative that a constant soil horizon is sampled as opposed

to a constant sampling depth due to the undulating nature of soil horizon contacts. These aspects were kept in mind in the collection of the soil samples for this study.

The Merelani soil surrounding the tanzanite deposit and which is represented in the trench was subdivided into eight soil zones, based mainly on the different C-horizons, which represent the underlying parent lithologies in the trench in terms of observed layering, lithological structure and colour quite well (Fig.11 – Fig.17). The only soil zone to contain a B-horizon is Zone 8 (Fig.17).

Samples were numbered according to the soil horizon and zone from which they were collected and the sequence in which they were collected. An example is the first sample, 01-A-001, which indicates that the sample was collected from soil zone 1, from the A-Horizon and that it is the first sample which was collected. The ca. 5kg samples were placed in plastic bags and stored in a dry freight container at the mine offices.

The 63 samples were oven dried at 50°C and subsequently sieved into three fractions: coarse (300-180µm), medium (180-90µm) and fine (<90µm). The coarse and medium fractions were milled in a tungsten mill for the XRF sample preparation. Powder briquettes were made of all three fractions for XRF trace element analysis. The XRF analyses were done on a Philips 1404 Wavelength Dispersive X-ray spectrometer at the University of Stellenbosch, South Africa. The spectrometer is fitted with a Rh tube, six analyzing crystals, namely LIF200, LIF220, LIF420, PE, TLAP and PX1. The detectors are a gas-flow proportional counter, a scintillation detector or a combination of the two. The gas-flow proportional counter uses P10 gas, which is a mixture of argon (90%) and methane (10%). The standards that were used for calibration purposes are shown in Table 3.

A 5g sample was weighed for the fine and medium fractions and leached with 50ml 1M HCl overnight (12 hours) and the mixture filtered the next morning according to the method suggested by Fletcher et al. (1987). The residue was discarded and the filtrate analysed by ICP-AE. The specific purpose for employing this method was to determine the concentration of the readily extractable (i.e. leachable) metals (cxMe) in order to resolve the question whether the elements of interest are present in the soil in leacheable form, or whether they are concentrated in mineral grains. The procedure replicates the mobilisation of trace elements by natural soil solutions in a much shorter

<b>Sample Name</b>	<b>Description</b>
AGV-1	Andesite from USGS
BHVO-1	Basalt from USGS
JG-1	Granodiorite from GSJ
JB-1	Granodiorite from GSJ
GSP-1	Granodiorite from USGS
SY-2	Syenite from CCRMP
SY-3	Syenite from CCRMP
STM-1	Syenite from USGS
NIM-G	Granite from MINTEK
NIM-S	Syenite from MINTEK
NIM-N	Norite from MINTEK
NIM-P	Pyroxeneite from MINTEK
NIM-D	Dunite from MINTEK
BCR	Basalt from USGS
GA	Granite from CRPG
GH	Granite from CRPG
DRN	Diorite from ANRT
BR	Basalt from CRPG

Abbreviations used:

- ANRT: Association Nationale de la Recherche Technique, Paris  
CCRMP: Canadian certified Reference Materials Project  
CRPG: Centre de Recherches Petrographiques et Geochimiques  
MINTEK: Council for Mineral Technology, South Africa  
GSJ: Geological Survey of Japan  
NIM: National Institute of Metallurgy, South Africa  
USGS: United States Geological Survey, Reston

timeframe. The ICP-AE analyses were done on a Varian Liberty II radial ICP with a 40MHz air cooled RF generator at the University of Stellenbosch. The samples were injected via an inert V-groove nebulizer into an inert Sturman masters double pass cyclonic action spray chamber. The torch is a standard single piece quartz torch. The conditions of operation are as follows: The nebulizer pressure was 185kPa, with the plasma power at 1.1kW. The argon flow rate was 15.0l.min<sup>-1</sup> for the plasma and 1.5l.min<sup>-1</sup> for the auxiliary. The pump rate was 15rpm, the integration time 3s and 4 replicates were done. The detection limits for the analysed elements are shown in Table 4.

<b>Element</b>	<b>Wavelength</b>	<b>LOD (mg.l<sup>-1</sup>)</b>
V	311.071	0.03
Cr	267.716	0.005
Ni	231.604	0.03
Cu	324.754	<0.006
U	367.007	0.3
Fe	259.940	<0.002
Mn	260.569	<0.002
Mg	279.553	<0.002

## **4.2 Stream Sediments**

Stream sediments were collected from an exploration concession. The concession was chosen on the basis of the presence of a few gemstone mines in the area, the presence of large streams and a variation in geology. No lithologic data exists for any lithologies outside the mining properties. Therefore the proximity of anomalous stream sediment samples to existing operating and abandoned tsavorite mines were used to evaluate the presence anomalous stream sediment samples. Tsavorite and tanzanite are paragenetic in the tanzanite deposits. The assumption is that the tsavorite deposit geology will be very similar to that of the tanzanite deposits (containing at least metasomatically altered layers which may be boudinaged and folded). This assumption is thought to be valid on the basis of the tsavorite deposits being found in the same regional structure, the Lelatema anticlinal structure and will be substantiated if the anomalies are similar to anomalies found in the soil samples collected from the trench.

One 2kg sample was taken every ca. 200m as suggested by Rose (Rose et al., 1979) with the distance measurements made via GPS (Fig.18). First and second order streams were sampled. The 46 samples were placed into plastic bags and stored at base camp till the stream sediment sampling program was completed. The samples were dried at 50°C and sieved into three fractions: coarse (600-180µm), medium (180-90µm) and fine (<90µm). The medium and fine fractions were analysed via XRF for their trace element content (Fig.19). The coarse fraction was to be submitted for heavy mineral separation, but due to severe time constraints this was never completed.

### **4.3 Calcrete Samples**

According to Anand et al. (1997) calcretes can concentrate elements during their formation. This application is often used in gold exploration (Anand et al; 1997). In order to determine whether the Merelani calcretes concentrate elements, four samples were collected from the natural wall of an old mine shaft, which was sunk by local miners. This shaft is situated directly above the tanzanite-mineralised JW-zone. The benefit of being able to use the calcretes in an exploration program lies in the fact that the Merelani calcretes are widespread and could be easily and therefore cheaply sampled.

The calcrete samples were analysed via XRF for their trace element content.

### **4.4 Precision**

Samples were randomly selected from the soil and stream sediment samples and duplicated. Each of these duplicates was analysed 5 times and the precision calculated according to the formula (Fletcher et al., 1987):

$$P_c(\%) = 200.S_c/c$$

where  $P_c$  is the analytical precision for concentration  $c$  as the percent relative variation at the 95% (two standard deviations) confidence level and  $S_c$  an estimate of the standard deviation at concentration  $c$ .

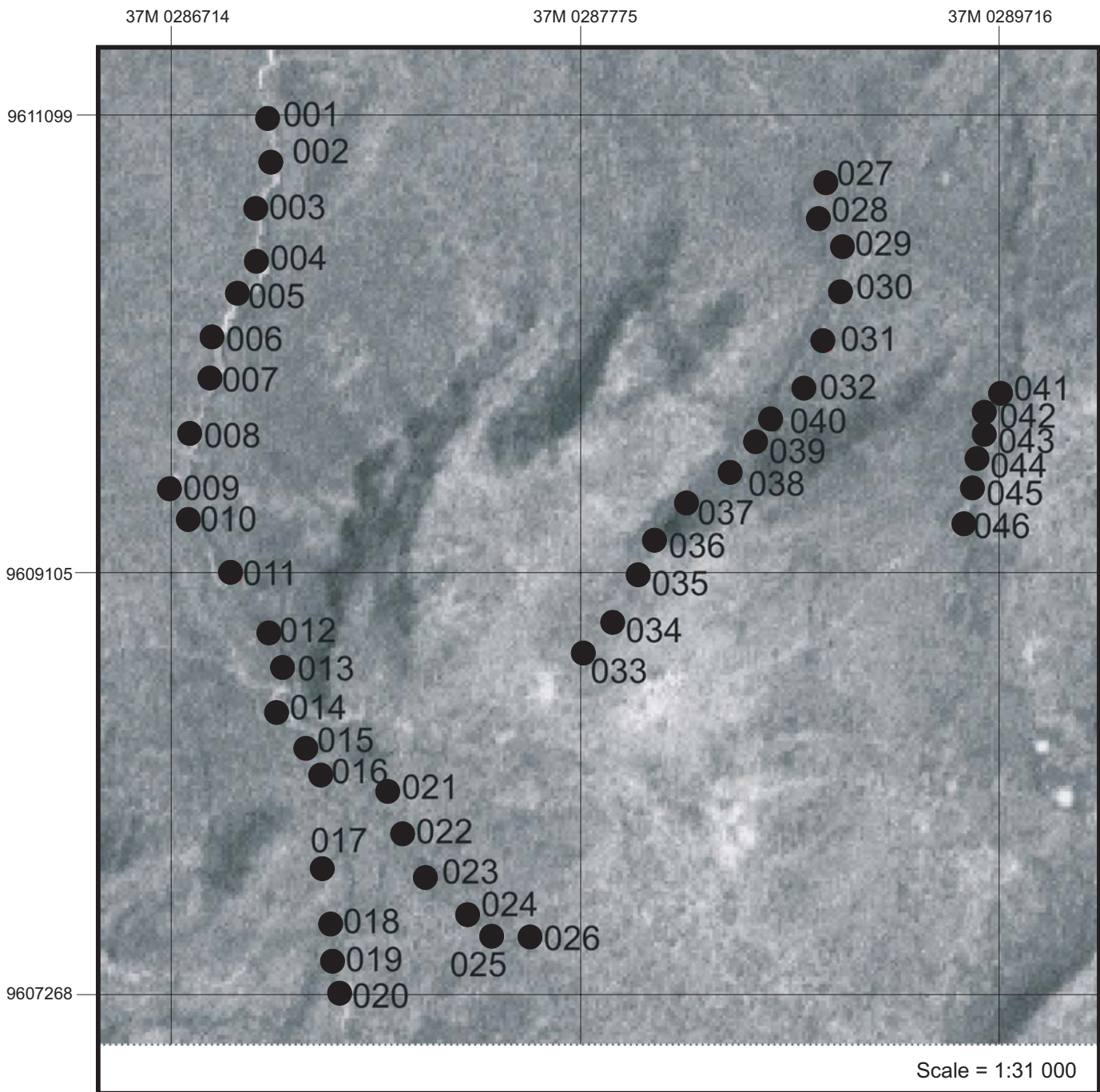


Fig.18 Satellite image of Stream Sediment Sampling Sites (coordinates in UTM/UPS and the Cape Datum was used). This image is an enlargement of Block A in Fig.1



## Flow Chart of Sample Collection and Preparation

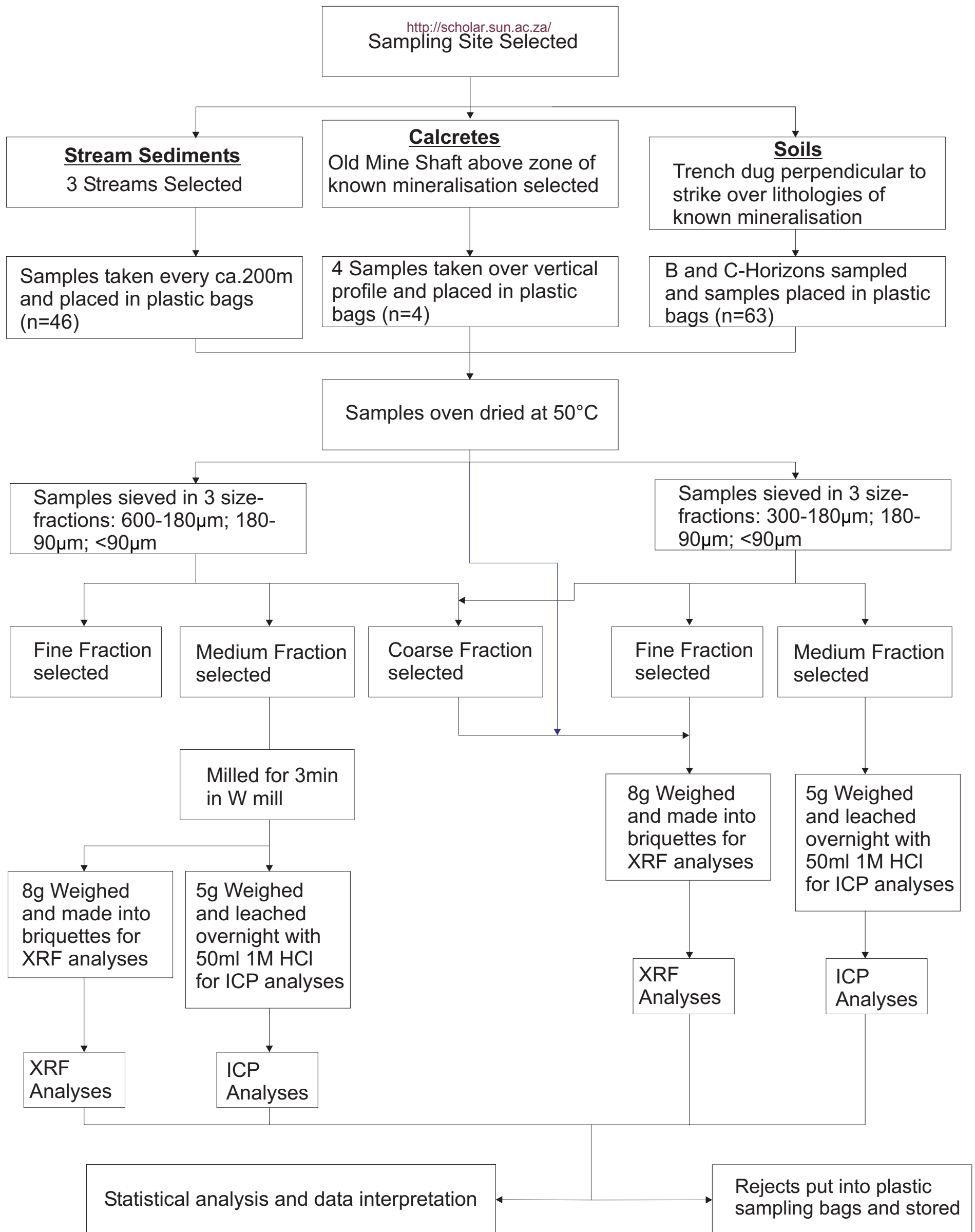


Fig.19 Flow chart of sample preparation and analytical methods employed

The results are given in Table 5.

Any precision below 15% is deemed acceptable (Fletcher et al., 1987) Although many of the trace elements show individual values above 15%, most of the data falls within the 15% acceptable limit. The exceptions are Ga, La, Pb, Th and U, which all show constant precision values above 15%. The reason for this is that these elements occur in concentrations close or below the XRF detection limits. On this basis these elements were not used in this study in the evaluation of techniques for geochemical exploration of tanzanite. They are shown in this thesis on the various diagrams, but this is only to observe trends in heavier elements. They were not considered in the final conclusions drawn from the overburden data.

Table 6 shows the XRF detection limits. Any data within 2ppm of any of the detection limits was not used in this study. Very few of the data points of the elements of interest are below the detection limits.

**Table 5 Summary of precision calculations of XRF analyses (all values in %)**

Sample Type	V	Cr	Co	Ni	Cu	Zn	Ga	Rb	Sr	Y	Zr	Nb	Ba	La	Ce	Nd	Pb	Th	U	
Stream Sediment Fine Fraction	SS-005a	5	10	3	11	13	9	27	12	4	5	4	8	17	3	10	80	33	168	
	SS-005b	6	12	3	13	10	15	23	9	3	8	3	8	12	5	4	85	31	119	
	SS-011a	5	10	4	9	38	4	9	6	4	9	4	8	7	33	4	39	83	56	
	SS-011b	9	12	4	10	34	6	25	6	4	4	4	6	7	31	6	69	13	114	
	SS-038a	5	5	3	20	18	8	26	3	3	7	4	4	7	18	6	9	79	25	14
	SS-038b	6	4	3	16	11	9	22	9	2	11	3	5	3	8	4	5	71	41	114
	SS-041a	6	5	0	8	32	12	18	8	4	8	4	8	8	24	7	12	38	22	299
	SS-041b	7	6	5	13	46	4	29	7	4	11	4	5	6	43	6	14	87	65	202
Stream Sediment Medium Fraction	SS-004a	2	4	0	28	6	14	13	8	2	1	3	3	19	4	7	74	14	111	
	SS-004b	5	7	3	21	5	12	21	20	0	6	1	2	24	5	10	35	39	82	
	SS-009a	7	6	0	21	183	5	33	6	2	9	3	4	34	7	22	78	21	63	
	SS-009b	8	12	0	14	481	16	16	11	2	6	3	4	56	10	15	83	27	88	
	SS-017a	6	5	3	26	6	10	17	10	1	4	2	4	6	23	2	7	43	28	56
	SS-017b	4	8	0	13	9	7	10	15	4	5	2	2	2	16	4	8	69	22	119
	SS-032a	3	9	2	26	5	14	24	20	1	2	2	1	4	5	2	59	11	34	
	SS-032b	4	6	0	22	5	12	23	16	2	2	2	2	9	9	2	39	16	46	
Soil Fine Fraction	01-C-012a	4	3	2	6	12	5	13	4	5	9	5	8	24	28	15	148	124	146	
	01-C-012b	5	1	2	7	9	5	18	5	3	8	3	12	9	17	10	52	48	217	
	03-C-021a	3	2	5	2	9	6	25	12	2	6	4	17	7	37	14	8	64	72	122
	03-C-021b	2	1	5	2	6	1	45	3	1	3	2	14	2	70	5	18	76	31	75
	06-C-032a	4	1	0	5	13	5	16	3	3	10	7	33	4	65	9	13	48	46	310
	06-C-032b	7	2	0	6	14	3	14	10	5	9	7	24	4	91	6	15	33	33	101
	07-C-040a	3	2	6	3	11	3	24	6	2	6	2	7	2	85	25	25	51	54	56
	07-C-040b	4	1	5	5	16	3	14	13	3	6	4	20	5	86	11	12	156	97	278
	08-B-044a	3	1	3	4	9	1	15	6	3	5	3	6	2	25	6	13	64	36	42
	08-B-044b	3	1	2	5	7	4	23	4	3	13	2	7	2	16	8	6	82	63	64
	01-B-050a	5	2	2	16	8	4	32	2	2	8	3	7	9	44	7	10	68	46	347
	01-B-050b	5	2	2	10	10	13	8	6	3	12	3	8	7	22	6	13	132	52	194
	08-A-060a	3	3	3	5	6	7	10	2	3	7	2	8	3	39	4	10	45	69	68
	08-A-060b	4	3	4	11	12	5	22	7	3	6	3	11	3	39	7	6	21	53	24

<b>Table 6a XRF major element detection limits</b>	
<b>Major element</b>	<b>Detection limit (Oxide wt%)</b>
Al <sub>2</sub> O <sub>3</sub>	0.20
CaO	0.01
Cr <sub>2</sub> O <sub>3</sub>	0.01
Fe <sub>2</sub> O <sub>3</sub>	0.06
K <sub>2</sub> O	0.05
MgO	0.04
MnO	0.01
Na <sub>2</sub> O	0.03
P <sub>2</sub> O <sub>5</sub>	0.01
SiO <sub>2</sub>	0.50
TiO <sub>2</sub>	0.02

<b>Table 6b XRF trace element detection limits</b>	
<b>Trace element</b>	<b>Detection limit (ppm)</b>
V	8
Cr	8
Co	1
Ni	9
Cu	1
Zn	8
Ga	3
Rb	5
Sr	4
Y	5
Zr	4
Nb	5
Ba	20
La	5
Ce	5
Nd	5
Pb	7
Th	11
U	6

## **5. Analysis of Soil XRF and ICP and Published XRF Data**

### **5.1. Introduction**

In this chapter, the data from the XRF and ICP trace element analyses of soil samples taken from the trench over Lower Horizon Merelani lithologies are evaluated and discussed. The soil samples are evaluated relative to the XRF analyses of samples of the lithological units from the Lower Horizon taken by Olivier (2006). The Lower Horizon lithological data from Olivier is derived from borehole core samples. The borehole positions are shown in Fig.6.

The chapter consists of two main sections:

1. geochemical soil characterisation and graphical data description and;
2. the study of correlation coefficients to discern probable mineralogic hosts for the various trace elements.

The first section of this chapter starts off with a lithologic characterisation. The lithologies were normalised to the Bulk Continental Crust (BCC) values of Taylor and McLennan (1995). The Merelani lithologies are comprised of various gneisses and schists and are interpreted as being of crustal origin (Maboko, 1995; Maboko 2000, Maboko and Nakamura, 1995; Maboko and Nakamura 2002). However, no genetic interpretations are made from the BCC normalised data, which serves only as a mutual reference between the Merelani lithologies and their derived soils.

### **5.2. Additional Samples**

In order to establish whether an external reference frame exists relative to which the trench geochemical data can be compared, additional surface soil samples were collected from A-horizon of the soil adjacent to the Merelani trench. Significant soil disturbance occurs in the area due to the presence of abandoned small scale mines. For this reason not all the soil zones could be sampled (Fig.20).

Data from the coarse, medium and fine fractions of each additional sample representing the different soil zones were compared to the data from the trench. The

# Map of Additional Sampling Points

<http://scholar.sun.ac.za/>

**Legend**

- Type 1
- Type 1 Transition Zone
- Type 2
- Type 3
- Type 4
- Type 5
- Type 6
- Type 7
- Type 8
- Old Mining Shafts
- Sampling Points

**Horizontal Legend**

0 1 2 3m

**Vertical Scale**

0 1 2 3m



● 50/51

● 52/53

● 54/55

● 56/57

● 58/59



● 60/61

Fig.20 Plan view of the trench, additional sampling points and old mine shafts

additional samples were collected 15 – 20m from the trench. The horizontal extent of each soil zone was determined by extrapolation of the width of the soil in the trench 20m to each side. Each additional sample could then be correlated with the correct soil zone in the trench. The additional samples were analysed by XRF and were compared to trench XRF data.

Statistical data limits were calculated by using the average and standard error values of each element for the various soil size fractions. The upper and lower limit are represented by the sum and difference of the average value for each element from each soil size fraction and the standard error respectively. Twice the standard deviation was used in calculating the standard error, thereby providing a 95% probability that a data point will fall within the statistical limits. The results are contained within Table 7.

Table 7 shows that data from Zone 1, Zone 1 TZ and Zone 2 for the fine and medium fraction correlate well with only a few data points occurring outside the data ranges for the fine and medium fractions. Zones 3 and 4 consistently show values which occur outside the data ranges. The coarse fraction data contains many data points which occur outside the data ranges. Only the data from Zone 8 shows good correlation between the additional sample and the trench samples. The coarser the fraction, the more data points in total occur outside the data ranges. This is taken as a first indication that at least the A-horizons of the different soil zones in the area surrounding the trench are disturbed and only show a slight correlation with relatively undisturbed soil from the trench. It is also indicative that if any geochemical anomalies are identified, they would have to occur within the C-horizon, as it is most probably the least disturbed horizon.

### **5.3. Merelani Lithology and Trench Soil Characterisation and Data Description**

The XRF results of the soil samples from the trench as well as the Merelani Lower Horizon litho-geochemical data were normalised to Bulk Continental Crust (BCC) values (Taylor and McLennan, 1995), rendering them comparable. This method was used on a study of the lower Amazon river by Vital and Statterger (2000). The results were subsequently plotted as spider diagrams (Fig.21 and Fig.23). To avoid clutter on the graphs, the average values were plotted together with the sum and difference of the

**Table 7a Comparison of the fine fraction trace element concentration between additional samples collected adjacent to the trench and trench samples**

		V	Cr	Ni	Cu	Zn	Ga	Rb	Sr	Y	Zr	Nb	Ba	La	Ce	Nd	Pb	Th	U
Zone 1	Average	477	901	91	43	208	26	90	267	46	928	41	700	60	126	57	3	11	3
	Std Error	29	22	23	55	38	2	2	25	1	151	2	65	6	26	11	0	2	0
	01-A-050	469	894	85	11	217	24	100	257	48	744	40	714	64	130	63	3	12	6
Zone 1 TZ	Average	595	833	213	69	355	25	83	282	51	787	40	740	59	119	58	3	11	6
	Std Error	109	44	128	16	163	2	4	22	8	121	6	40	10	25	15	0	2	3
	01-A-052	519	962	107	75	206	26	86	265	41	1016	44	740	58	129	61	3	13	7
Zone 2	Average	740	802	197	86	327	25	72	299	49	646	41	886	66	128	62	3	9	5
	Std Error	397	50	116	68	122	1	16	19	10	89	1	334	13	23	11	0	7	5
	02-A-054	828	882	173	73	264	29	72	328	55	783	44	1076	71	144	76	3	14	6
Zone 3	Average	1660	706	639	6	1160	14	40	416	58	427	27	1113	39	83	54	2	10	9
	Std Error	20	61	22	0	300	3	2	68	16	93	3	77	1	7	2	0	1	2
	03-B-056	858	868	164	29	253	28	71	332	58	807	45	1124	77	170	73	3	14	8
Zone 4	Average	1039	708	372	51	587	22	63	349	60	560	41	1124	63	117	63	5	12	8
	Std Error	153	67	108	48	152	6	4	38	8	127	6	11	12	24	11	3	5	4
	04-B-058	764	934	254	60	339	26	77	296	61	1129	47	876	76	179	93	3	18	9
Zone 8	Average	737	742	223	40	368	25	65	290	49	670	47	1002	63	122	57	2	14	8
	Std Error	153	46	67	38	113	1	5	14	6	61	6	46	5	10	7	0	0	2
	08-A-060	642	776	191	33	317	24	67	266	45	606	48	970	64	124	60	9	13	5

**Table 7b Comparison of the medium fraction trace element concentration between additional samples collected adjacent to the trench and trench samples**

		V	Cr	Ni	Cu	Zn	Ga	Rb	Sr	Y	Zr	Nb	Ba	La	Ce	Nd	Pb	Th	U
Zone 1	Average	299	201	61	60	133	30	75	221	37	343	40	526	147	300	125	11	41	10
	Std Error	19	12	2	7	16	1	9	12	4	99	2	60	20	51	25	2	10	7
	01-A-050	283	209	64	60	132	29	79	217	32	250	39	501	97	202	82	8	31	9
Zone 1 TZ	Average	405	200	141	63	259	29	76	241	39	362	39	672	107	227	86	12	29	12
	Std Error	119	10	95	8	147	6	10	24	8	77	2	164	27	47	20	4	7	3
	01-A-052	329	288	54	62	133	35	71	219	32	354	39	602	135	288	112	12	30	11
Zone 2	Average	538	192	130	57	235	28	71	261	40	272	39	942	94	221	78	11	29	11
	Std Error	387	1	89	9	138	6	1	54	14	71	5	650	32	61	13	2	0	2
	02-A-054	540	192	101	58	157	27	65	277	39	315	38	1212	82	233	80	10	25	11
Zone 3	Average	1248	190	428	52	930	17	46	346	46	222	26	1138	62	155	56	12	26	15
	Std Error	83	23	27	2	227	1	6	48	9	70	3	135	2	12	9	4	1	4
	03-A-056	552	202	94	59	162	30	64	275	40	289	37	1274	112	231	79	11	25	9
Zone 4	Average	644	168	201	53	349	23	68	266	44	195	36	1154	74	178	57	15	24	12
	Std Error	168	11	74	6	130	1	8	39	9	22	6	167	26	48	25	7	8	2
	04-A-058	435	202	125	58	191	28	60	224	42	254	42	814	146	302	123	4	42	12
Zone 8	Average	387	163	105	55	192	23	61	216	33	249	38	1059	67	172	58	11	24	9
	Std Error	13	18	2	2	6	5	5	9	3	64	2	37	13	1	2	4	5	4
	08-A-060	465	184	136	62	241	24	70	247	35	321	46	1112	88	196	58	5	21	9

**Table 7c Comparison of the coarse fraction trace element concentration between additional samples collected adjacent to the trench and trench samples**

		V	Cr	Ni	Cu	Zn	Ga	Rb	Sr	Y	Zr	Nb	Ba	La	Ce	Nd	Pb	Th	U
Zone 1	Average	268	242	24	10	146	35	59	200	43	285	29	2	135	291	117	14	52	5
	Std Error	6	10	2	1	22	4	7	10	3	21	1	3	23	35	20	1	8	5
	01-A-050	273	190	44	19	335	26	94	240	31	174	16	234	32	116	37	5	47	1
Zone 1 TZ	Average	348	224	48	10	255	33	59	222	46	285	26	61	98	206	80	18	48	5
	Std Error	91	9	25	6	115	5	5	28	7	29	1	115	21	28	10	8	4	2
	01-A-052	294	267	71	7	228	32	108	160	40	262	23	87	106	226	98	20	44	5
Zone 2	Average	476	214	50	8	263	30	57	241	46	276	26	264	80	197	74	12	45	1
	Std Error	329	26	31	0	135	7	2	47	10	29	4	536	26	32	5	1	2	1
	02-A-054	302	257	25	15	145	37	59	195	44	306	29	221	103	307	124	15	52	8
Zone 3	Average	1054	165	147	2	939	17	38	320	50	193	14	446	48	136	62	13	27	8
	Std Error	44	11	2	1	294	9	5	32	8	71	4	156	21	34	8	6	5	1
	03-A-056	426	229	59	12	260	30	51	215	52	323	31	518	126	319	128	19	55	3
Zone 4	Average	496	165	65	3	340	23	58	228	48	197	23	464	49	120	51	15	33	5
	Std Error	125	17	21	3	106	5	6	40	6	5	4	185	7	12	4	3	4	4
	04-A-058	470	220	71	6	308	31	53	219	50	290	27	622	124	240	95	5	47	5
Zone 8	Average	412	173	45	5	210	22	46	202	39	204	23	727	59	84	41	16	33	6
	Std Error	211	18	19	2	40	5	6	48	1	6	5	257	17	21	6	4	10	6
	08-A-060	309	192	35	5	186	25	47	175	38	205	27	635	54	116	54	21	36	7



average and standard error, thus defining a data range for each element. The average and standard error values were calculated separately for each individual soil zone as well as for each soil horizon. Twice the standard deviation was used in the calculation of the standard error, thus implying a 95% probability that a given value will fall within the calculated data ranges.

The trace element pattern defined by the spider diagrams will be used as a geochemical signature for the lithological units.

### ***5.3.1. Lithology Characterisation***

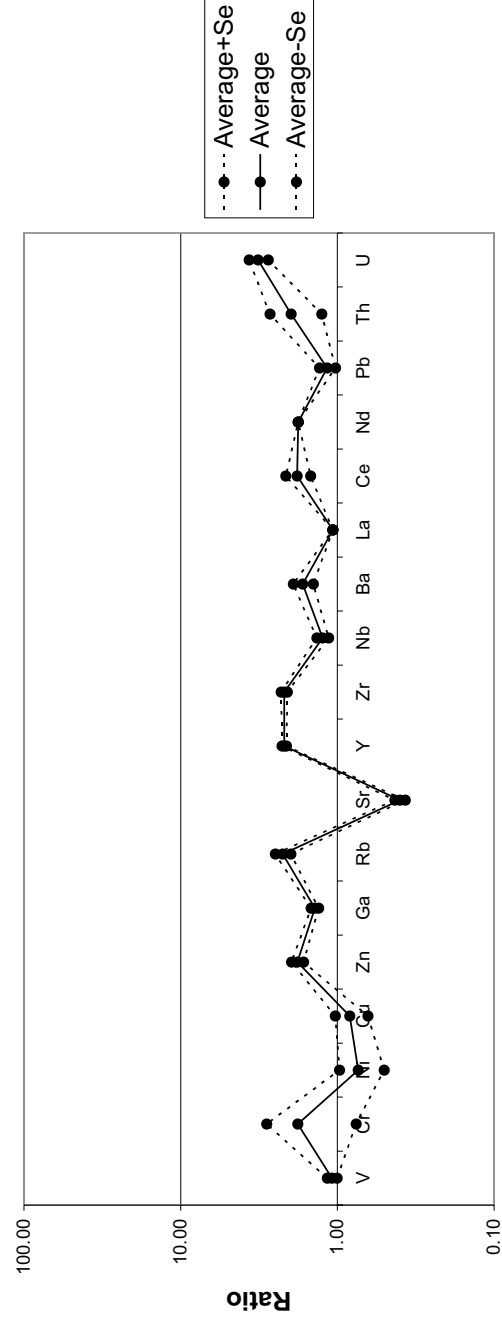
The results of the BCC normalised Merelani lithological units are presented in Fig.21. Most of the lithological units contain statistically significant elevated concentrations of Zn, Ba, Pb, Th and U relative to BCC. The only exception is the Central Dolomite, which only has an elevated relative concentration of Th and U. The latter relative concentration is by far the most pronounced in all the Merelani Lower Horizon lithologies. Most of the lithologies contain elevated relative concentrations of V and Ni. Exceptions are the garnet gneiss and banded calc-silicate fels units as well as the Central Dolomite.

In addition, except for corresponding lithological units such as the Kyanite Gneiss LK3 and LK4 units and the C-Zone sandwiched between them, each lithology has its own unique pattern. Also the patterns for corresponding lithological units on either side of the Central Dolomite, such as the Banded Calc-Silicate Fels 1 and 2 units, are practically identical. Folding in the Merelani Lower Horizon lithologies is well documented from the tanzanite mining and evidence was found that suggests that folding exists on a local scale in the rocks underlying the trench (Fig.22). The trace element patterns of the Merelani lithological units (Fig.21) also show that duplication of the stratigraphic succession around the Central Dolomite is a distinct possibility.

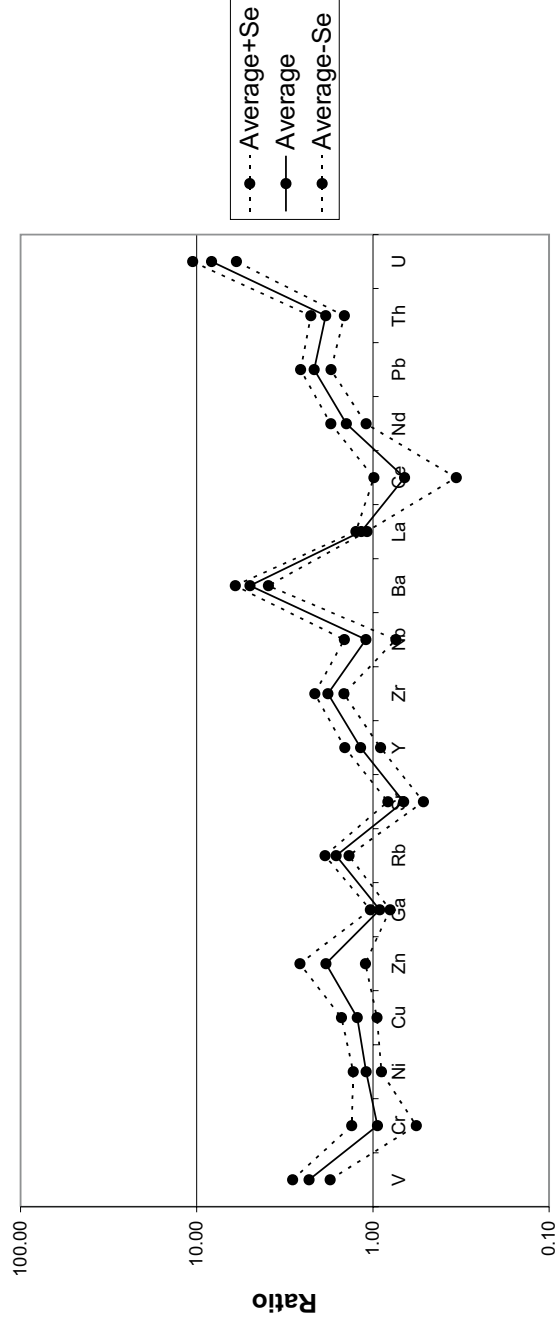
### ***5.3.2. Soil Characterisation***

The XRF trace element data for each individual soil zone and soil horizon and normalised to BCC is presented in Fig.23.

### Spider Diagram of Trace Element Concentrations of the Garnet Gneiss 1 Lithological Unit Normalised to Bulk Continental Crust

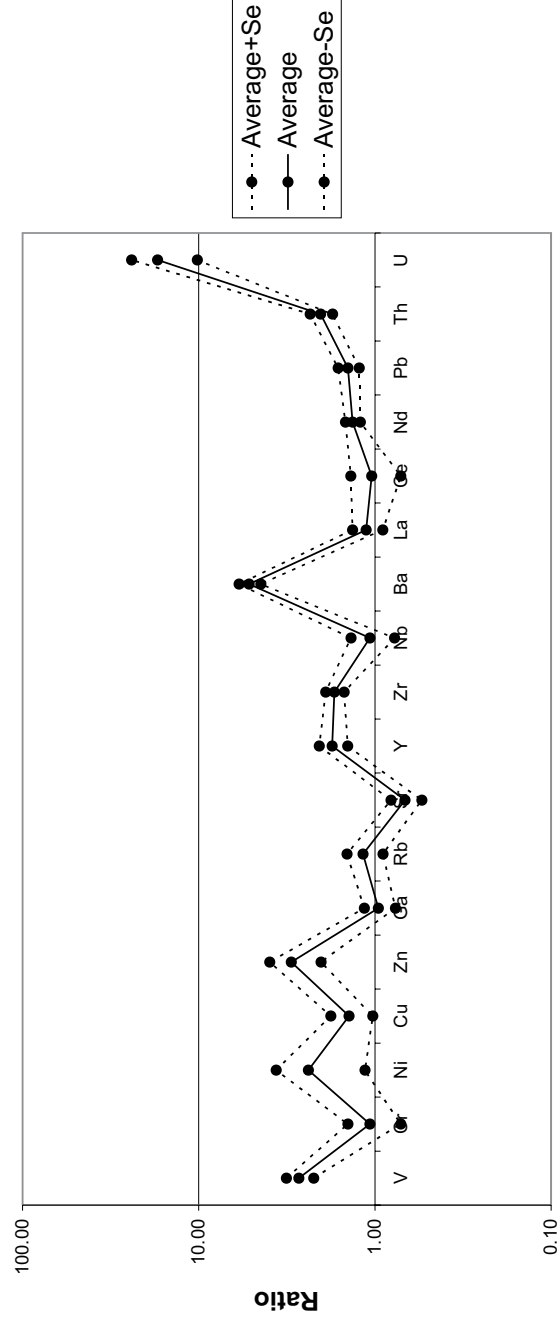


### Spider Diagram of Trace Element Concentrations of the Kyanite 4 Lithological Unit Normalised to Bulk Continental Crust



<http://scholar.sun.ac.za/>

### Spider Diagram of Trace Element Concentrations of the C-Zone Lithological Unit Normalised to Bulk Continental Crust



### Spider Diagram of the Trace Element Concentrations of the Kyanite 3 Lithological Unit Normalised to Bulk Continental Crust

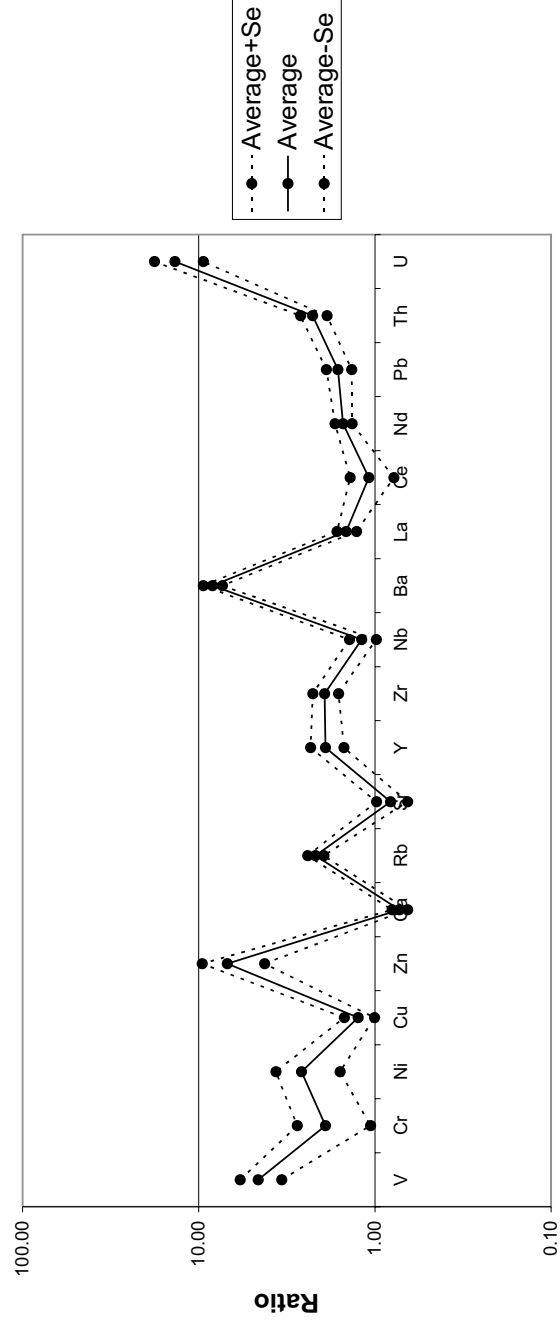
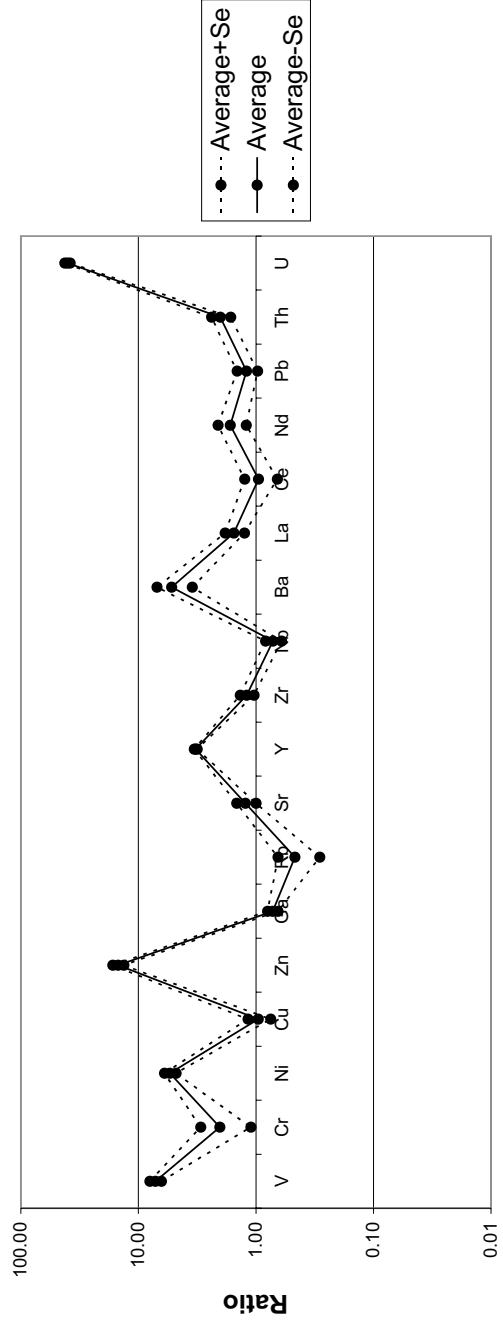
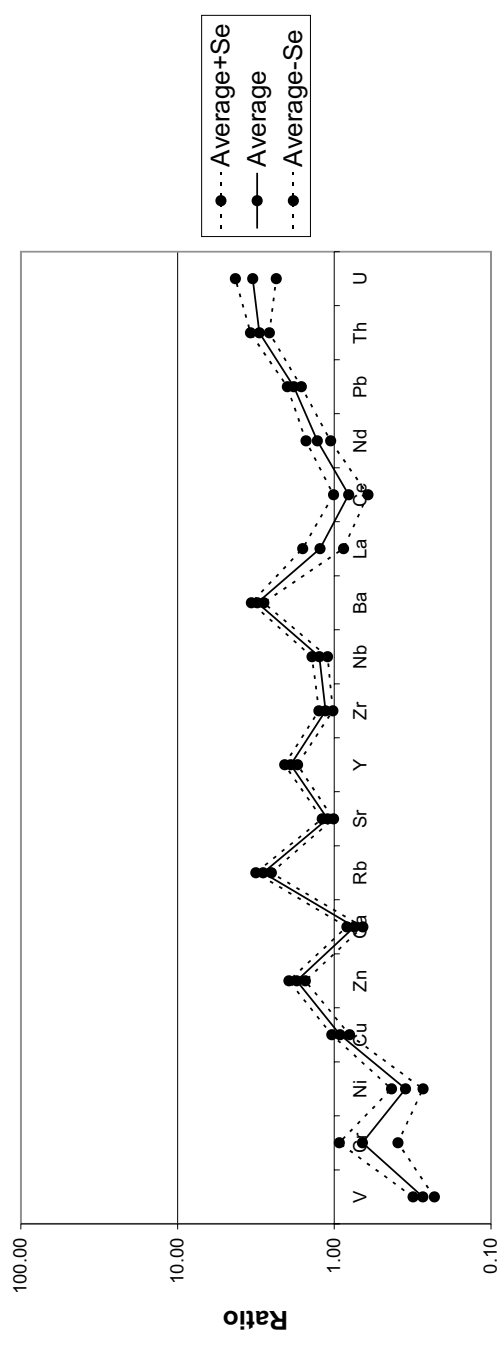


Fig.21 Spider diagrams of the Merehani lithological units normalised to bulk continental crust

**Spider Diagram of the Trace Element Concentrations of the Graphitic Calc-Silicate Schist 2 Lithological Unit Normalised to Bulk Continental Crust**

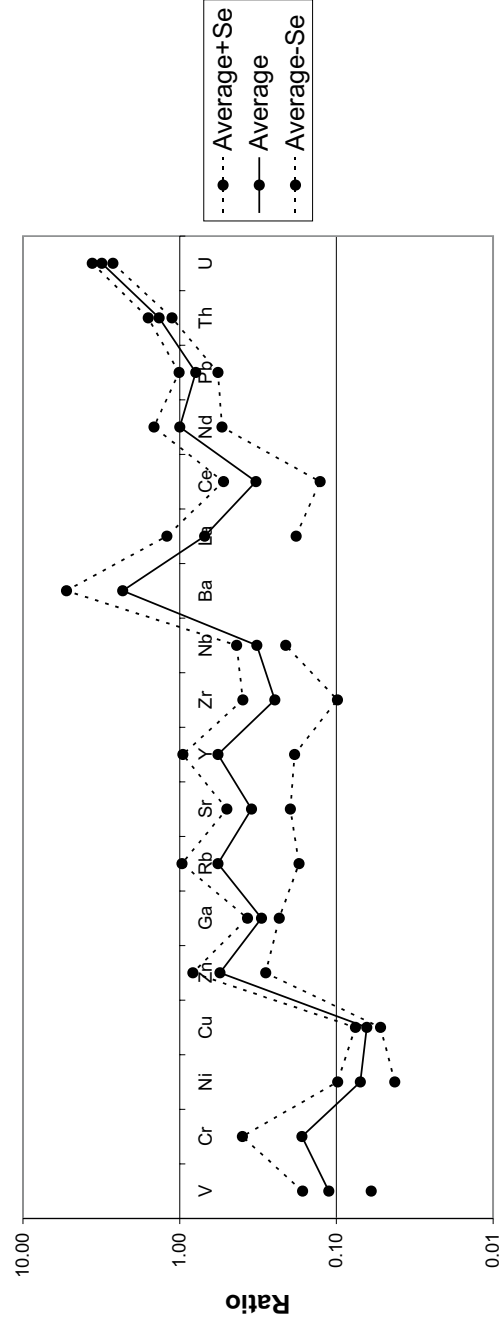


**Spider Diagram of the Trace Element Concentrations of the Banded Calc-Silicate Fels 2 Lithological Unit Normalised to Bulk Continental Crust**

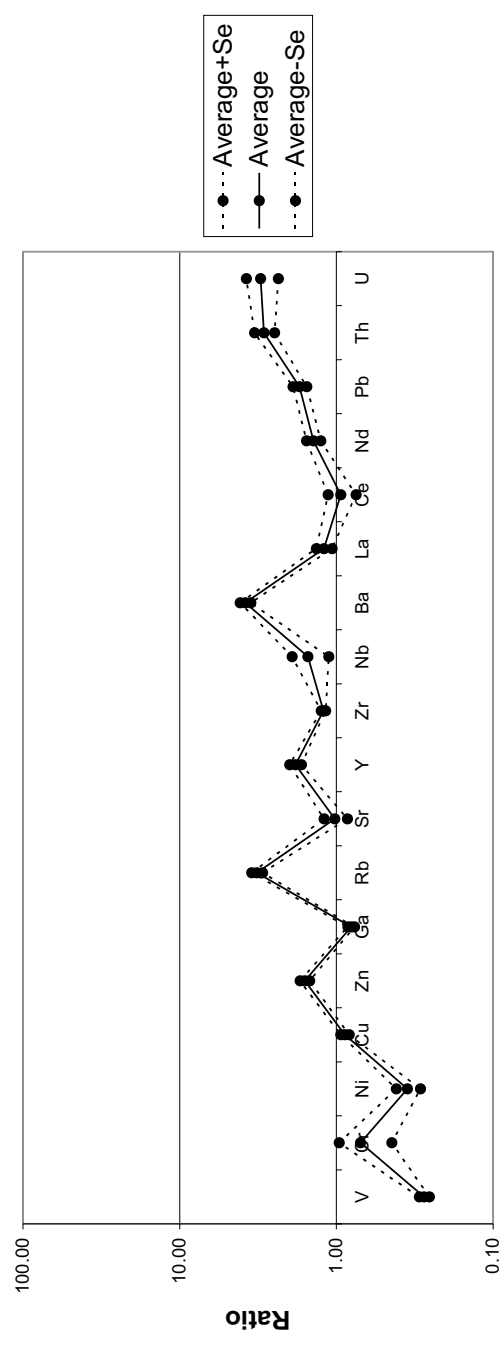


<http://scholar.sun.ac.za/>

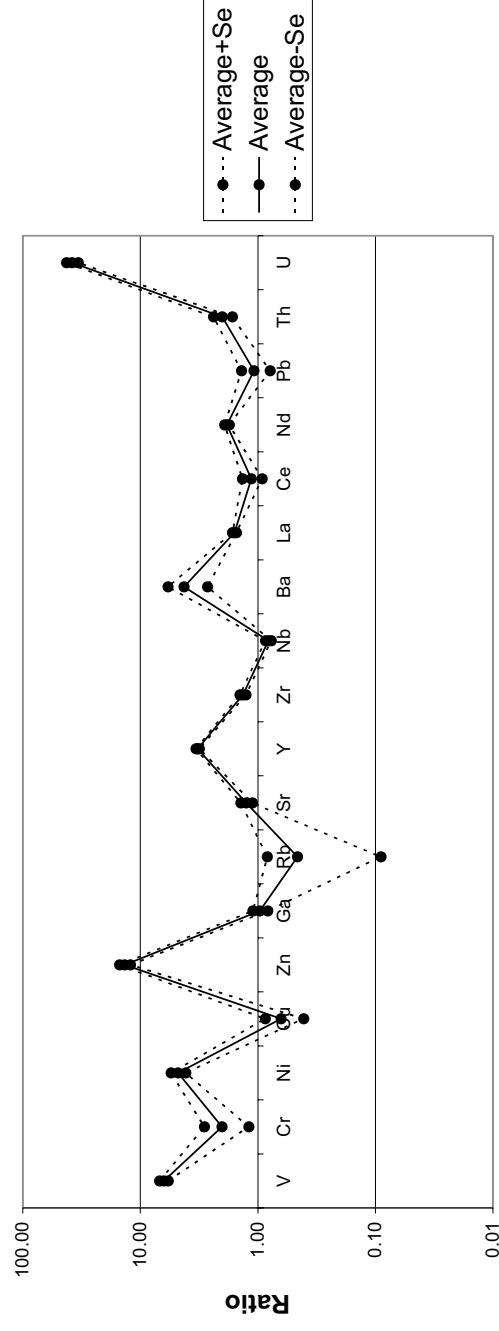
**Spider Diagram of the Trace Element Concentrations of the Central Dolomite Lithological Unit Normalised to Bulk Continental Crust**



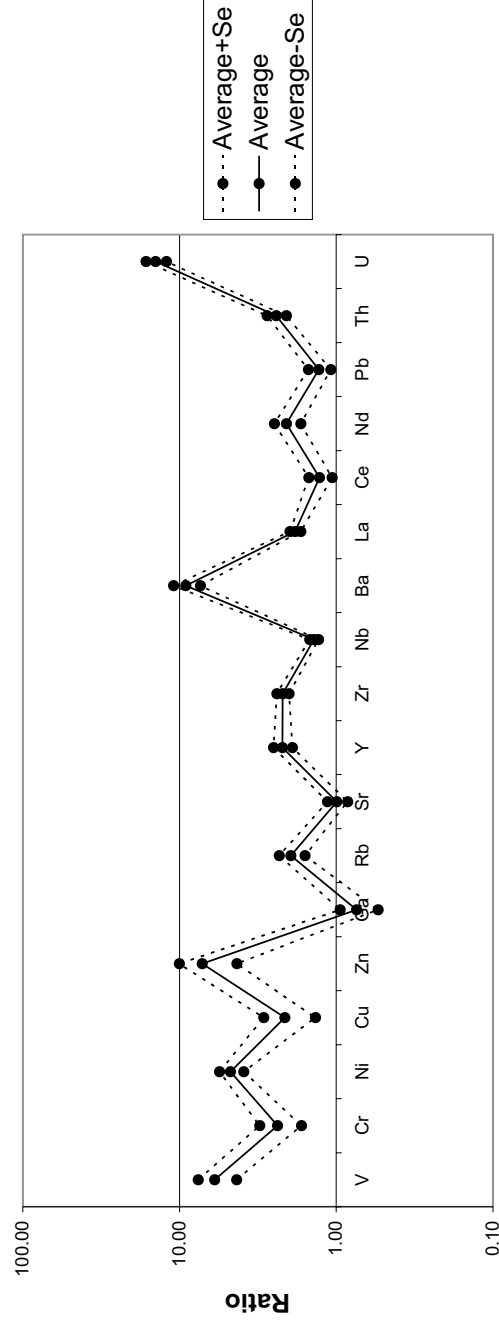
**Spider Diagram of the Trace Element Concentrations of the Banded Calc-Silicate Fels 1 Lithological Unit Normalised to Bulk Continental Crust**



**Spider Diagram of the Trace Element Concentrations of the Graphitic Calc-Silicate Schist 1 Lithological Unit Normalised to Bulk Continental Crust**

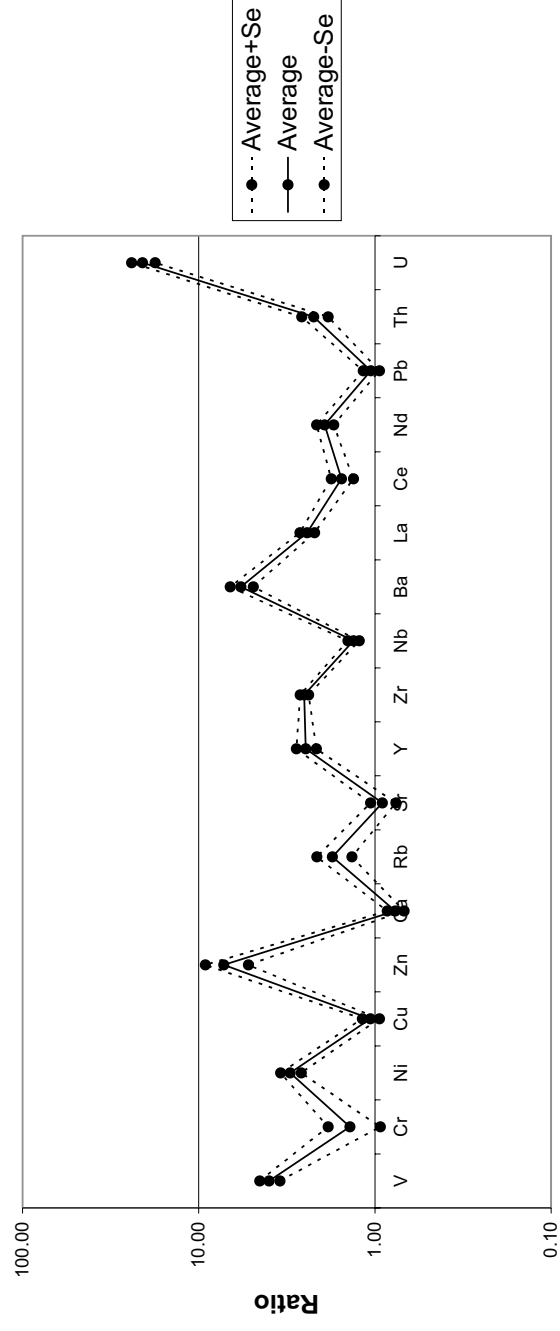


**Spider Diagram of the Trace Element Concentrations of the Kyanite Gneiss LK2 Lithological Unit Normalised to Bulk Continental Crust**



<http://scholar.sun.ac.za/>

**Spider Diagram of the Trace Element Concentrations of the JWZ Lithological Unit Normalised to Bulk Continental Crust**



**Spider Diagram of the Trace Element Concentrations of the Kyanite Gneiss LK1 Lithological Unit Normalised to Bulk Continental Crust**

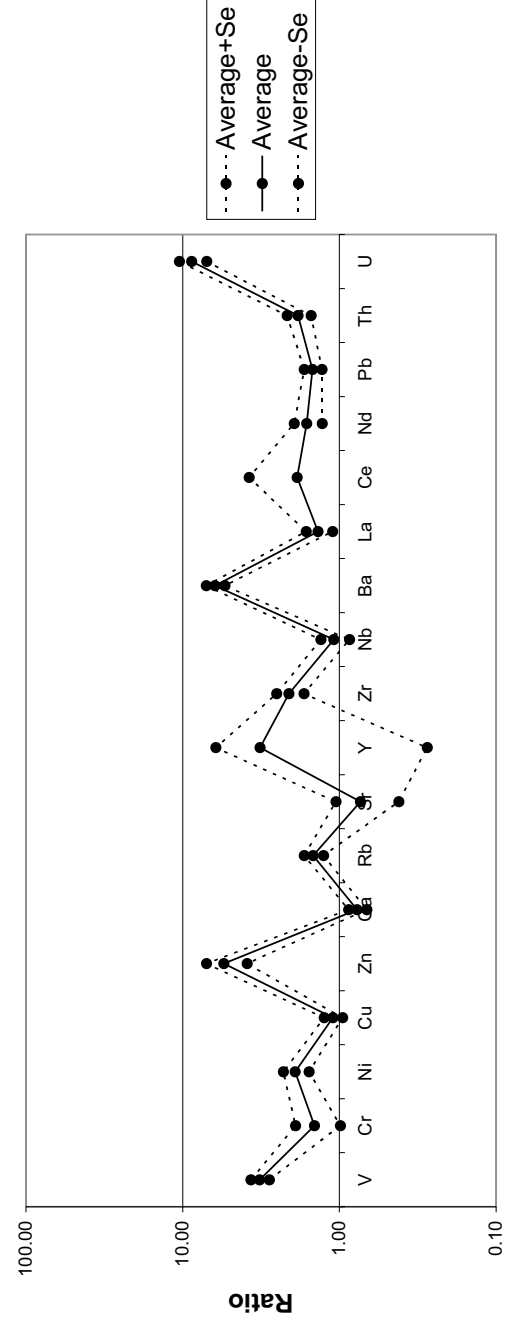




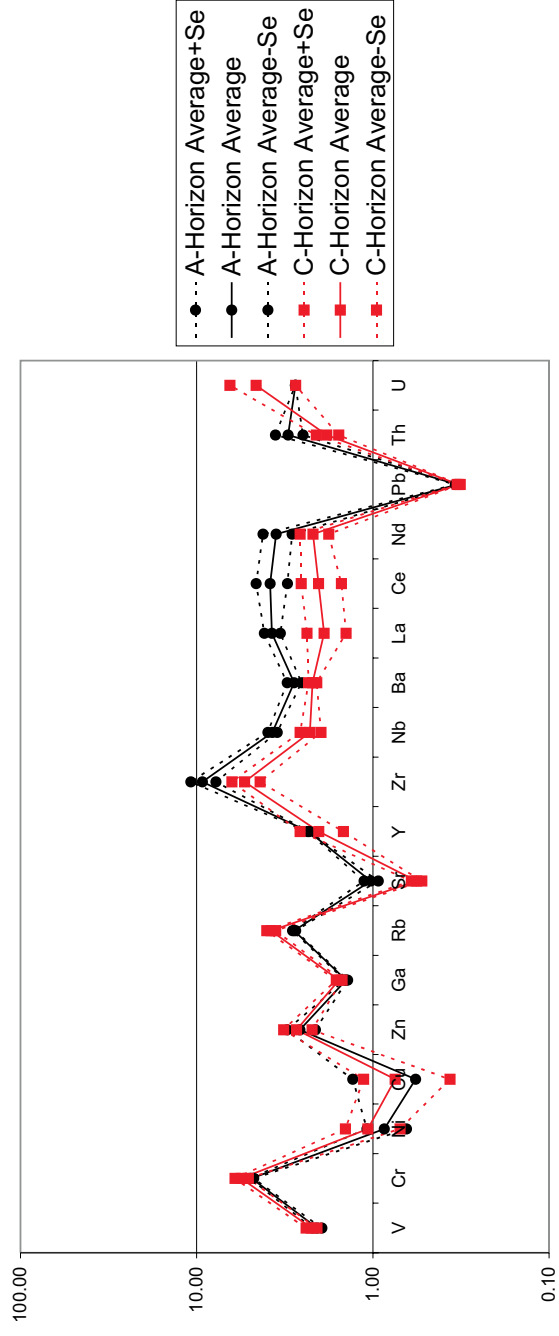
Fig.22a

Fig.22 Folding in the JWZ, located in the C-Horizon of Type 7 Soil. This indicates that folding is definitely present within at least the JWZ and is evidence that folding on a larger scale could exist.

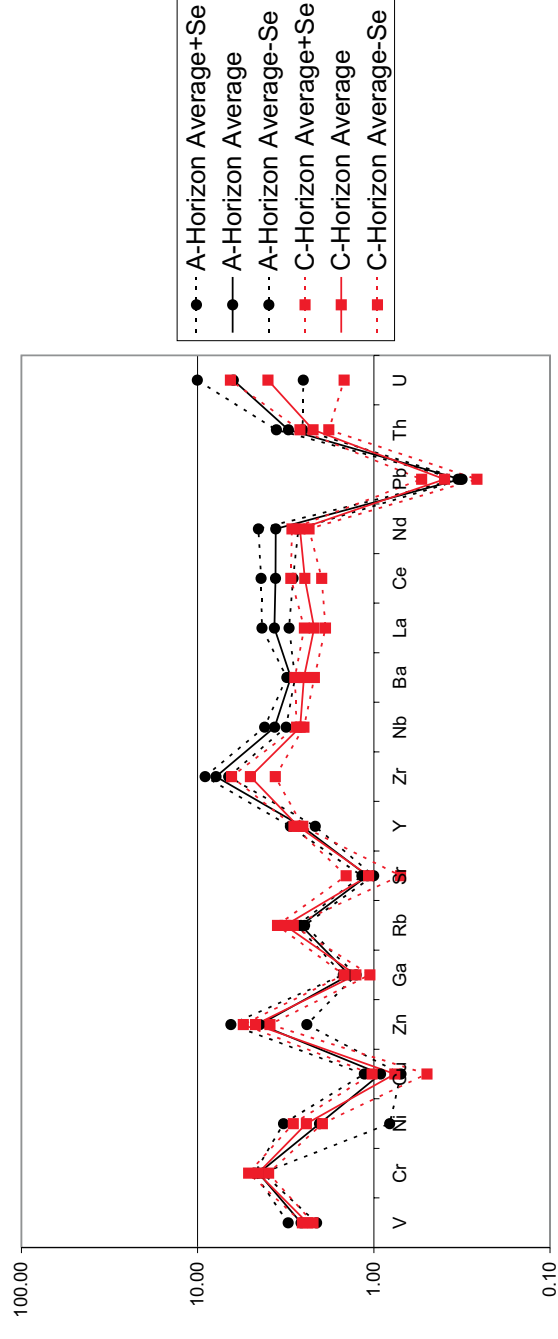


Fig.22b

### Spider Diagram of the Fine Fraction of the A- and C-Horizon of Zone 1 Soil Normalised to Bulk Continental Crust

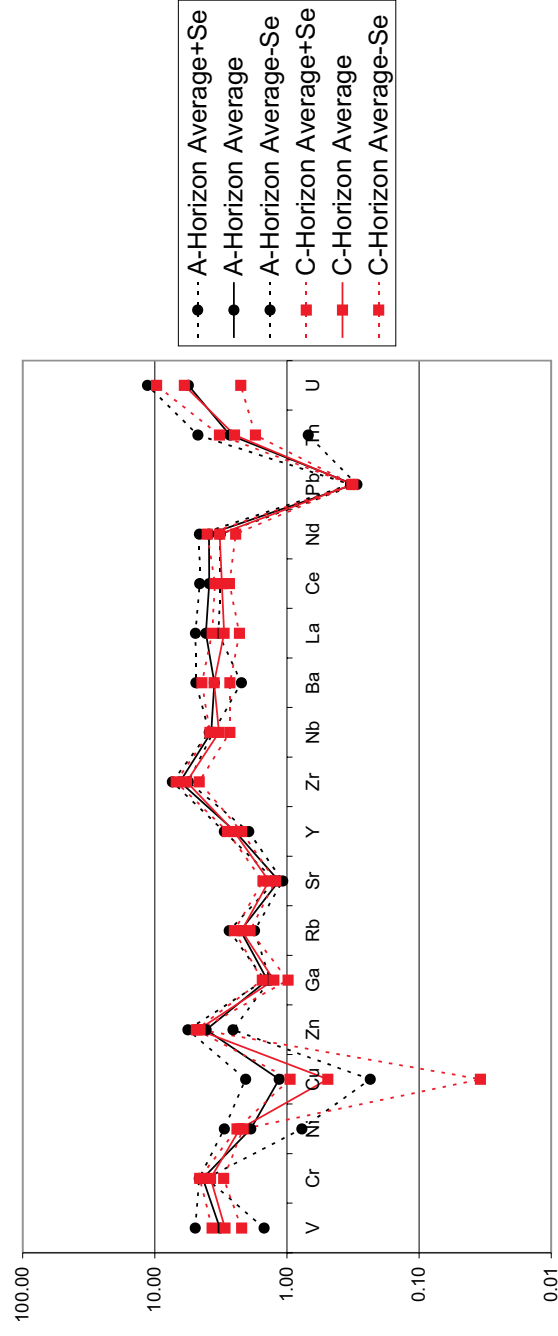


### Spider Diagram of the Fine Fraction of the A- and C-Horizon of Zone 1 TZ Soil Normalised to Bulk Continental Crust



<http://scholar.sun.ac.za/>

### Spider Diagram of the Fine Fraction of the A- and C-Horizon of Zone 2 Soil Normalised to Bulk Continental Crust



### Spider Diagram of the Fine Fraction of the A- and C-Horizon of Zone 3 Soil Normalised to Bulk Continental Crust

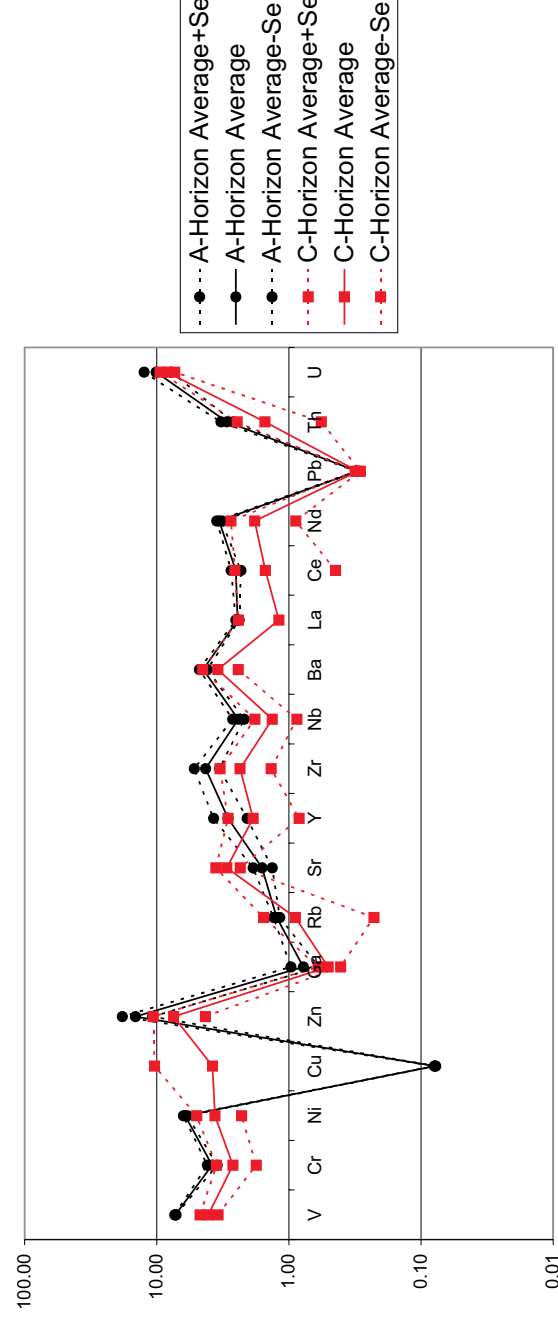
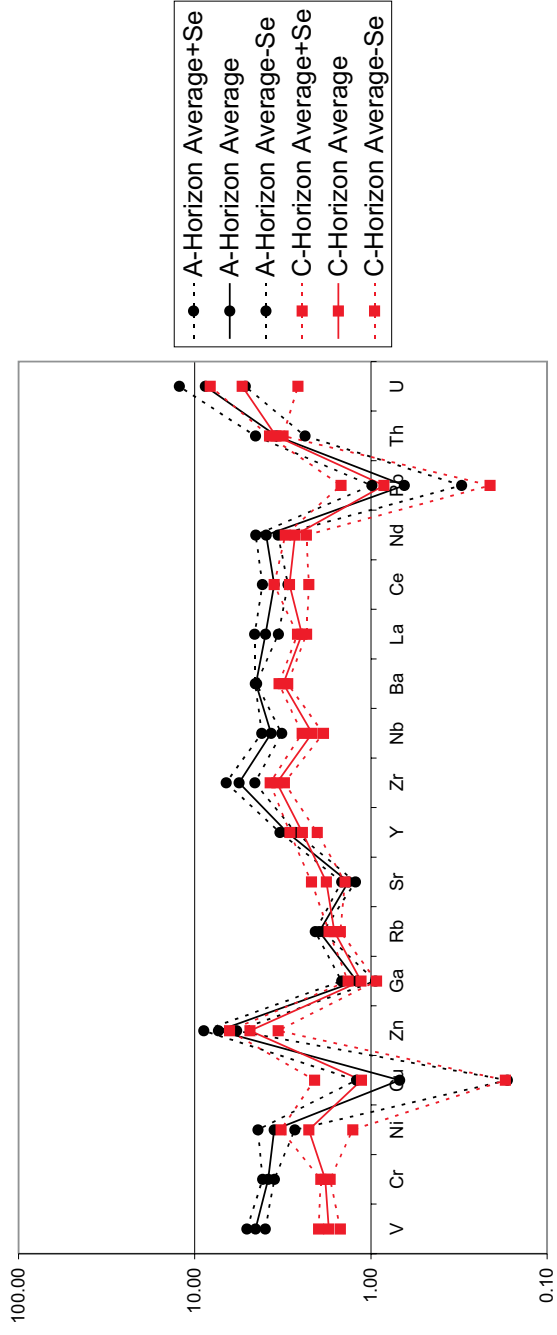


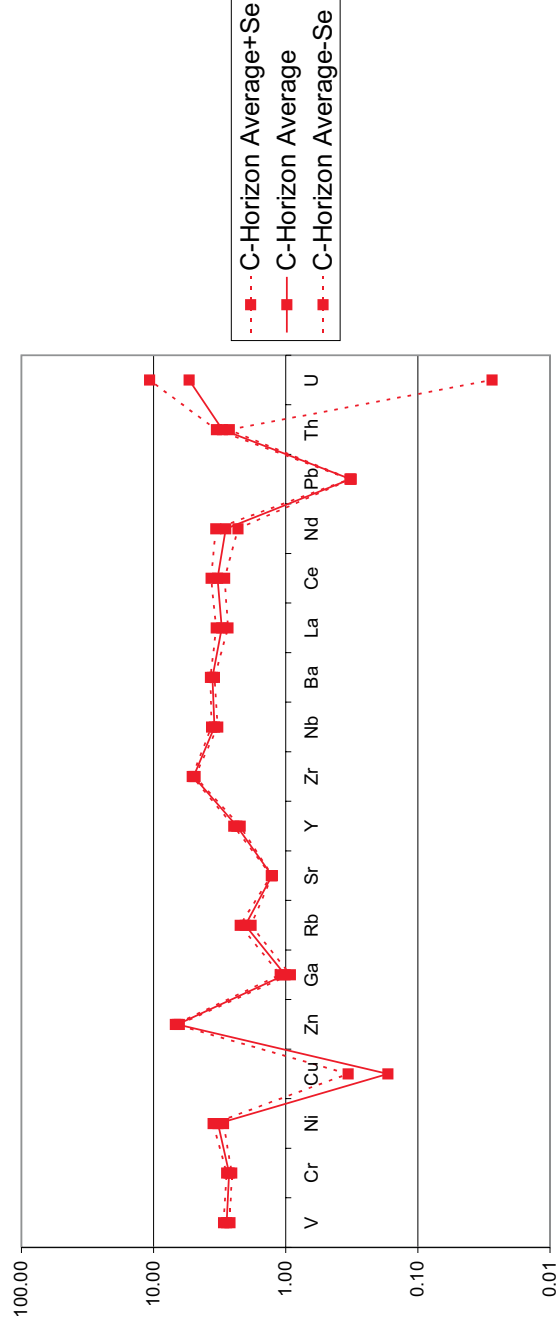
Fig.23 Spider diagrams of the trace element concentrations of the soil samples from the Merelani trench normalised to bulk continental crust

### Spider Diagram of the Fine Fraction of the A- and C-Horizon of Zone 4 Soil Normalised to Bulk Continental Crust

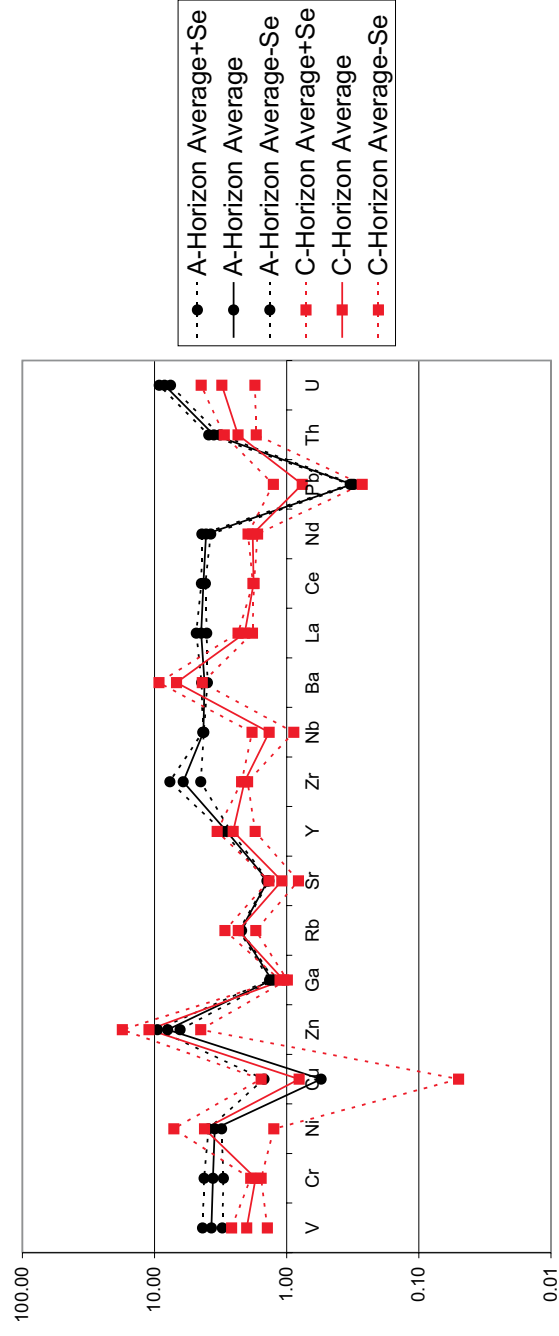


<http://scholar.sun.ac.za>

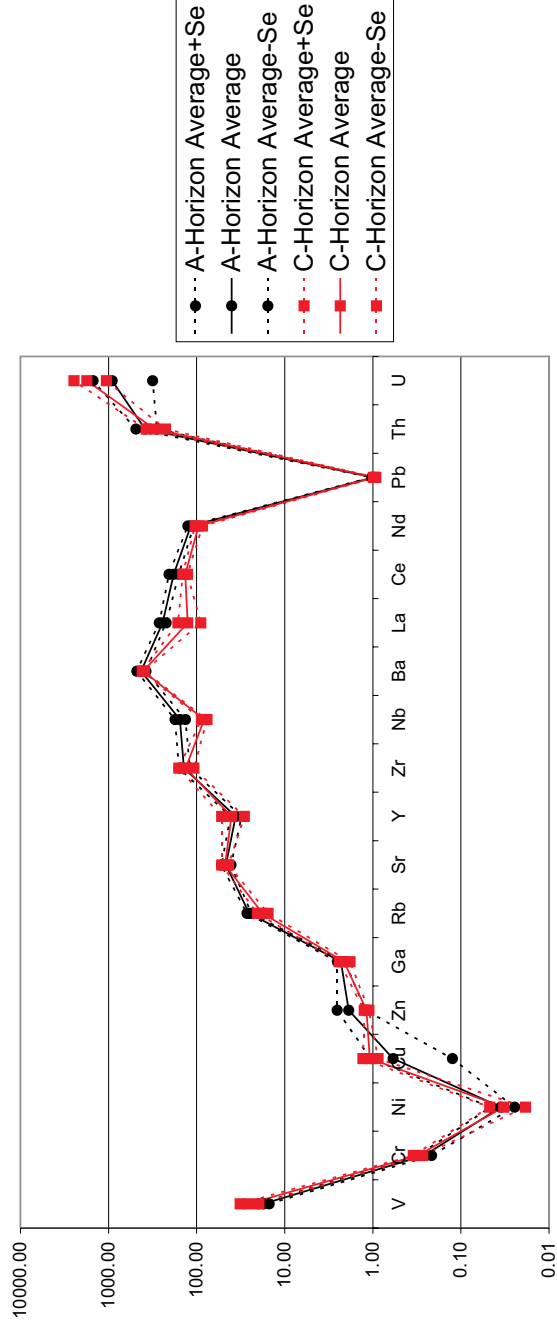
### Spider Diagram of the Fine Fraction of the A- and C-Horizon of Zone 5 Soil Normalised to Bulk Continental Crust



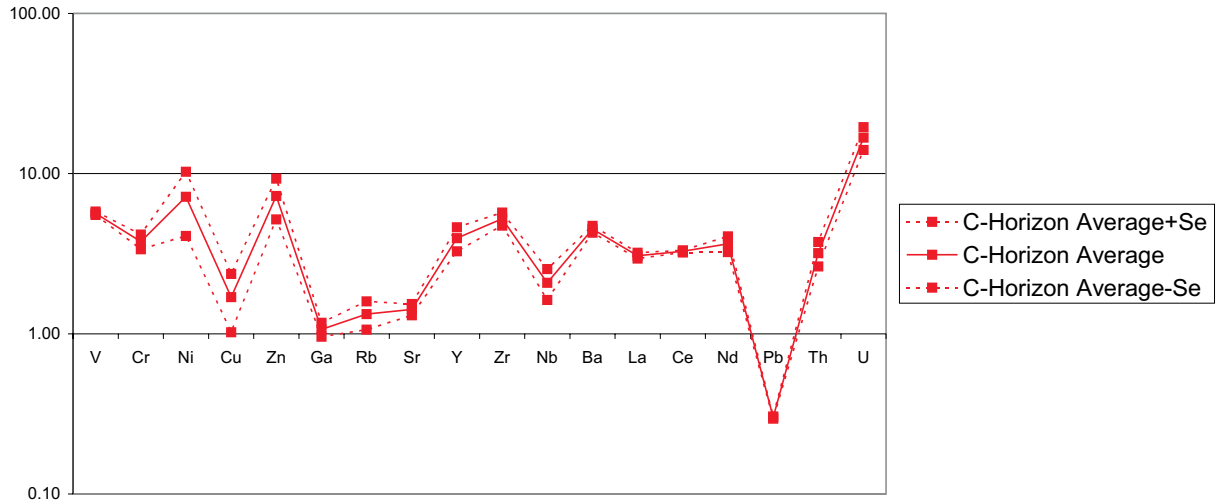
### Spider Diagram of the Fine Fraction of the A- and C-Horizon of Zone 6 Soil Normalised to Bulk Continental Crust



### Spider Diagram of the Fine Fraction of the A- and C-Horizon of Zone 7 Soil Normalised to Bulk Continental Crust



### Spider Diagram of the Fine Fraction of the A- and C-Horizon of Zone JWZ Soil Normalised to Bulk Continental Crust



### Spider Diagram of the Fine Fraction of the A- and C-Horizon of Zone 8 Soil Normalised to Bulk Continental Crust

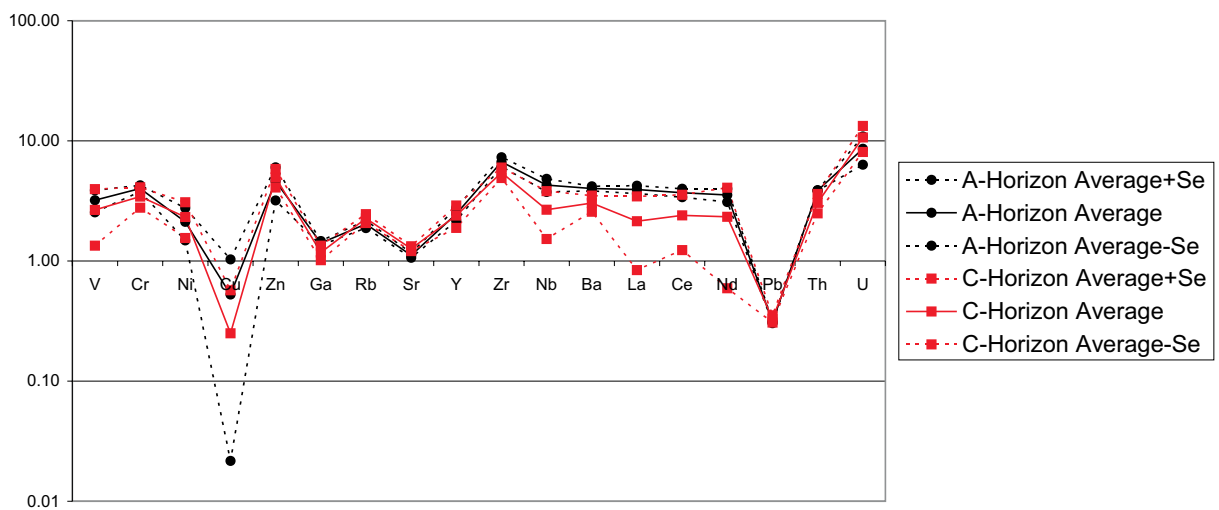
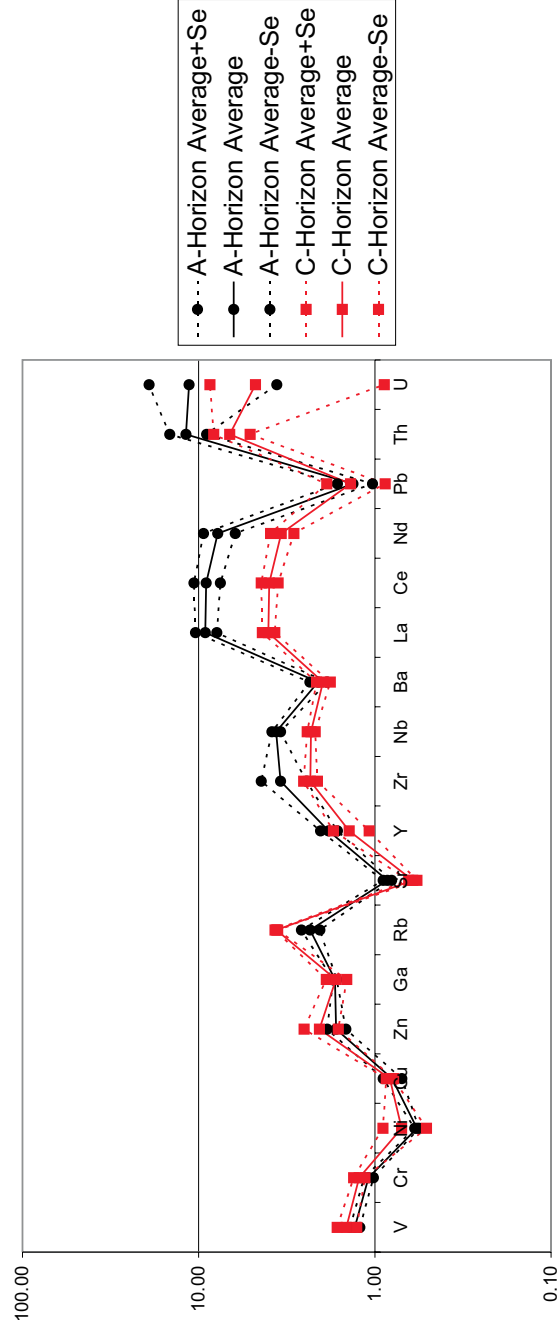


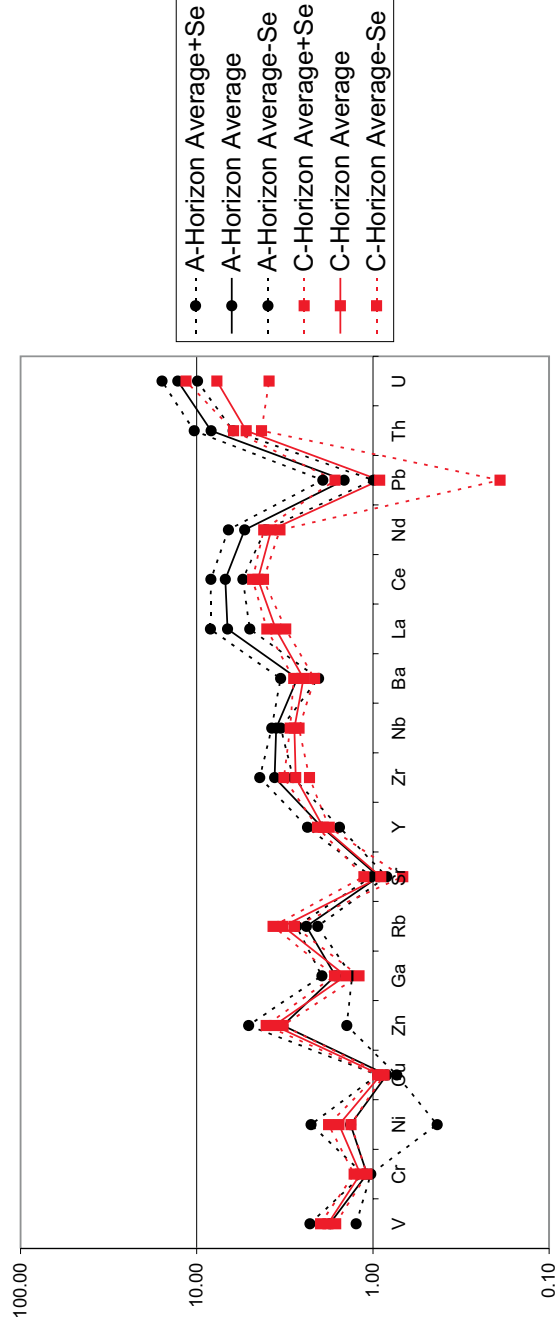
Fig.23 ...continued



### Spider Diagram of the Medium Fraction of the A- and C-Horizon of Zone 1 Soil Normalised to Bulk Continental Crust

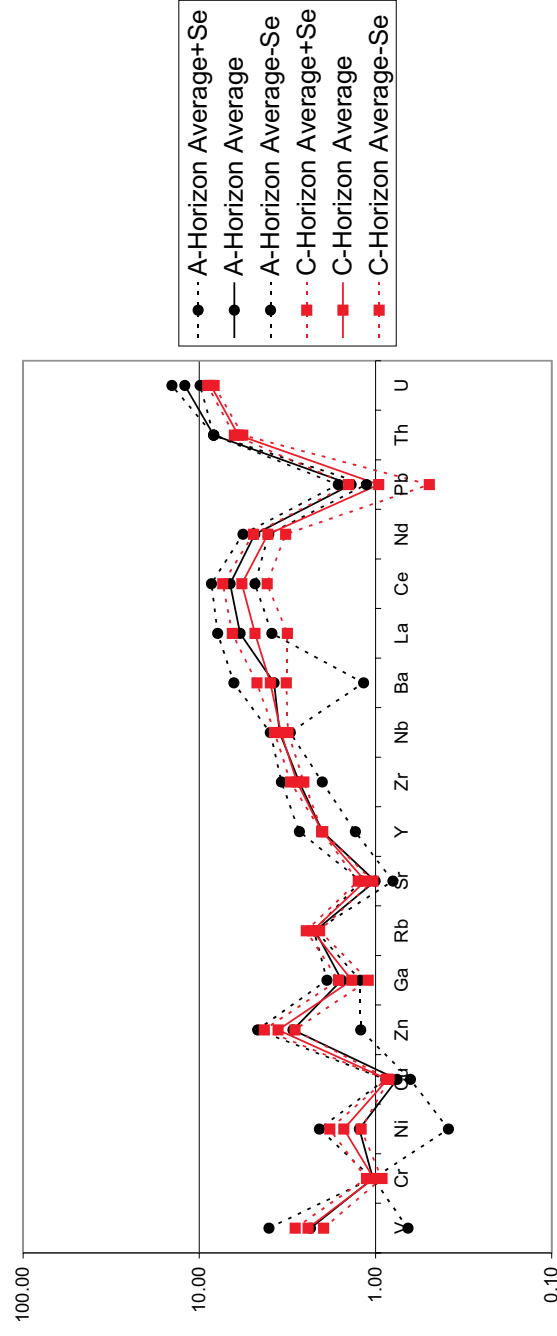


### Spider Diagram of the Medium Fraction of the A- and C-Horizon of Zone 1 TZ Soil Normalised to Bulk Continental Crust

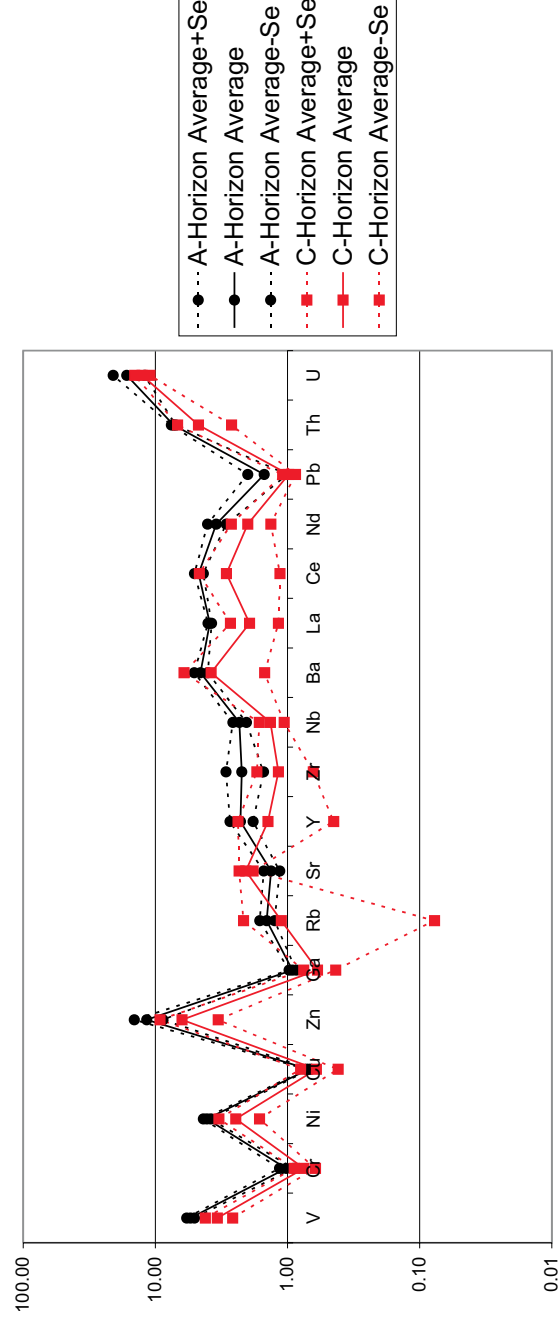


<http://scholar.sun.ac.za/>

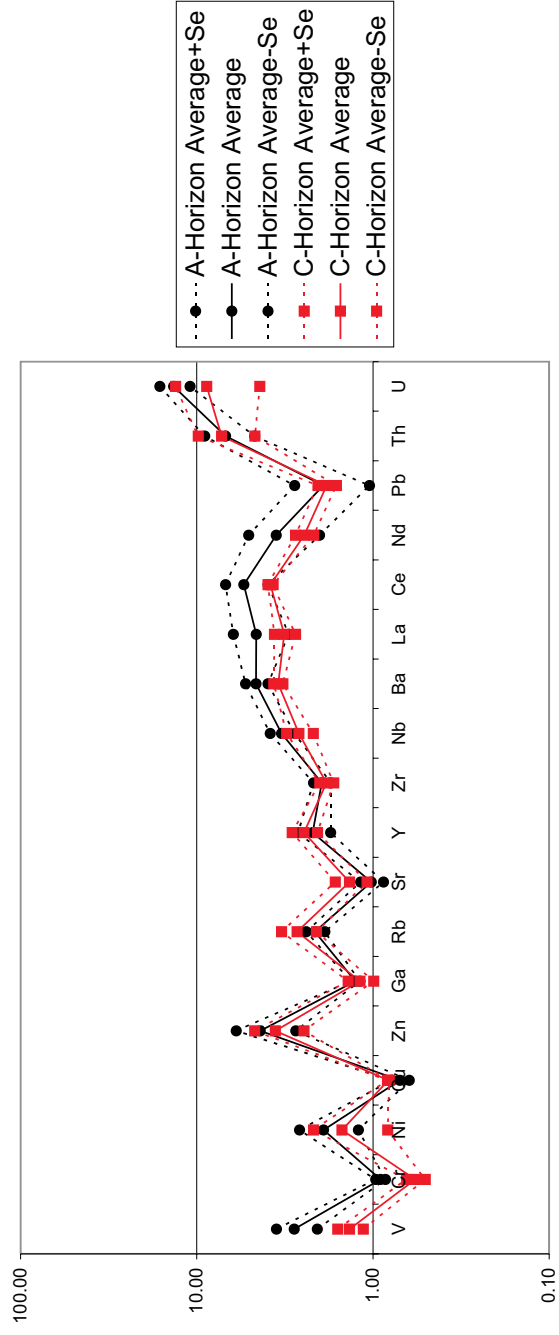
### Spider Diagram of the Medium Fraction of the A- and C-Horizon of Zone 2 Soil Normalised to Bulk Continental Crust



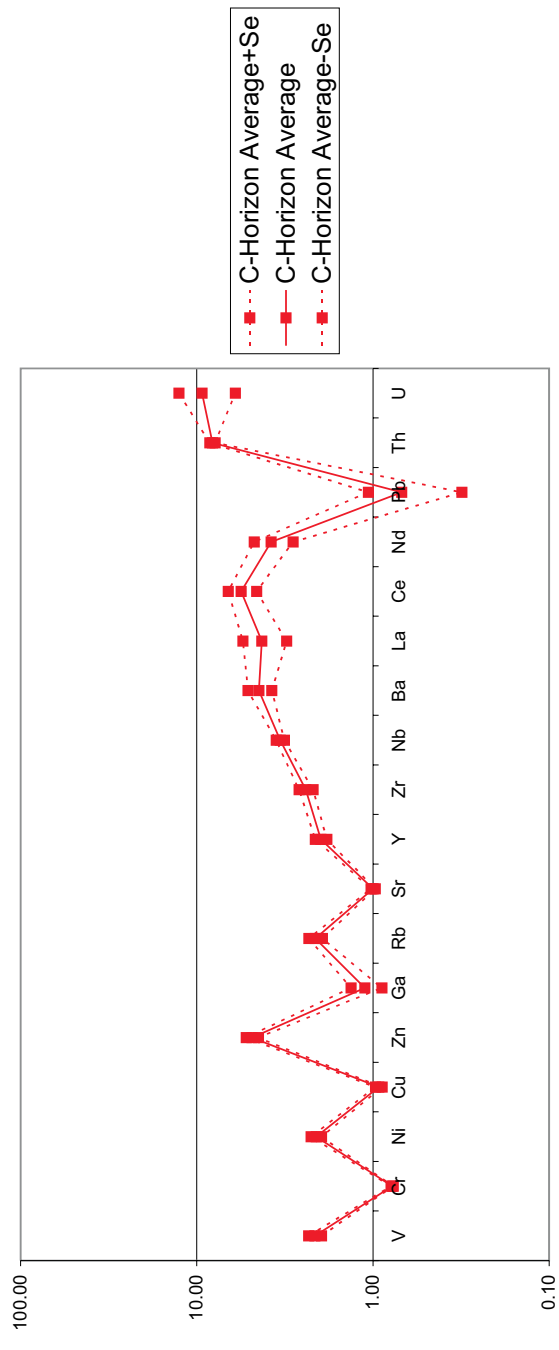
### Spider Diagram of the Medium Fraction of the A- and C-Horizon of Zone 3 Soil Normalised to Bulk Continental Crust



### Spider Diagram of the Medium Fraction of the A- and C-Horizon of Zone 4 Soil Normalised to Bulk Continental Crust

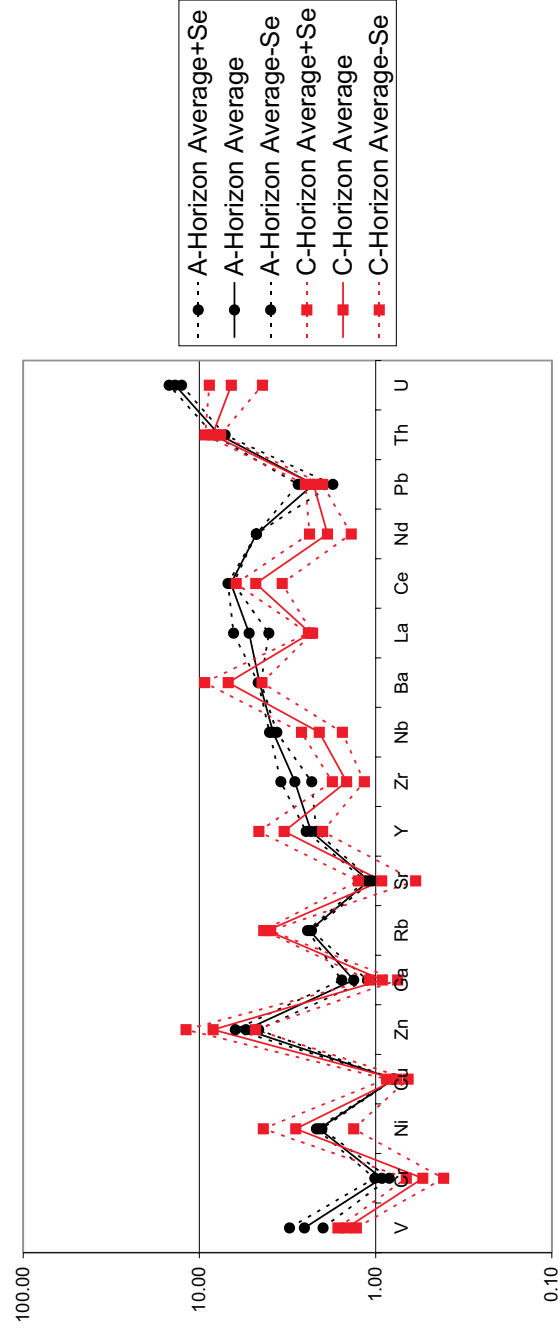


### Spider Diagram of the Medium Fraction of the A- and C-Horizon of Zone 5 Soil Normalised to Bulk Continental Crust

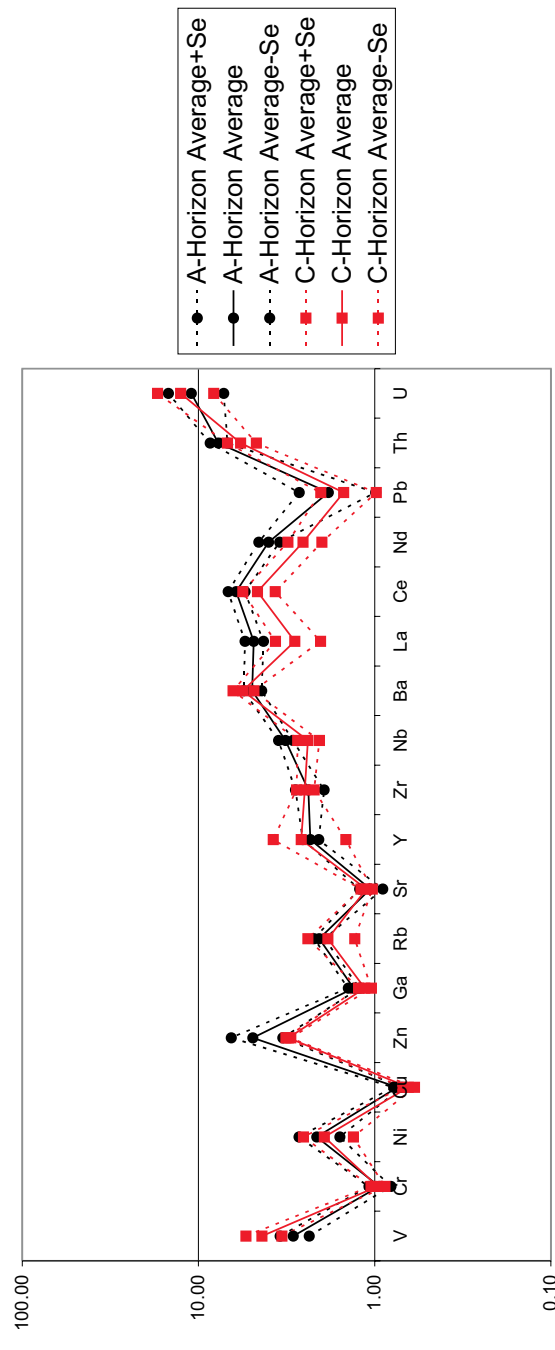


<http://scholar.sun.ac.za/>

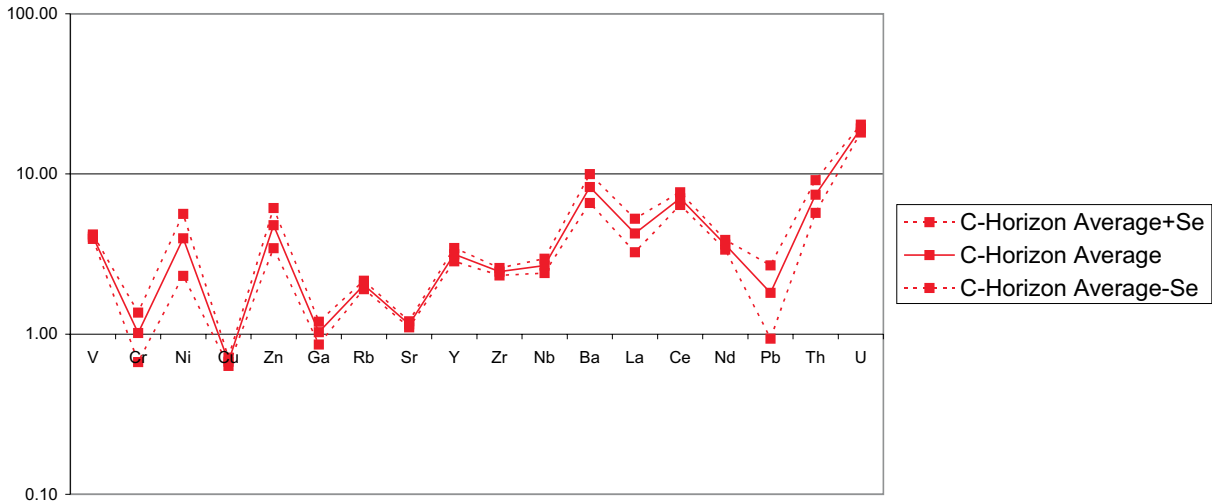
### Spider Diagram of the Medium Fraction of the A- and C-Horizon of Zone 6 Soil Normalised to Bulk Continental Crust



### Spider Diagram of the Medium Fraction of the A- and C-Horizon of Zone 7 Soil Normalised to Bulk Continental Crust



### Spider Diagram of the Medium Fraction of the A- and C-Horizon of Zone 7 (JWZ) Soil Normalised to Bulk Continental Crust



### Spider Diagram of the Medium Fraction of the A- and C-Horizon of Zone 8 Soil Normalised to Bulk Continental Crust

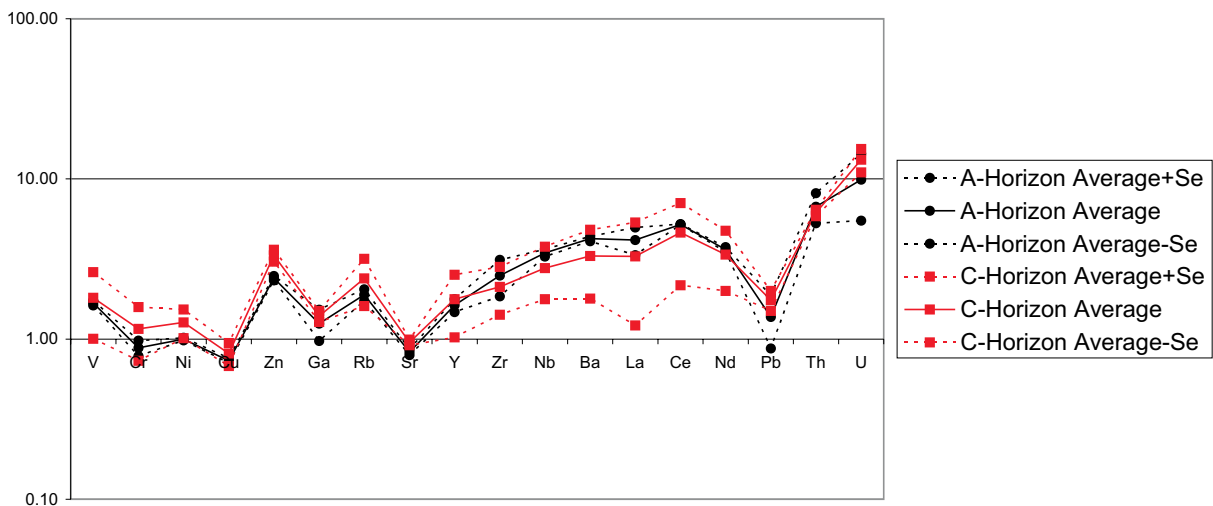
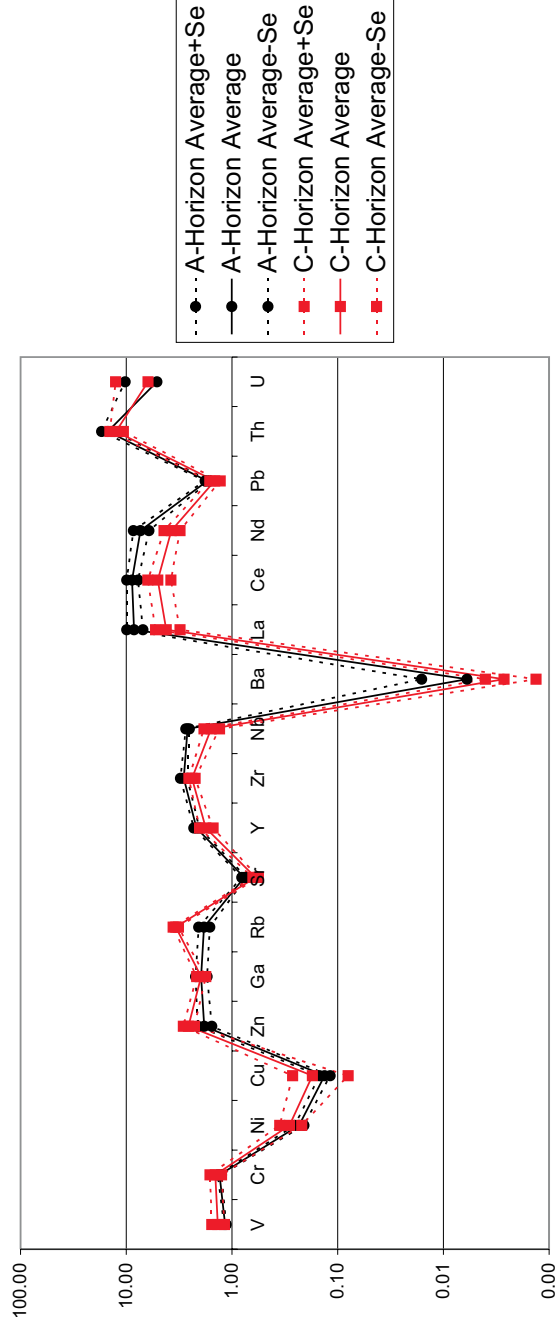
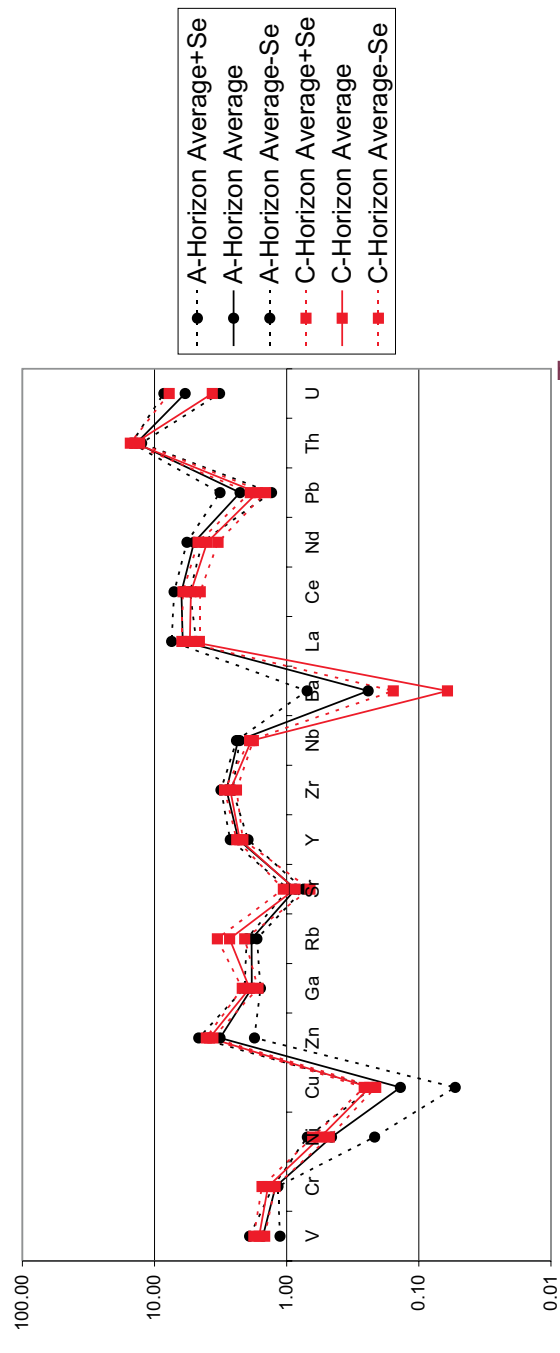


Fig.23 ...continued

### Spider Diagram of the Coarse Fraction of the A- and C-Horizon of Zone 1 Soil Normalised to Bulk Continental Crust

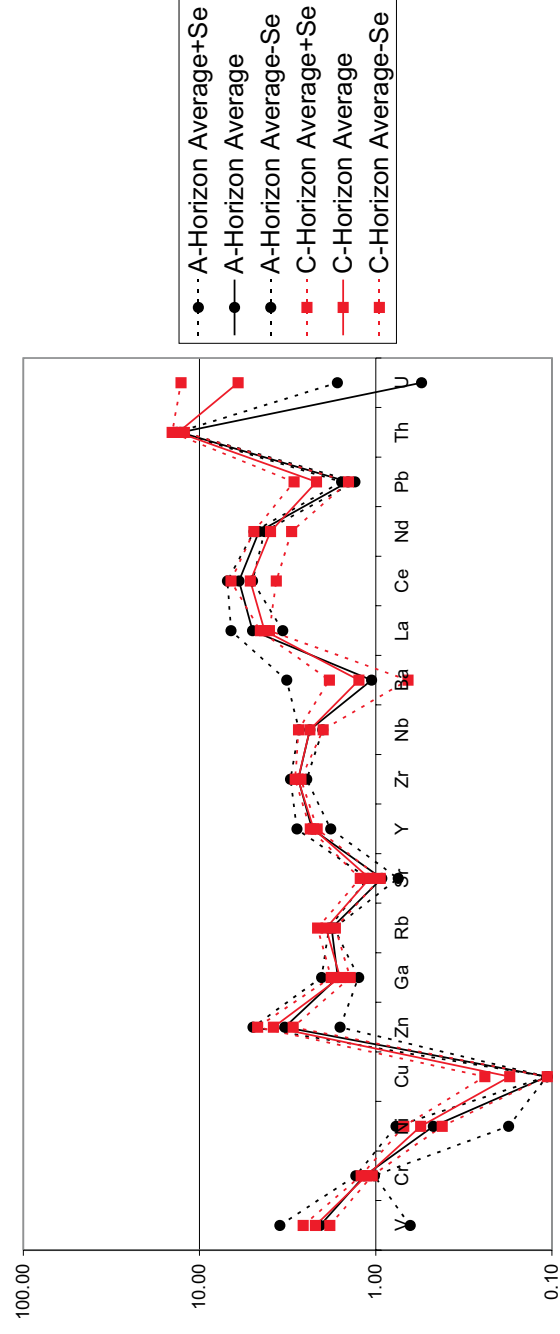


### Spider Diagram of the Coarse Fraction of the A- and C-Horizon of Zone 1 TZ Soil Normalised to Bulk Continental Crust

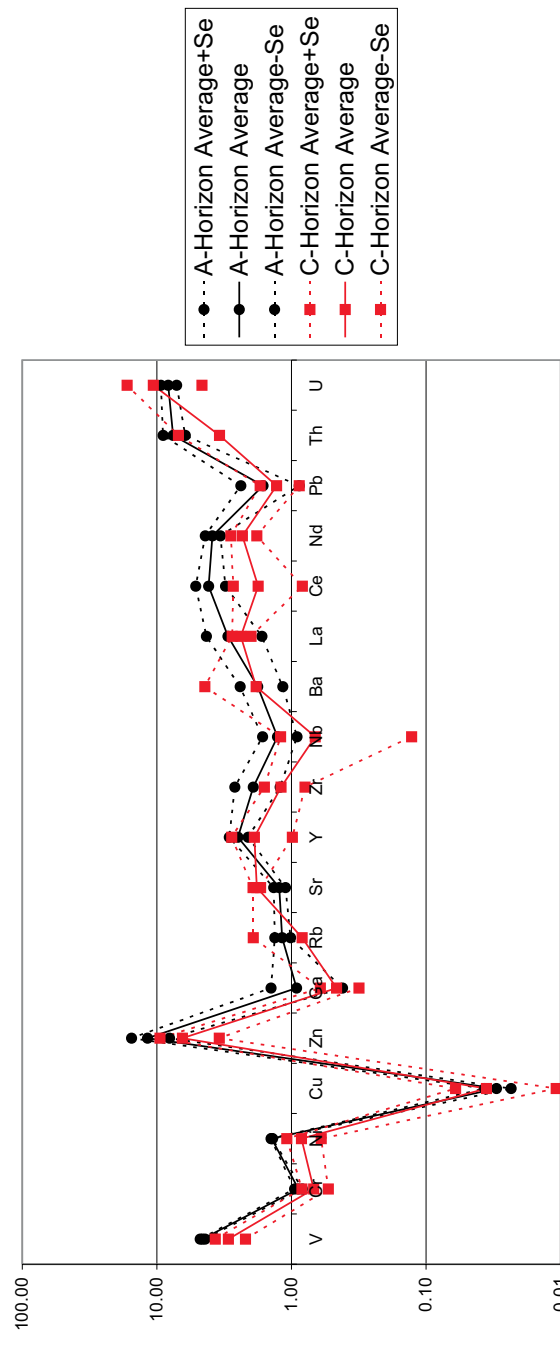


<http://scholar.sun.ac.za/>

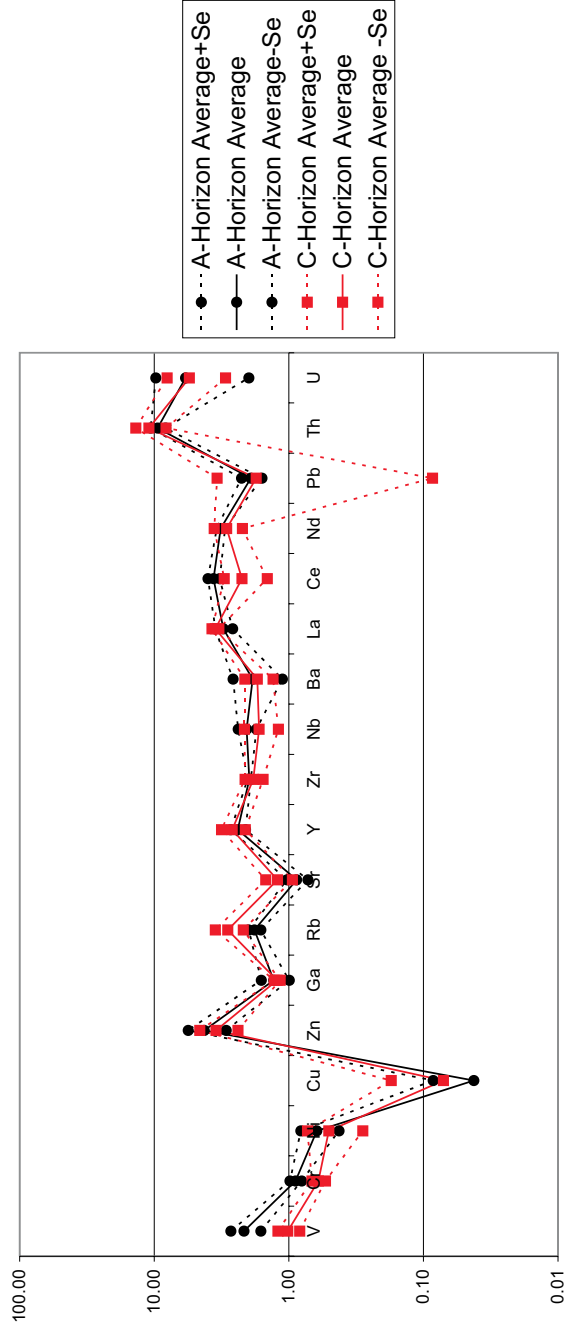
### Spider Diagram of the Coarse Fraction of the A- and C-Horizon of Zone 2 Soil Normalised to Bulk Continental Crust



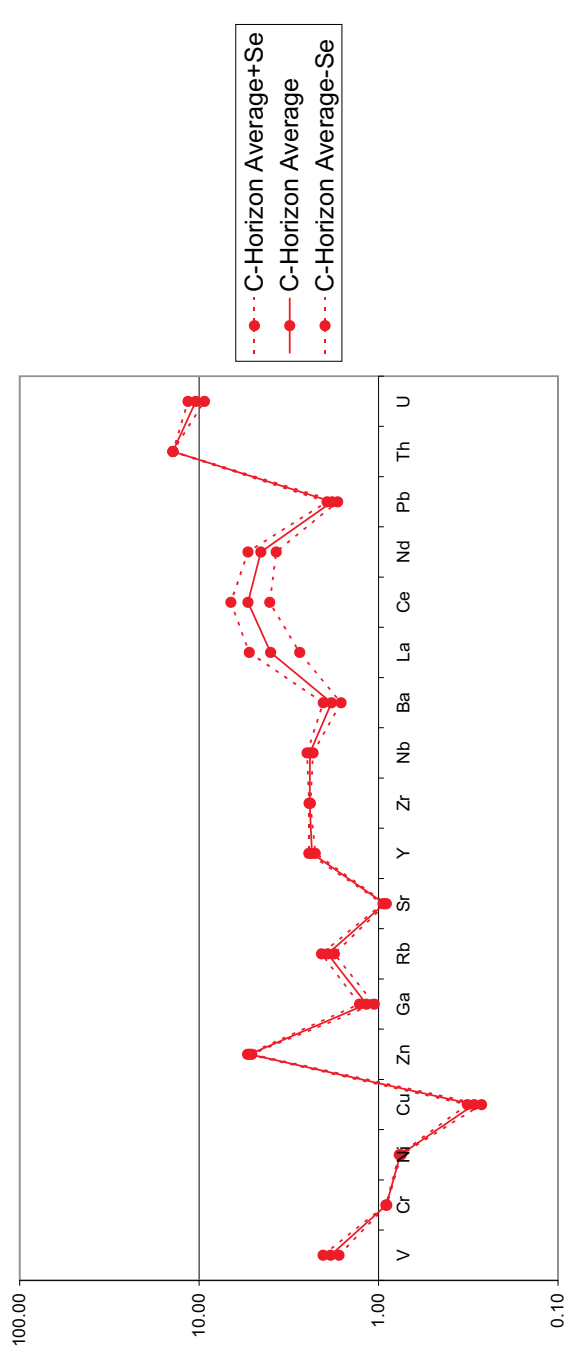
### Spider Diagram of the Coarse Fraction of the A- and C-Horizon of Zone 3 Soil Normalised to Bulk Continental Crust



### Spider Diagram of the Coarse Fraction of the A- and C-Horizon of Zone 4 Soil Normalised to Bulk Continental Crust

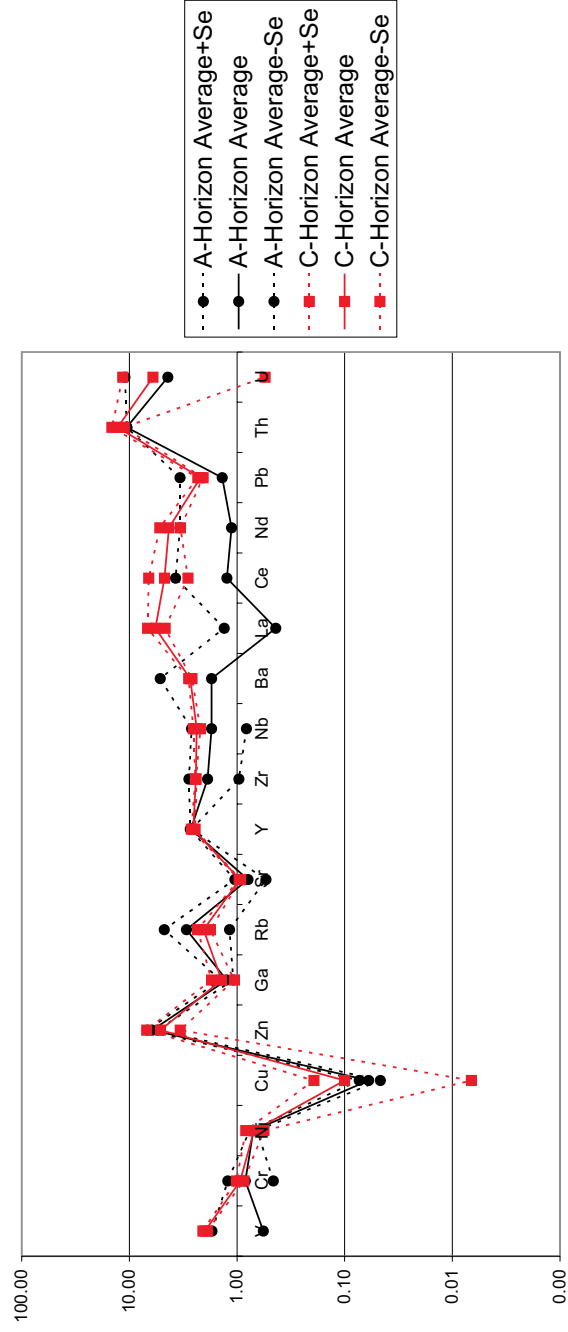


### Spider Diagram of the Coarse Fraction of the A- and C-Horizon of Zone 5 Soil Normalised to Bulk Continental Crust

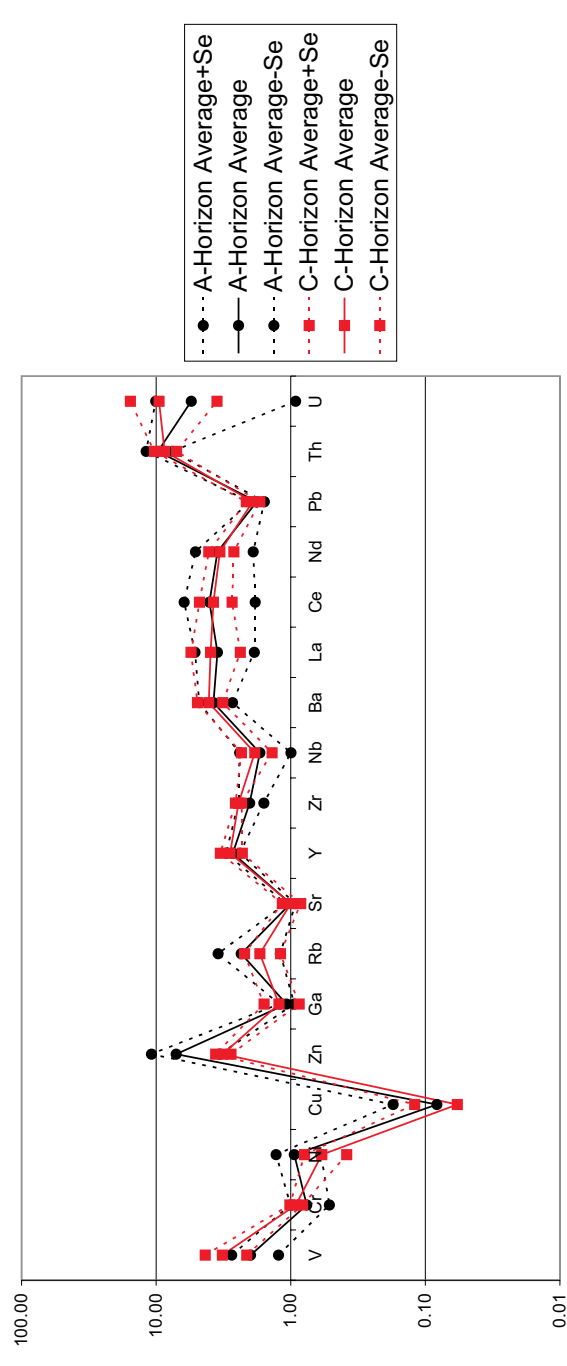


<http://scholar.sun.ac.za>

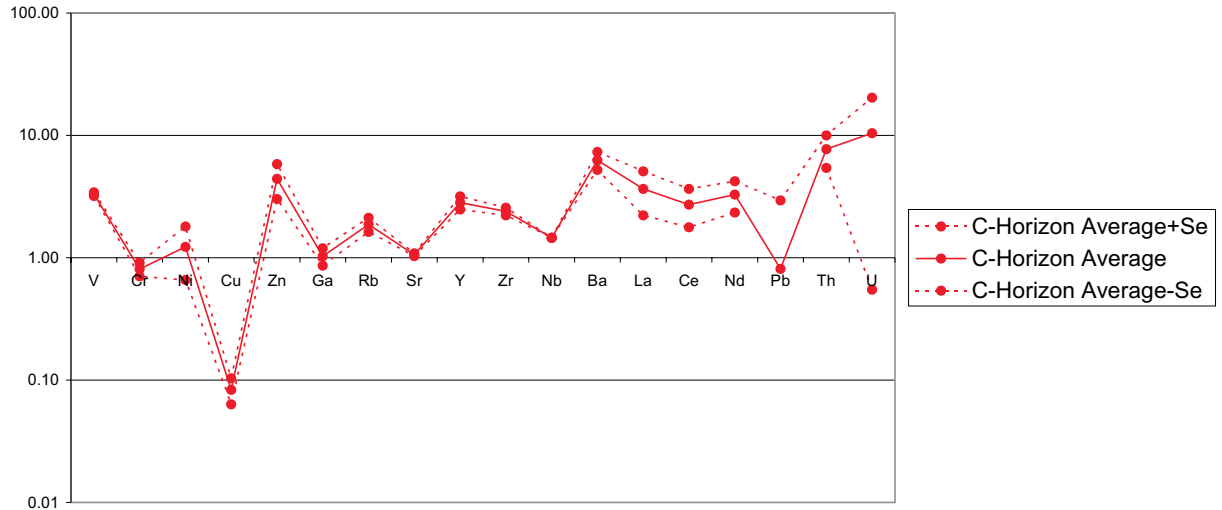
### Spider Diagram of the Coarse Fraction of the A- and C-Horizon of Zone 6 Soil Normalised to Bulk Continental Crust



### Spider Diagram of the Coarse Fraction of the A- and C-Horizon of Zone 7 Soil Normalised to Bulk Continental Crust



### Spider Diagram of the Coarse Fraction of the A- and C-Horizon of Zone 7 (JWZ) Soil Normalised to Bulk Continental Crust



### Spider Diagram of the Coarse Fraction of the A- and C-Horizon of Zone 8 Soil Normalised to Bulk Continental Crust

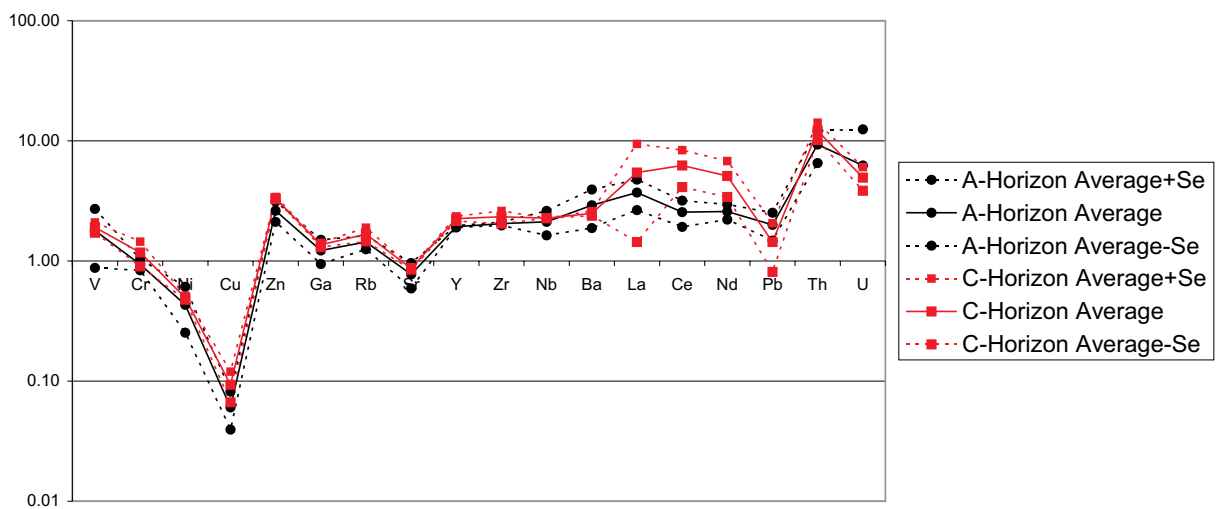


Fig.23 ...continued

All the soil zones as well as the different soil horizons and soil size fractions display elevated concentrations of V, Zn, REE, Zr, Th and U relative to BCC. There is no difference in the patterns of the A-Horizons compared to those of C-Horizons for any of the three size fractions. Small differences between the trace element patterns become apparent when the different size fractions from the same soil zones are compared with each other. Where all the trace element patterns show a relatively lower BCC normalised Cr value compared to BCC normalised V value, the coarse fraction of soil Zone 1, the medium fraction of soil Zone 1, 1 TZ and 2 show the reverse. Other comparative differences are the significant negative BCC normalised Ba anomaly of the coarse fraction of soil Zone 1 and the negative Cu anomaly of the Coarse fraction of soil Zone 3 relative to the other soil zones and soil size fractions. Another comparative difference is the anomalous BCC normalised values of the heavier elements in the fine fraction of soil Zone 7, with the exception of Pb, relative to the other soil zones and size fractions.

The patterns of Zone 1 and Zone 1 TZ soils are almost identical for all three size fractions. They are both situated on the Garnet Gneiss 1 unit. The same scenario exists for Zone 7 and Zone JWZ soils, with the exception of the much higher relative heavy element values of the coarse fraction of soil Zone 7 compare to the values for the same elements of soil Zone JWZ.

### **5.3.3. Comparison between lithologies and soils**

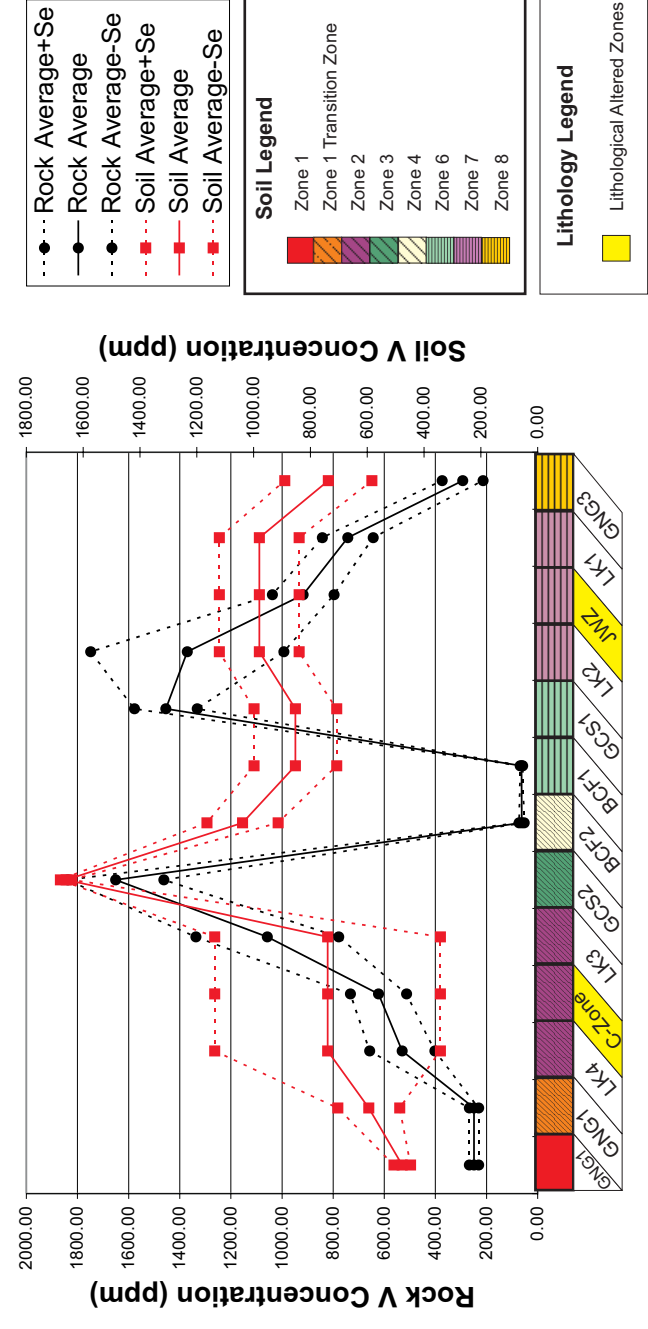
Geochemical profiles over the Merelani lithologies and the soils that overly them, as represented in the trench, were constructed by plotting both the soil trace element XRF data for all three size fractions and for both soil horizons as well as the lithology trace element XRF data on the same graph (Fig.24). The lithology and soil data were plotted on two corresponding y-axes, due to the difference in trace element concentration for some of the lithologies compared to the soils which overly them.

All the trace element profiles of the soil zones in the trench correlate with those of the lithologies, which lie beneath them. However, some trace element profiles, such as those of V and Cr, correlate to a larger degree than some of the others, such as Y and Ce. Only the profiles in which the soil profiles most closely represent those of the lithology profiles are shown in Fig.24. The rest can be found in the addendum (addendum CD). In general, the closest correlations between the profiles of the soils and lithologies exist in the profiles of the fine and medium fractions of the C-horizons of the soils. The A-horizon profiles generally correlate well with the lithological profiles from the Garnet Gneiss Unit 1 to the Central Dolomite, but then they “deviate” and the profile is smoothed compared to the lithological profiles. The profiles of V, Ni and Zn are similar to each other as well as the profiles of Cr and Ga and Ba and Sr, which may suggest a correlation between these elements. The trace elements which show the closest correlation between the soil and lithology trace element profiles are C-Horizon profiles of the fine and medium fractions of V, Cr, Ni, Zn, Ga, Rb, Ba. Of these elements V shows the closest correlation between the soil and lithology profile patterns. The heavier elements, such as Pb and U show a correlation between soil and lithology profiles, however, the statistical error is so large, due to the low concentrations of these elements, that it is difficult to say whether the correlations actually exist.

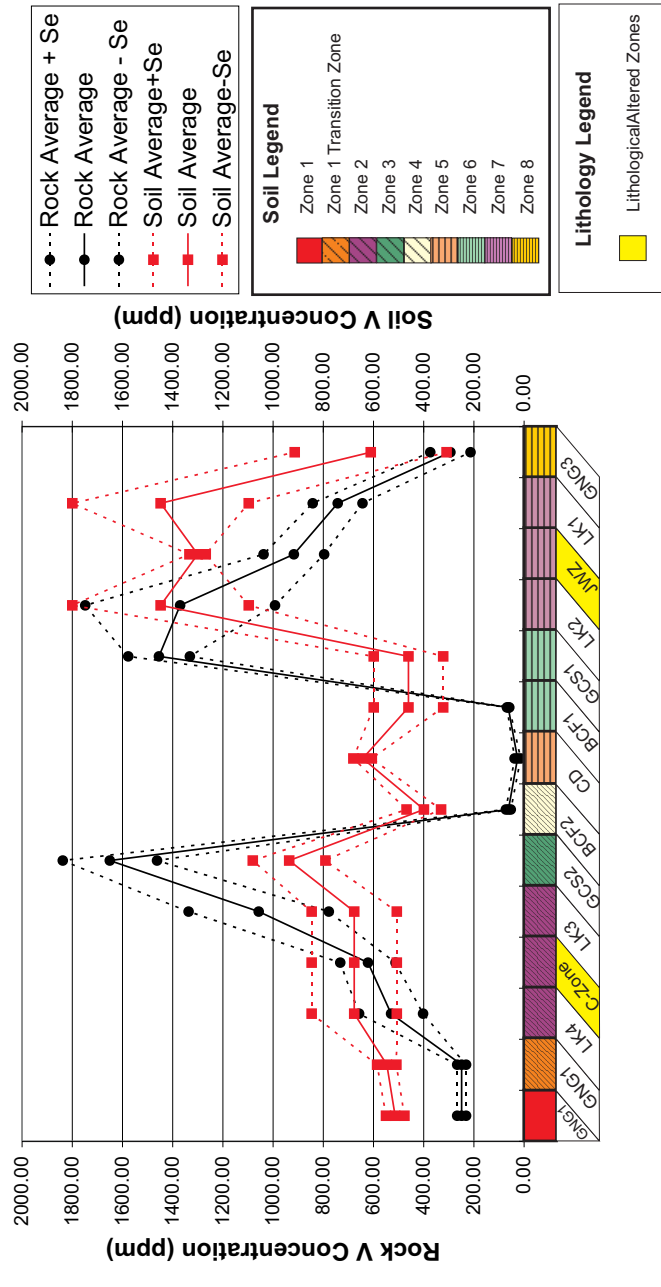
One reason for the weaker correlation with regard to the A-horizon profiles is that the A-horizon is more susceptible to soil creep and soil disturbance than the C-horizon, which is situated deeper in the soil profile. The implications for exploration are thus that the C-horizon provides a more accurate comparison between soil and lithology and should therefore be the soil horizon to be sampled in an exploration survey.



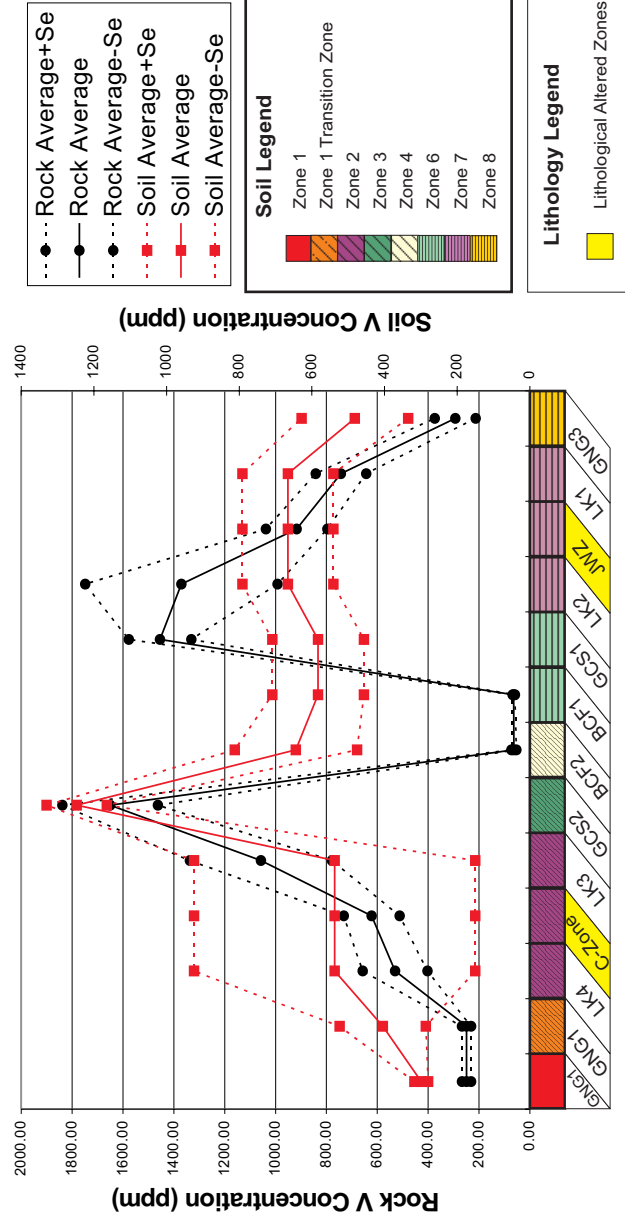
## Lithology and Fine Fraction Soil Profiles for V - A Horizon



## Lithology and Fine Fraction Soil Profiles for V - C-Horizon



## Lithology and Medium Fraction Soil Profiles for V - A Horizon



## Lithology and Medium Fraction Soil Profiles for V - C Horizon

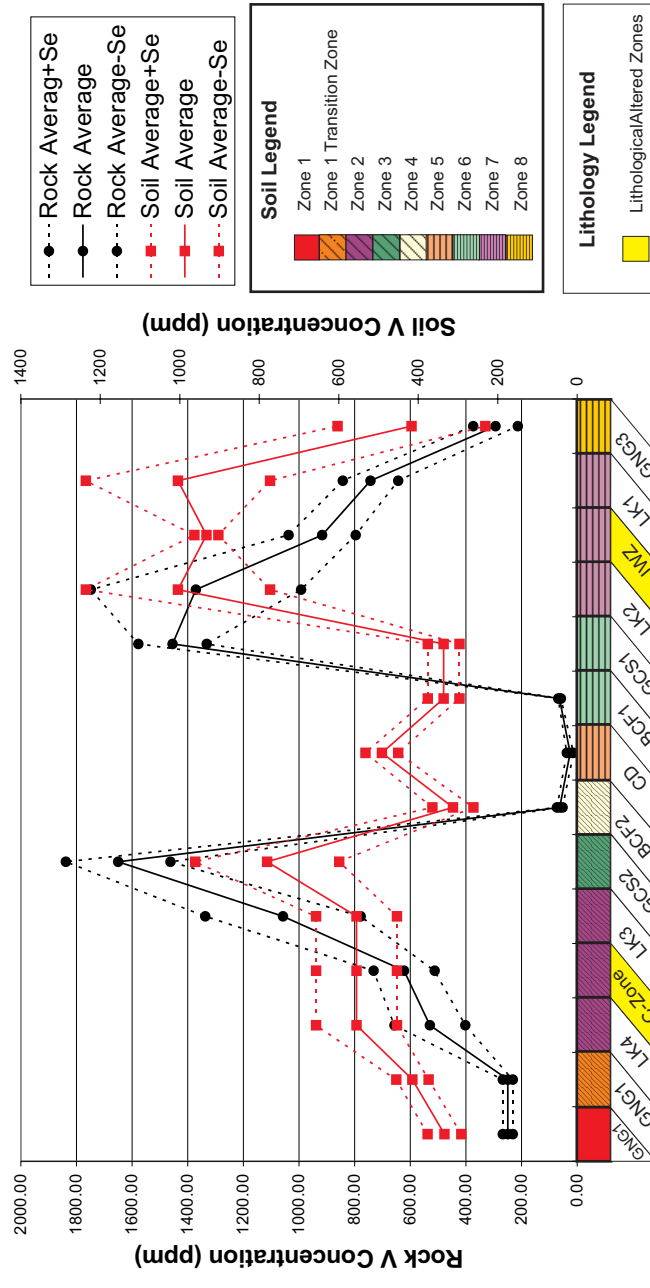
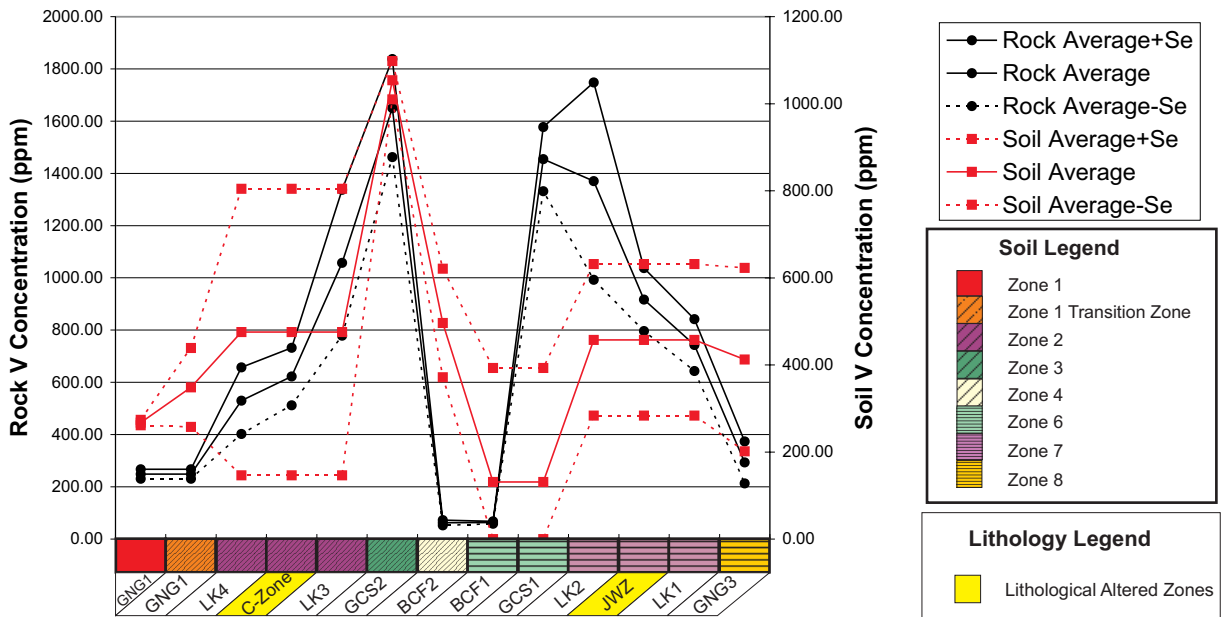


Fig.24 Profile plot of trace elements over the trench for Merelani lithological units as well as for the A- and C-Horizons and fine, medium and coarse fractions of the soil zones. The Central Dolomite does not contain an A-Horizon and for this reason it has been left out of the diagram at the bottom of each graph. Some soil zones cover more than one lithological unit. In these cases the values for the specific soil zone was plotted over all the lithological units it covers. The Garnet Gneiss 1 unit is covered by both the Zone 1 and Zone 1 TZ soil zones. This has been incorporated in the underlying diagrams of the trench and Meleni lithologies by "adding" an additional GNG1 unit to the diagram and legend. The altered zones have been coloured yellow on the diagram as it is the JWZ which is host to the tanzaniite mineralisation and the C-Zone which potentially hosts tanzanite mineralisation and is therefore important units to exploration.

## Lithology and Coarse Fraction Soil Profiles for V - A Horizon



## Lithology and Coarse Fraction Soil Profiles for V - C-Horizon

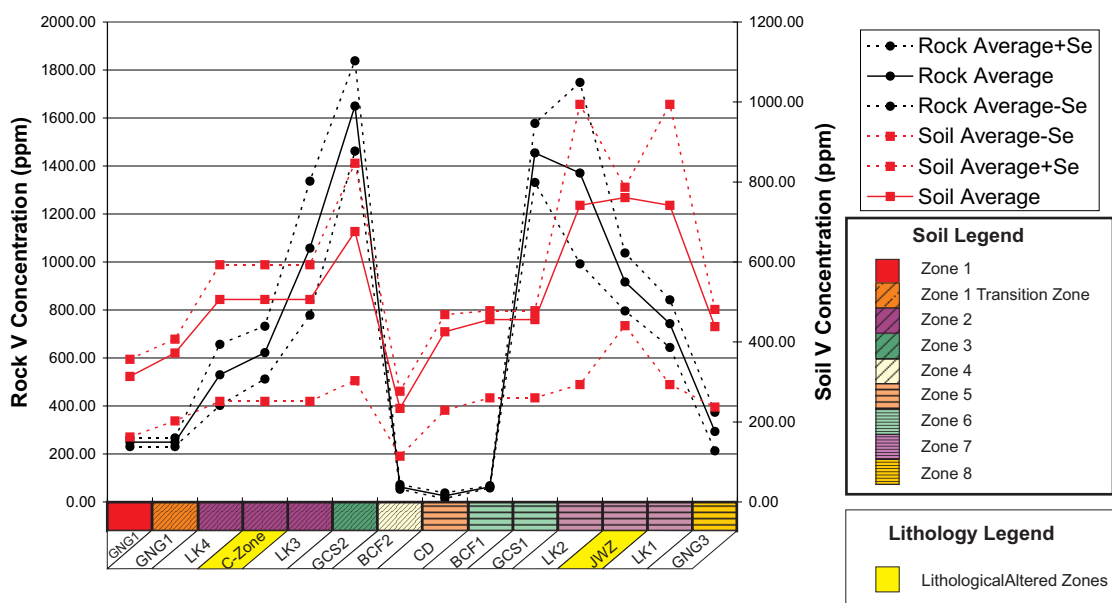
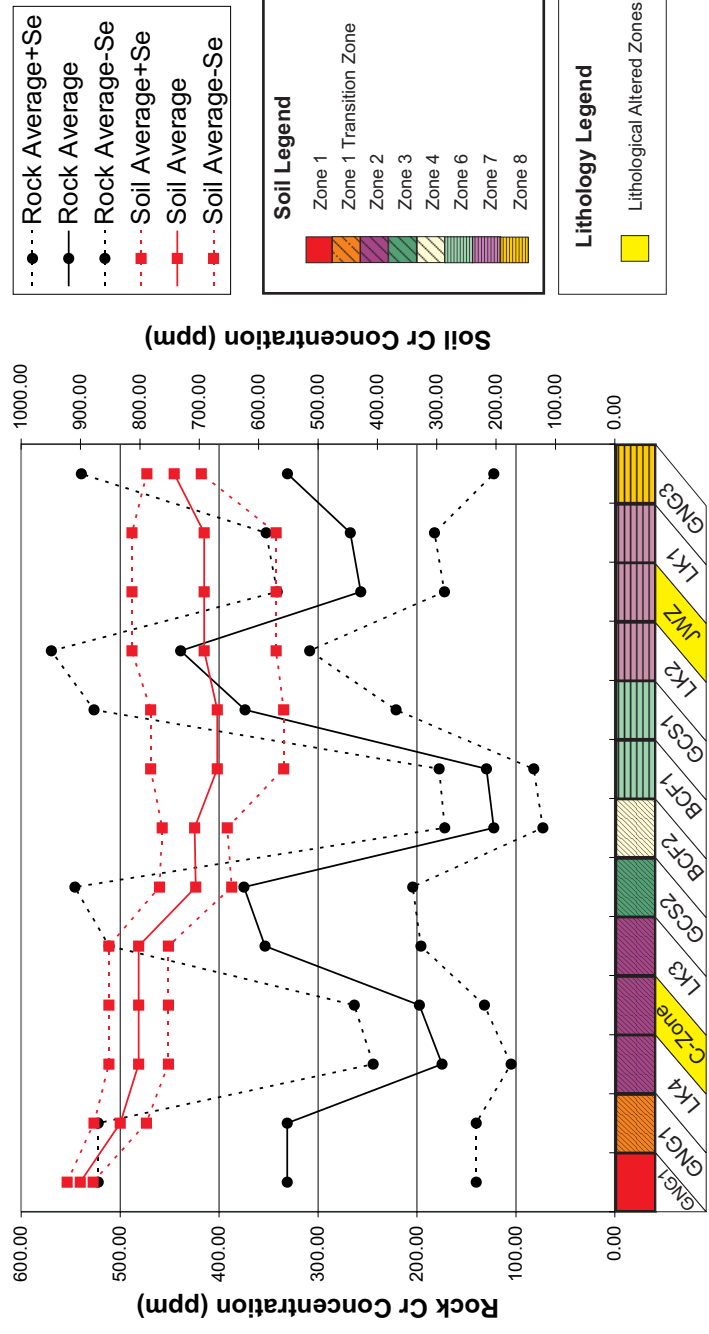


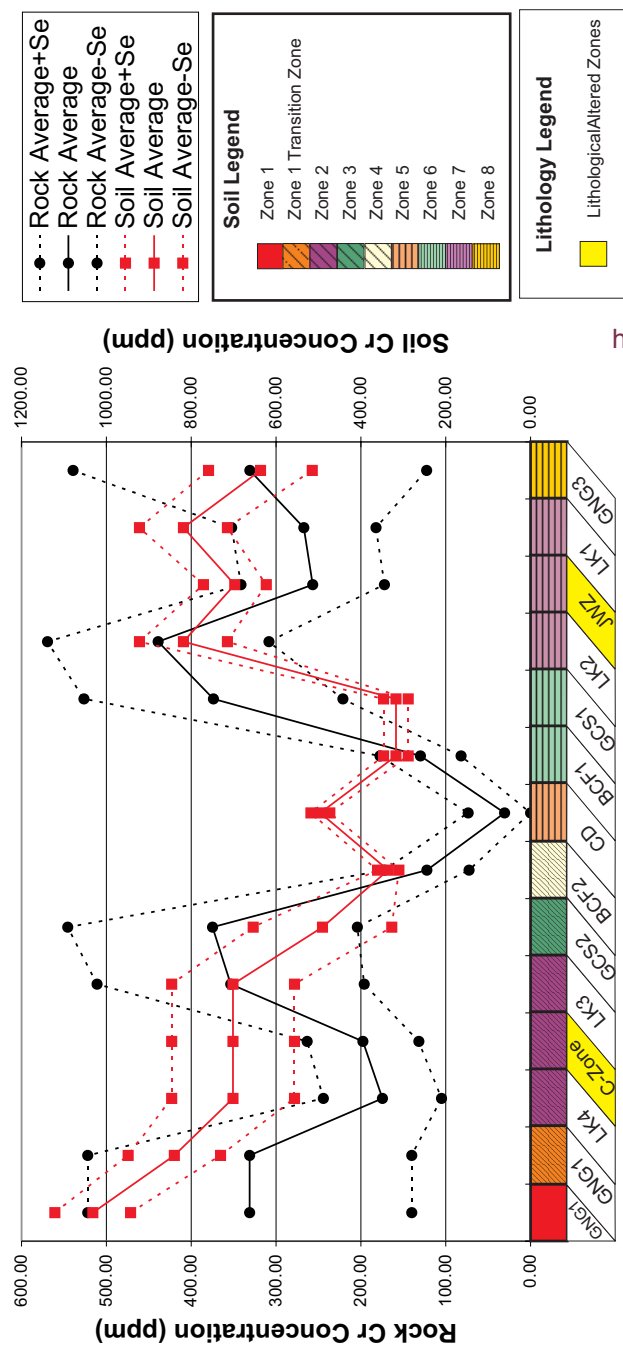
Fig.24 ...continued

### Lithology and Fine Fraction Soil Profiles for Cr - A-Horizon

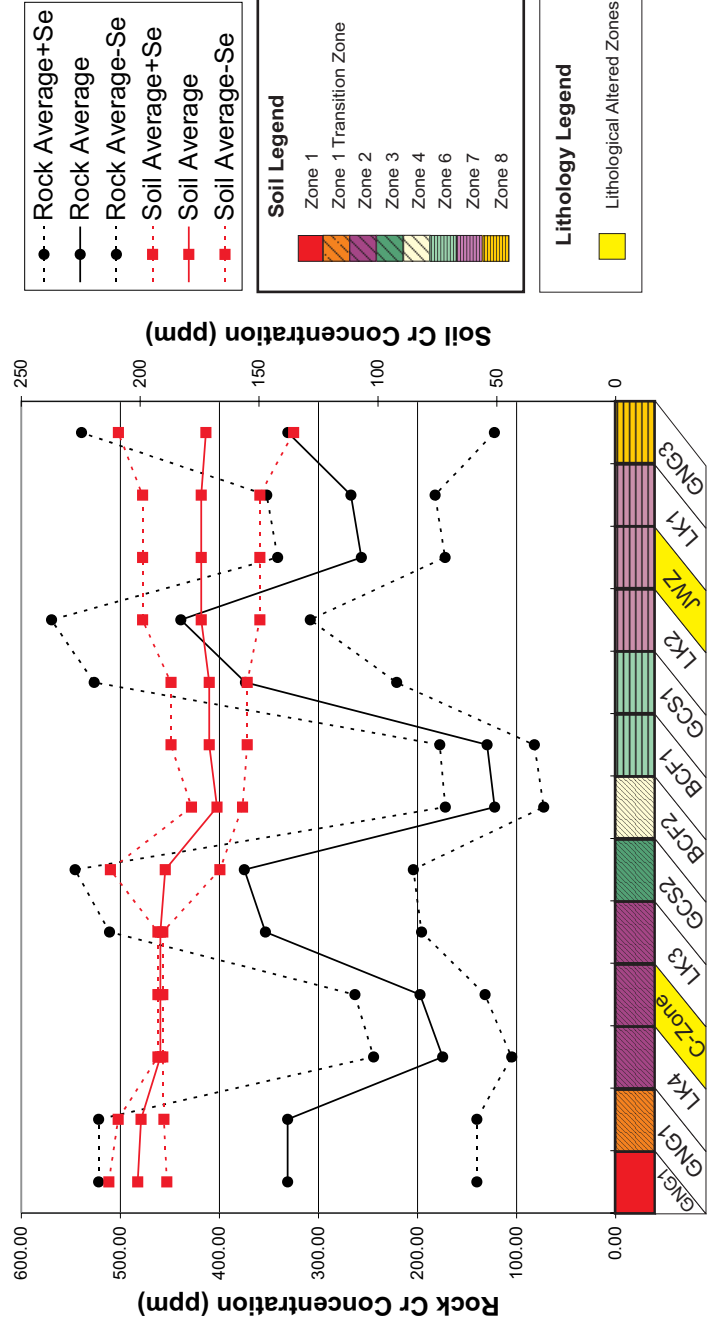


<http://scholar.sun.ac.za/>

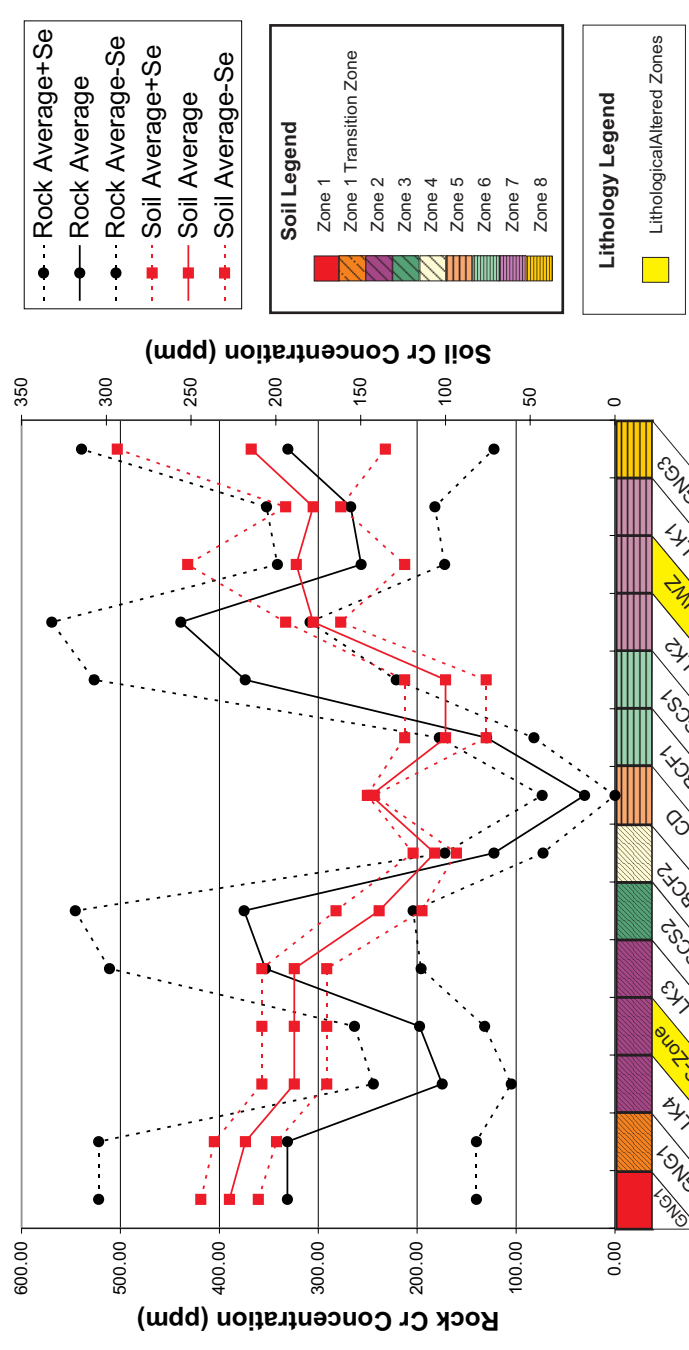
### Lithology and Fine Fraction Soil Profiles for Cr - C-Horizon



### Lithology and Medium Fraction Soil Profiles for Cr - A-Horizon



### Lithology and Medium Fraction Soil Profiles for Cr - C-Horizon



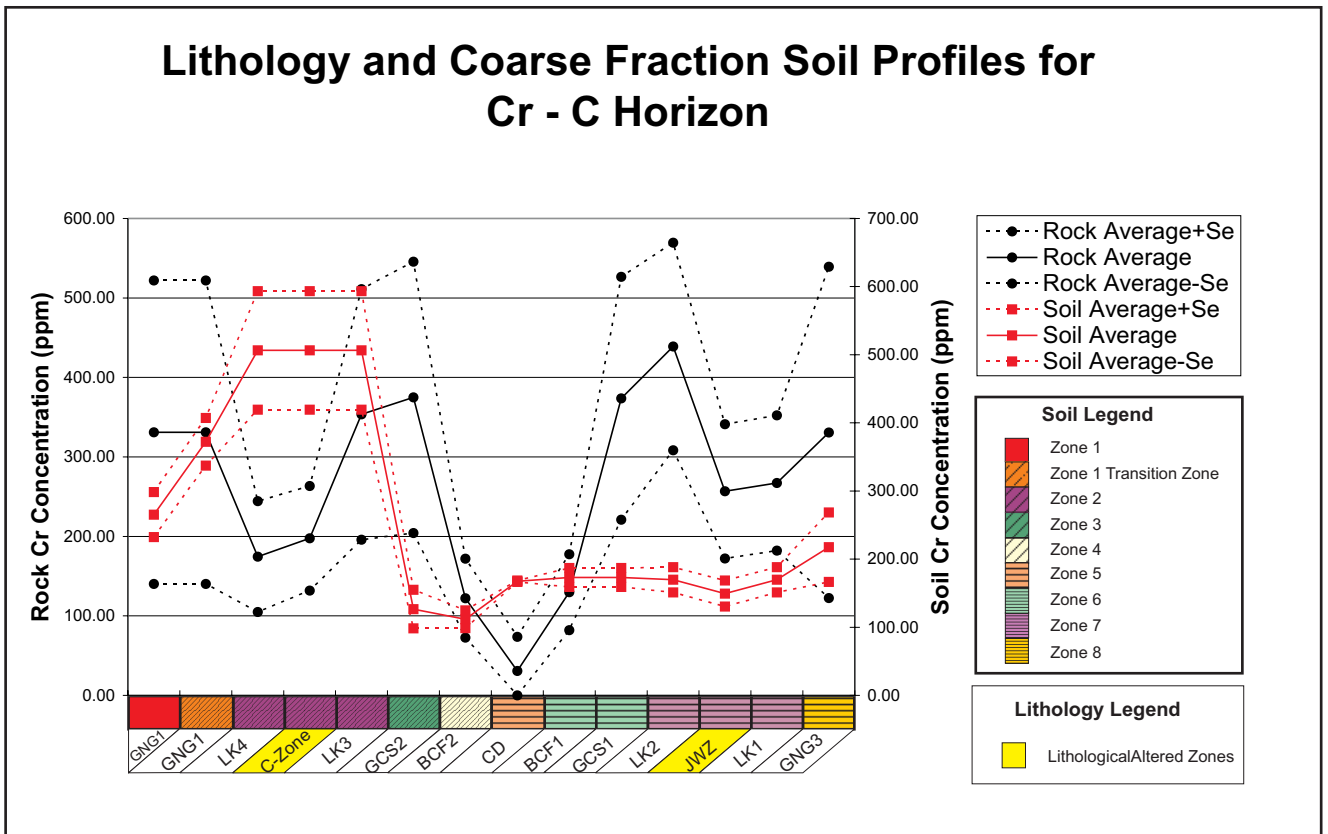
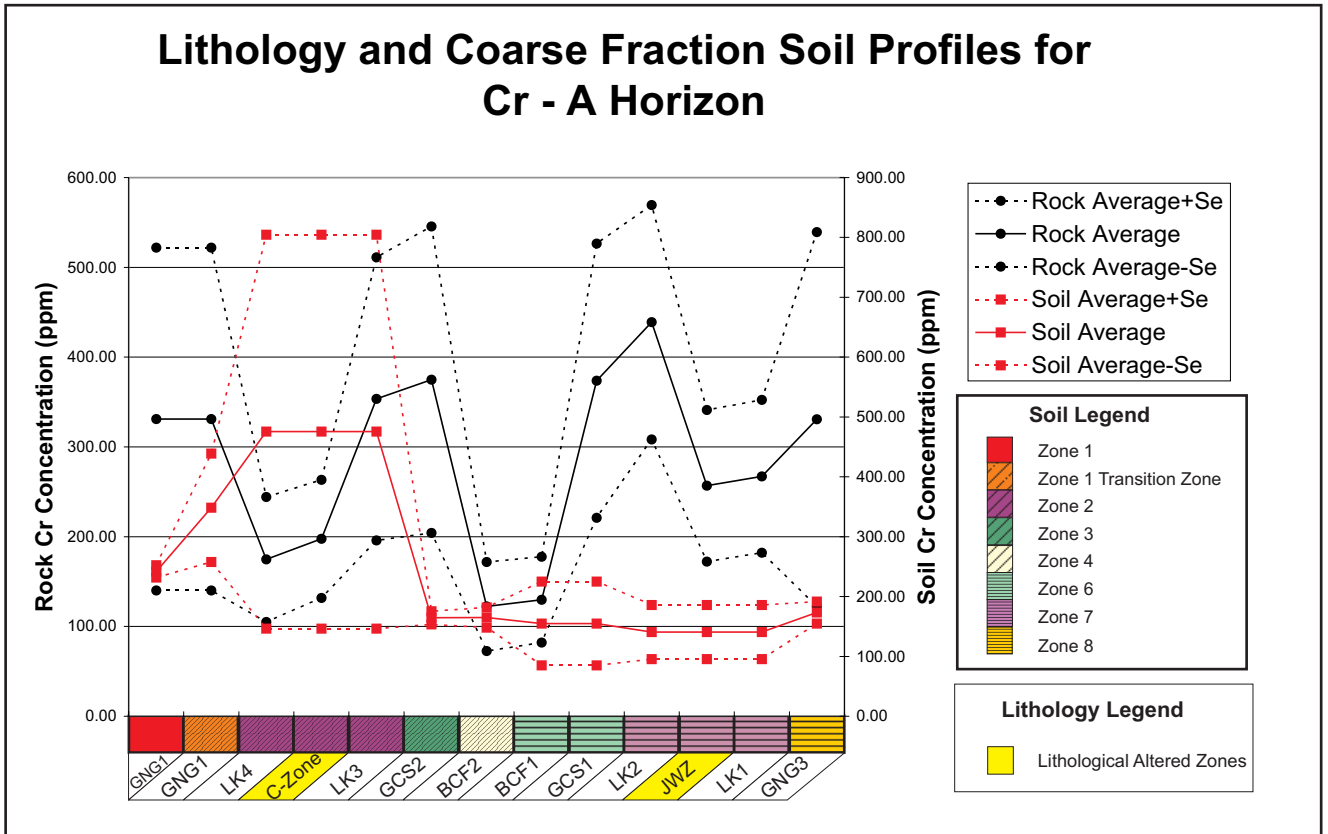
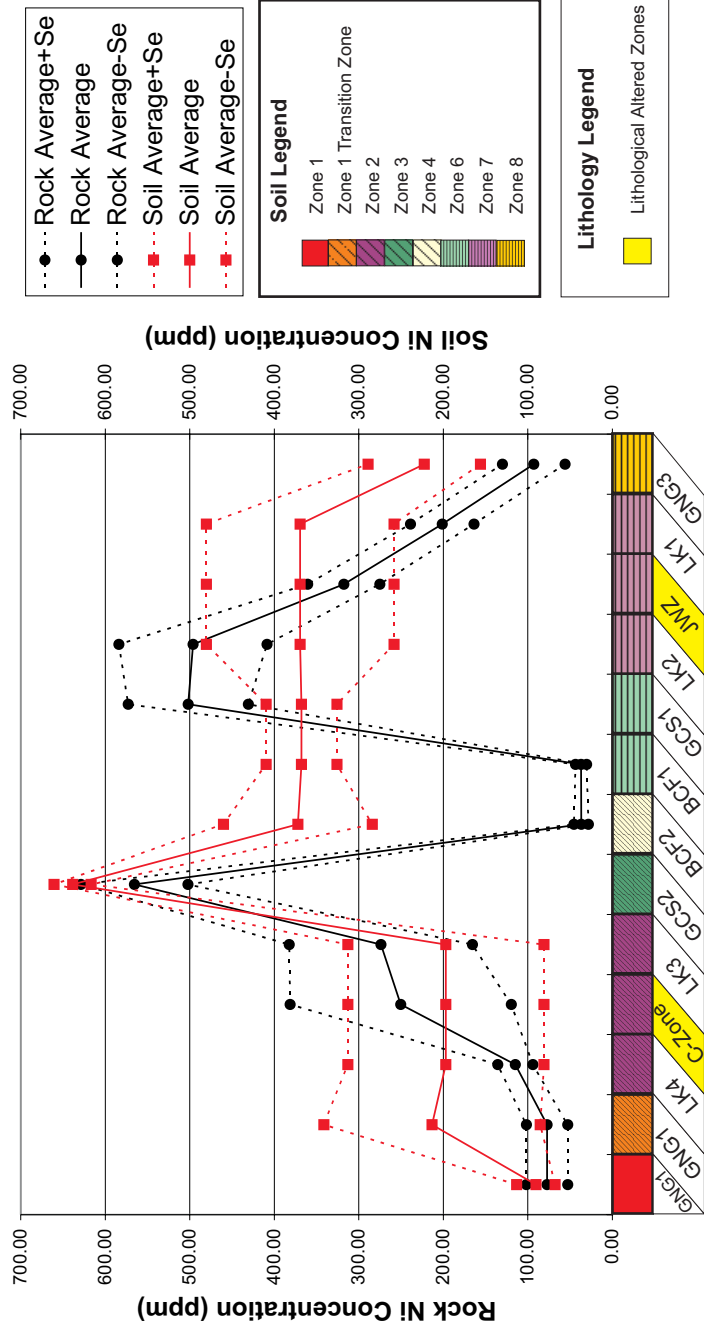
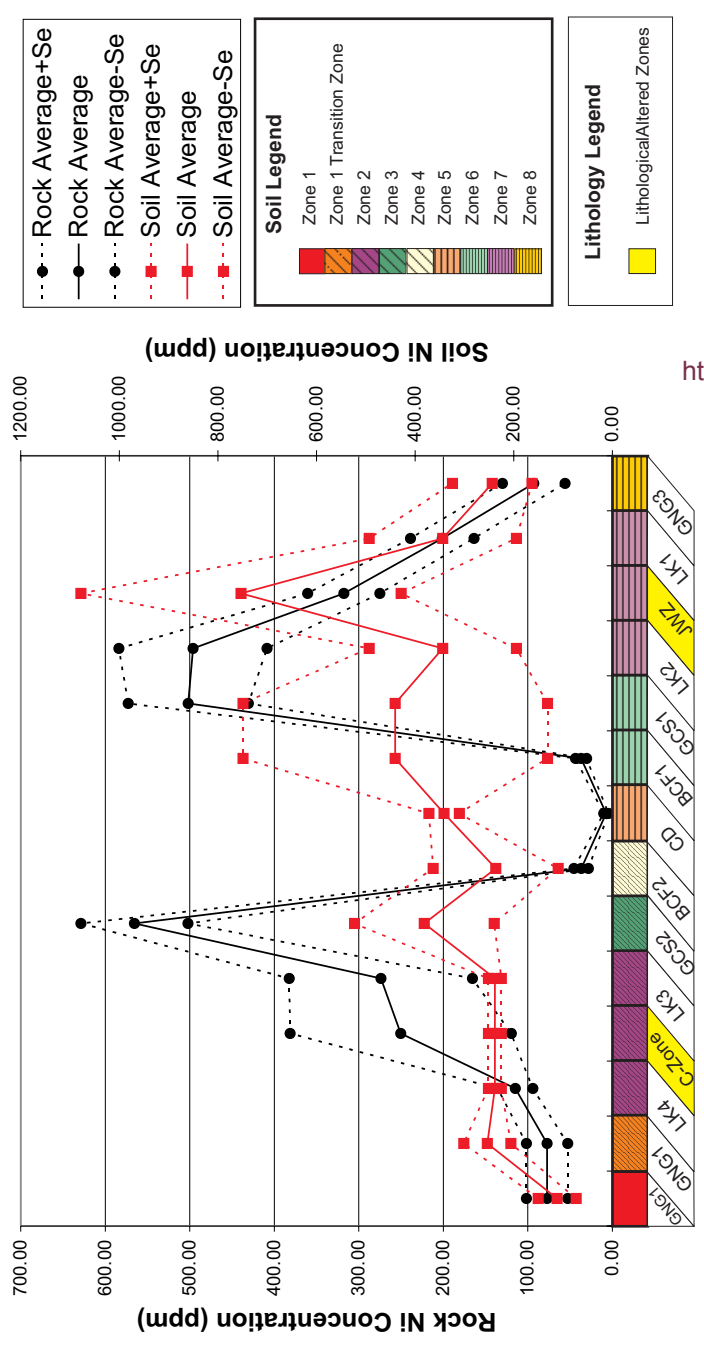


Fig.24 ...continued

### Lithology and Fine Fraction Soil Profiles for Ni - A-Horizon

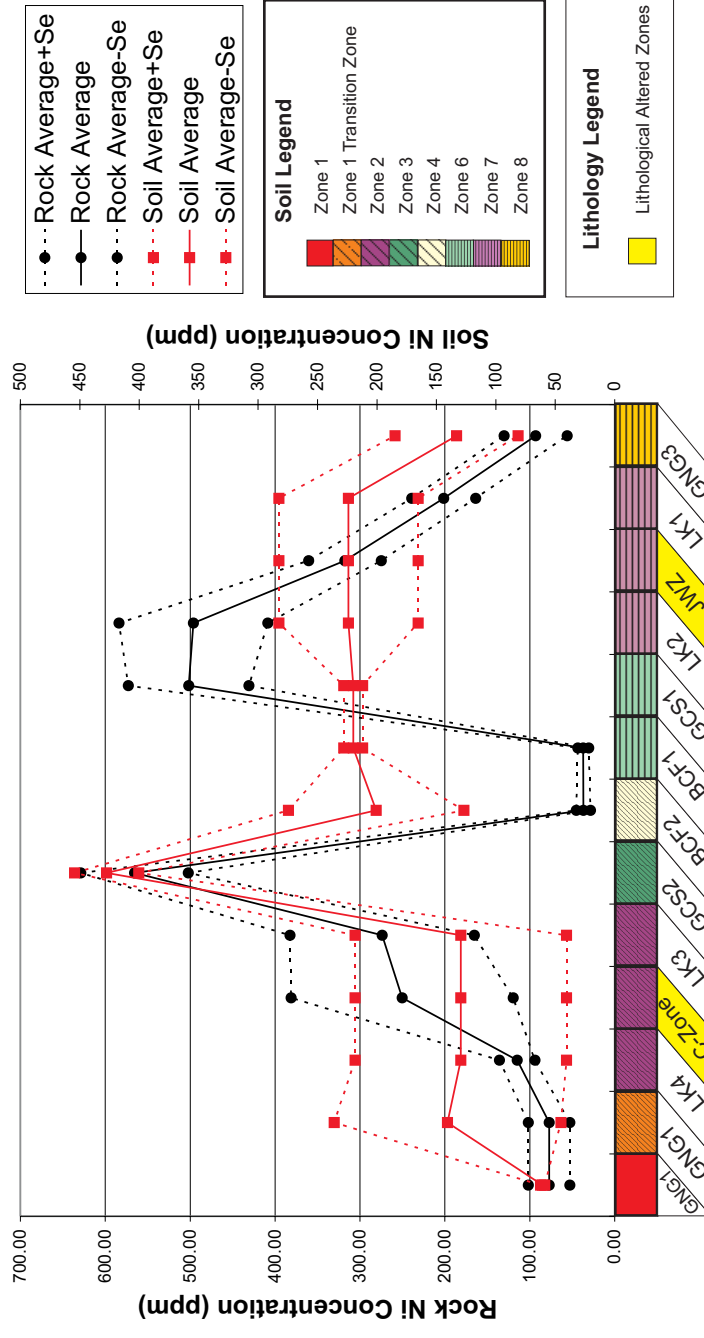


### Lithology and Fine Fraction Soil Profiles for Ni - C-Horizon

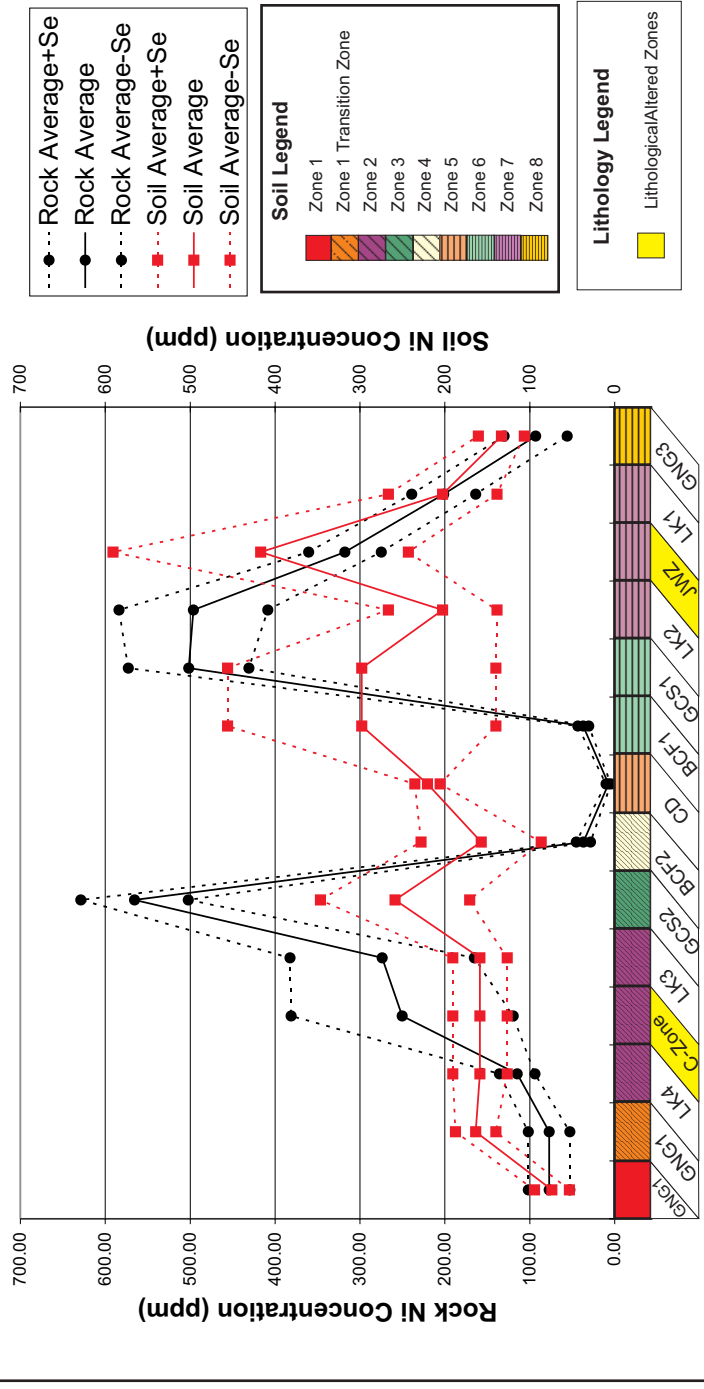


<http://scholar.sun.ac.za/>

### Lithology and Medium Fraction Soil Profiles for Ni - A-Horizon



### Lithology and Medium Fraction Soil Profiles for Ni - C-Horizon



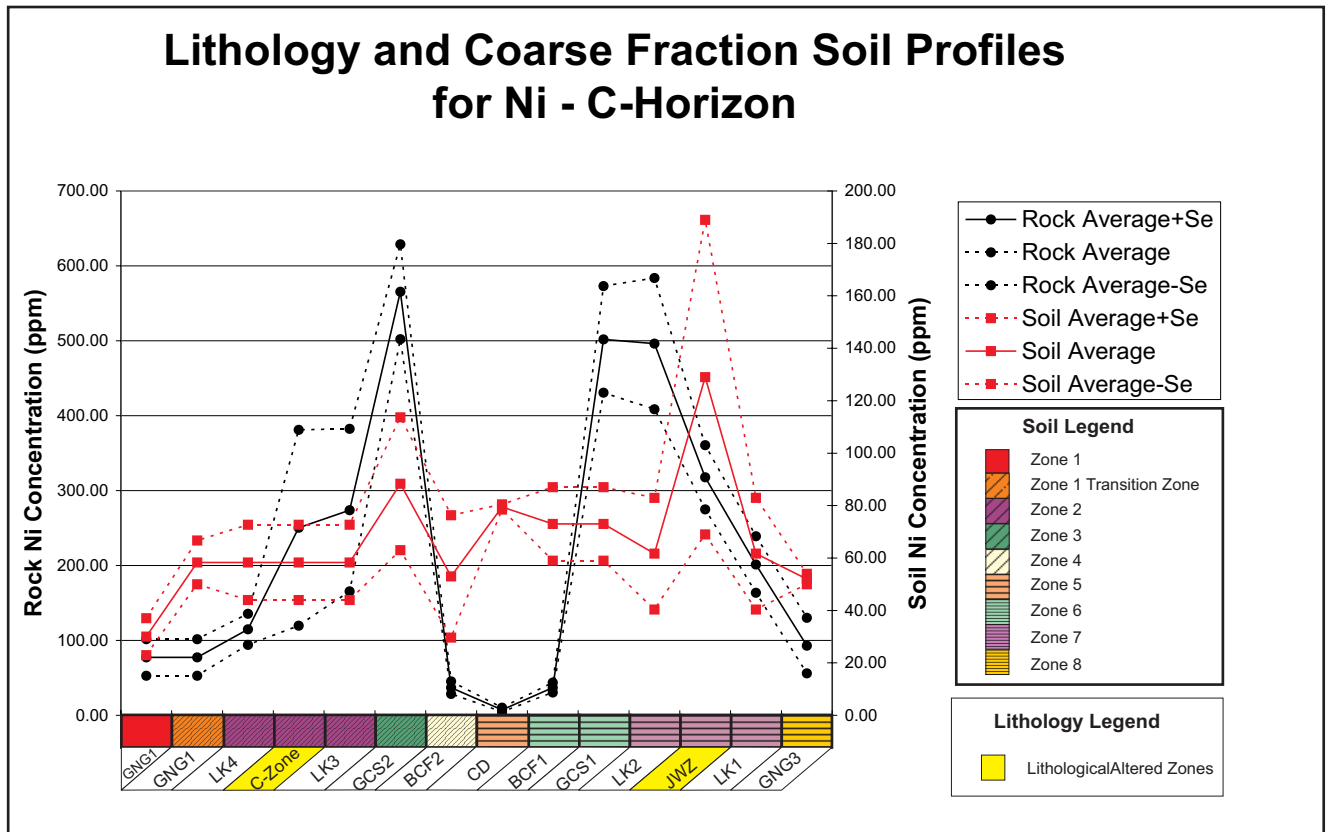
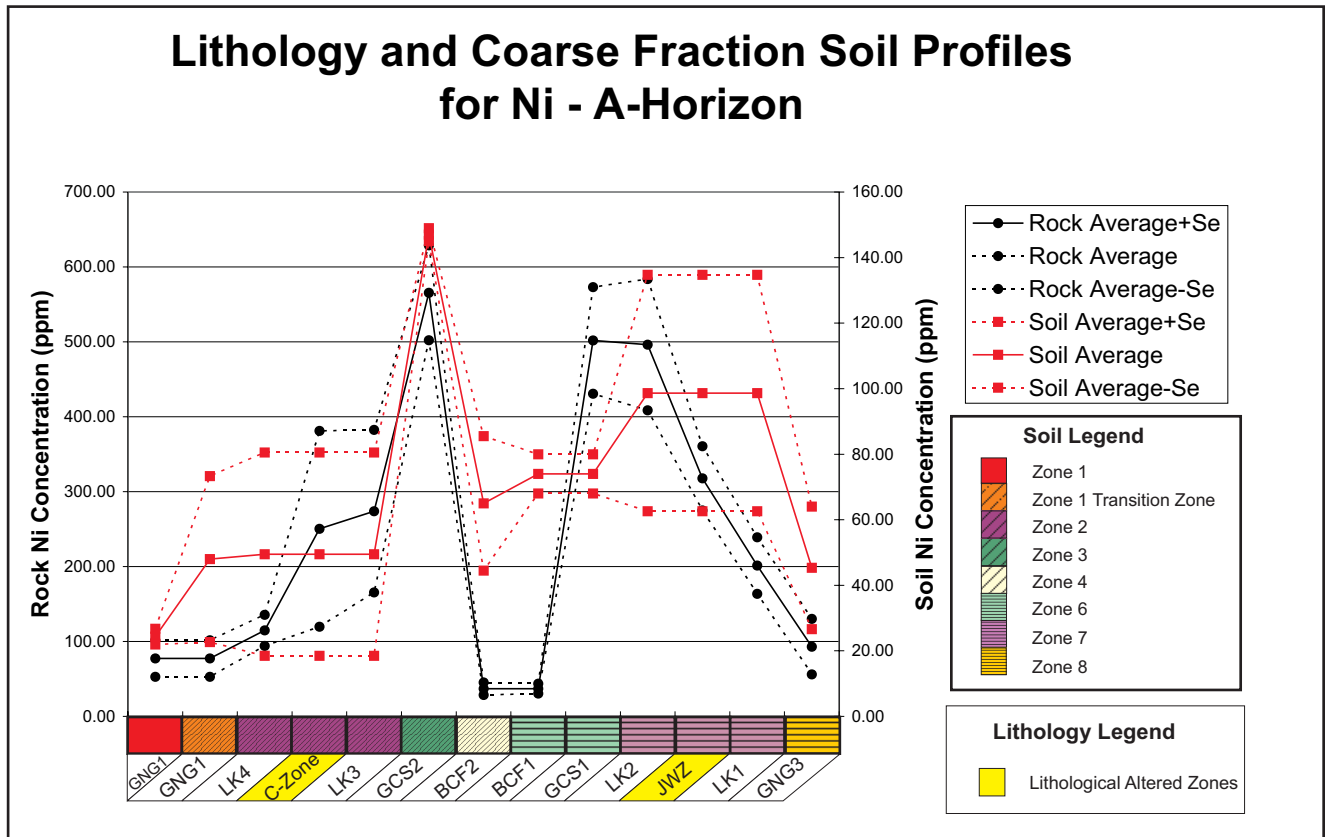
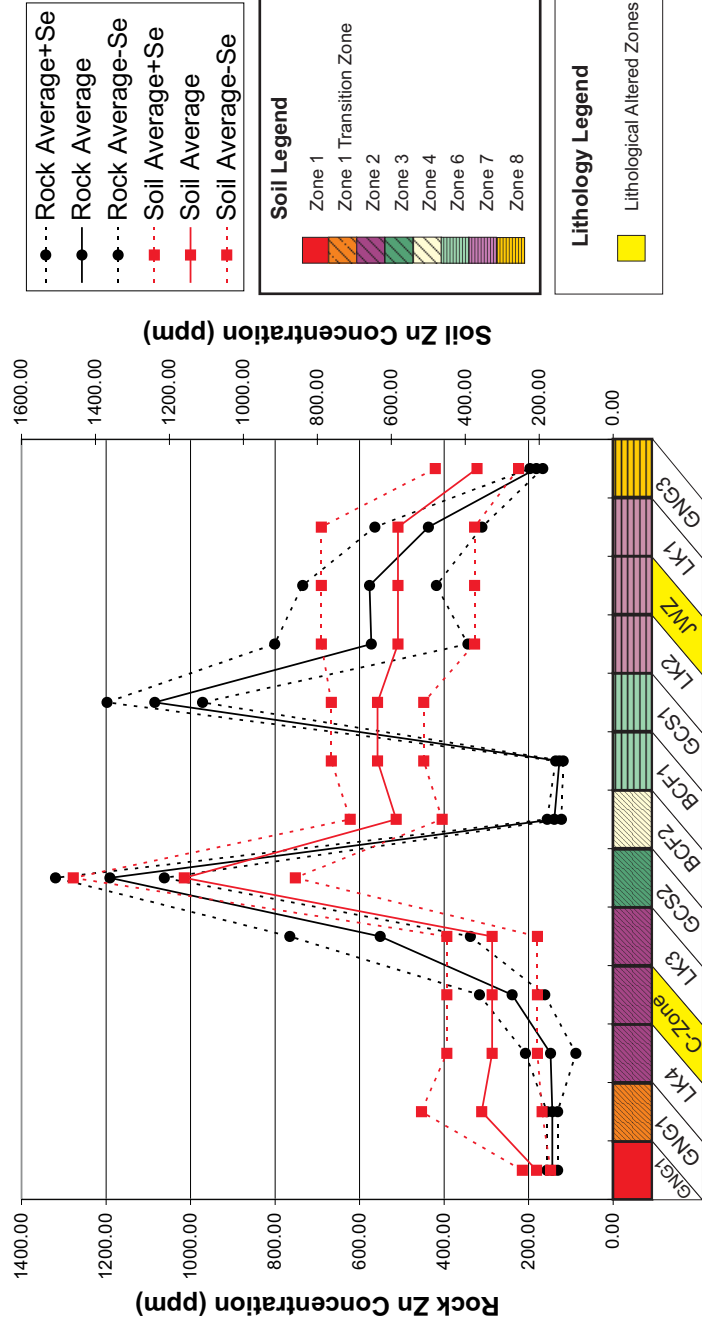


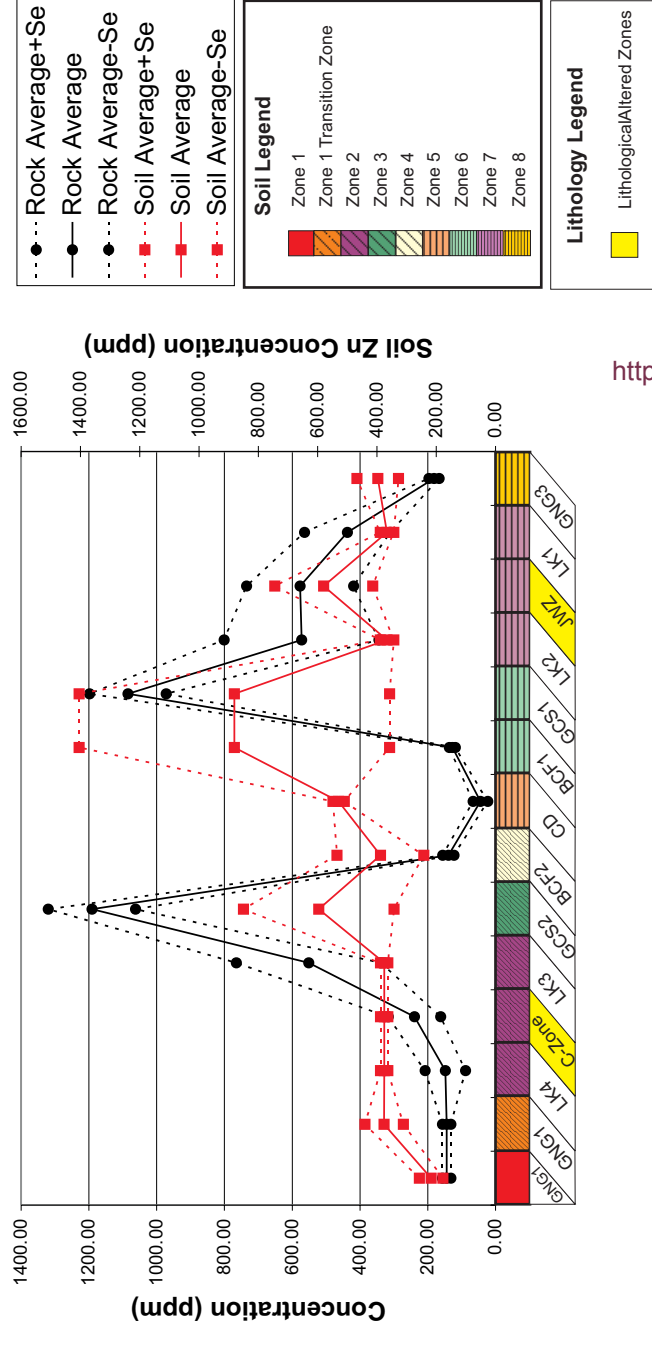
Fig.24 ...continued

### Lithology and Fine Fraction Soil Profiles for Zn - A-Horizon

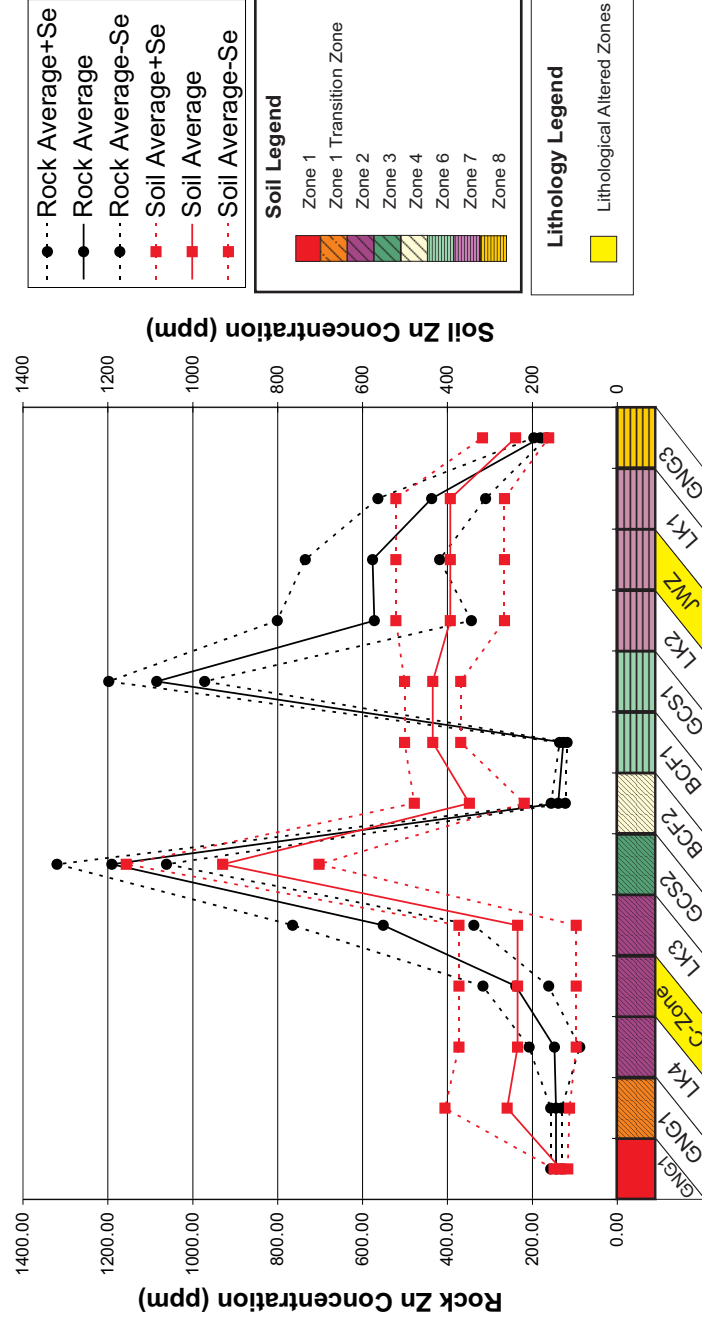


<http://scholar.sun.ac.za>

### Lithology and Fine Fraction Soil Profiles for Zn - C-Horizon



### Lithology and Medium Fraction Soil Profiles for Zn - A-Horizon



### Lithology and Medium Fraction Soil Profiles for Zn - C-Horizon

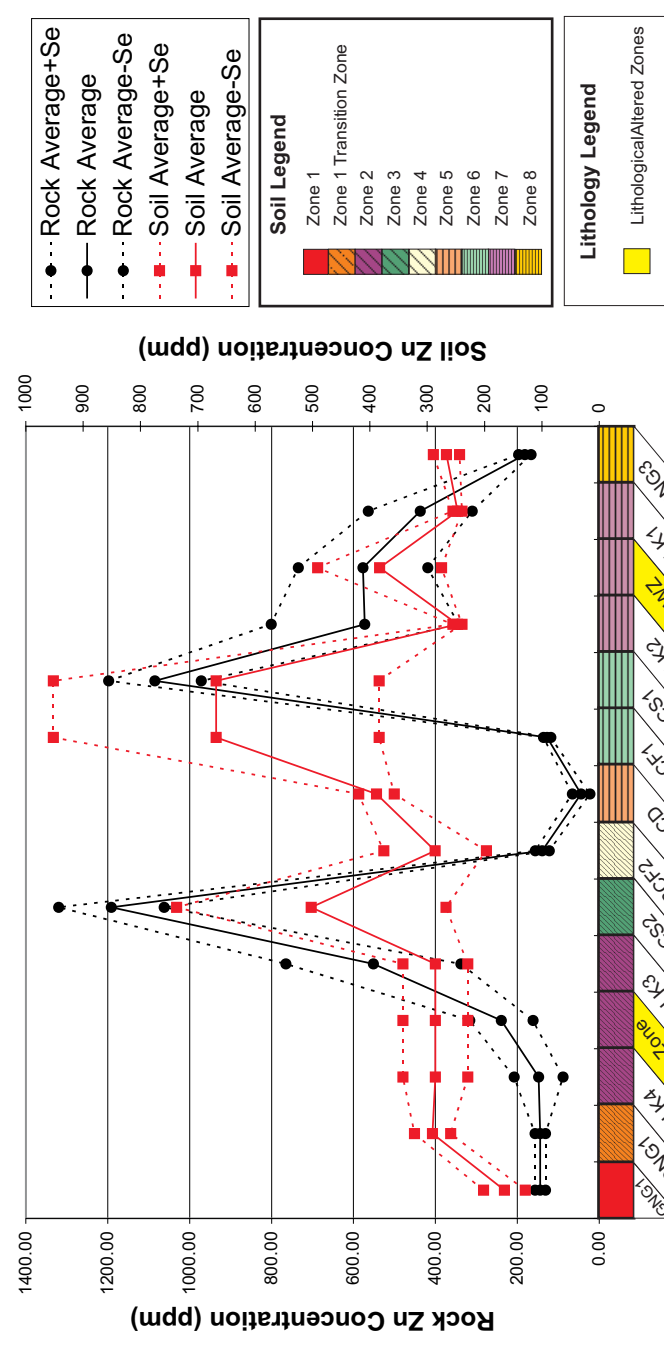


Fig.24 ....continued

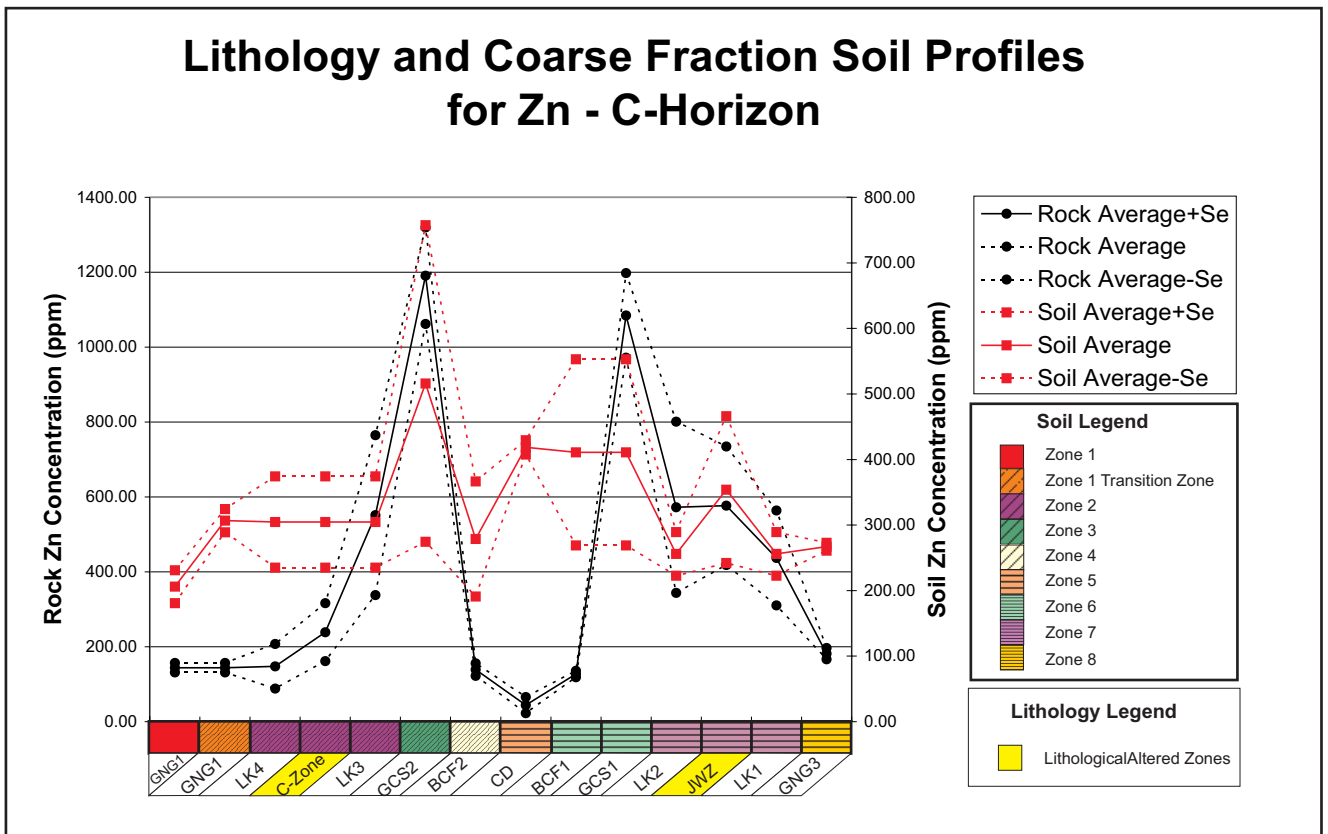
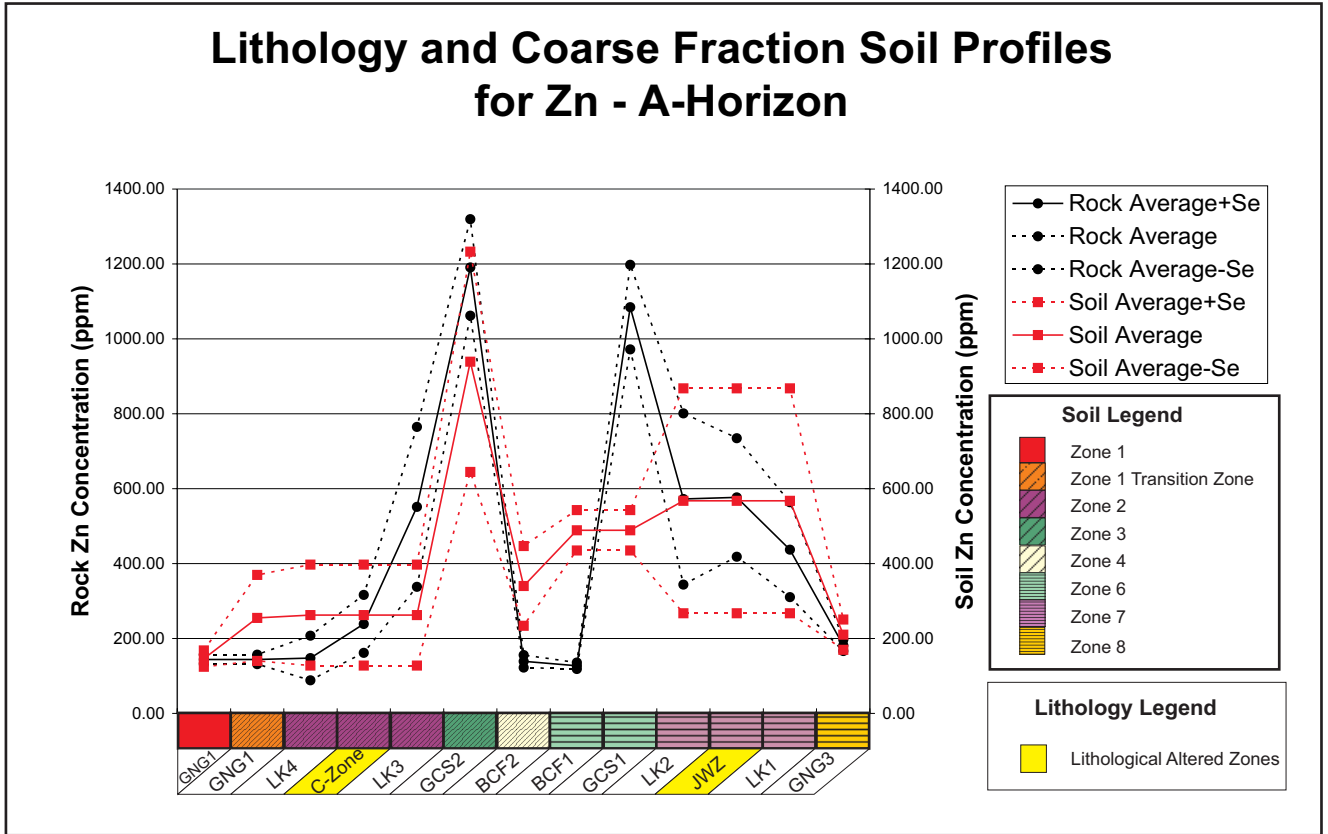
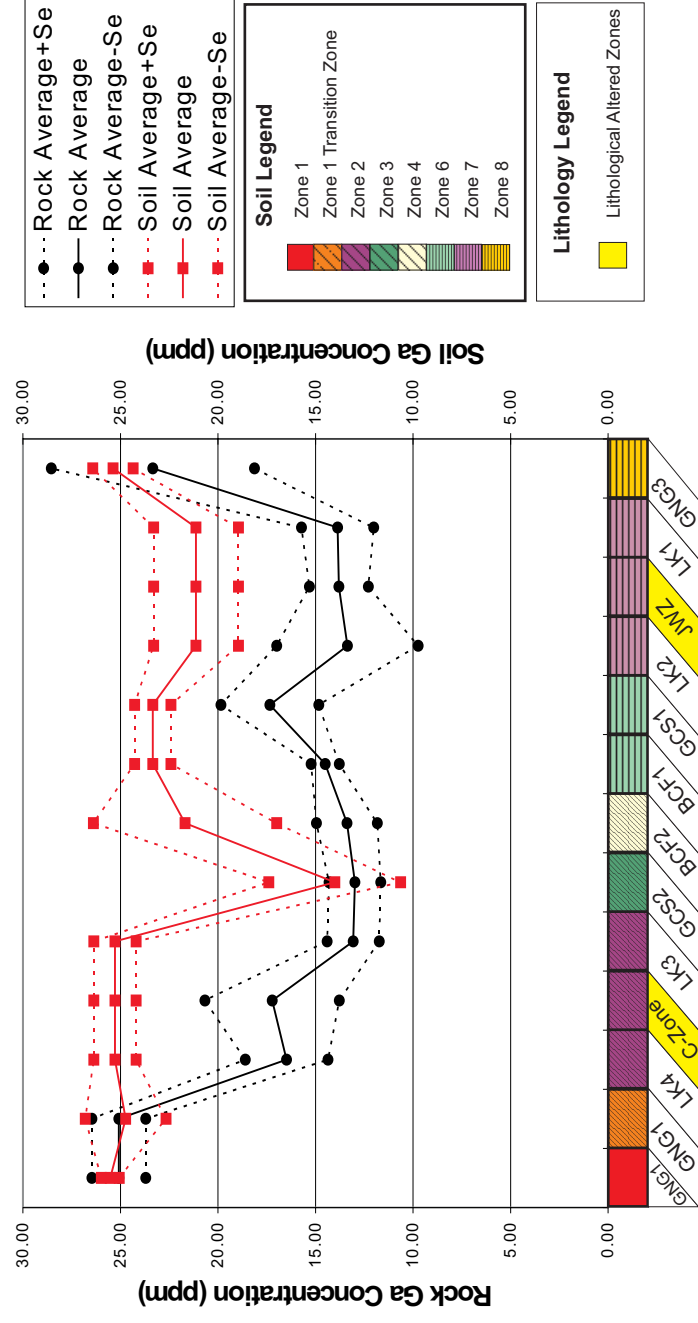


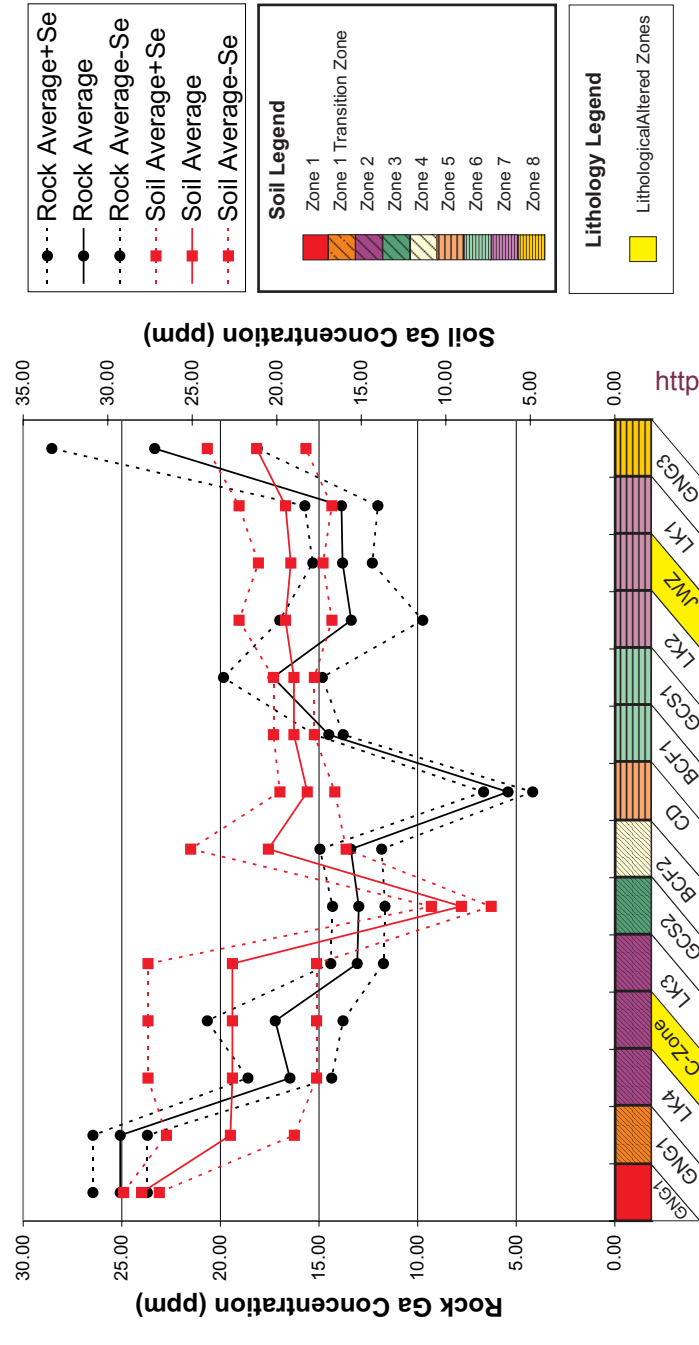
Fig.24 ...continued



### Lithology and Fine Fraction Soil Profiles for Ga - A-Horizon

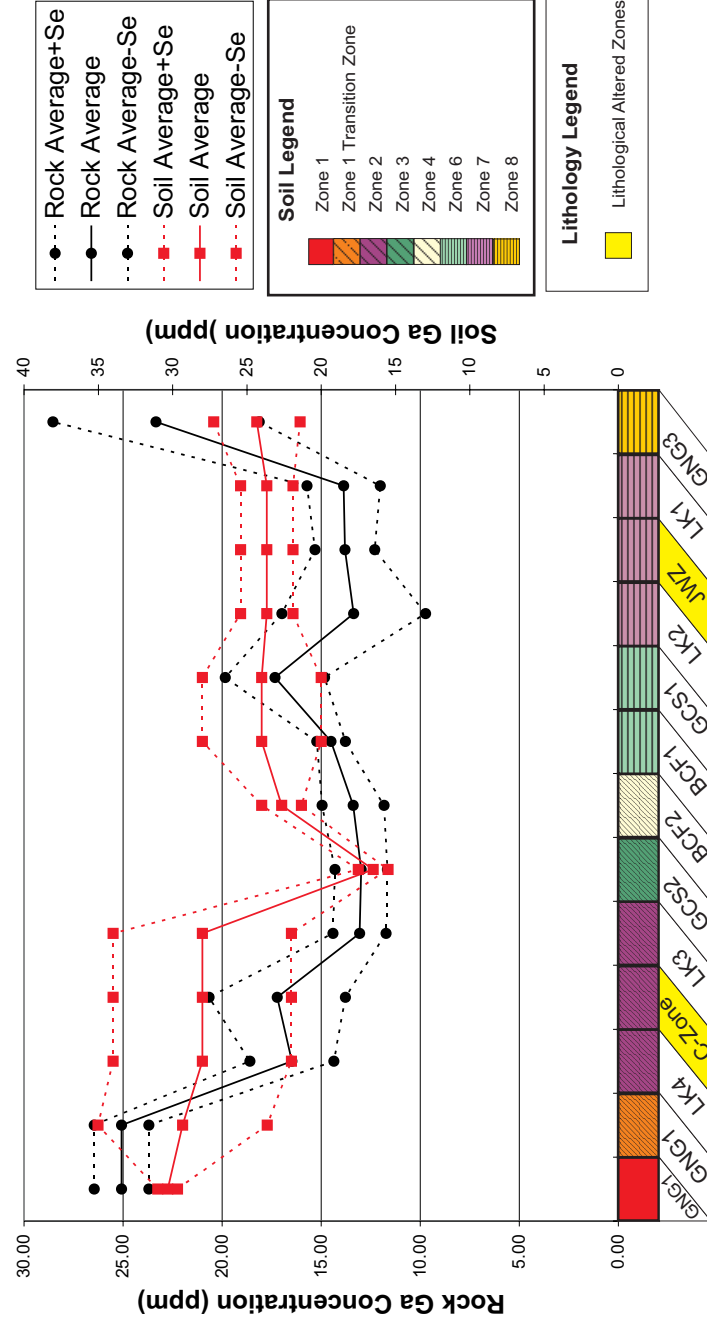


### Lithology and Fine Fraction Soil Profiles for Ga - C-Horizon

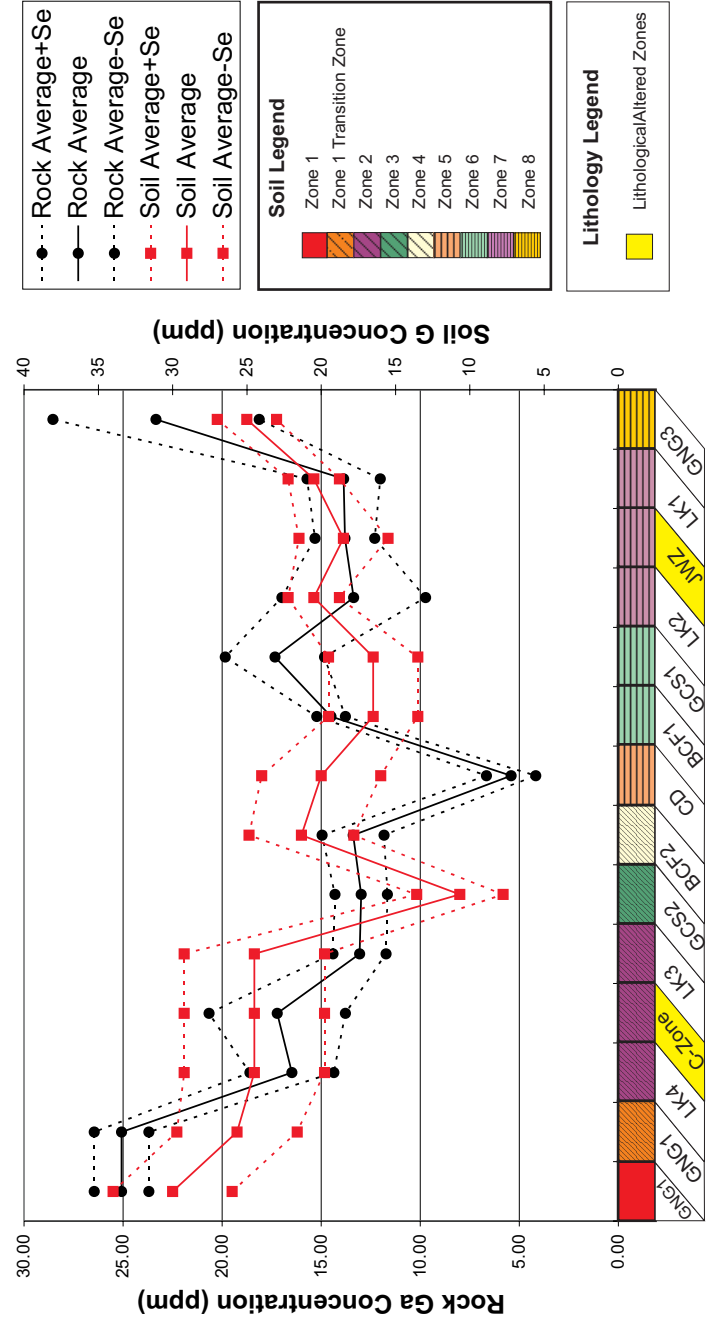


<http://scholar.sun.ac.za/>

### Lithology and Medium Fraction Soil Profiles for Ga - A-Horizon



### Lithology and Medium Fraction Soil Profiles for Ga - C-Horizon



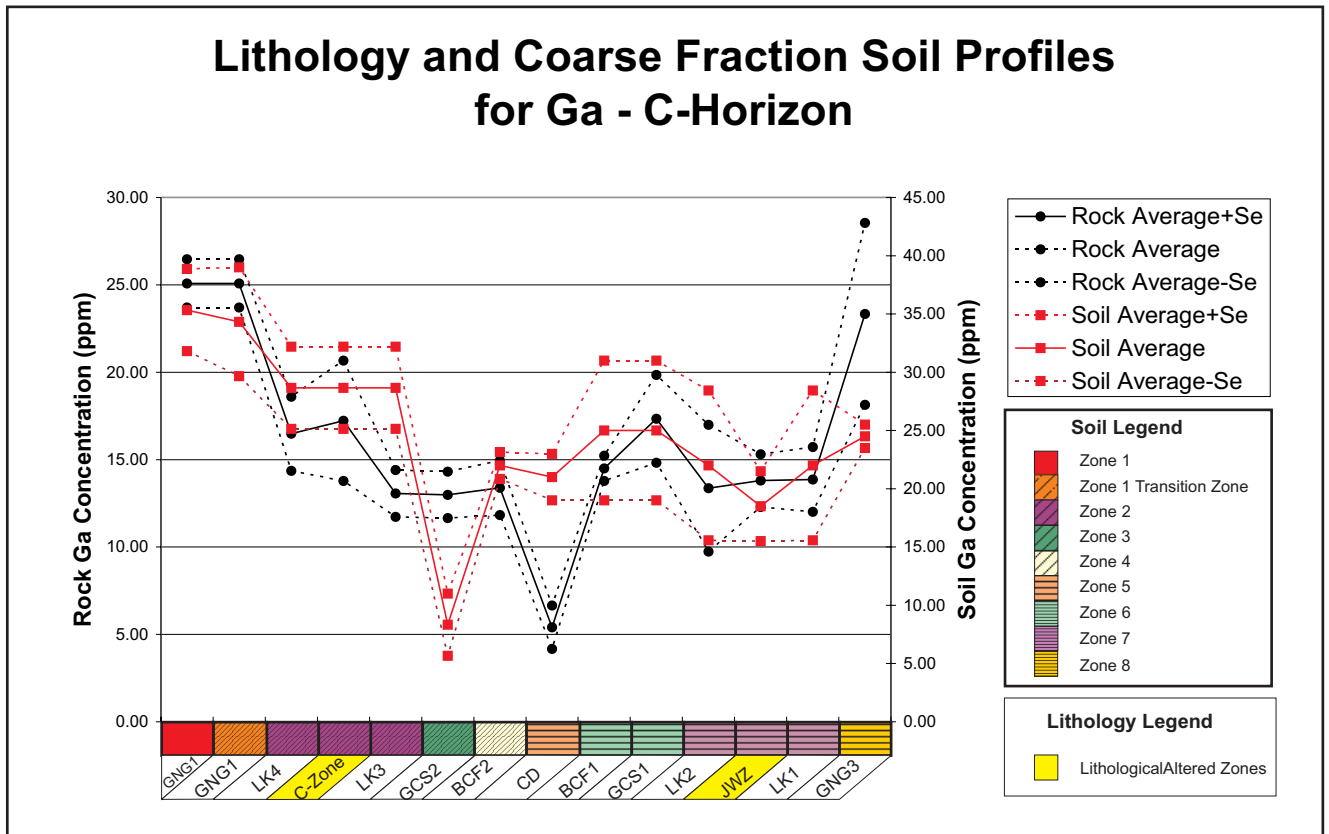
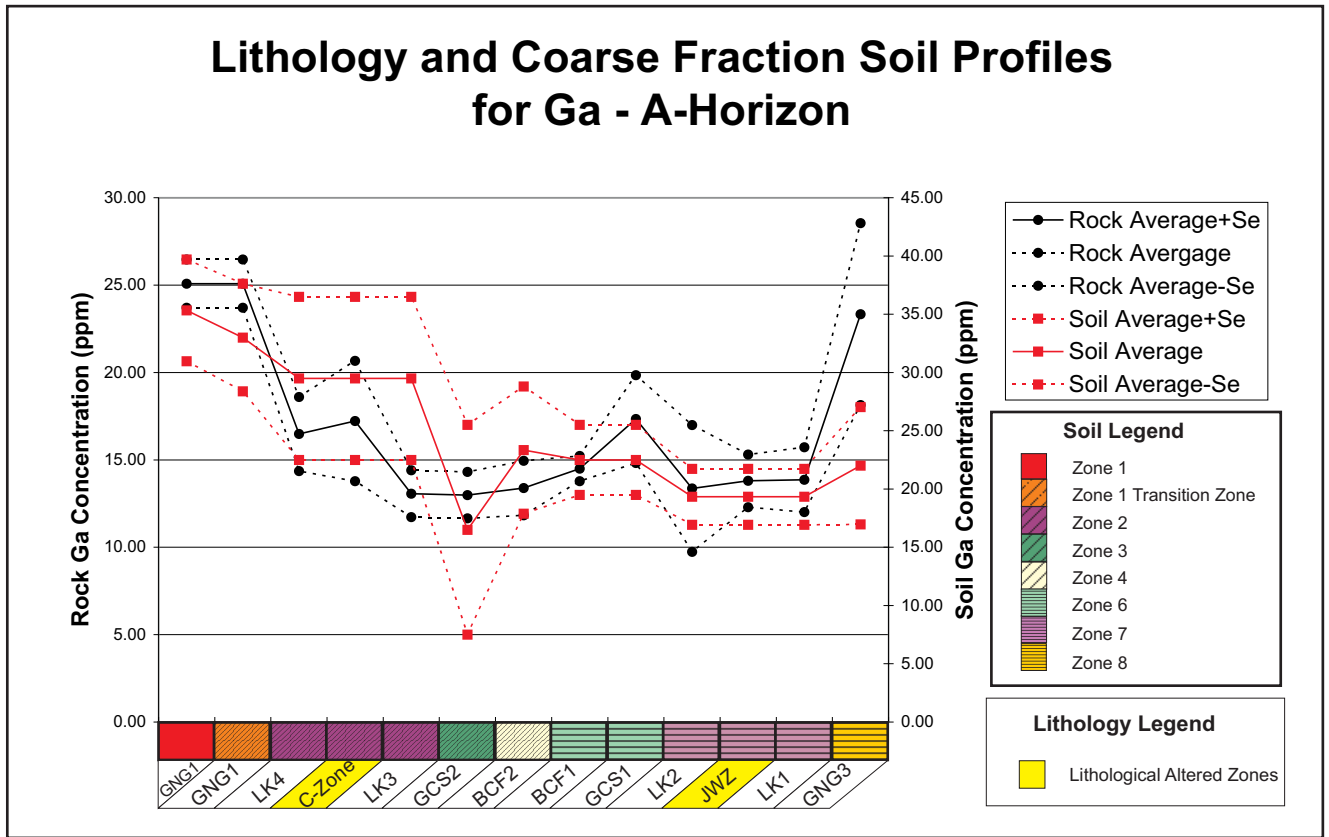
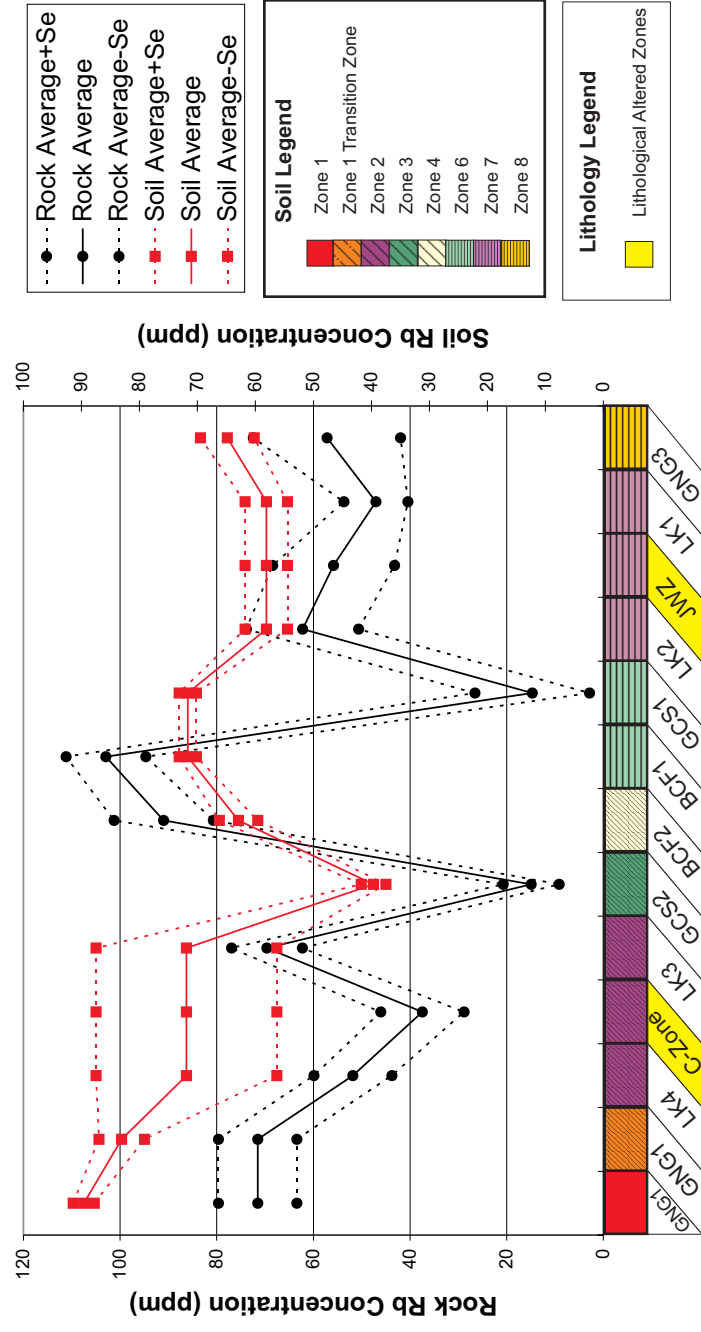
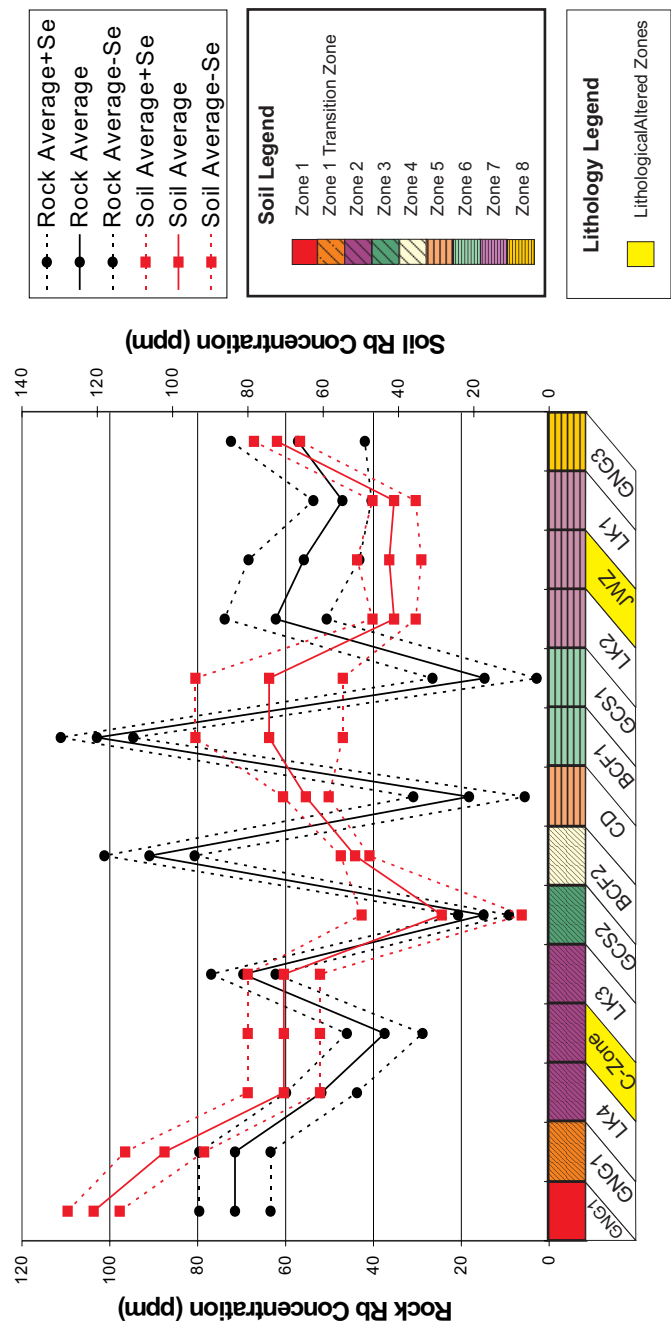


Fig.24 ...continued

### Lithology and Fine Fraction Soil Profiles for Rb - A-Horizon

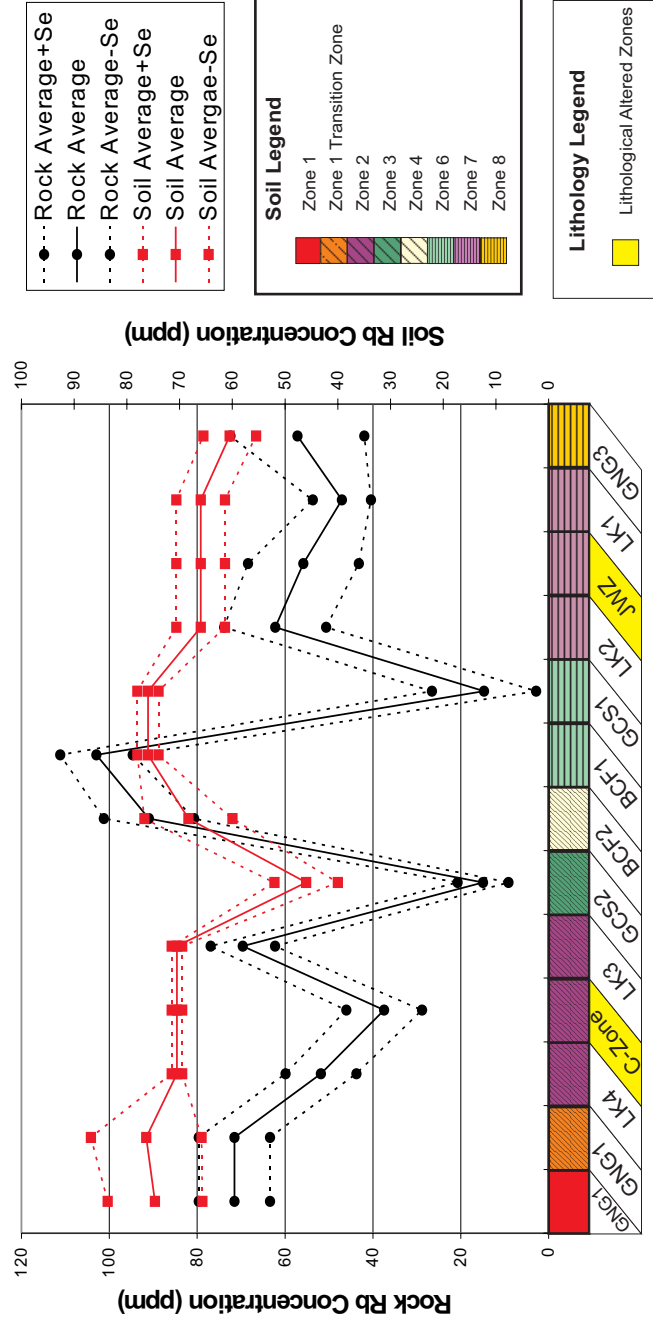


### Lithology and Fine Fraction Soil Profiles for Rb - C-Horizon

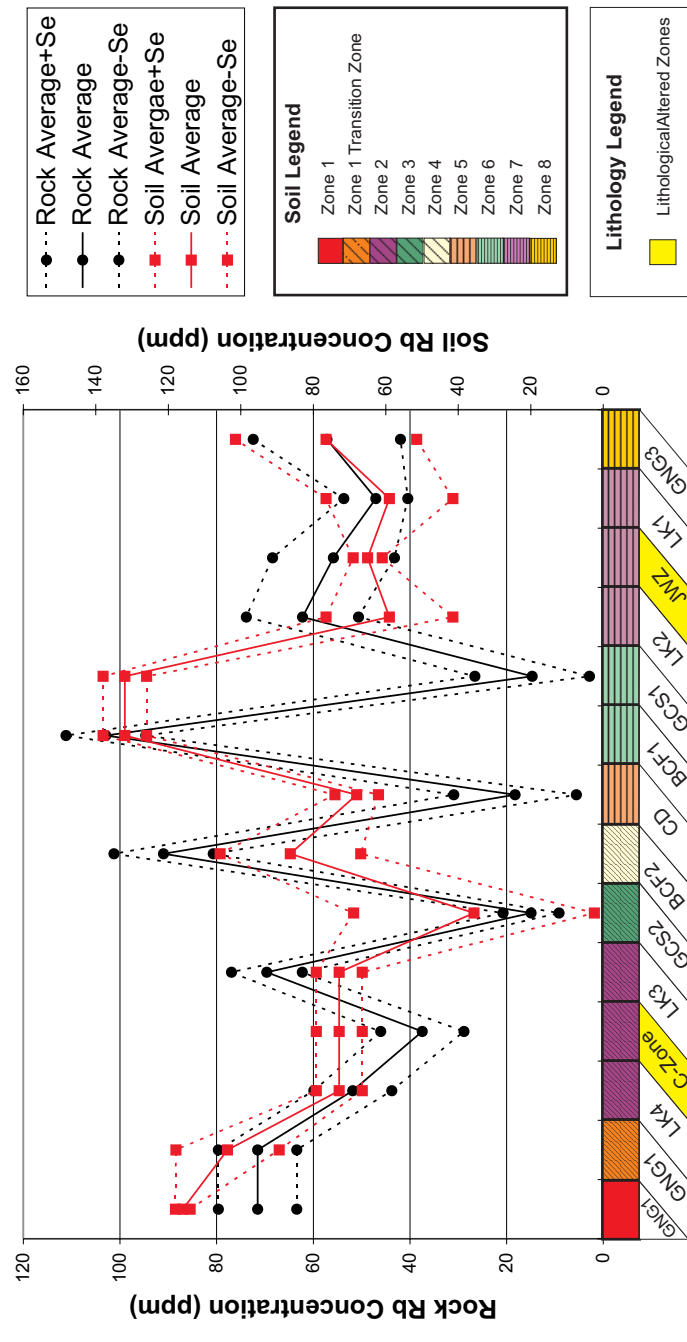


<http://scholar.sun.ac.za/>

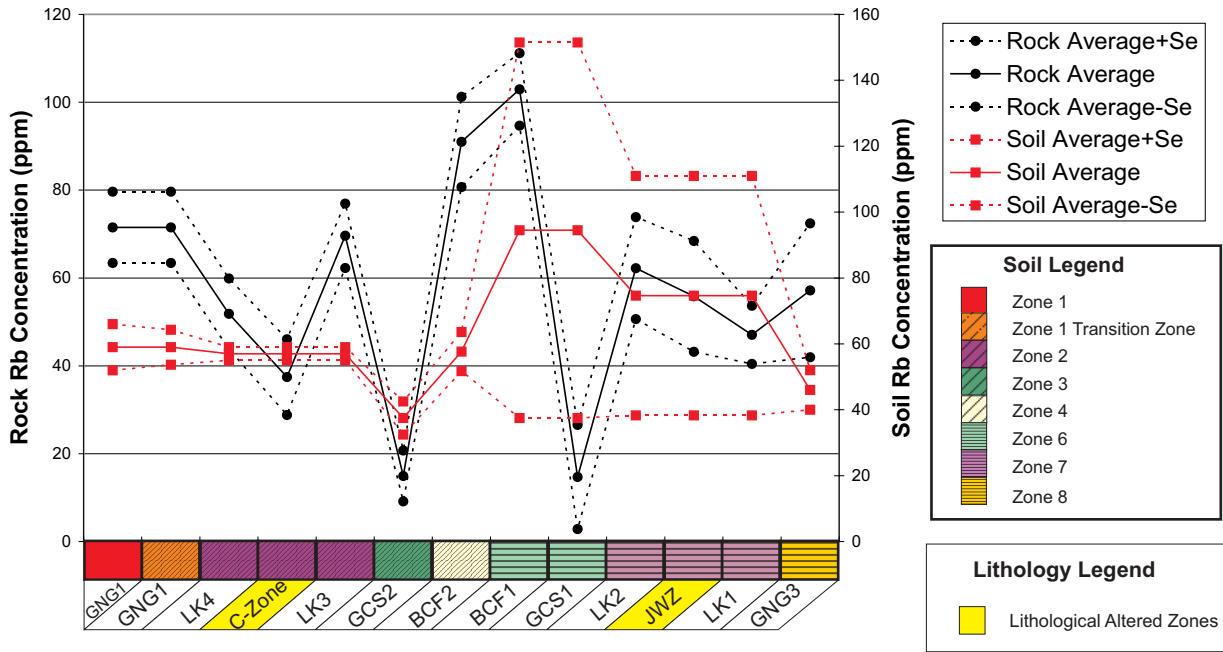
### Lithology and Medium Fraction Soil Profiles for Rb - A-Horizon



### Lithology and Medium Fraction Soil Profiles for Rb - C-Horizon



## Lithology and Coarse Fraction Soil Profiles for Rb - A-Horizon



## Lithology and Coarse Fraction Soil Profiles for Rb - C-Horizon

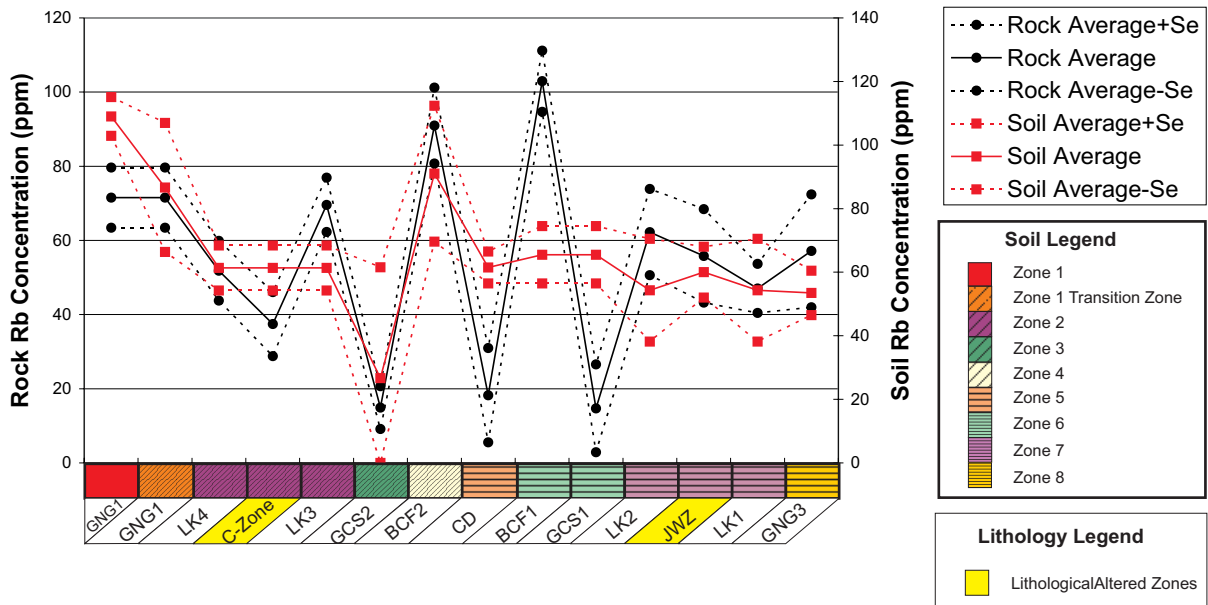
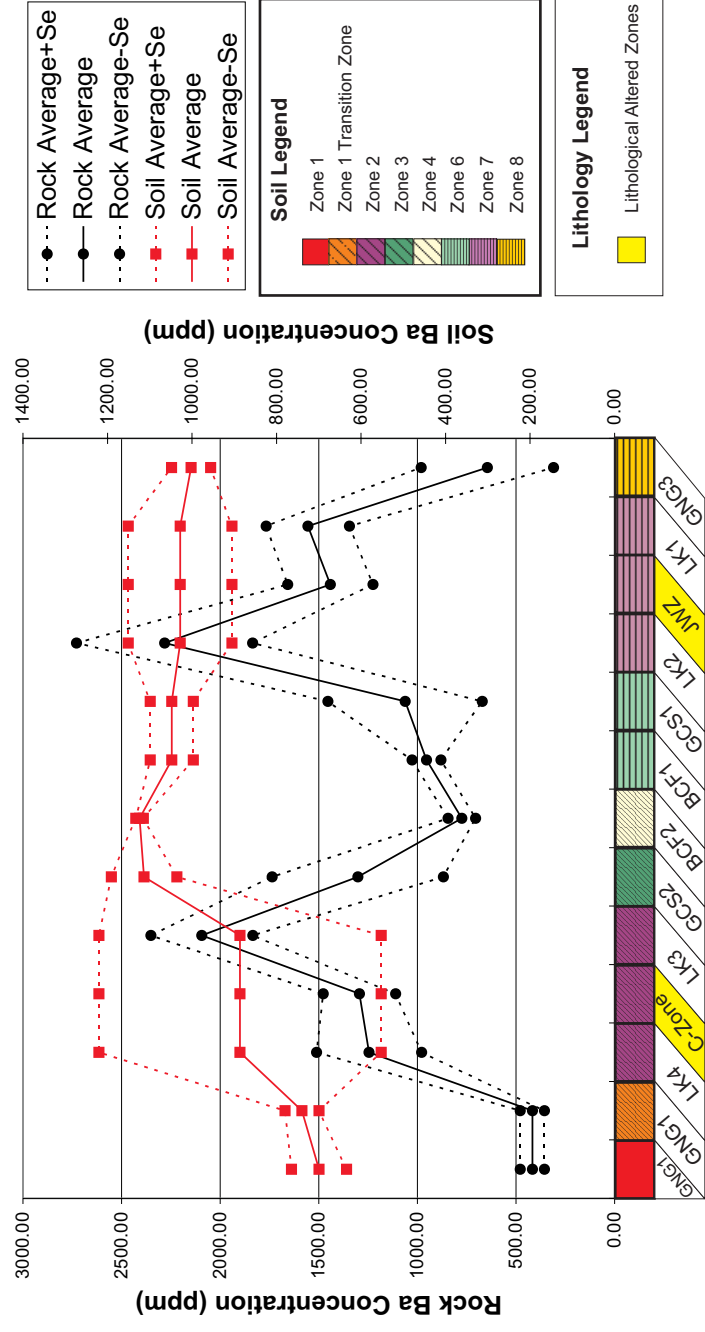
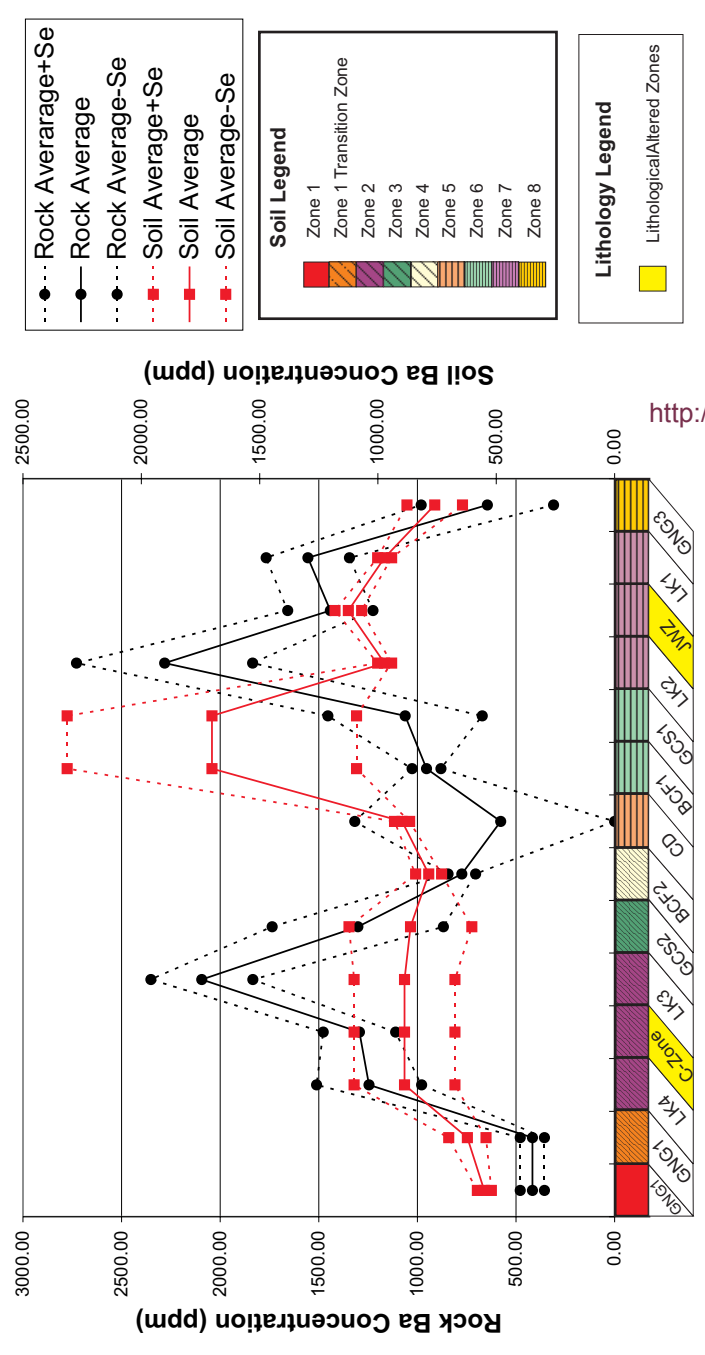


Fig.24 ...continued

### Lithology and Fine Fraction Soil Profiles for Ba - A-Horizon

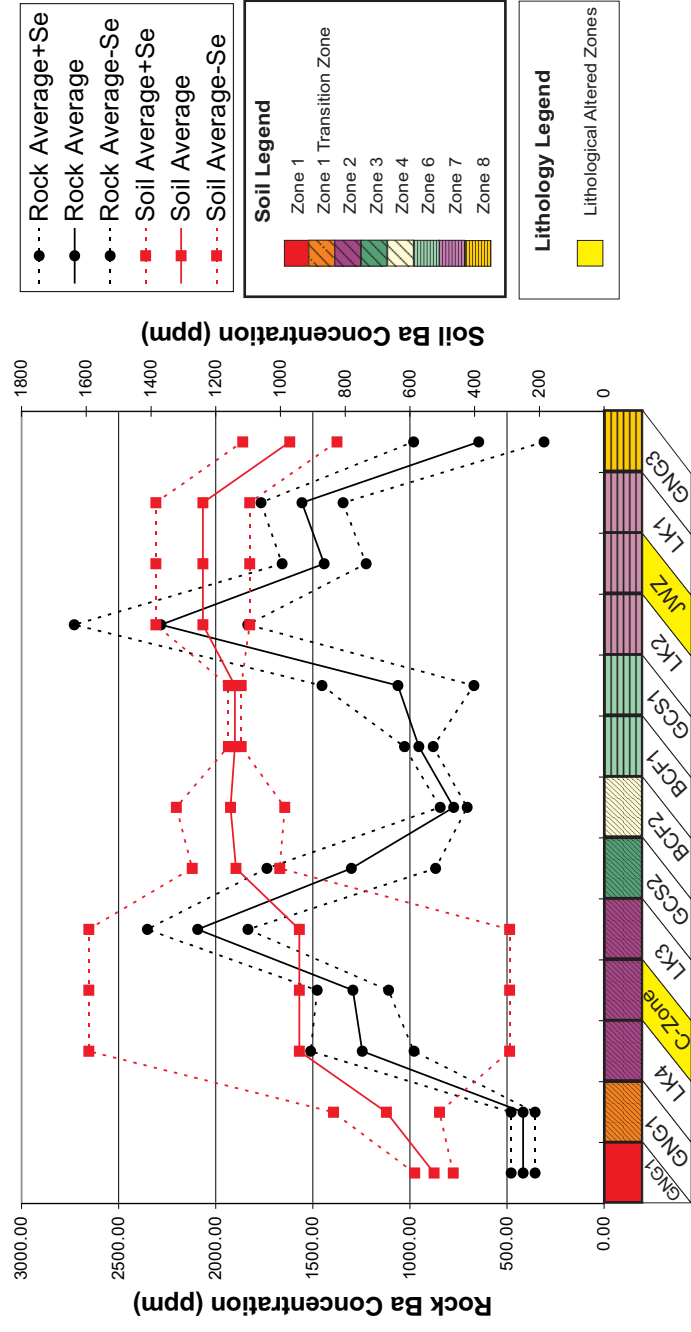


### Lithology and Fine Fraction Soil Profiles for Ba - C-Horizon

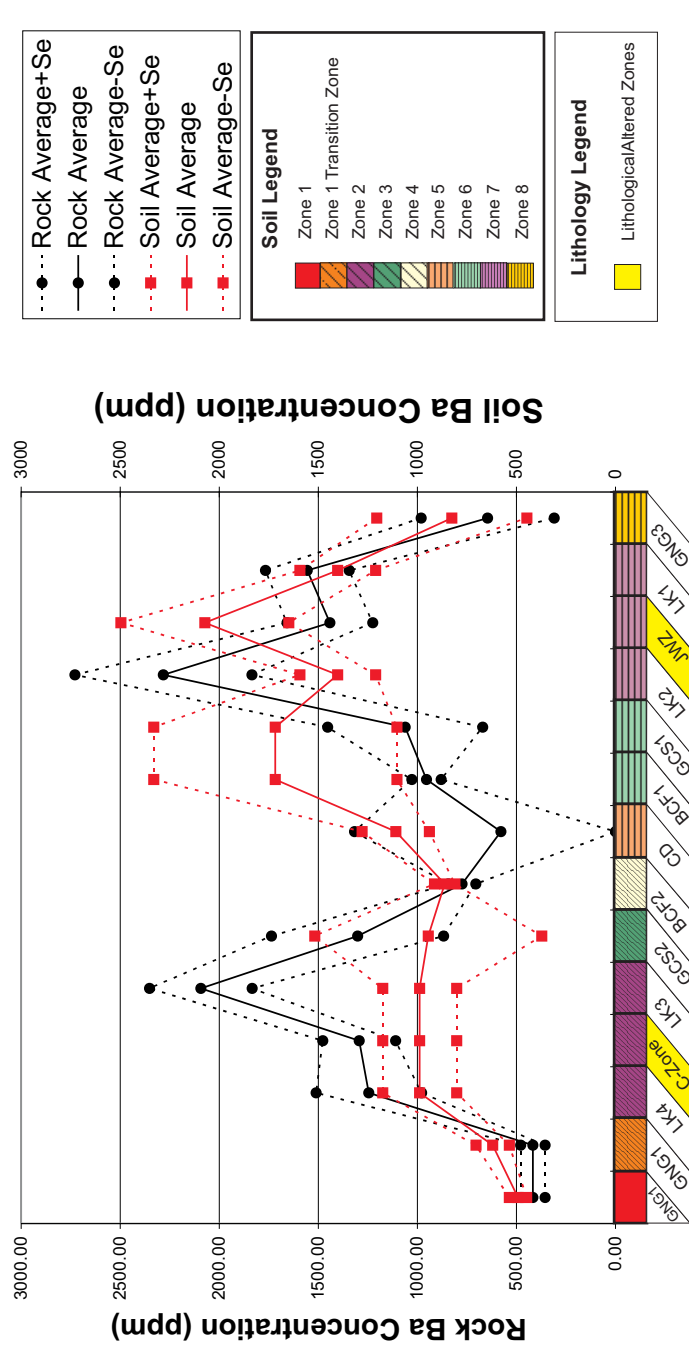


<http://scholar.sun.ac.za/>

### Lithology and Medium Fraction Soil Profiles for Ba - A-Horizon



### Lithology and Medium Fraction Soil Profiles for Ba - C-Horizon



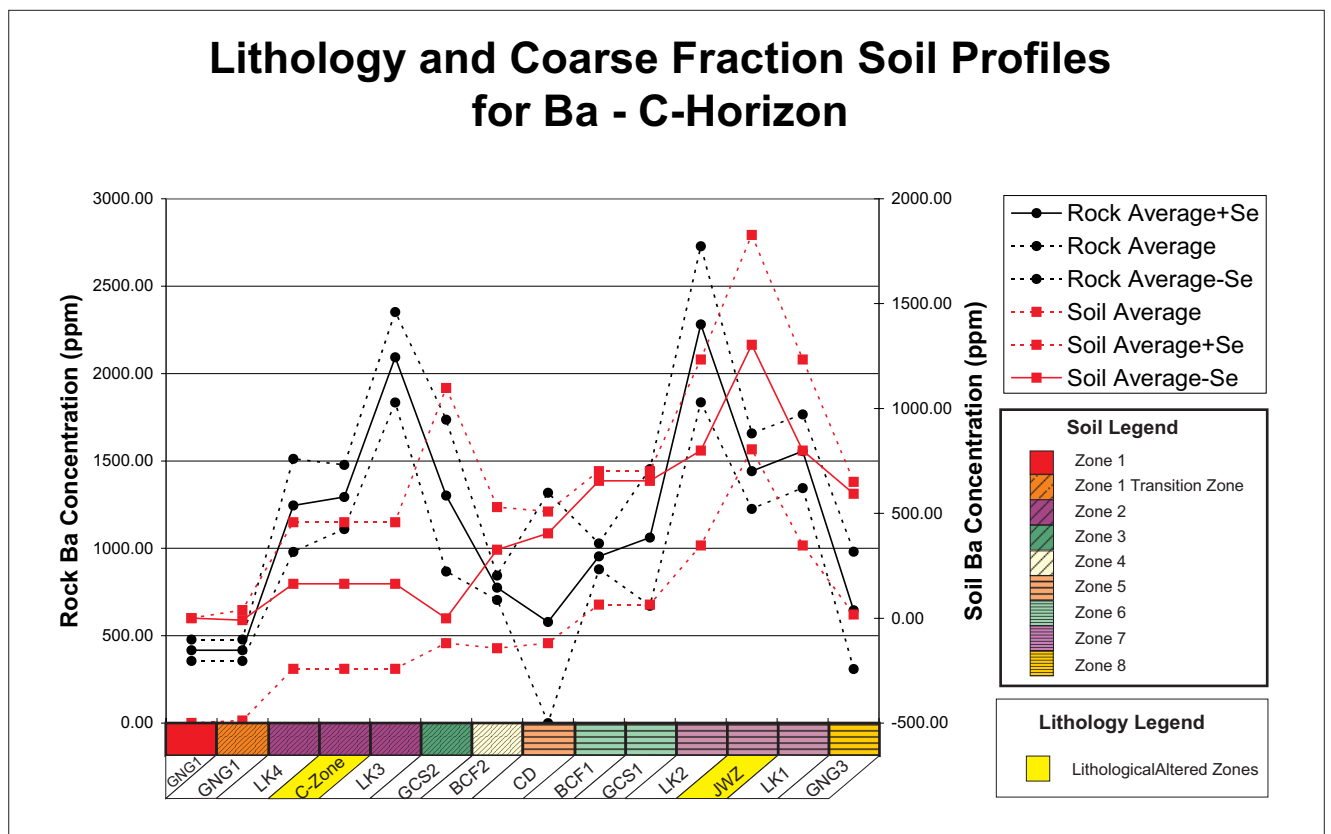
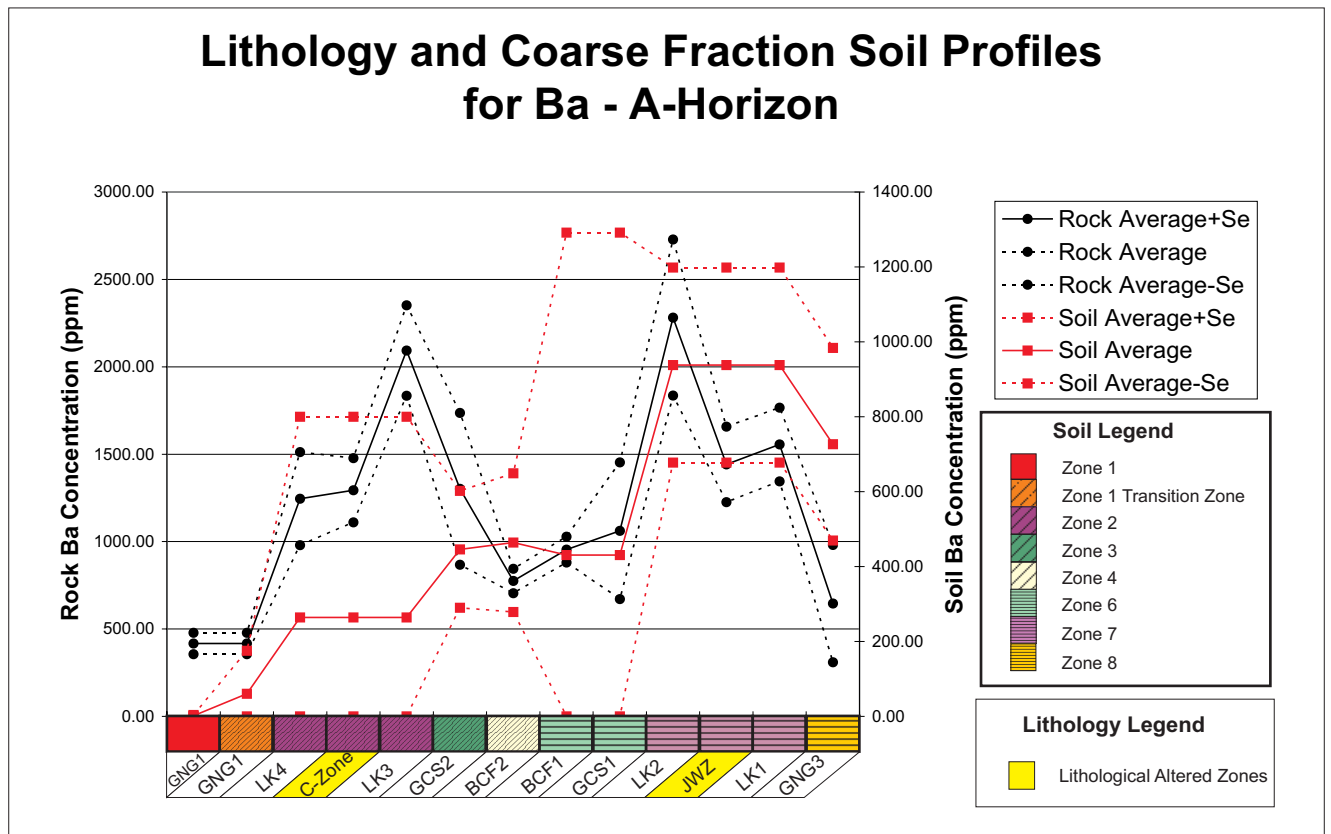


Fig.24 ...continued

When the trace element profiles of the Merelani Lower Horizon lithologies are considered, it can be seen that most of the trace elements show relatively high concentrations in either the Graphitic Calc-Silicate schist or in the Kyanite Gneiss units. Exceptions are Zr, Ga and Rb, which show relatively high values in the Garnet Gneiss units. The Garnet Gneiss units also contain, along with the Kyanite Gneiss Units, high values of Cr relative to the other trace element concentrations.

An important trend in the trace element profiles of the Merelani lithologies is that the profiles are mirrored on either side of the Central Dolomite. From the tanzanite mining complex folding is known to exist the Lower Horizon Lithologies. The geochemical duplication is therefore indicative of possible structural duplication around the Central Dolomite.

Fig.24 shows that the resolution, i.e. the contrast between high and low concentrations for a specific element, of the trace elements plotted as the soil trace element profiles is much less than that of the Merelani lithologies' trace element resolution.

It should be noted that the Graphitic Calc-Silicate schist units have the highest V concentrations and that these units are in close proximity to the Lower Horizon Kyanite Gneiss units 1 and 2, which host the tanzanite mineralisation.

To shed further light on the trace element profiles, the anomalous values for each trace element in each of the soils and the Merelani lithologies were calculated. The anomalous values are defined by all values above the 97.5<sup>th</sup> percentile for a specific trace element while the background values are all values below the median value as suggested by Rose et al. (1979).

Only the summary results are shown in the text; the detailed tabulated results can be found in the addendum compact disc. The tables for the Merelani lithologies will be described first, followed by a comparative description of the soils. The elements which show anomalous values for each lithological unit are presented in Table 8.

<b>Table 8 Trace elements showing anomalous values in the Merelani Lithologic units</b>	
<b>Merelani Lithological Unit</b>	<b>Element in Anomalous Concentration</b>
GNG1	Ga, Th
LK4/C-Zone/LK3	V, <b>Ni<sup>1</sup></b> , <b>Cu</b> , Ga, Zr, <b>Nb</b> , <b>Ce</b> , Pb, <b>U</b> , Ba
GCS2	V, Cr, Ni, Zn, Y, Nd, U
BCF2	Rb, Th
CD	Ba
BCF1	Rb, Sr, Nb, Th
GCS1	U
LK2/JWZ/LK1	V, Cr, Ni, Cu, <b>Zn</b> , Ga, <b>Sr</b> , Y, <b>Zr</b> , Nb, <b>La</b> , <b>Ce</b> , Nd, Ba
GNG3	Ga, Nb, Ce

1. Bold implies element anomalies which occur in the JWZ and/or C-Zone

The only element which displays anomalous values in only one specific lithology is Rb in both BCF units. The following observations are made when the table of the spread of anomalous values and values between background and anomalous are studied:

- V, Ni, Zn and U show anomalous and high values in the GCS and Kyanite Gneiss units with background values in both Garnet Gneiss, both BCF and the Central Dolomite units;
- Cr has background values in the Central Dolomite and has mostly background values in both BCF units, with isolated high values;
- The high and anomalous values of Zr are situated exclusively in the Garnet and Kyanite Gneiss units with background values in both GCS and both BCF units as well as in the Central Dolomite Unit.

Zone 1 and Zone 1 TZ soil zones are regarded as one soil zone, as they both cover the Garnet Gneiss 2 unit. When the spread of anomalous, high and background values of the soils are compared (addendum compact disc) it becomes apparent that almost none of the elements are exclusively anomalous in any one soil zone, horizon or size fraction. Rb is the only exception. However, when the tables of anomalous



values for the soils and lithologies are viewed in conjunction, the following observations are made:

- Cr, Ga and Rb have the majority of their anomalous and high values in Zone 1, Zone 1 TZ and Zone 8 soils, which are representative of the Garnet Gneiss units;
- V, Ni, Zn, Sr and Ba have the majority of their anomalous and high values in Zone 2, Zone 3 and Zone 4 soils (representing the Kyanite Gneiss, GCS and BCF units above the Central Dolomite) and in Zone 6 and Zone 7 soils (representing the GCS, BCF and Kyanite Gneiss units below the Central Dolomite).

#### **5.3.4. Ti and Zr normalisation as a test of trace element mobility**

Two immobile elements are used to quantify element mobility during weathering (Nesbitt, 1979). These are Zr and Ti. It is, however, Zr which is most frequently used in mass balance calculations (Colin et al., 1993). Ti is, however, also used (Scheepers and Rozendaal, 1993). The potential problem however, is that in both cases the Ti and/or Zr is assumed to be the immobile element and all mass balance calculations are based on this assumption. Therefore Ti and Zr were used to test whether they are discernibly mobile relative to each other, thus indicating whether any soil movement has taken place, as neither of these elements are mobile in a system dominated by chemical weathering. The mass balance calculations were performed using the equation of Nesbitt (1979):

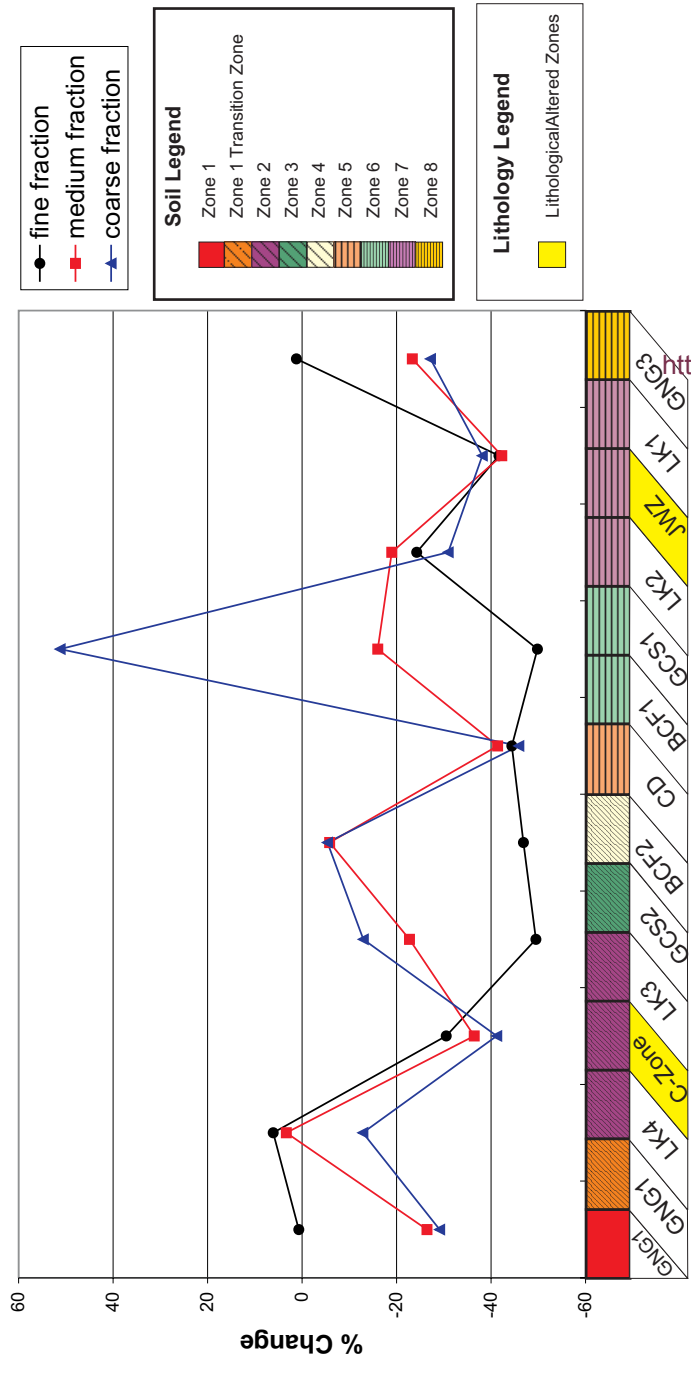
$$\% \text{ Change} = 100 \left( \frac{\left( \frac{x_s}{i_s} \right)}{\left( \frac{x_p}{i_p} \right)} - 1 \right)$$

The percentage increase or decrease of an element  $x$  in the sample  $s$  compared to its concentration in the parent rock  $p$  can be calculated relative to an assumed immobile element  $i$  (Ti or Zr).

The results are presented diagrammatically as spider diagrams in Fig.26 and Fig.27. The results of Zr- and Ti percentage change relative to each other is important for inferring soil particle mobility. A summary of the values of Zr- and Ti-percentage change for each of the soil horizons and size fractions of the different soil zones is presented in Table 9 and Fig.25.

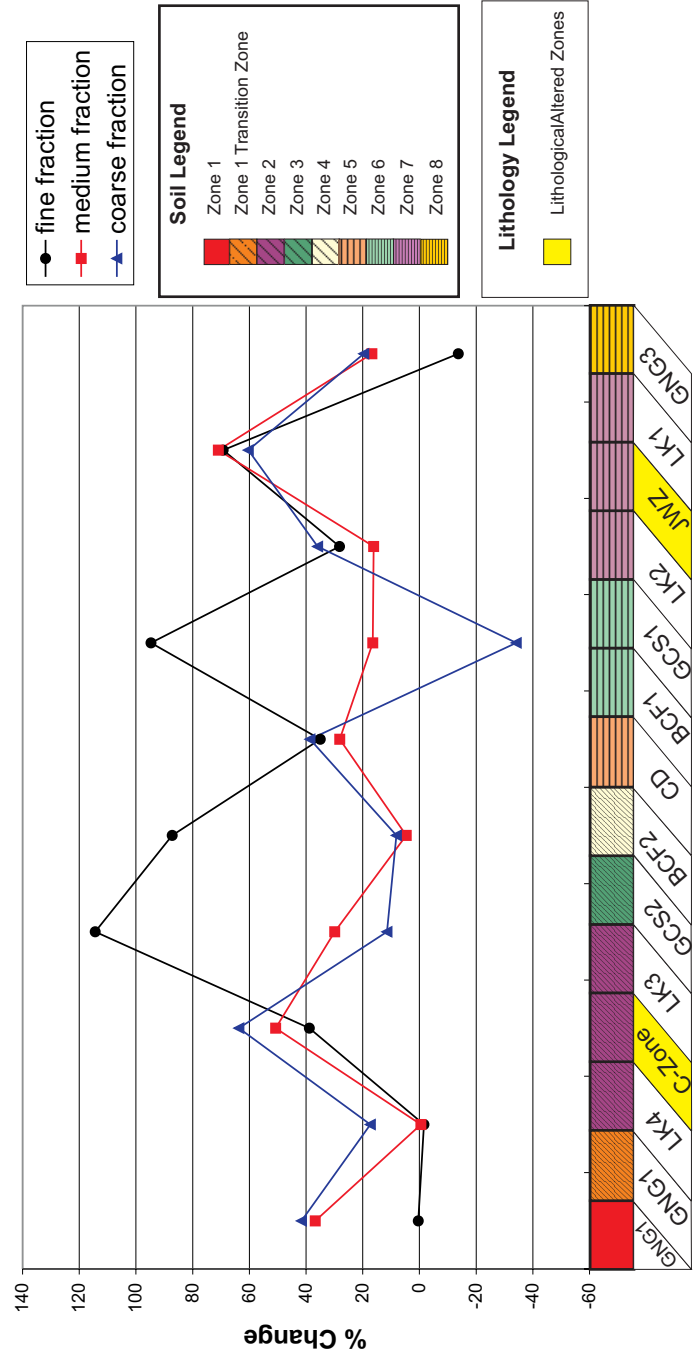
From Table 9 and Fig.25 it becomes apparent that Zr and Ti are mobile relative to each other. One would expect that in the event of hydromorphic trace element depletion or enrichment a percentage change of various mobile elements relative to Ti and Zr would result, but certainly not any percentage change of Ti relative to Zr. Even though Ti and Zr are mobile relative to each other, the correlations between the percentage change of Zr relative to Ti for the different size fractions and soil horizons is remarkable (Table 8). This would imply that the elements, although mobile, are mobile together. With both elements being inert in chemical weathering systems, the only deduction that can be made is that the elements are mobilised physically. Fig.26 and Fig.27 also shows a correlation between the Zr- and Ti-normalised patterns when the percentage change values are plotted on a type of spider diagram. The only general trend that can be observed in Fig.26 and Fig.27 is the generally larger percentage change of the heavier elements. Exceptions however are the Ti and Zr-normalised spider plots of Zone 4 and Zone 5, which both show high percentage changes for V and Ni. Fig.25 shows that no clear trend can be discerned in the Zr- and Ti-percentage change profiles over the trench. This would imply limited mobility, despite the seemingly large percentage change values.

### Profile of Percentage Change for Ti- Normalised Zr - C-Horizon

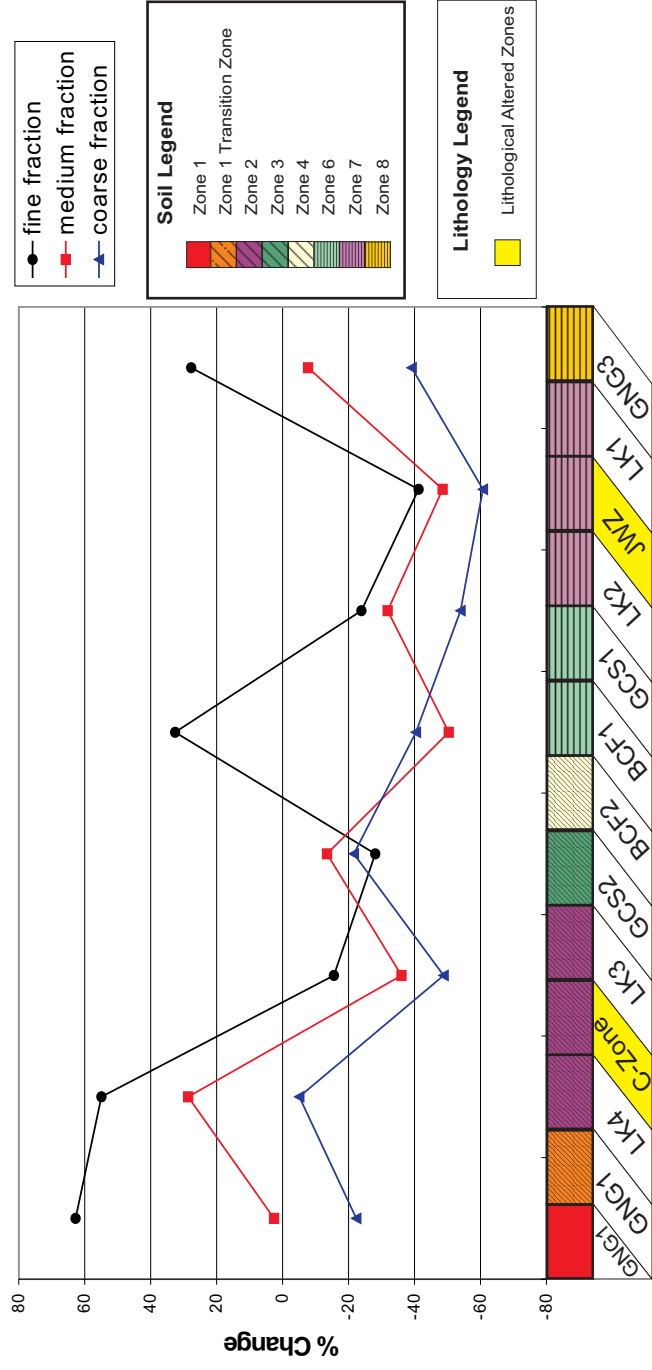


<http://scholar.sun.ac.za/>

### Profile of Percentage Change for Zr- Normalised Ti - C-Horizon



### Profile of Percentage Change for Ti- Normalised Zr - A-Horizon



### Profile of Percentage Change for Zr- Normalised Ti - A-Horizon

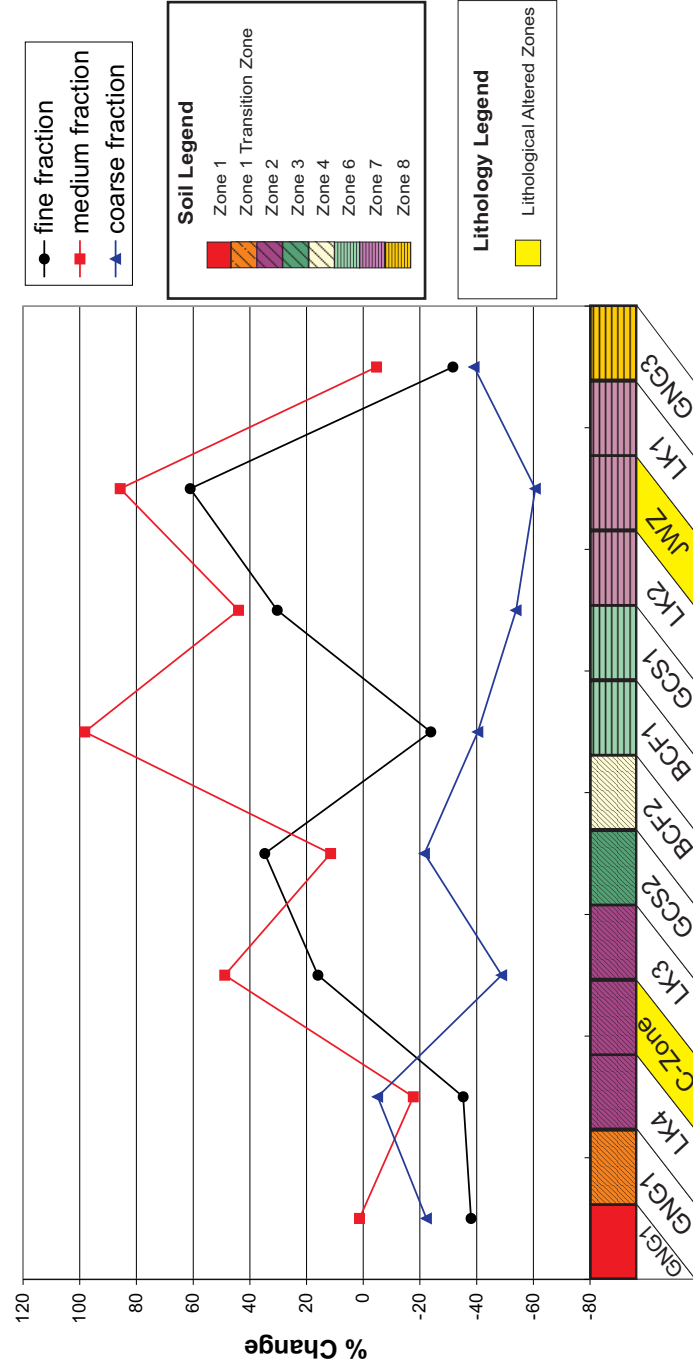
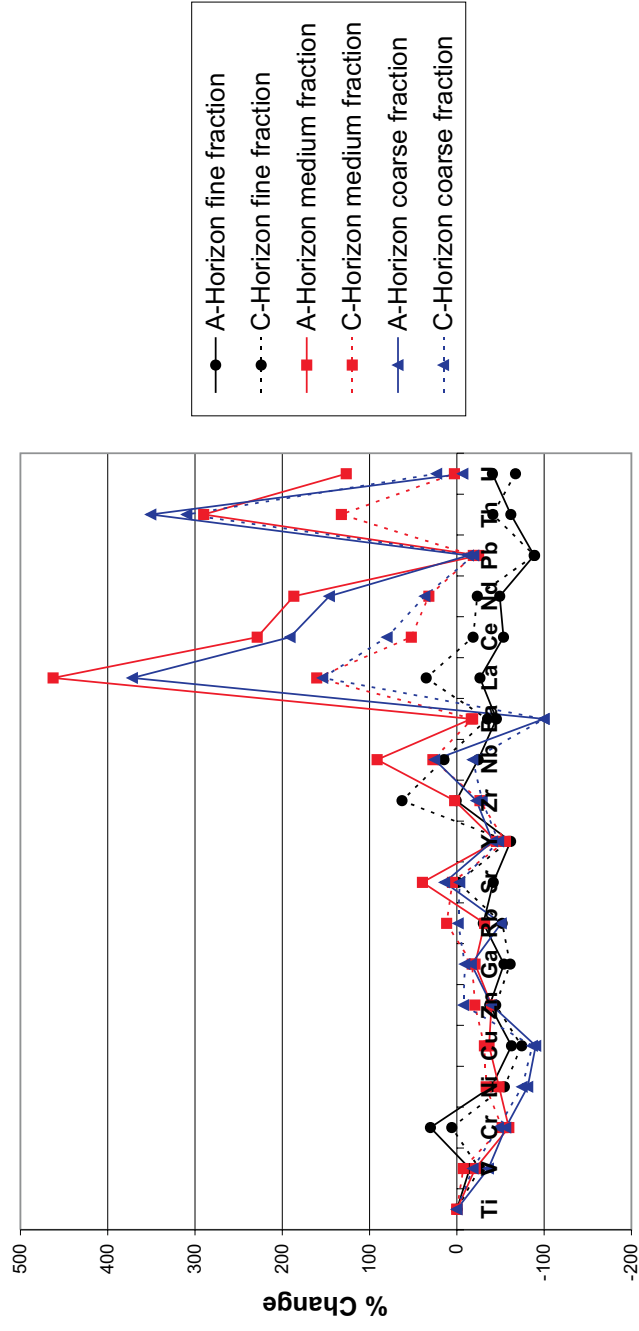
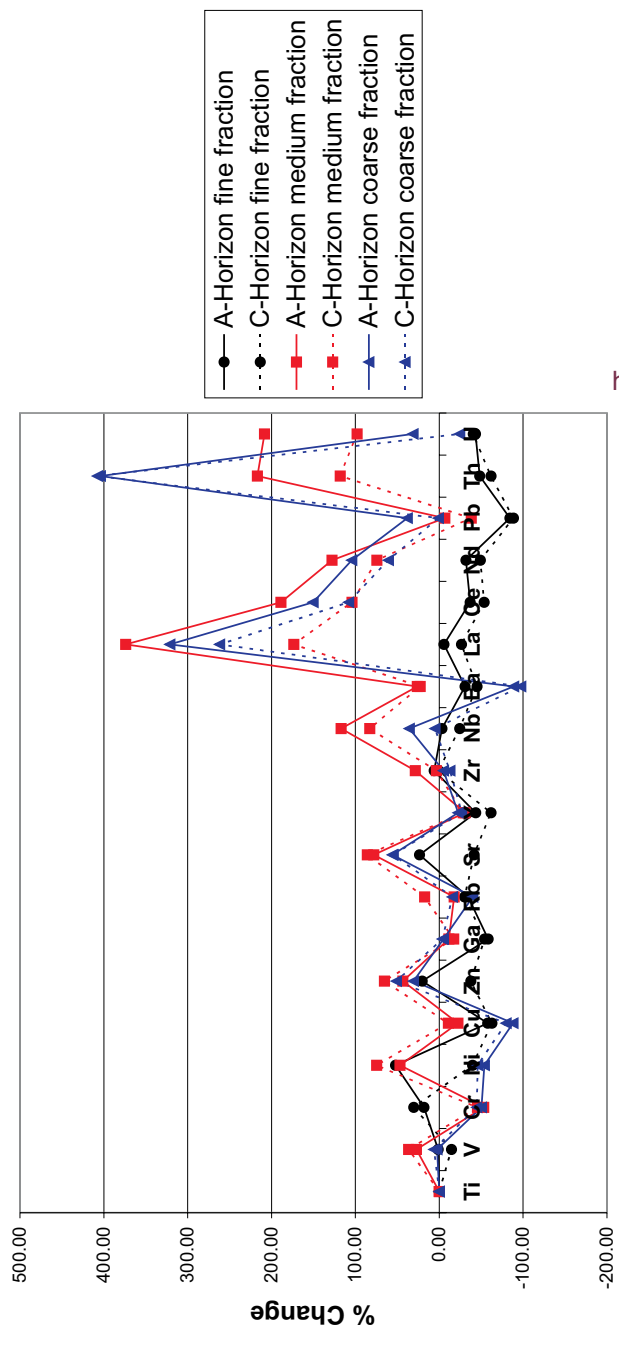


Fig.25 Profile of Ti- and Zr-Normalised percentage change values for the A- and C-Horizons and the different size fractions over the Merelani trench.

### Zone 1 Soil Ti-Normalised Percentage Change

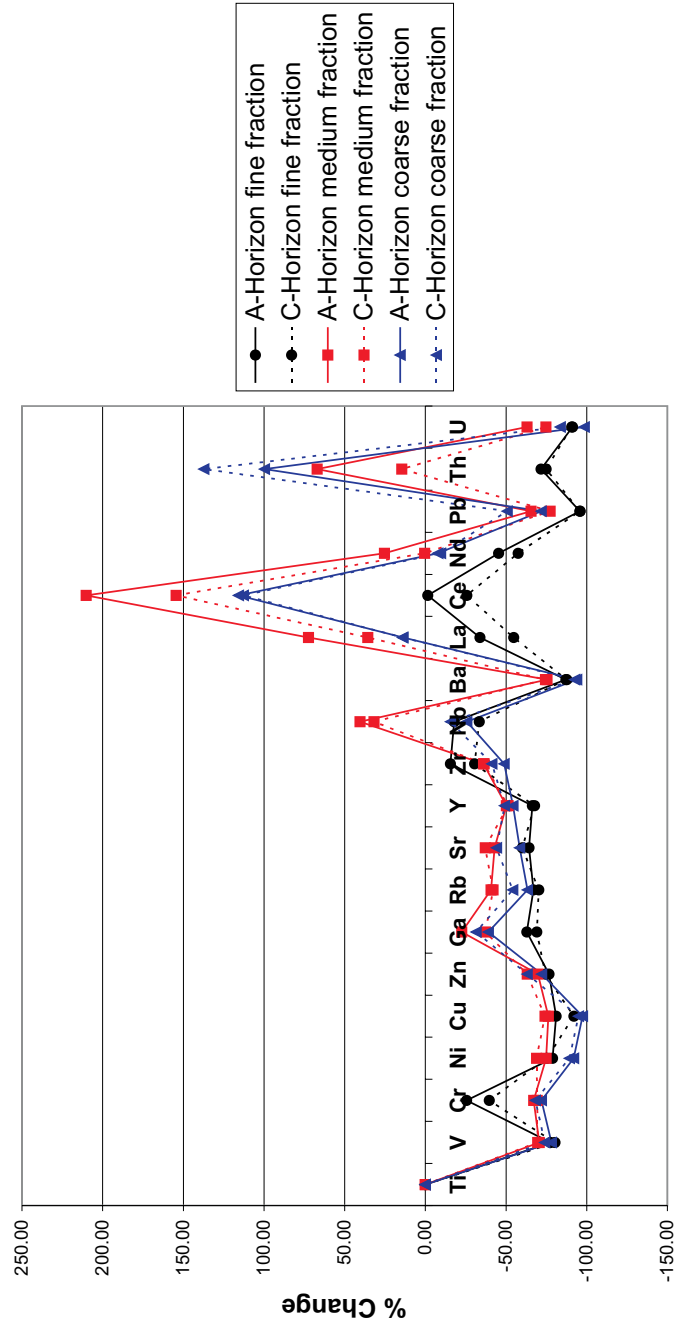


### Zone 1 TZ Soil Ti-Normalised Percentage Change



<http://scholar.sun.ac.za/>

### Zone 2 Soil Ti-Normalised Percentage Change



### Zone 3 Soil Ti-Normalised Percentage Change

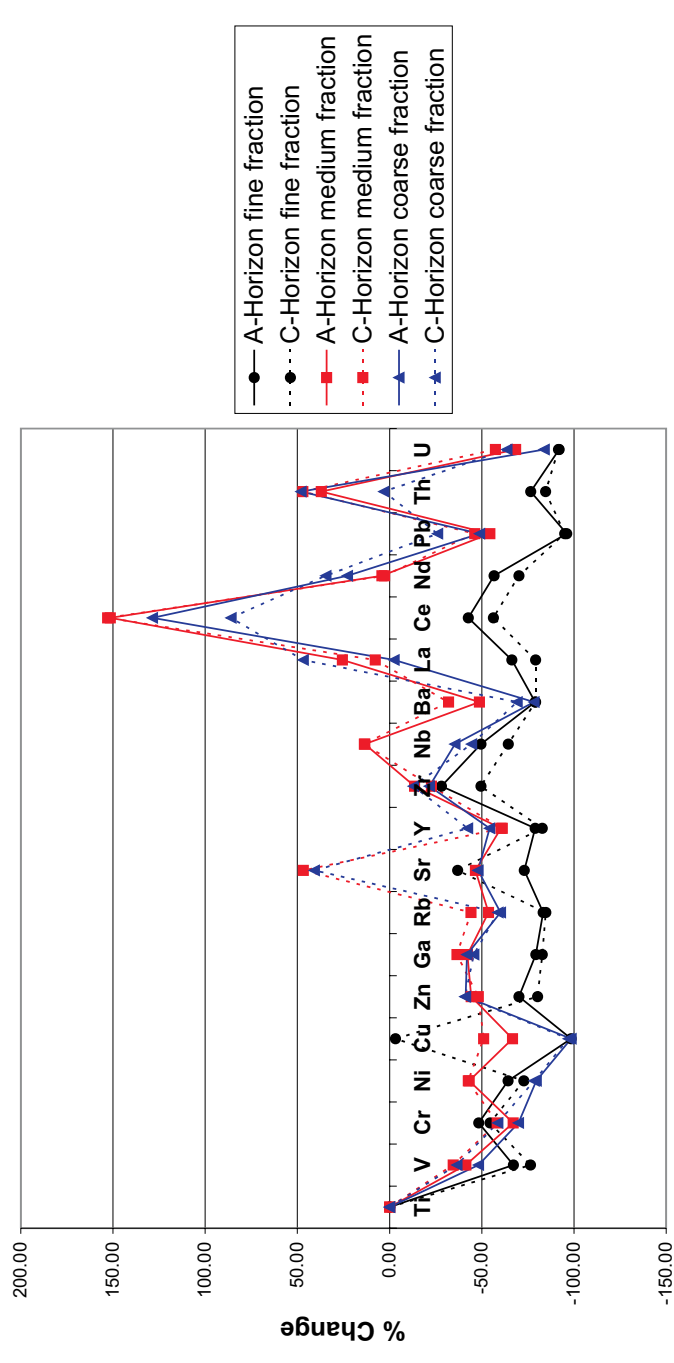
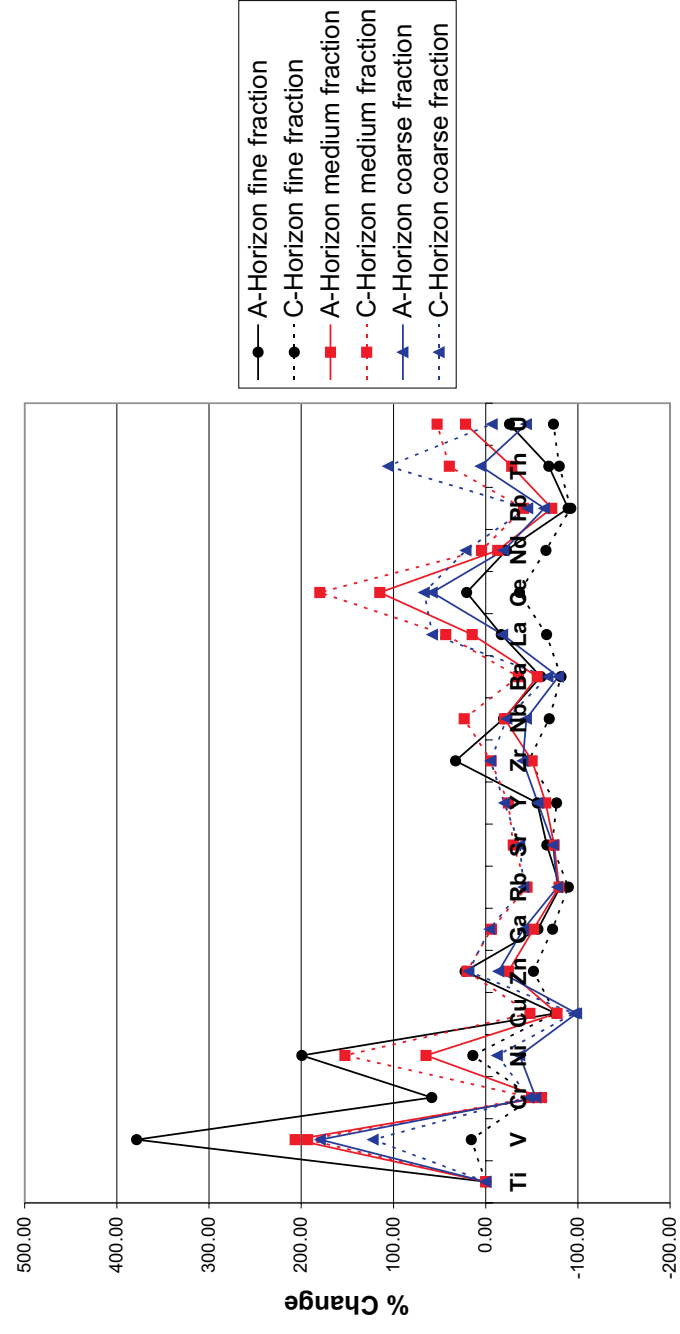
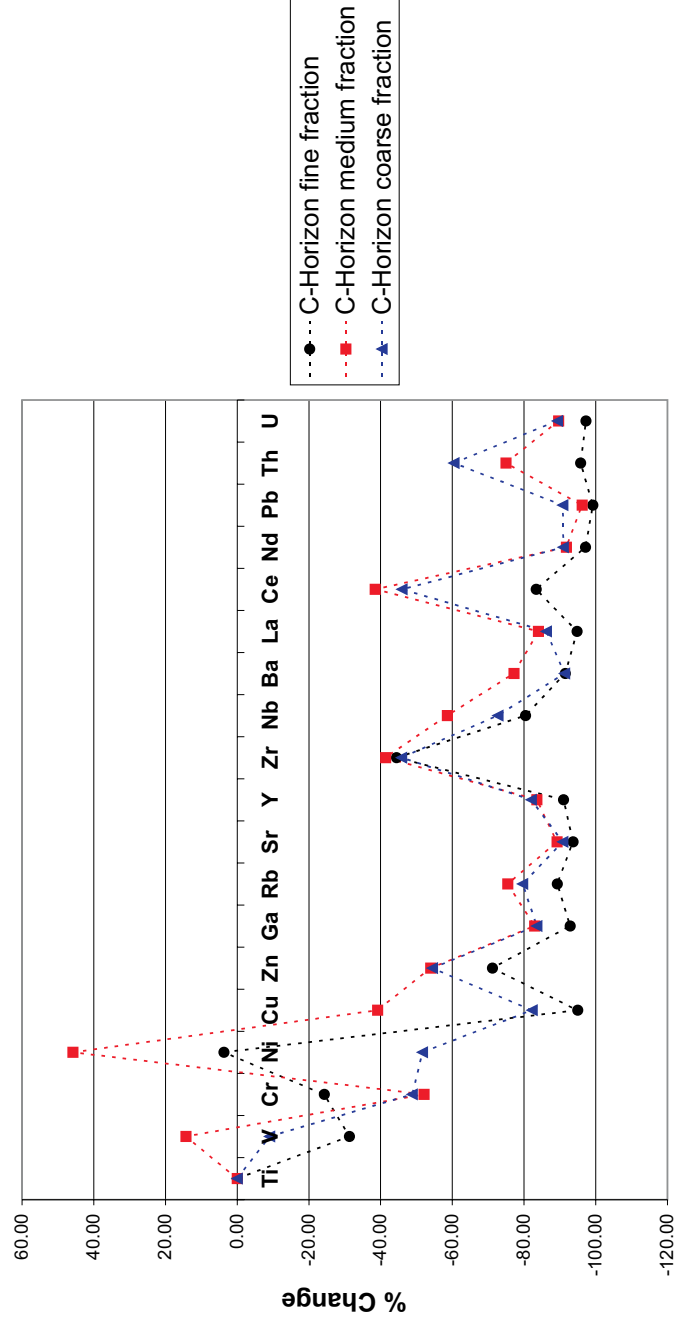


Fig.26 Spider diagrams of Ti-normalised percentage change values for the A- and C-Horizons and the three size fractions for the soil zones represented in the trench

### Zone 4 Soil Ti-Normalised Percentage Change

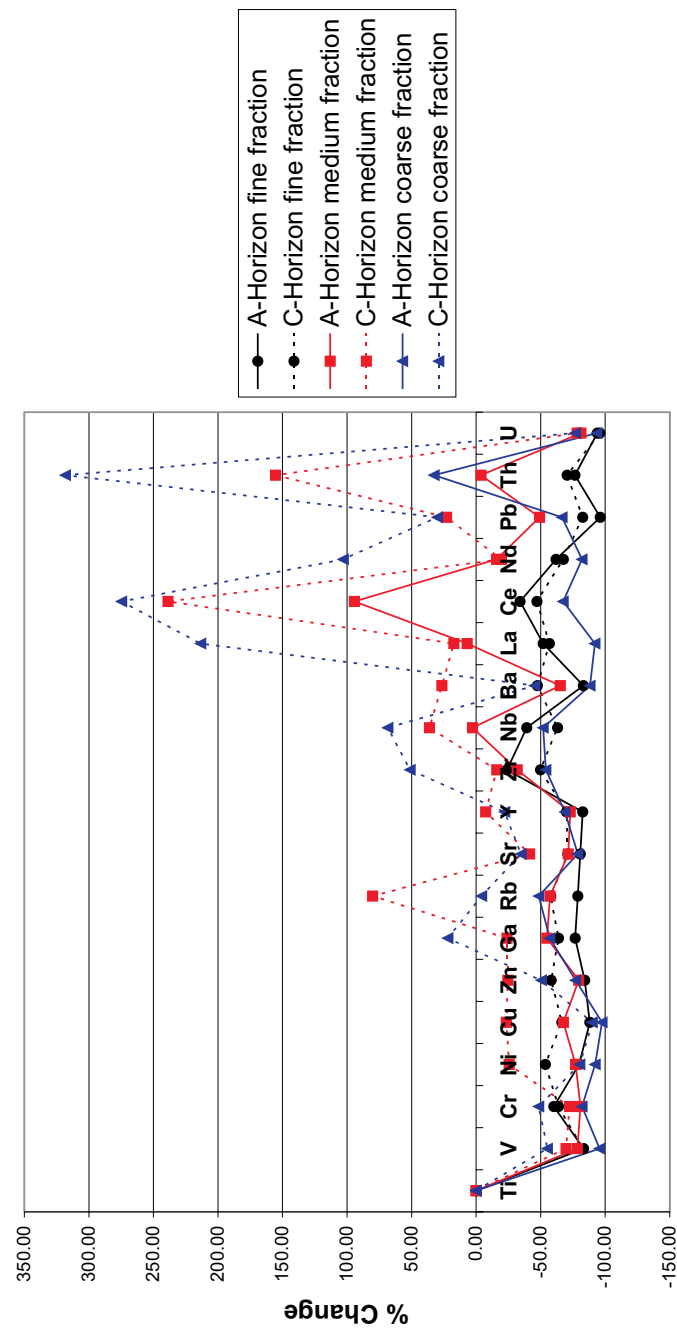


### Zone 5 Soil Ti-Normalised Percentage Change

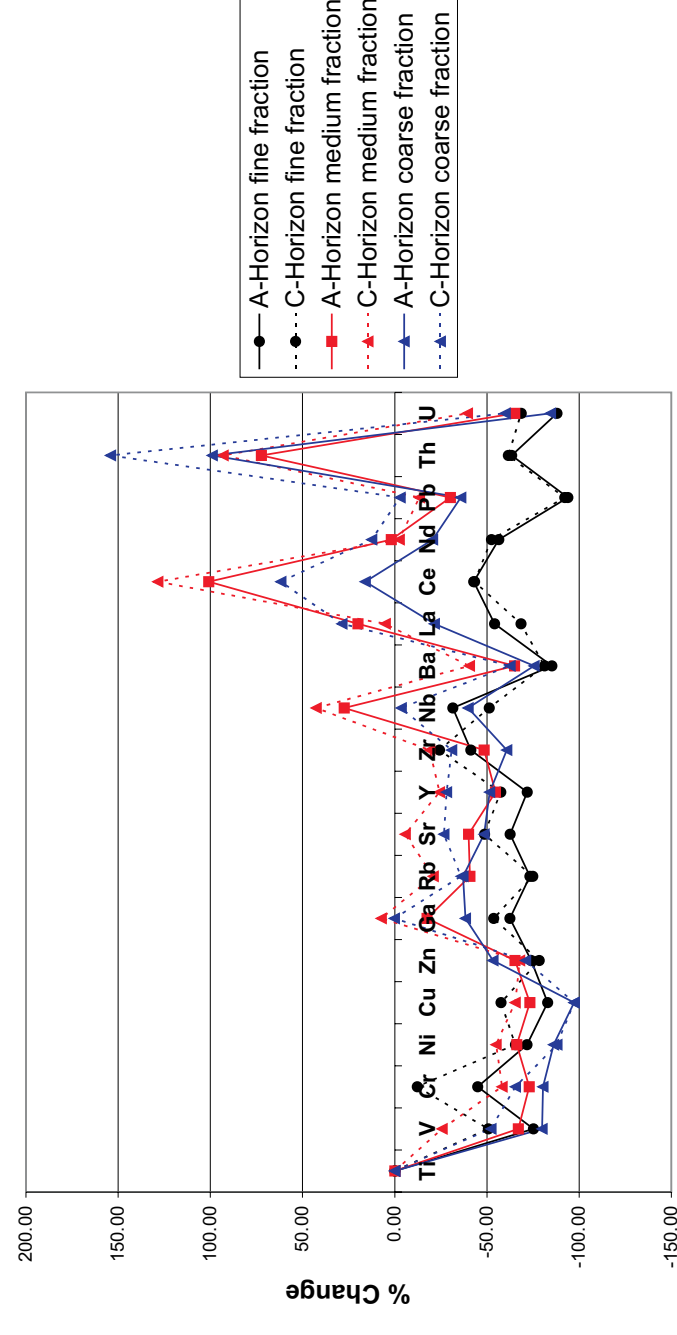


<http://scholar.sun.ac.za/>

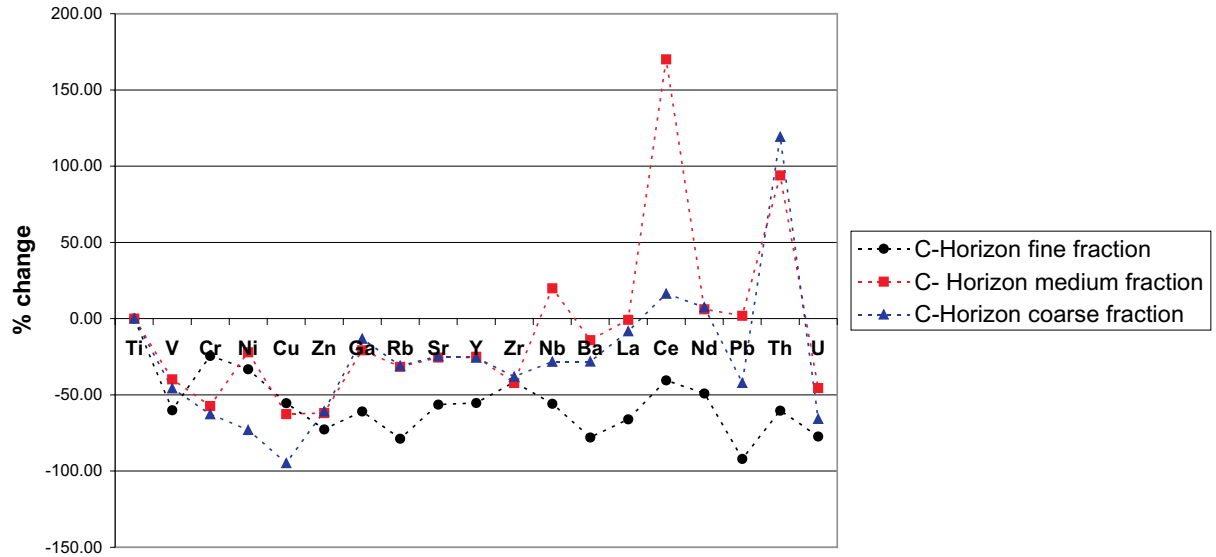
### Zone 6 Soil Ti-Normalised Percentage Change



### Zone 7 Soil Ti-Normalised Percentage Change



### Zone 7 (JWZ) Soil Ti-Normalised Percentage Change



### Zone 8 Soil Ti-Normalised Percentage Change

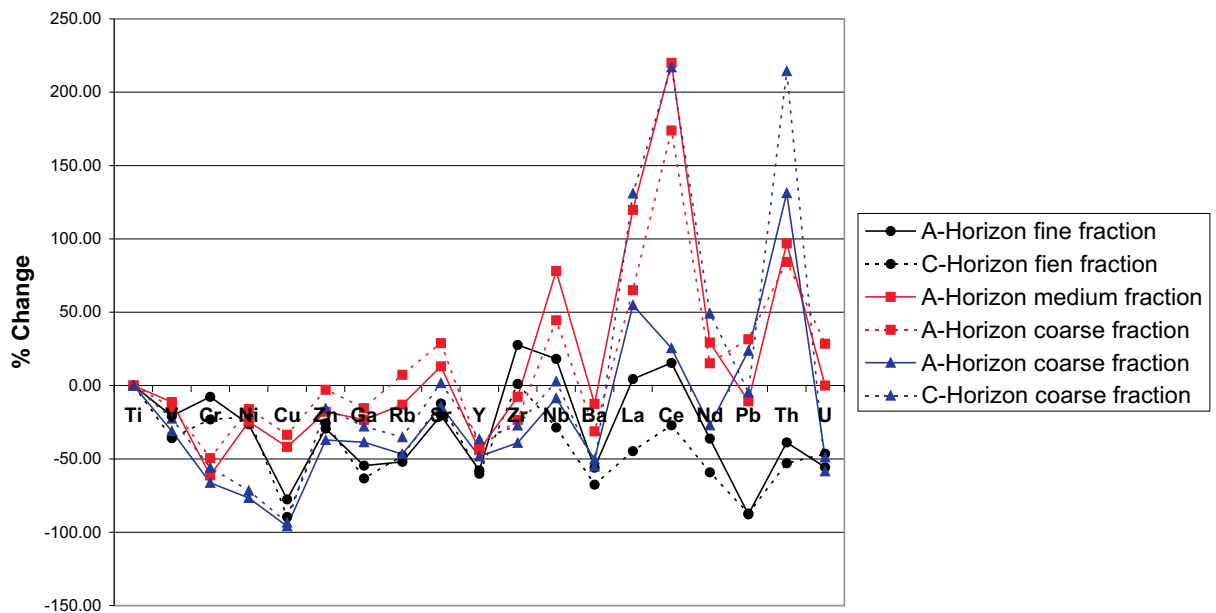
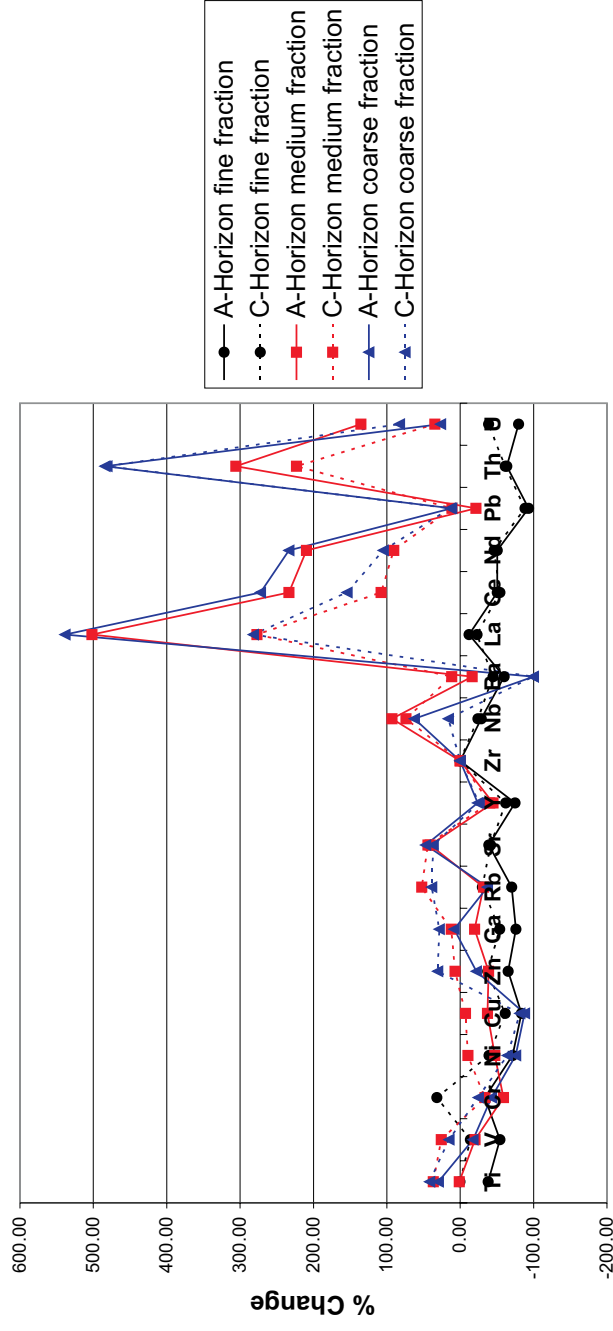
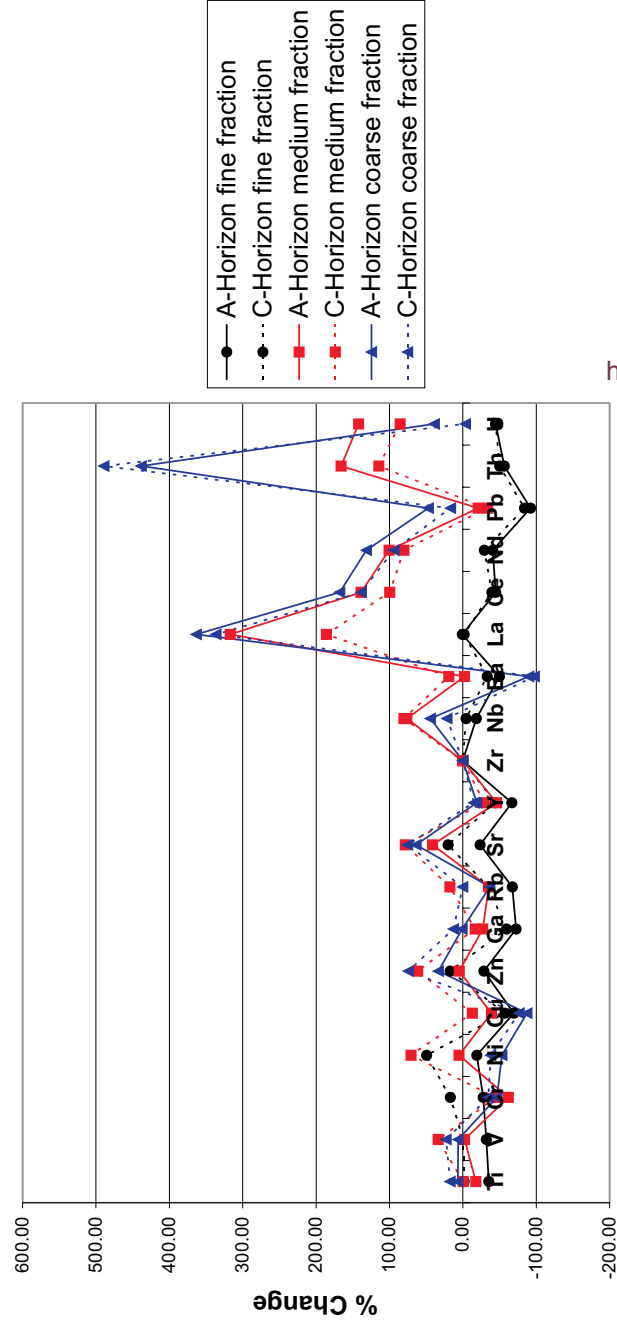


Fig.26 ...continued

### Zone 1 Soil Zr-Normalised Percentage Change

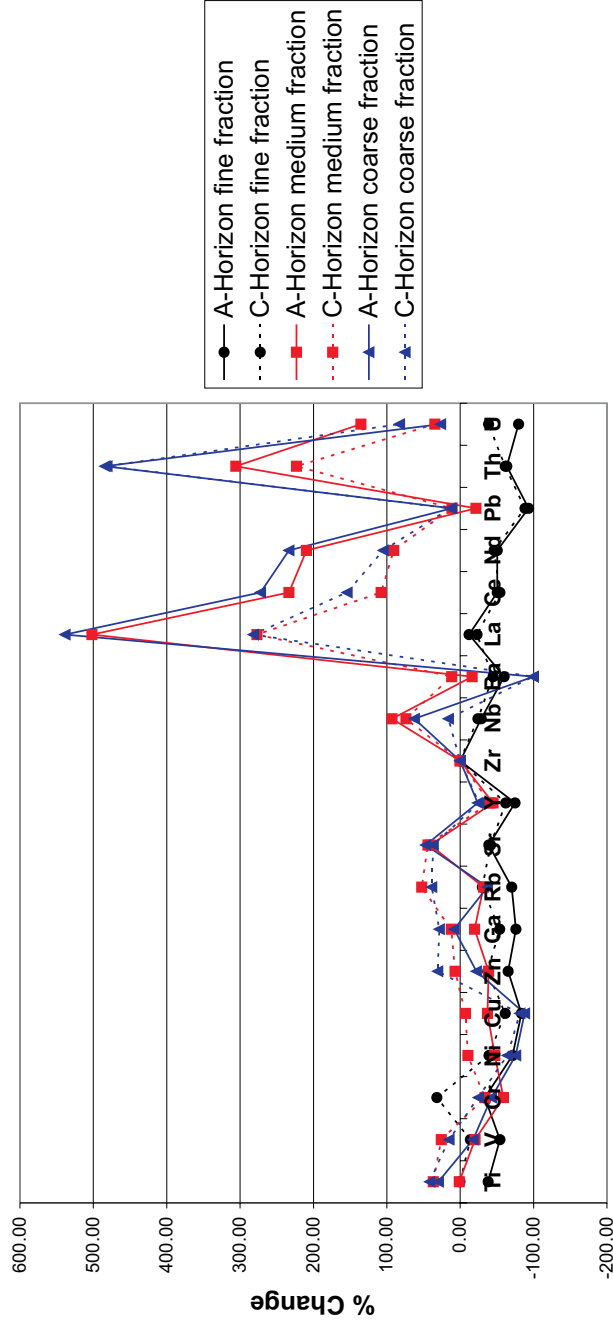


### Zone 1 TZ Soil Zr-Normalised Percentage Change

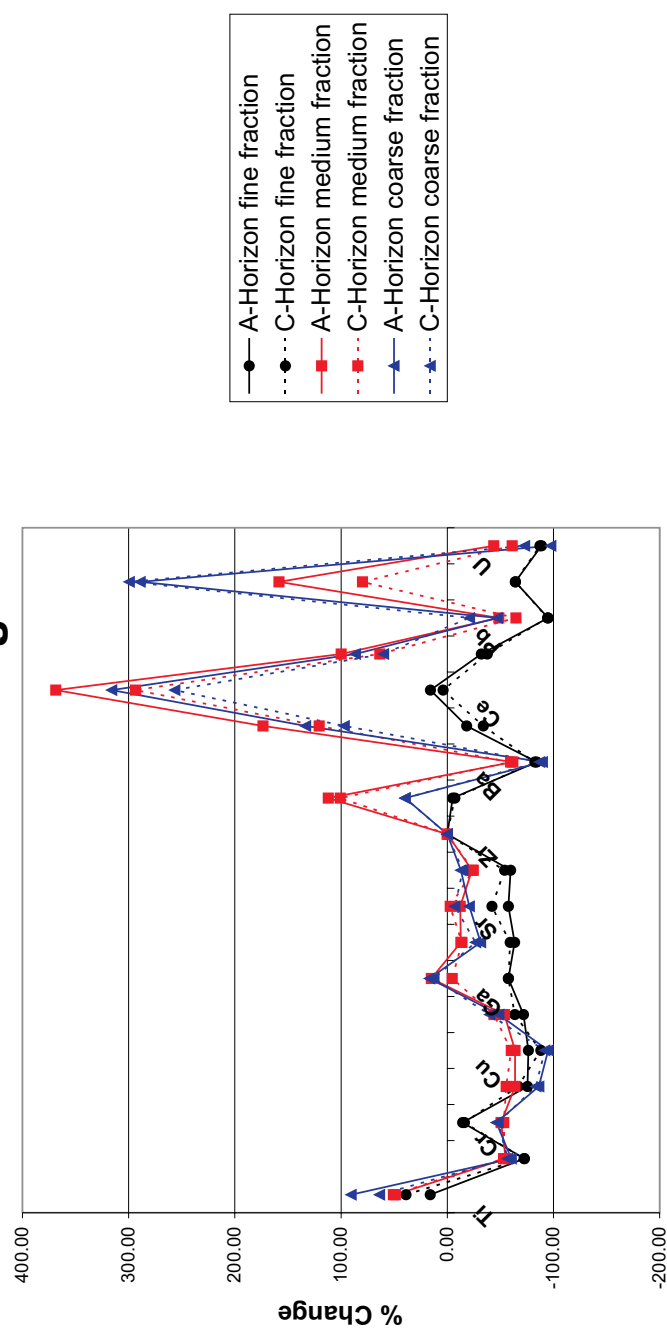


<http://scholar.sun.ac.za/>

### Zone 2 Soil Zr-Normalised Percentage Change



### Zone 2 Soil Zr-Normalised Percentage Change



### Zone 3 Soil Zr-Normalised Percentage Change

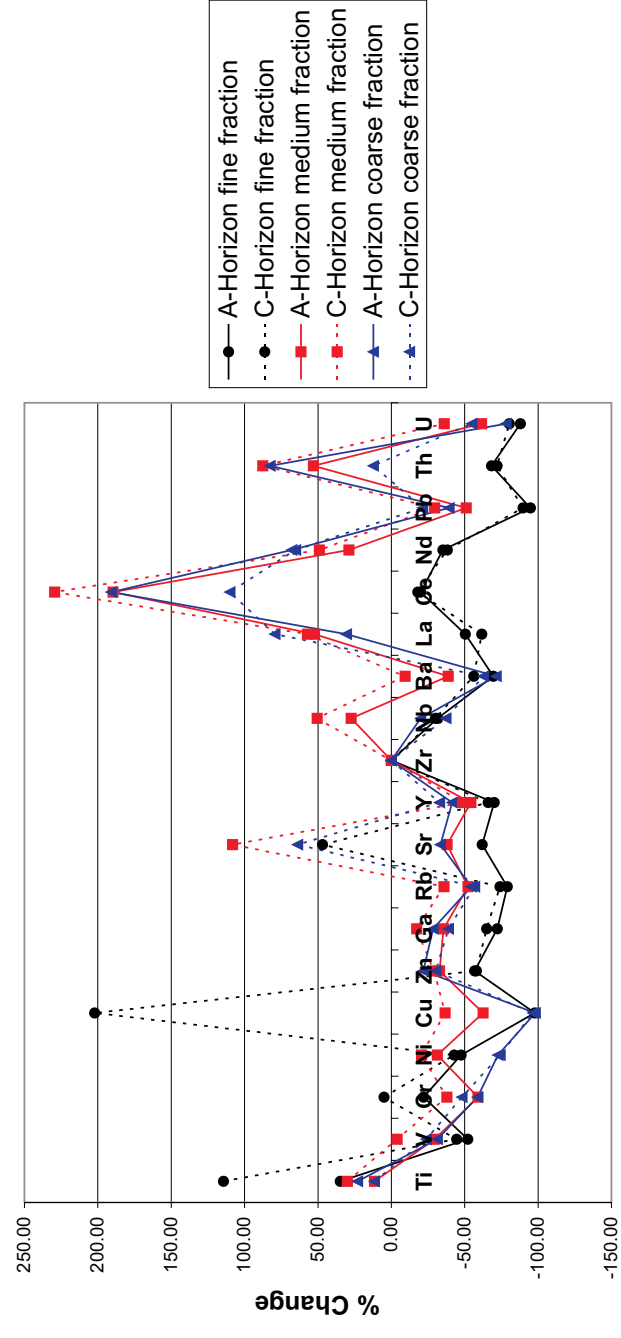
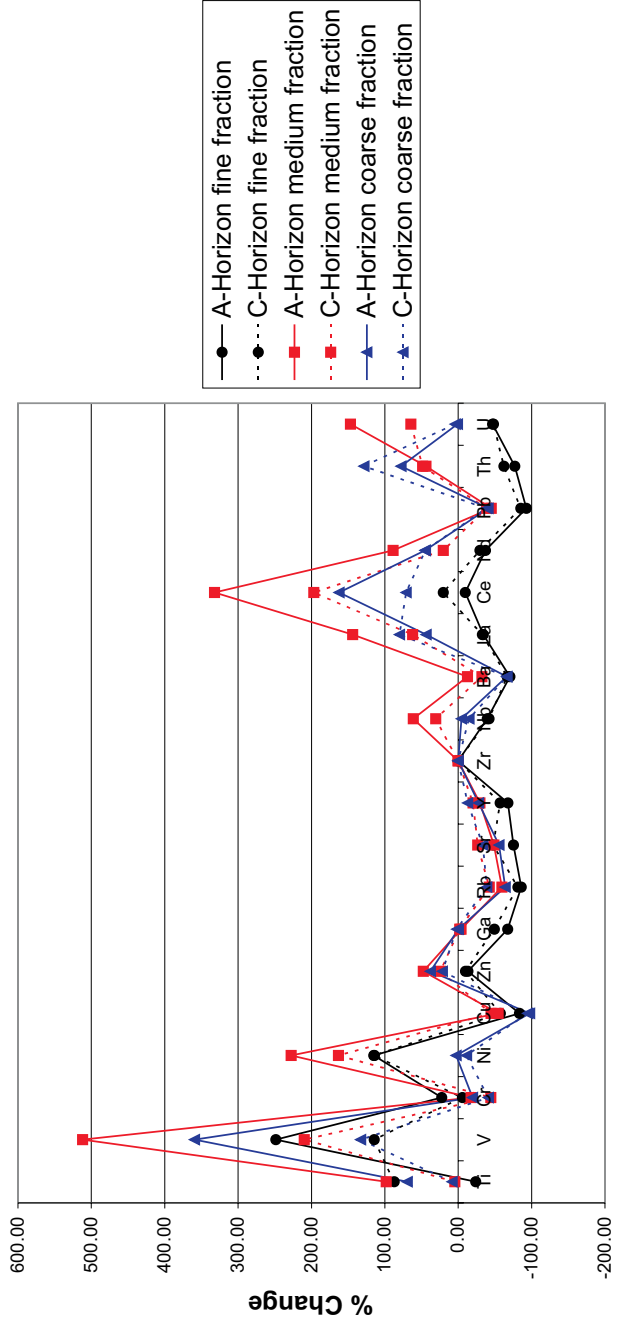
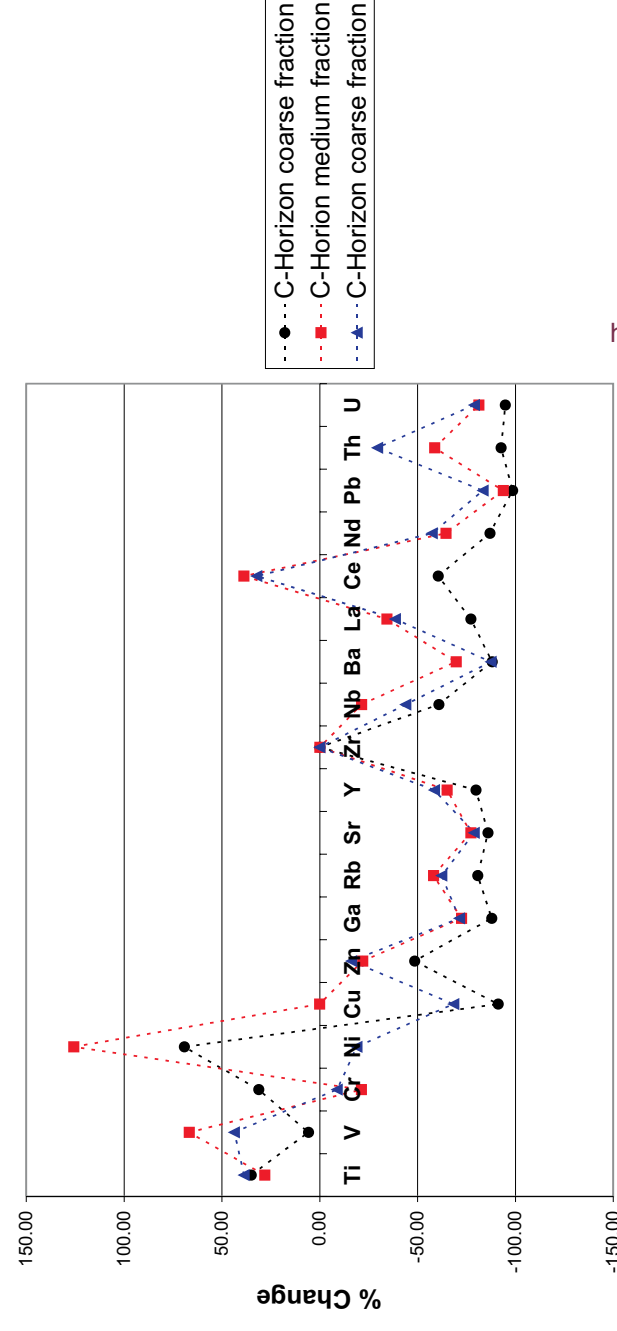


Fig.27 Spider diagrams of Zr-normalised percentage change values for the A- and C-Horizons and the three size fractions for the soil zones represented in the trench

### Zone 4 Soil Zr-Normalised Percentage Change

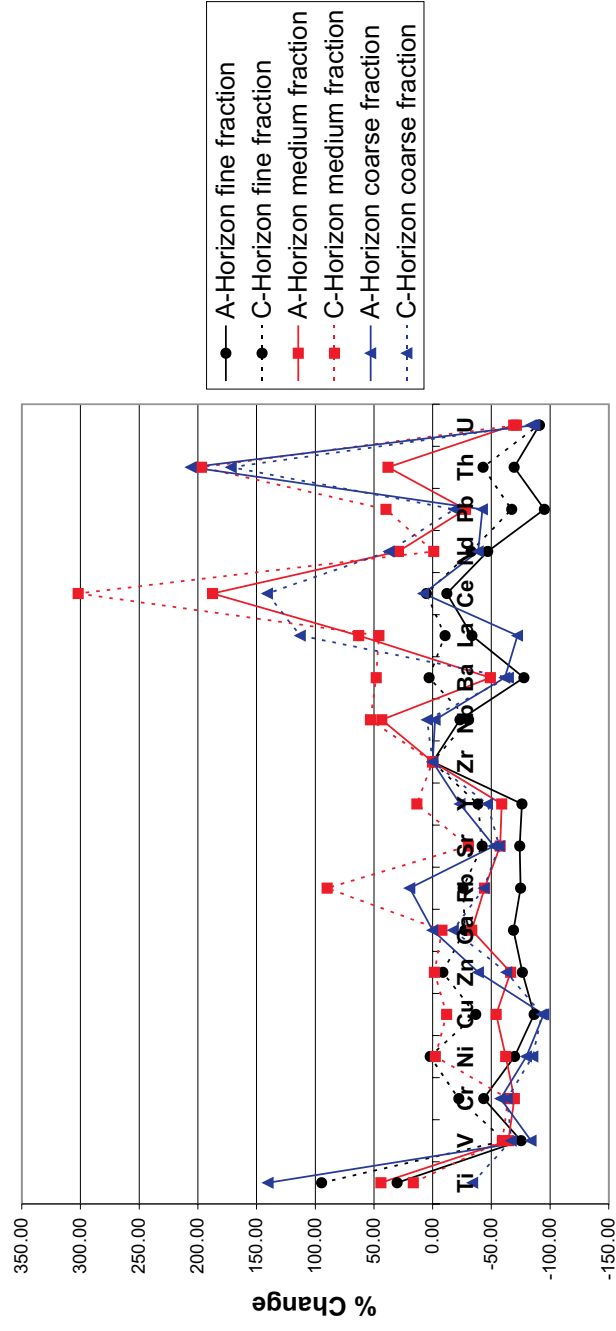


### Zone 5 Soil Zr-Normalised Percentage Change

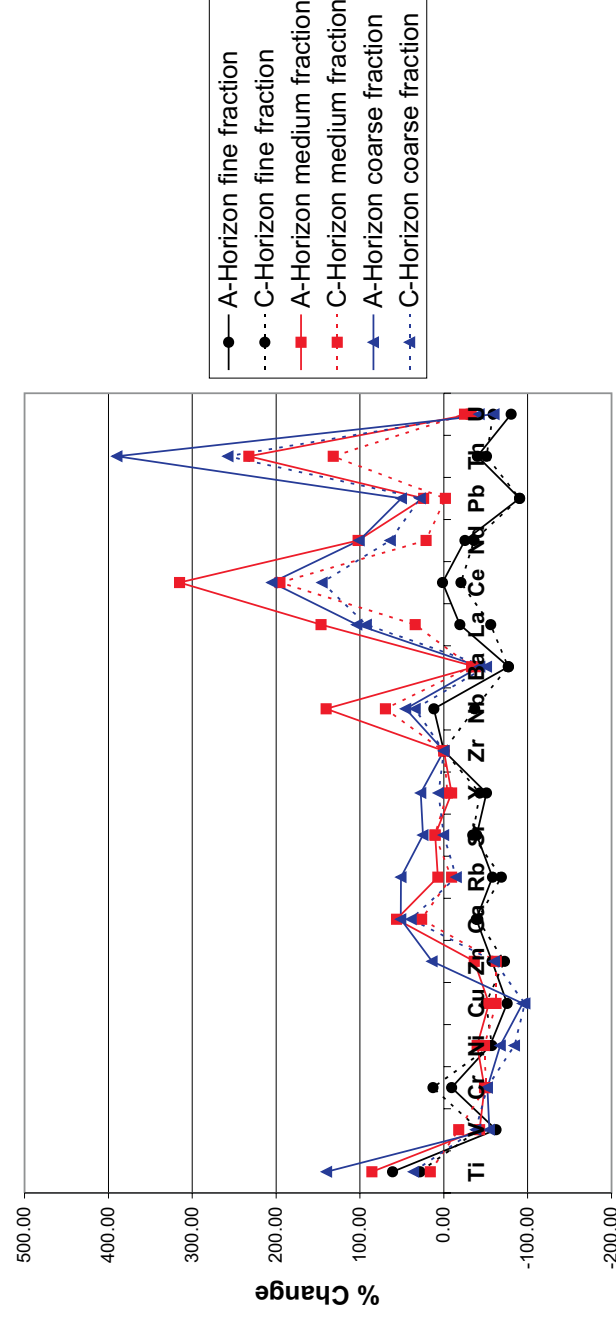


<http://scholar.sun.ac.za/>

### Zone 6 Soil Zr-Normalised Percentage Change

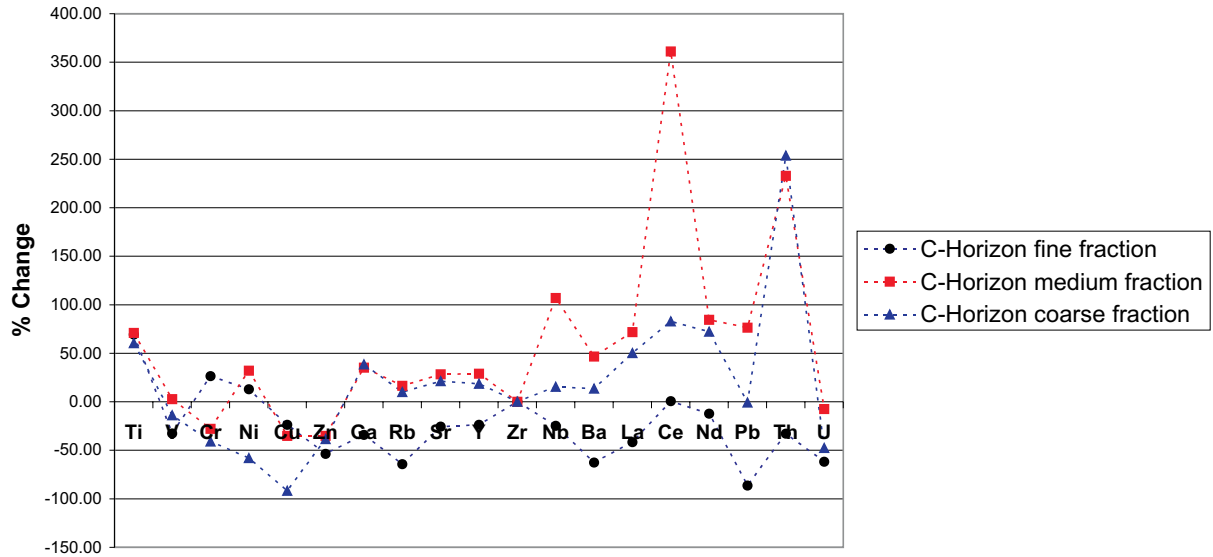


### Zone 7 Soil Zr-Normalised Percentage Change





### Zone 7 (JWZ) Soil Zr-Normalised Percentage Change



### Zone 8 Soil Zr-Normalised Percentage Change

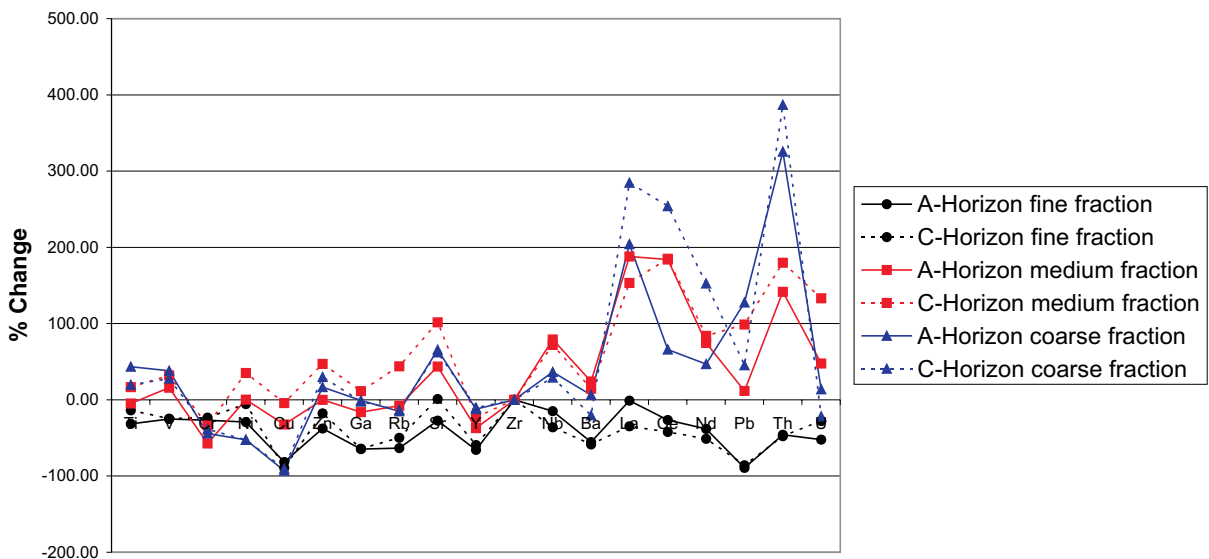


Fig.27 ...continued

<b>Table 8. Correlation coefficient of the percentage change of Zr and Ti (calculated from Table 7)</b>			
	<b>fine fraction</b>	<b>medium fraction</b>	<b>coarse fraction</b>
<b>A-Horizon</b>	-0.97	-0.94	-0.93
<b>C-Horizon</b>	-0.90	-0.85	-0.92

<b>Table 9 Percentage change of Ti and Zr of the Merelani soils relative to the Merelani lithologies</b>						
	<b>Fine Fraction</b>		<b>Medium Fraction</b>		<b>Coarse Fraction</b>	
	<b>Ti Normalised</b>	<b>Zr Normalised</b>	<b>Ti Normalised</b>	<b>Zr Normalised</b>	<b>Ti Normalised</b>	<b>Zr Normalised</b>
	<b>Zr % Change</b>	<b>Ti % Change</b>	<b>Zr % Change</b>	<b>Ti % Change</b>	<b>Zr % Change</b>	<b>Ti % Change</b>
<b>A-Horizon</b>						
<b>Zone 1</b>	63	-38	3	1	-22	30
<b>Zone 1 TZ</b>	55	-35	29	-18	-5	7
<b>Zone 2</b>	-16	16	-36	49	-49	90
<b>Zone 3</b>	-28	35	-13	11	-22	23
<b>Zone 4</b>	33	-24	-50	98	-40	69
<b>Zone 6</b>	-24	30	-32	44	-54	140
<b>Zone 7</b>	-41	61	-49	86	-61	140
<b>Zone 8</b>	28	-32	-8	-5	-39	43
<b>C-Horizon</b>						
<b>Zone 1</b>	1	0	-26	37	-29	42
<b>Zone 1 TZ</b>	6	-2	3	-1	-13	17
<b>Zone 2</b>	-30	39	-36	51	-41	64
<b>Zone 3</b>	-50	114	-23	30	-13	11
<b>Zone 4</b>	-47	87	-6	5	-5	8
<b>Zone 5</b>	-44	35	-41	28	-46	39
<b>Zone 6</b>	-50	95	-16	16	51	-34
<b>Zone 7</b>	-24	28	-19	16	-31	36
<b>Zone 7 (JWZ)</b>	-42	69	-42	71	-38	60
<b>Zone 8</b>	1	-14	-23	17	-27	20

In addition to the possible use of partial extraction methods in the exploration for additional tanzanite deposits, it is also a useful tool in testing the above hypothesis of Merelani trace element mobility. Thus the following section will deal with the quantification of the mobility of selected trace elements, which could prove useful in an exploration venture for additional tanzanite deposits.

### **5.3.5. Total (XRF) and Partial (ICP) trace element extraction and analysis**

Four trace elements were chosen for the ICP analyses for several reasons: V was chosen due to the fact that it is the chromophoric element in tanzanite (Olivier, 2006) and because it has been shown to have a good correlation between the Merelani soils and lithologies and might prove useful in an exploration program and because of its mobility in oxygenating environments. Cr, Ni and Cu were chosen for their chromophoric properties in a plethora of coloured gemstones (Fritsch et al., 1987 and 1988) and budget constraint allowed for only the four elements to be analysed. The coarse fraction was not chosen for analysis because of the fact that the elements chosen for the ICP-AE analysis show a better correlation between the Merelani soils and lithologies in the fine and medium fractions.

The leachate of the medium and fine fractions of the Merelani trench soil samples was analysed by ICP-AE. The ICP analyses are expressed relative to the XRF analyses as a percentage and presented in Table 10 and Table 11. The following equation was used to calculate the values presented in the afore-mentioned tables:

$$\text{Percentage Metal Leached} = 100 \left( \frac{x_{\text{Average}}^{\text{ICP}}}{x_{\text{Average}}^{\text{XRF}}} \right)$$

Table 10 and 11 show that there is generally an order of magnitude or two difference between the concentration of extractable metal in the A- and C-Horizons. However, values are still less than 2ppm for Cr, Ni and V, which is low relative to the concentration of these elements in the soil. The percentage extractable Cu in the fine fraction of Zone 3 A-Horizon and Zone 5 as well as the C-Horizon of the medium fraction of Zone 3 are high relative to the percentage extractable metal available for the other three elements and reaches a value of 73ppm in the A-Horizon of Zone 3. In

<b>Table 10 Percentage Extractable Metal of the Fine Fraction</b>				
	<b>Cr</b>	<b>Ni</b>	<b>V</b>	<b>Cu</b>
<b>A Horizon</b>				
<b>Type 1</b>	0.012	1.319	0.260	3.938
<b>Type 1 TZ</b>	0.018	1.322	0.417	3.701
<b>Type 2</b>	0.016	1.468	0.377	2.409
<b>Type 3</b>	0.040	0.733	0.398	72.982
<b>Type 4</b>	0.037	1.486	0.775	4.561
<b>Type 6</b>	0.051	2.092	1.082	7.939
<b>Type 7</b>	0.031	1.726	0.795	4.463
<b>Type 8</b>	0.026	1.691	0.646	5.330
<b>C Horizon</b>				
<b>Type 1</b>	0.009	0.684	0.204	4.428
<b>Type 1 TZ</b>	0.009	1.239	0.478	5.743
<b>Type 2</b>	0.015	1.493	0.435	7.999
<b>Type 3</b>	0.048	0.819	0.472	5.969
<b>Type 4</b>	0.025	1.470	1.199	2.218
<b>Type 5</b>	0.019	1.719	1.070	21.367
<b>Type 6</b>	0.001	0.011	0.020	0.037
<b>Type 7</b>	0.027	1.437	0.636	3.257
<b>Type JWZ</b>	0.038	1.726	0.753	3.818
<b>Type 8</b>	0.047	1.562	0.779	12.017

<b>Table 11 Percentage Extractable Metal of the Medium Fraction</b>				
	<b>Cr</b>	<b>Ni</b>	<b>V</b>	<b>Cu</b>
<b>A Horizon</b>				
<b>Type 1</b>	0.49	2.03	0.80	2.81
<b>Type 1 TZ</b>	0.38	2.16	0.81	3.08
<b>Type 2</b>	0.43	2.24	0.67	2.77
<b>Type 3</b>	0.48	1.86	1.00	3.74
<b>Type 4</b>	0.30	2.23	1.09	2.60
<b>Type 6</b>	0.33	2.56	1.25	3.54
<b>Type 7</b>	0.35	2.59	1.14	4.02
<b>Type 8</b>	0.33	2.47	0.94	2.33
<b>C Horizon</b>				
<b>Type 1</b>	0.36	1.08	0.61	2.61
<b>Type 1 TZ</b>	0.33	2.02	0.83	3.51
<b>Type 2</b>	0.19	1.93	0.55	2.93
<b>Type 3</b>	0.42	1.92	0.82	42.25
<b>Type 4</b>	0.44	2.17	1.51	2.41
<b>Type 5</b>	0.23	2.52	1.54	2.61
<b>Type 6</b>	0.87	2.49	2.38	2.38
<b>Type 7</b>	0.40	2.32	1.03	5.11
<b>Type JWZ</b>	0.41	2.98	1.28	6.77
<b>Type 8</b>	0.26	2.55	1.11	2.00

addition to the high analytical precision values for Cu, the average Cu concentration in the Merelani trench soils is low and ranges from 32 - 74ppm. Thus caution is called for in interpreting the amount of Cu potentially leacheable from the soils.

The ICP-AE analyses therefore show that the trace elements investigated, with perhaps the exception of Cu, is not significantly mobilised by soil solutions and must therefore be mobile by physical means such as soil creep down-slope and/or flash floods.

### **5.3.6. Chemical evaluation of various size fractions**

In geochemical exploration it is important to know how the elements of interest are distributed throughout the sampled medium and where they occur for the purposes of planning and implementing a geochemical exploration programme. Thus the trace element data of the fine, medium and coarse fractions from the Merelani soils were geochemically evaluated in terms of trace element distribution.

V, Ni, Cr, Zn and Th were chosen for the study. The first four elements were chosen due to their positive geochemical correlation between the Merelani lithologies and soils. Th was chosen as a reference frame because of its known association with heavy minerals (Dill, 1998; Wederpohl, 1978) and thus coarse fraction in soils and stream sediments. Ni, is concentrated in the fine fraction. This, as well as the association of Th with the coarse fraction in the Merelani soils, is demonstrated in Fig.28b. Ni and Th display an antipathetic relationship with a linear correlation coefficient of -0.586, which is significant (see section 4.3 for a more detailed discussion on correlation coefficients). Ni displays maximum concentrations in the fine fraction and Th maximum concentrations in the coarse fraction.

V shows a slight vertical trend towards higher concentrations in the fine fraction (Fig.28a). The highest Cr values are found in the fine fraction, with no significant separation of the spread of values between the medium and coarse fractions. Zn shows the same trend and to the same degree as V.

V, Ni, Cr and Zn all display trends towards enrichment in the fine fraction. The only difference is the degree of enrichment of individual elements, as can be seen from the

### Evaluation of the Effect of Grain Size of V and Th Values

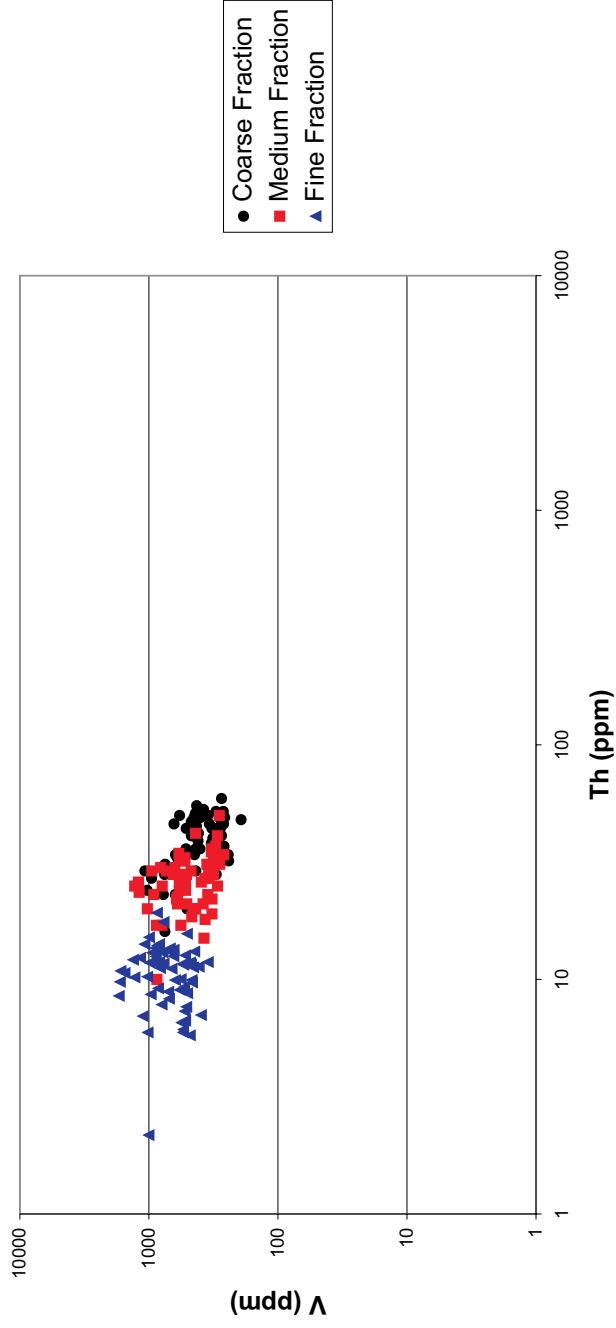
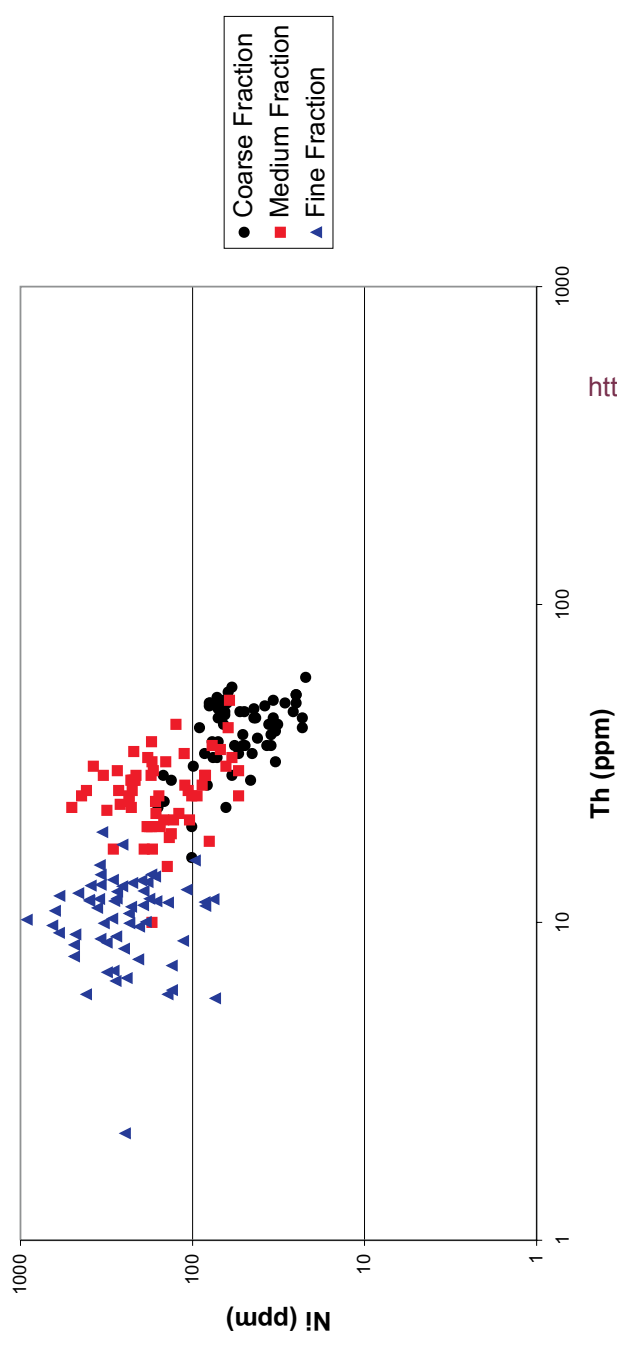


Fig.28a

### Evaluation of the Effect of Grain Size on Ni and Th



<http://scholar.sun.ac.za>

Fig.28b

### Evaluation of the Effect of Grain Size on Cr and Th

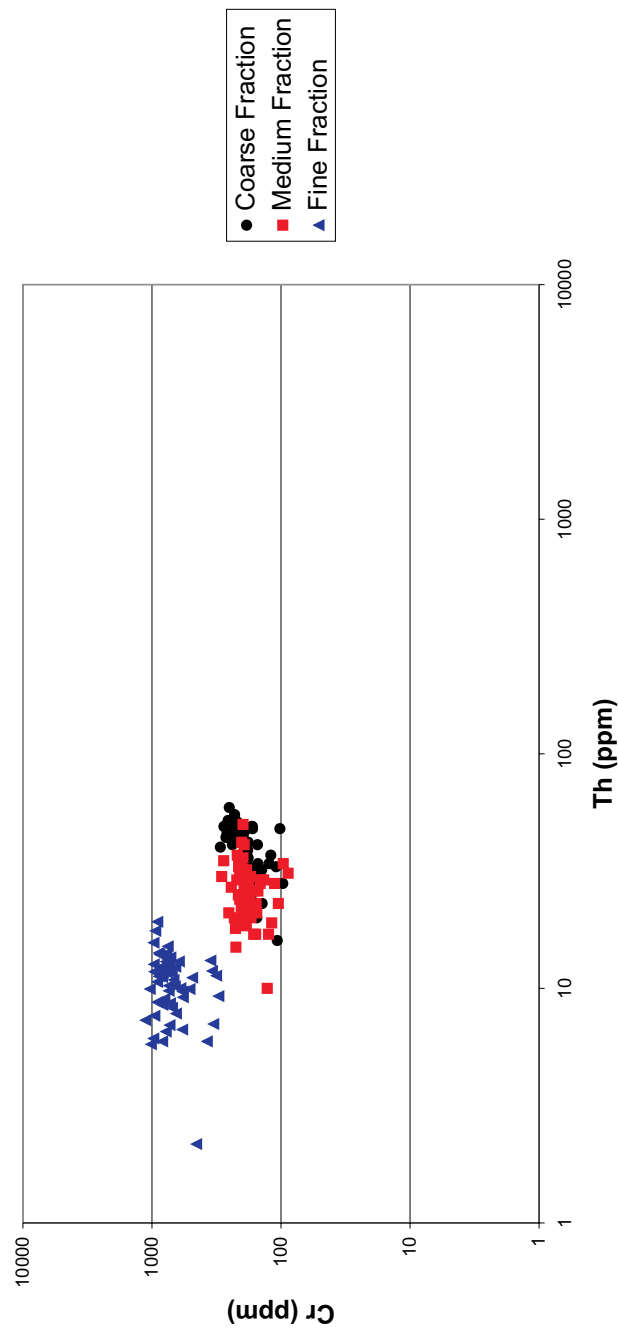


Fig.28c

### Evaluation of the Effect of Grain Size on Zn and Th

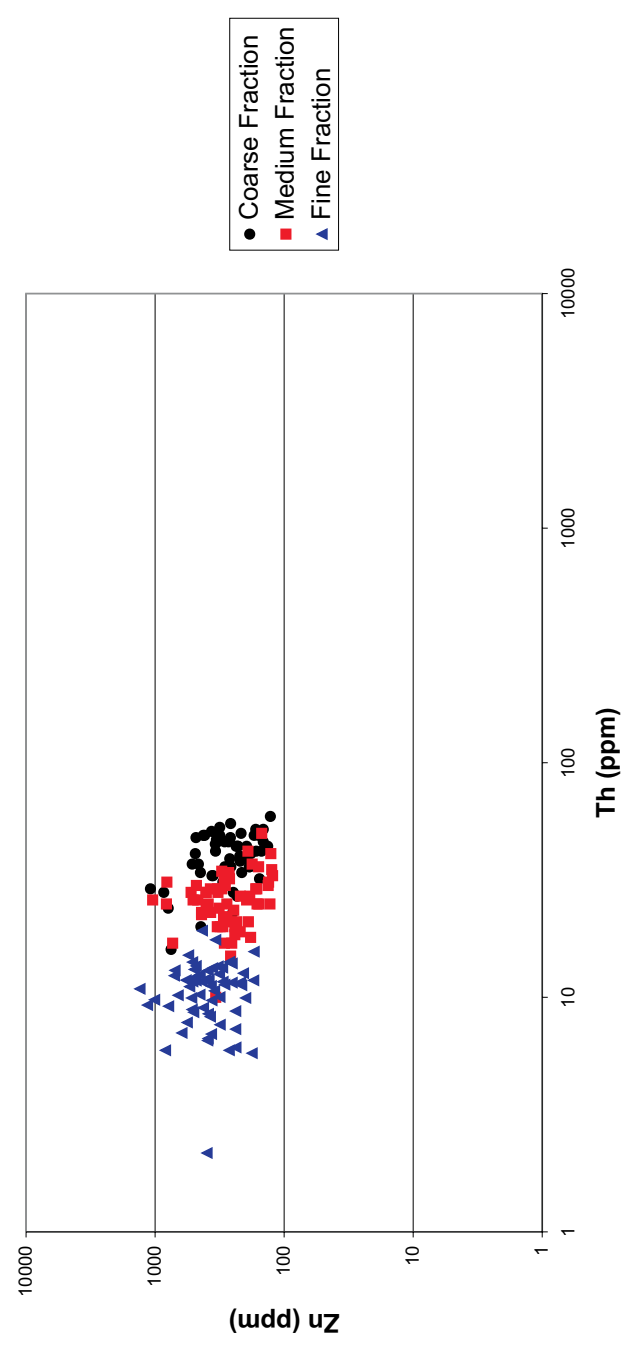


Fig.28d

Fig.28 Scatterplots of V, Ni, Cr, Zn and Th as a tool for the evaluation of the effect of grain size on trace element chemistry.

### Evaluation of the Effect of Grain Size on V and Ni Values

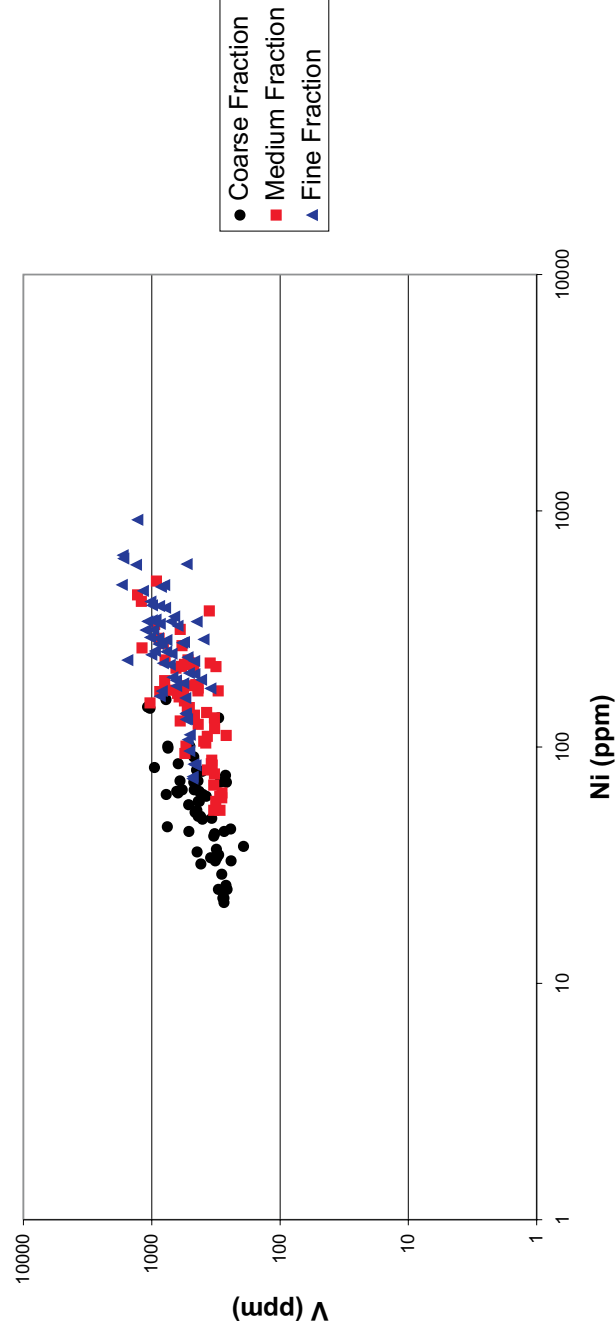
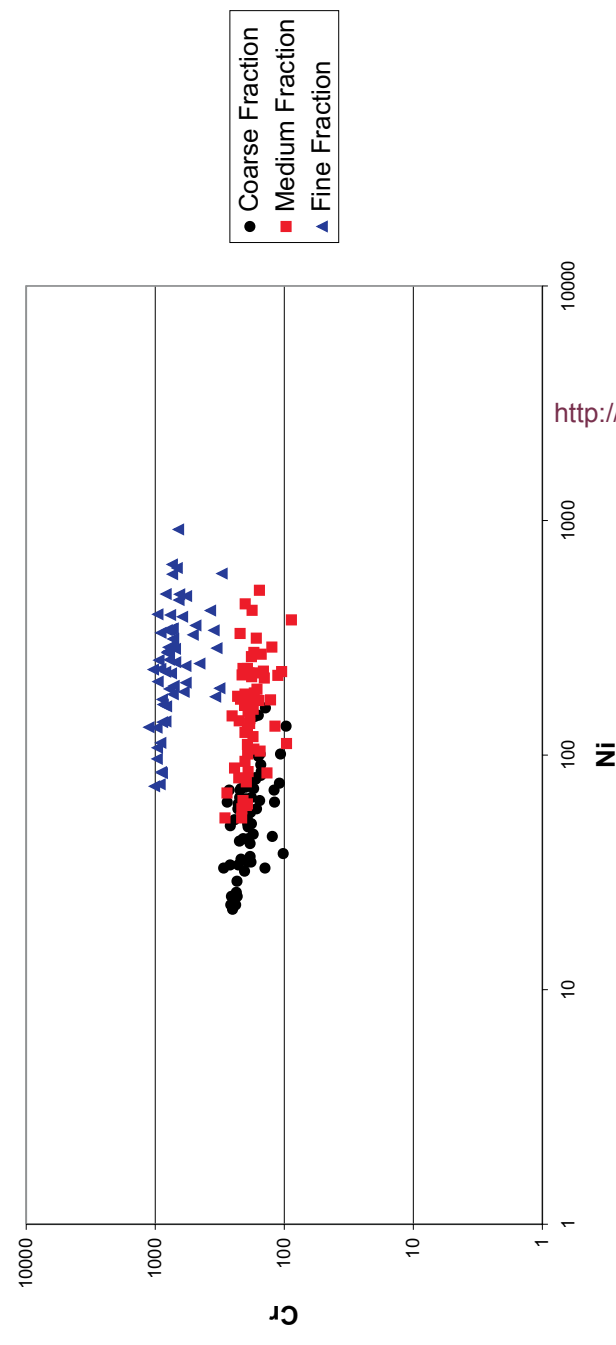


Fig.28e

### Avaluation of the Effect of Grain Size on Cr and Ni



<http://scholar.sun.ac.za/>

Fig.28f

### Evaluation of the Effect of Grain Size on Zn and Ni

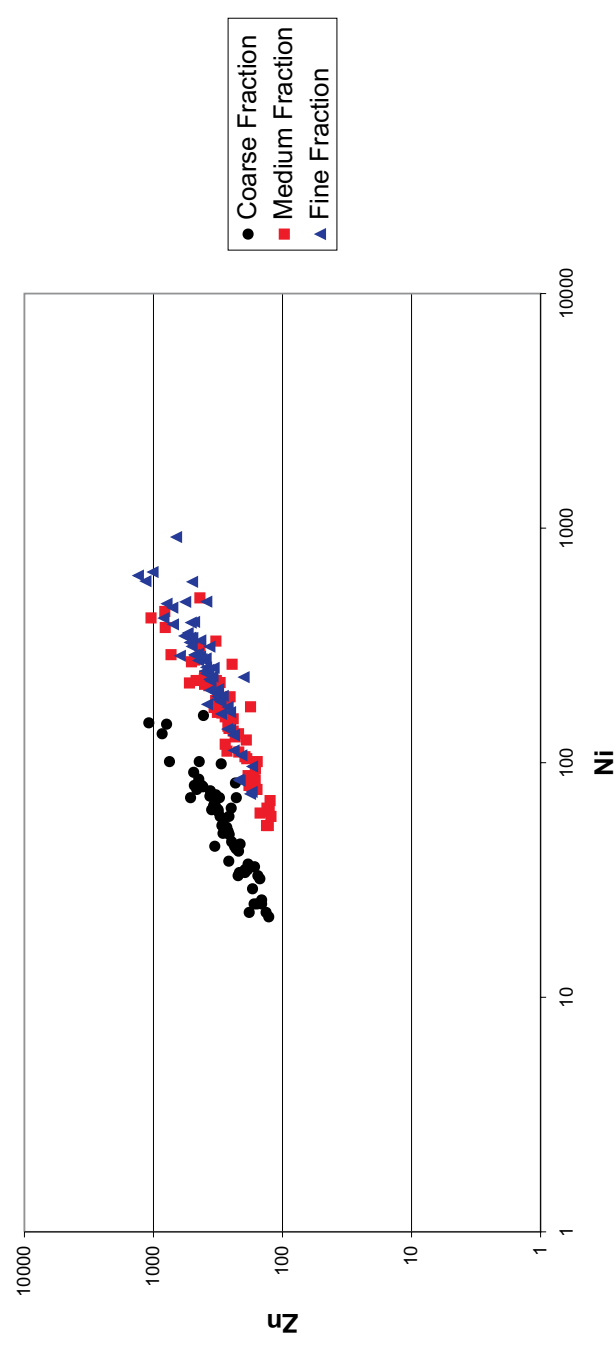


Fig.28g

Fig.28 ...continued

plots of V, Zn and Cr against Ni. Cr shows a strong trend of enrichment in the fine fraction relative to the medium and coarse fractions relative to Ni (Fig.28e). V and Zn both show more gradual trends of enrichment towards the fine fraction relative to Ni (Fig.30f-g).

As an aid to the above scatterplots in the study of trace element distribution, the average and standard errors of the chosen elements were calculated and are presented in Table 12.

<b>Element</b>	<b>Fraction</b>	<b>Average</b>	<b>Standard Error</b>
<b>V</b>	Coarse	440.27	51.61
	Medium	541.60	62.39
	Fine	779.50	82.12
<b>Ni</b>	Coarse	60.86	7.85
	Medium	177.54	24.82
	Fine	287.93	40.52
<b>Zn</b>	Coarse	318.85	45.33
	Medium	311.23	45.73
	Fine	438.54	56.60
<b>Cr</b>	Coarse	192.04	11.83
	Medium	183.65	10.08
	Fine	739.01	47.99
<b>Ba</b>	Coarse	465.46	98.67
	Medium	990.28	99.02
	Fine	910.61	60.80
<b>Th</b>	Coarse	39.52	2.70
	Medium	26.48	1.78
	Fine	10.73	0.77

Twice the standard deviation ( $\sigma$ ) was used in the calculation of the standard error implying a 95% certainty that a data point will be located in a certain data range (Fletcher et al., 1987), defined by the sum of and difference between the average ( $\bar{x}$ ) and the standard error. The calculation is expressed by the following equation:

$$\text{Data Range} = \bar{x} \pm \left( \frac{2\sigma}{\sqrt{n}} \right)$$



The data is presented schematically in Fig.29. From Fig.29 it becomes clear that no data overlap exists (except for a few samples which fall outside the 95% confidence limits) between the various size fractions for the individual trace elements. The differentiation of Ni values from lower values in the coarse fraction to higher values in the fine fraction is much more pronounced than that of V and Zn as was shown in the scatterplots (Fig.28a and Fig.28d). The highest values of Cr are in the fine fraction, but no clear distinction can be made between the coarse and medium fractions when viewing the spread of Cr concentration values (Fig.29). Thus Table 12 is a compliment to Fig.28.

#### 5.4. Correlation

The linear correlation coefficient ( $r$ ), is a dimensionless statistical parameter to quantify the extent to which the values of a specific variable vary relative to the values of a second variable and is defined by the following equation:

$$r = \frac{\text{Cov}_{xy}}{S_x \cdot S_y}$$

with  $\text{Cov}_{xy}$  the covariance of variable  $\chi$  and  $y$  defined by:

$$\text{Cov}_{xy} = \frac{1}{n-1} \sum_{i=1}^n (x_i - \bar{x})(y_i - \bar{y})$$

with  $n$  the number of data points,  $\chi_i$  the  $i^{\text{th}}$  value of variable  $\chi$ ,  $\bar{x}$  the average for all values of variable  $\chi$ ,  $y_i$  the  $i^{\text{th}}$  value of variable  $y$ ,  $\bar{y}$  the average for all values of variable  $y$  and  $S_x$  and  $S_y$  the standard deviations of variables  $\chi$  and  $y$  respectively. The upper and lower limits of the coefficient vary between the values of  $-1$  and  $1$ .  $1$  indicates a perfect sympathetic (positive) correlation, or simultaneous variability, while  $-1$  indicates a perfect antipathetic (negative) correlation.  $0$  indicates the total absence of any correlation between the values of two respective variables. A few examples from the Merelani lithologic data set were chosen as examples of the relation of numerical integer values of  $r$  and their data distribution patterns in a scatterplot and presented in Fig.30.

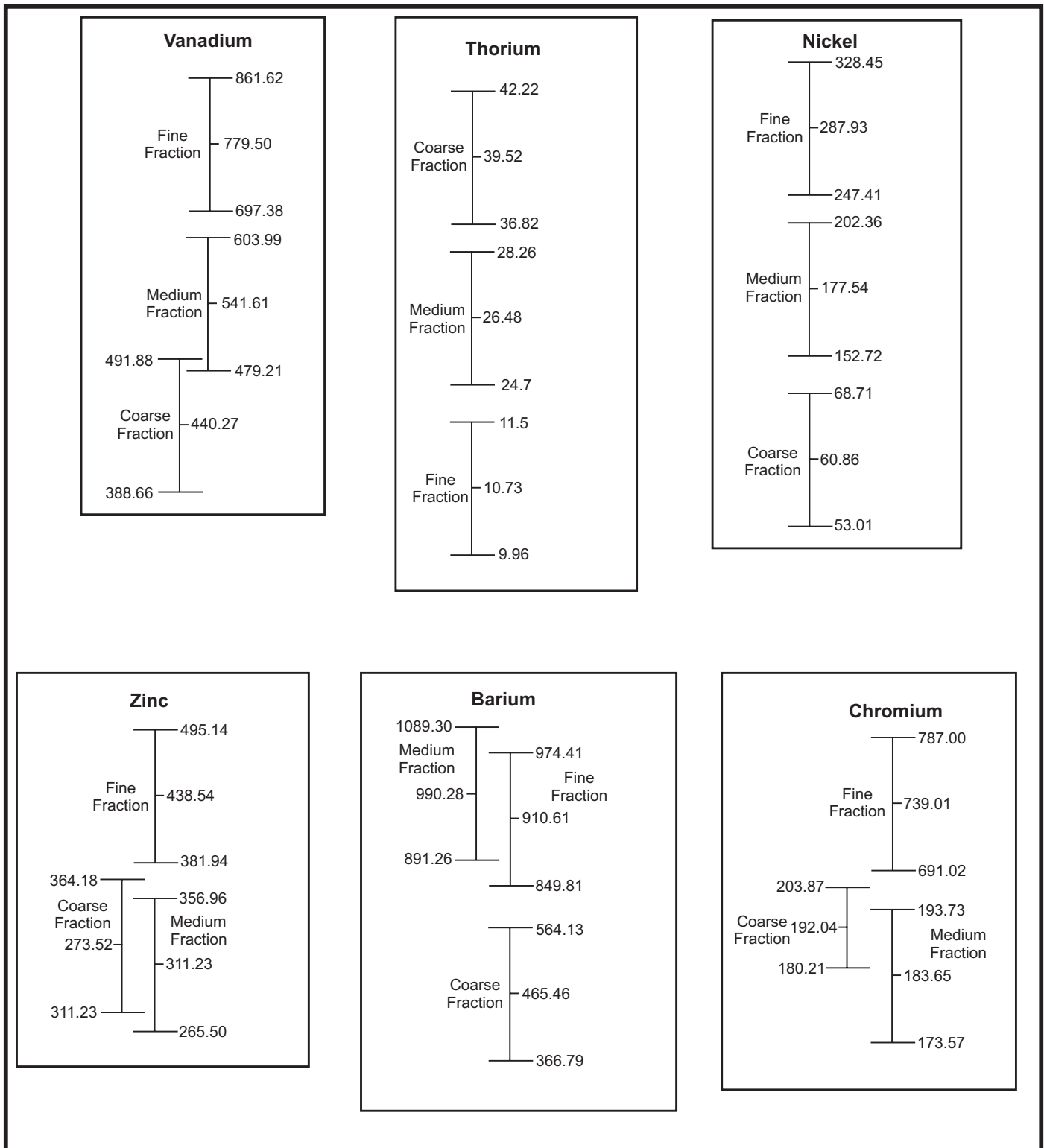


Fig.29 Schematic diagram of trace element data ranges (as described in the text)

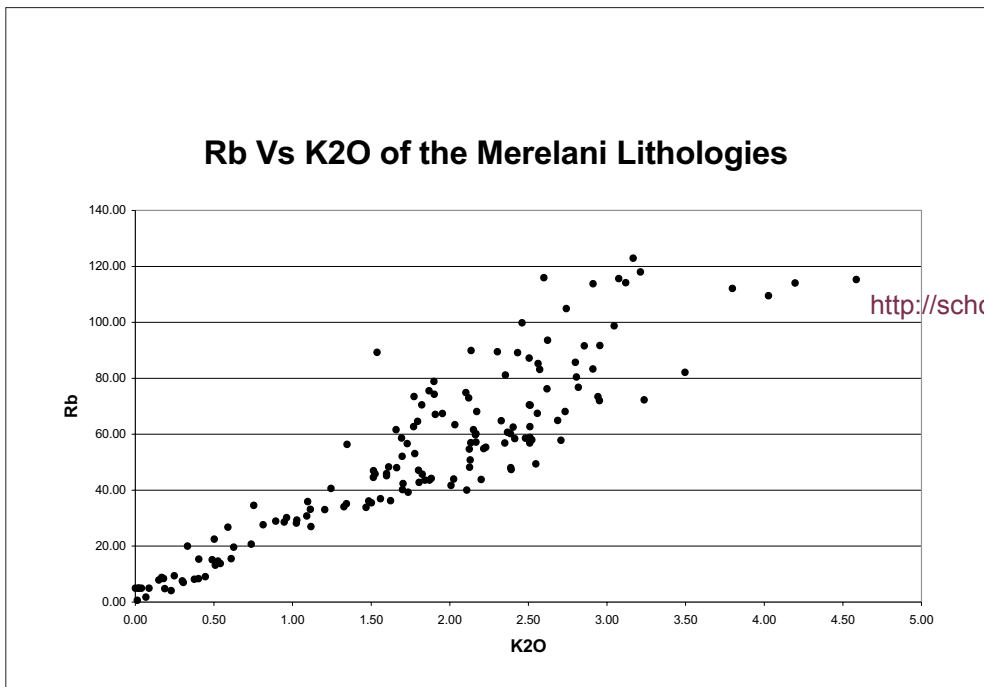


Fig.30a r~1

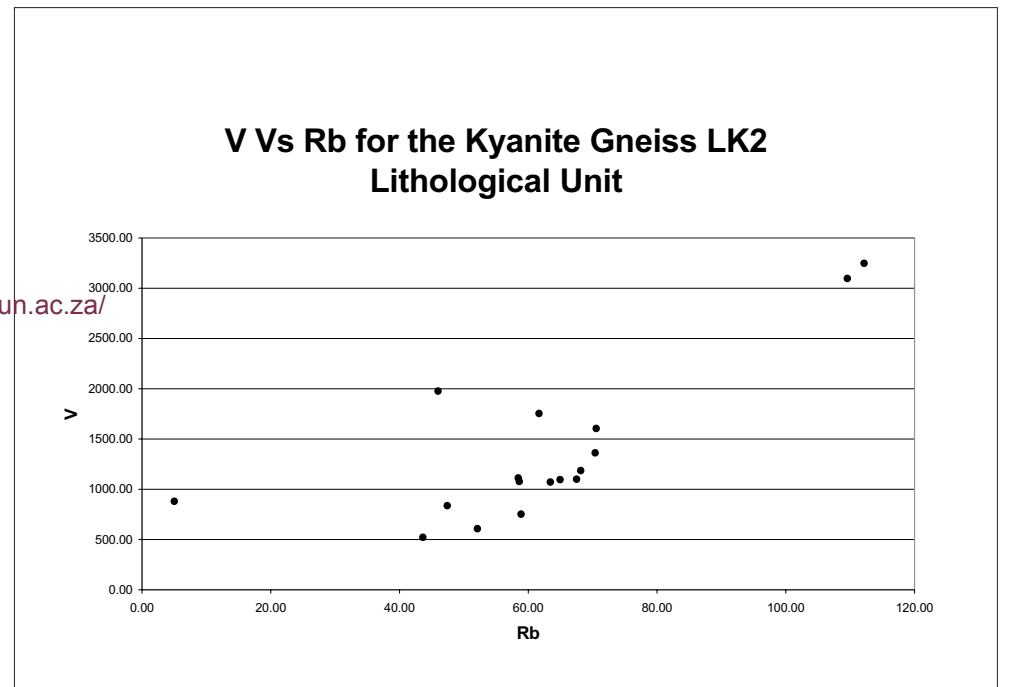


Fig.30b r~0.8

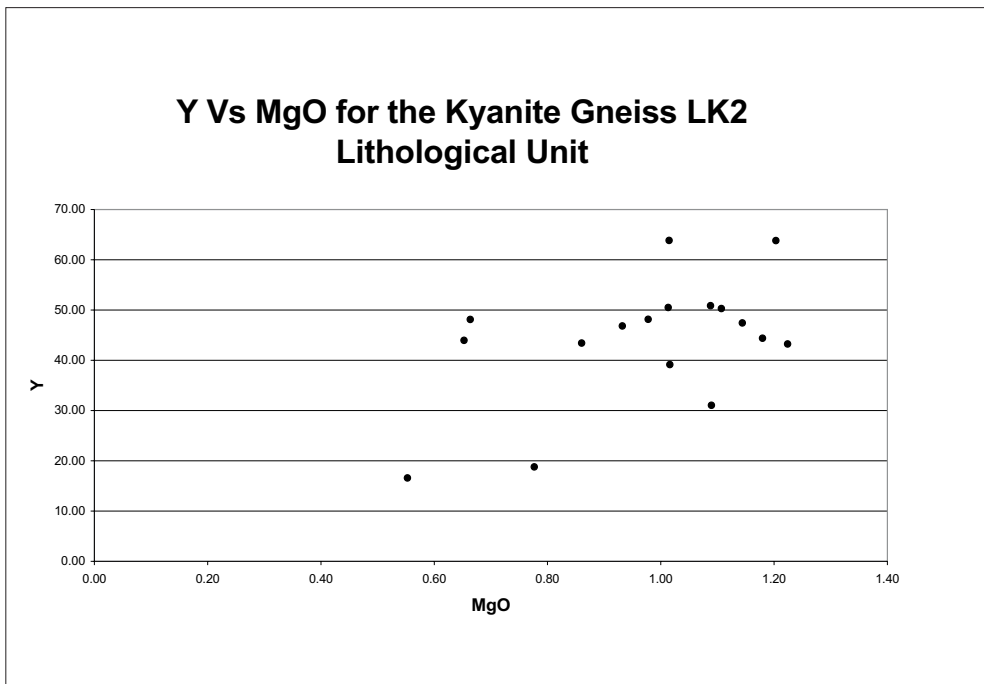


Fig.30c r~0.5

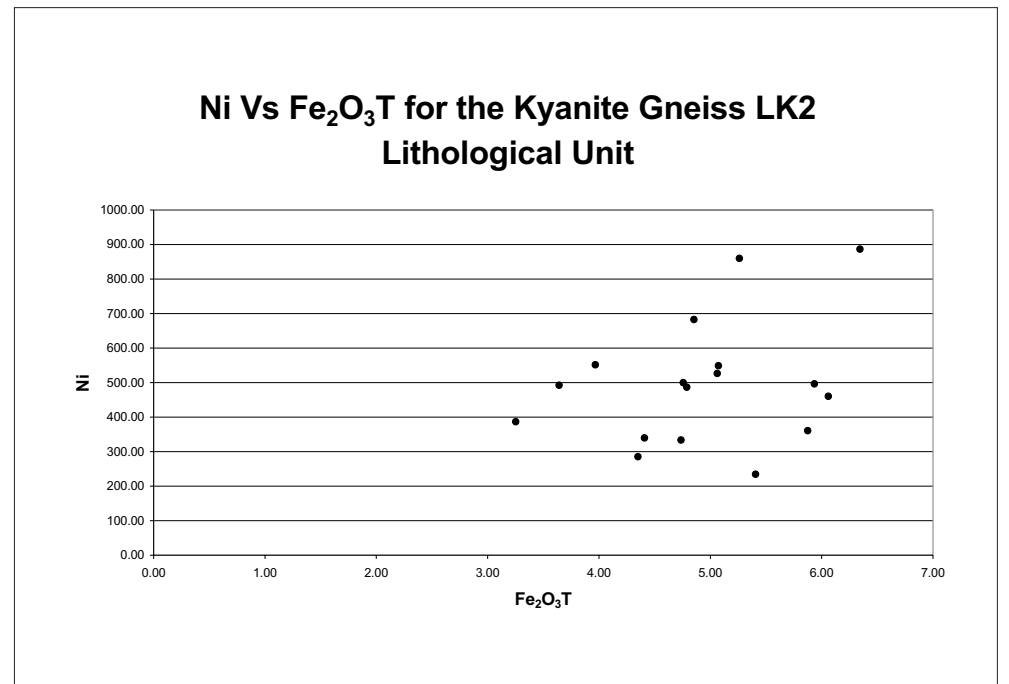


Fig.30d r~0.3

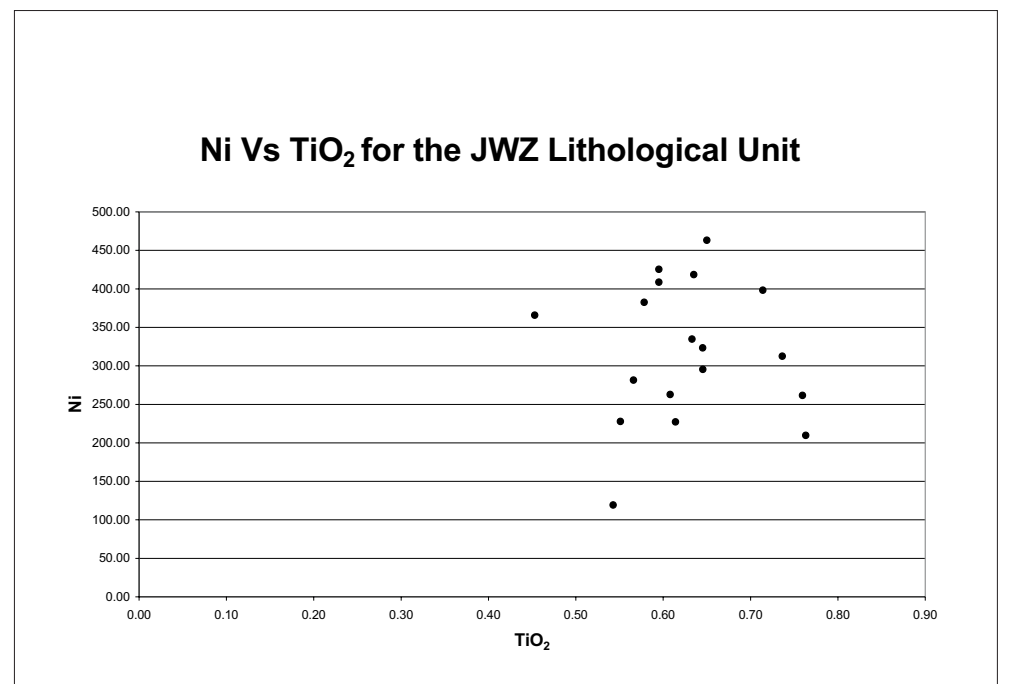


Fig.30e r~0

Fig.30 Graphic representations as examples of different values of r

There is one difficulty regarding  $r$ , inherent in its name, which must be taken into account. The linear correlation coefficient is a measure of linear trends and does not show any polynomial trends of data variability (Fig.31a (i - ii) and Fig.31b (i - ii)). The numerical value of the coefficient should therefore always be interpreted in conjunction with the relevant scatterplots.

#### **5.4.1. Merelani Lithology Trace Element Correlations**

Correlation matrices of the major and trace elements of the Merelani lithologies and soils were constructed (addendum compact disc). A value of  $r \geq 0.500$  was taken as a significant correlation. These matrices were constructed in order to identify certain element groups within the major and trace element data sets, which show mutual variation trends. The aim was to discern possible mineralogic hosts for the various trace elements. The study was performed in three main phases. In the first phase correlations between the trace and major elements for the Merelani lithologies were calculated. Various groups with mutually correlating trace elements and major element oxides were identified. These groups are referred to as “mutually correlating” groups. In the second phase, the correlation coefficients for the trace elements from the Merelani trench soils were calculated. Once again, trace elements displaying mutual correlations were identified and grouped. In the third phase the groups from the Merelani lithologies and soils were compared with each other and with published data on mineral chemistry. This was done to discern possible mineralogic hosts for the trace elements of the soils, based on the groups of mutual correlation in which specific elements occur. The results of this study are easily verified by LA-ICP-MS.

The Kyanite Gneiss (LK4) unit is taken as an example of the process.

Four groups of mutually correlating trace elements were identified from the correlation matrix for the Kyanite Gneiss LK4 unit (Table 13) compared to the six groups of mutually correlating trace elements and major element oxides, as show in Table 14. It can be seen from both these tables that there are subtle differences between the groups of mutually correlating trace elements and of the groups of trace elements and major element oxides. However, when the groups mutually correlating elements in Table 14 is studied, it becomes apparent that the groups of Table 13 are grouped

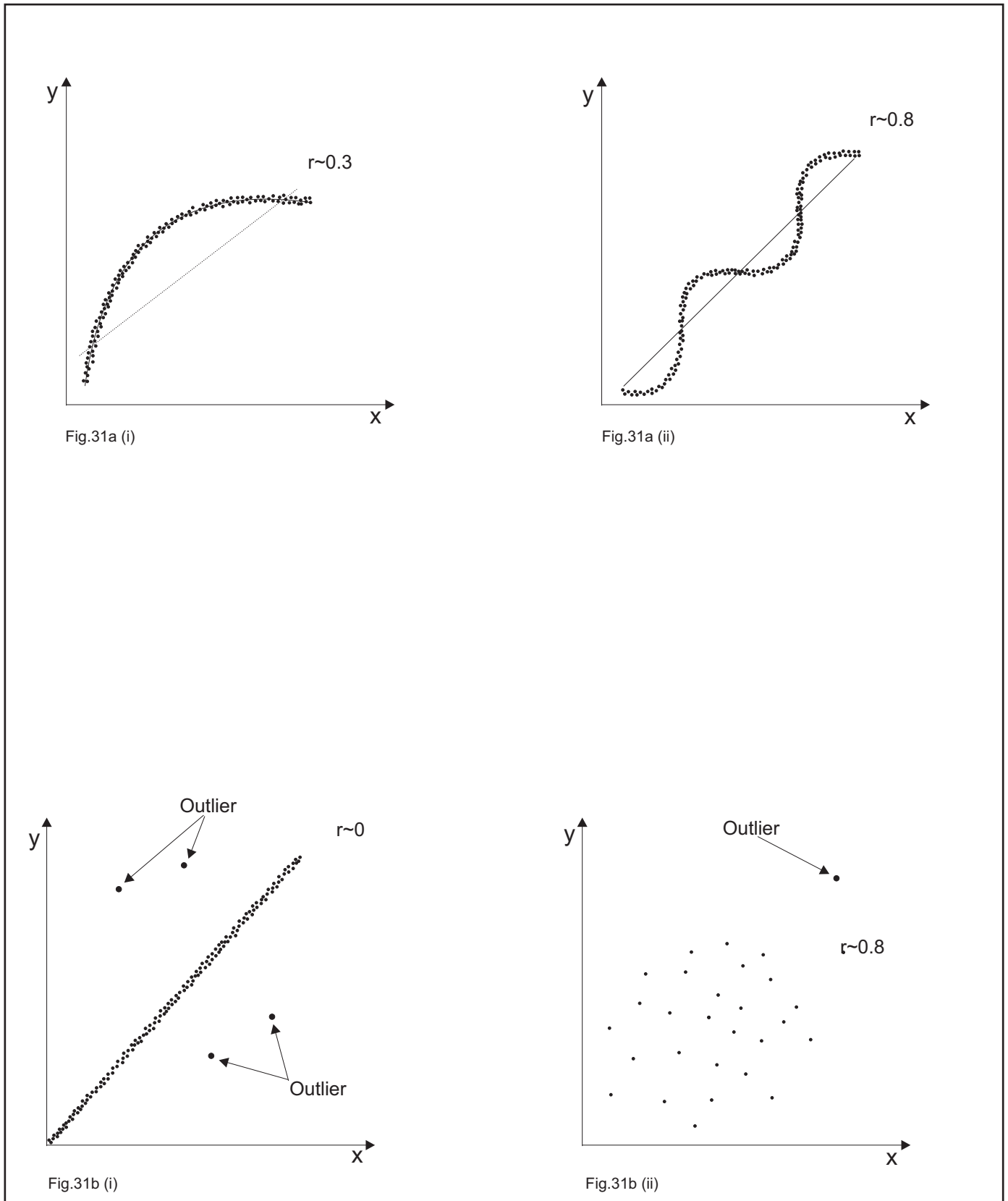


Fig.31 Schematic diagram of potentials problems when using r (after Fletcher, 1987)

<b>Table 13 Groups of mutually correlating trace elements in the Kyanite Gneiss (LK4)</b>	
<b>Group<sup>1</sup></b>	<b>Elements</b>
1	V, Ba, Sr
2	Ga, Rb, Sr, Ce, Y, La, Nd, Th
3	Th, Y, Ce, U, Zn, Cr, Nb
4	Zr, Cu, Pb, Nb

<b>Table 14 Groups of mutually correlating trace elements and major element oxides in the Kyanite Gneiss (LK4)</b>	
<b>Group</b>	<b>Elements</b>
1	TiO <sub>2</sub> , Zr, Nb, Ce, Th, MgO
2	CaO, P <sub>2</sub> O <sub>5</sub> , Ga, Rb, La, Ce, Nd, Sr, Zr, U, Na <sub>2</sub> O, MgO
3	K <sub>2</sub> O, Al <sub>2</sub> O <sub>3</sub> , V, Ba, Ga, Rb, Sr, Y, Ce, Ni, Cu, U, Cr, Zn, Na <sub>2</sub> O, MnO
4	Fe <sub>2</sub> O <sub>3</sub> T, La, Nd, Ni, Zr, Zn, Ga, MnO
5	Zr, Cu, Nb, Nd, Pb, Ni, LOI
6	Zn, Y, La, Nd, MnO, K <sub>2</sub> O

<sup>1</sup> a "Group" is defined by values of r defining mutual correlations between the elements of a specific group as represented in the above tables.

together to form the larger groups in Table 14. This is a result of adding the major element oxides to the correlation matrix of the trace elements and recalculating the correlations.

The groups of mutually correlating trace elements and major element oxides identified for the Merelani Lower Horizon lithologies are shown in Table 14. The groups of mutually correlating major element oxides and trace elements were ascribed to a mineral phase(s) depending on the dominant major element component for a specific mineral phase (Table 15b) based on published data on mineral chemistry (Deer et al., 1966, Klein and Hurlbut, 1993, Wederpohl, 1978).

In order to identify general groups of mutually correlating trace elements in the Merelani lithologies, all the lithological units were placed in a single spreadsheet and a correlation matrix constructed (Table 16). The resultant matrix is therefore an average of all the Merelani lithologies potentially rendering it comparable to a matrix of the entire soil data set as certain soils cover more than one lithological unit.

Five groups were identified for both the major and trace elements (Table 15). The only element in the Merelani lithologies with which  $\text{SiO}_2$  shows a significant correlation is Zr. This is an indication that Zr is predominantly incorporated into silicate minerals and the mineral zircon is inferred, as this mineral does occur in many of the Merelani lithologies (see Chapter 2, section 2). This is also substantiated by the correlation between Zr and Y in many of the Merelani lithologies as these two elements commonly group together (Wederpohl, 1978). The second group is interpreted as being contained in the heavy minerals, including garnet due to the  $\text{TiO}_2\text{-Al}_2\text{O}_3$  correlation. The third group is inferred as representing the carbonates, due to the mutual correlation of CaO, MgO and LOI. The fourth group is seen to represent the feldspars and micas, based on published data (Icenhower and London, 1996). It must be noted that the Rb- $\text{K}_2\text{O}$  correlation is remarkable (Fig.32) with  $r = 0.906$ . This excellent correlation exists despite the fact that the correlation matrix represents the entire group of Merelani lithologies. This strongly suggests that both Rb and  $\text{K}_2\text{O}$  are located in a very limited amount of mineral phases. The last group is a group containing  $\text{P}_2\text{O}_5$  and the Rare Earth Elements (REE).

<b>Table.15 Table of various groups extracted via intercorrelatory trace element and trace element-major element oxide relationships</b>		
<b>Major or Trace Element</b>	<b>Element</b>	<b>Correlated with</b>
<b>Major Element Correlations</b>	SiO <sub>2</sub>	Zr
	TiO <sub>2</sub>	Ga, Zr, Nb, <i>Al<sub>2</sub>O<sub>3</sub><sup>1</sup></i> , Fe <sub>2</sub> O <sub>3</sub> T
	Al <sub>2</sub> O <sub>3</sub>	Ga, Zr, Nb, <i>TiO<sub>2</sub></i> , Fe <sub>2</sub> O <sub>3</sub> T, LOI
	Fe <sub>2</sub> O <sub>3</sub> T	Ga, TiO <sub>2</sub> , Al <sub>2</sub> O <sub>3</sub>
	MgO	CaO, LOI
	K <sub>2</sub> O	<b>Rb</b>
	CaO	MgO, LOI
	P <sub>2</sub> O <sub>5</sub>	<b>Y, Ce</b>
	LOI	MgO, LOI
	<b>Trace Element Correlations</b>	V
Ni		V, Zn, U
Cu		V, Ba
Zn		V, Ni, U
Ga		TiO <sub>2</sub> , Al <sub>2</sub> O <sub>3</sub> , Fe <sub>2</sub> O <sub>3</sub> T
Rb		<b>K<sub>2</sub>O</b>
Y		La, <b>Ce</b> , Nd, P <sub>2</sub> O <sub>5</sub>
Zr		Nb, La, Ce, Nd, SiO <sub>2</sub> , TiO <sub>2</sub> , Al <sub>2</sub> O <sub>3</sub>
Nb		Zr, TiO <sub>2</sub> , Al <sub>2</sub> O <sub>3</sub>
Ba		Cu
Ce		<b>Y</b> , Zr, La, Nd, <b>P<sub>2</sub>O<sub>5</sub></b>
U		V, Ni, Zn

Major Element Groups:

1. SiO<sub>2</sub>, Zr
2. TiO<sub>2</sub>, Al<sub>2</sub>O<sub>3</sub>, Fe<sub>2</sub>O<sub>3</sub>T, Ga, Zr
3. MgO, CaO, LOI
4. K<sub>2</sub>O, Rb
5. P<sub>2</sub>O<sub>5</sub>, Rare Earth Elements

Trace Element Groups:

1. V, Ni, Zn, U, Cu, Ba<sup>2</sup>
2. Y, La, Ce, Nd, P<sub>2</sub>O<sub>5</sub>, Zr
3. Zr, Nb, La, Ce, Nd, SiO<sub>2</sub>, TiO<sub>2</sub>, Al<sub>2</sub>O<sub>3</sub><sup>3</sup>
4. Rb, K<sub>2</sub>O
5. Ga, TiO<sub>2</sub>, Fe<sub>2</sub>O<sub>3</sub>T, Al<sub>2</sub>O<sub>3</sub><sup>4</sup>

<b>Table.15b Table of various groups extracted via intercorrelatory trace element and trace element-major element oxide relationships</b>		
<b>Group</b>	<b>Elements</b>	<b>Associated mineral(s)</b>
1	V, Ni, Zn, U, Cu, Ba, Cr, Sr, Th	Graphite
2	Fe <sub>2</sub> O <sub>3</sub> T, MnO, Na <sub>2</sub> O, H <sub>2</sub> O <sup>+</sup>	Fe-Minerals
3	Zr, Nb, SiO <sub>2</sub> , TiO <sub>2</sub> , Al <sub>2</sub> O <sub>3</sub> , Ga	Heavy Minerals (especially, Zircon, Rutile, Ilmenite, Kyanite, Garnet)
4	Rb, Pb, K <sub>2</sub> O	Feldspars and Micas
5	CaO, MgO, LOI	Carbonates
6	REE, P <sub>2</sub> O <sub>5</sub>	Apatite, Allanite

<sup>1</sup> Italics implies 0.8<r<0.9 and bold implies r>0.9

<sup>2</sup> This group is not significantly associated with any major element oxides and could be associated with graphite, as graphite is a major mineral phase in many of the Merelani lithologies

<sup>3</sup> It could be that Zr is associated with the mineral zircon as well as with another phase, such as rutile and the clay minerals. Nb displays the same behaviour

<sup>4</sup> Ga seems to be associated with the heavy mineral phase, although the Al<sub>2</sub>O<sub>3</sub> could represent the garnets as well as the clay minerals or feldspar – the garnets or feldspars are preferred as the clay minerals only form a major phase in the altered zones



Table 16 Correlation Matrix of the entire Merelani lithology data set

	V	Cr	Ni	Cu	Zn	Ga	Rb	Sr	Y	Zr	Nb	Ba	La	Ce	Nd	Pb	Th	U	SiO2	TiO2	Al2O3	Fe2O3T	MnO	MgO	CaO	Na2O
V	1.000	0.297	0.855	0.540	0.765	-0.026	-0.198	0.338	0.165	0.133	-0.083	0.475	0.437	0.042	0.457	0.027	-0.144	0.677	0.128	-0.021	-0.040	-0.102	-0.200	-0.390	-0.304	0.055
Cr	0.297	1.000	0.449	0.132	0.343	-0.033	-0.110	0.181	0.112	0.189	0.084	0.253	0.445	-0.044	0.601	-0.360	0.450	0.309	0.170	0.195	0.223	0.115	-0.061	-0.259	-0.305	0.026
Ni	0.855	0.449	1.000	0.479	0.732	0.021	-0.185	0.253	0.192	0.135	0.033	0.400	0.494	0.073	0.500	-0.086	-0.022	0.735	0.100	0.055	-0.052	-0.081	-0.179	-0.345	-0.269	-0.035
Cu	0.540	0.132	0.479	1.000	0.147	-0.049	0.312	0.135	0.010	0.232	0.239	0.514	0.094	0.062	0.069	0.362	-0.001	0.031	0.277	0.235	0.173	0.253	-0.194	-0.317	-0.425	0.264
Zn	0.765	0.343	0.732	0.147	1.000	-0.023	-0.239	0.318	0.163	-0.055	-0.199	0.170	0.396	-0.016	0.430	-0.161	-0.027	0.738	0.054	-0.172	-0.117	-0.162	-0.017	-0.313	-0.132	-0.070
Ga	-0.026	-0.033	0.021	-0.049	-0.023	1.000	0.067	0.077	0.051	0.220	0.327	-0.258	0.143	0.143	0.324	0.101	0.008	0.087	0.253	0.589	0.618	0.564	0.366	-0.190	-0.358	0.037
Rb	-0.198	-0.110	-0.185	0.312	-0.239	0.067	1.000	0.055	-0.162	0.113	0.489	0.254	-0.035	-0.008	-0.101	0.452	0.238	-0.477	0.307	0.370	0.398	0.277	0.168	-0.129	-0.269	0.099
Sr	0.338	0.181	0.253	0.135	0.318	0.077	0.055	1.000	0.127	-0.015	0.162	0.248	0.369	-0.016	0.227	0.089	0.260	0.346	0.087	-0.126	0.037	-0.122	0.307	-0.310	-0.031	0.057
Y	0.165	0.112	0.192	0.010	0.163	0.051	-0.162	0.127	1.000	0.429	0.118	-0.085	0.550	0.915	0.576	-0.079	0.043	0.256	0.015	0.101	0.087	0.108	0.325	-0.211	-0.015	-0.086
Zr	0.133	0.189	0.135	0.232	-0.055	0.220	0.113	-0.015	0.429	1.000	0.540	0.297	0.615	0.542	0.619	0.026	0.079	0.007	0.546	0.600	0.550	0.333	0.097	-0.464	-0.629	0.390
Nb	-0.083	0.084	0.033	0.239	-0.199	0.327	0.489	0.162	0.118	0.540	1.000	0.174	0.504	0.256	0.475	0.221	0.302	-0.180	0.351	0.632	0.541	0.351	0.229	-0.245	-0.393	0.201
Ba	0.475	0.253	0.400	0.514	0.170	-0.258	0.254	0.248	-0.085	0.297	0.174	1.000	0.288	-0.067	0.260	0.171	0.022	0.086	0.340	0.096	0.124	-0.103	-0.353	-0.359	-0.436	0.280
La	0.437	0.445	0.494	0.094	0.396	0.143	-0.035	0.369	0.550	0.615	0.504	0.288	1.000	0.688	0.678	-0.298	0.311	0.335	0.222	0.248	0.348	-0.095	0.214	-0.320	-0.334	0.066
Ce	0.042	-0.044	0.073	0.062	-0.016	0.143	-0.008	-0.016	0.915	0.542	0.256	-0.067	0.688	1.000	0.819	-0.020	-0.039	0.064	0.025	0.287	0.233	0.223	0.326	-0.138	-0.064	-0.016
Nd	0.457	0.601	0.500	0.069	0.430	0.324	-0.101	0.227	0.576	0.619	0.475	0.260	0.678	0.819	1.000	-0.287	0.272	0.292	0.194	0.476	0.478	0.082	0.219	-0.246	-0.408	0.045
Pb	0.027	-0.360	-0.086	0.362	-0.161	0.101	0.452	0.089	-0.079	0.026	0.221	0.171	-0.298	-0.020	-0.287	1.000	-0.074	-0.242	0.269	0.111	0.068	0.077	0.979	-0.199	-0.213	0.097
Th	-0.144	0.450	-0.022	-0.001	-0.027	0.008	0.238	0.260	0.043	0.079	0.302	0.022	0.311	-0.039	0.272	-0.074	1.000	0.005	0.210	0.032	0.136	0.052	0.326	-0.171	-0.112	-0.113
U	0.677	0.309	0.735	0.031	0.738	0.087	-0.477	0.346	0.256	0.007	-0.180	0.086	0.335	0.064	0.292	-0.242	0.005	1.000	0.009	-0.195	-0.197	-0.155	-0.221	-0.297	-0.071	-0.174
SiO2	0.128	0.170	0.100	0.277	0.054	0.253	0.307	0.087	0.015	0.546	0.351	0.340	0.222	0.025	0.194	0.269	0.210	0.009	1.000	0.331	0.483	0.255	0.046	-0.815	-0.896	0.381
TiO2	-0.021	0.195	0.055	0.235	-0.172	0.589	0.370	-0.126	0.101	0.600	0.632	0.096	0.248	0.287	0.476	0.111	0.032	-0.195	0.331	1.000	0.856	0.736	0.232	-0.193	-0.556	0.171
Al2O3	-0.040	0.223	-0.052	0.173	-0.117	0.618	0.398	0.037	0.087	0.550	0.541	0.124	0.348	0.233	0.478	0.068	0.136	-0.197	0.483	0.856	1.000	0.748	0.293	-0.337	-0.663	0.382
Fe2O3T	-0.102	0.115	-0.081	0.253	-0.162	0.564	0.277	-0.122	0.108	0.333	0.351	-0.103	-0.095	0.223	0.082	0.077	0.052	-0.155	0.255	0.736	1.000	0.748	0.344	-0.179	-0.450	0.144
MnO	-0.200	-0.061	-0.179	-0.194	-0.017	0.366	0.168	0.307	0.325	0.097	0.229	-0.353	0.214	0.326	0.219	0.079	0.126	-0.021	0.046	0.232	0.293	0.344	1.000	-0.063	0.030	-0.092
MgO	-0.390	-0.259	-0.345	-0.317	-0.313	-0.190	-0.129	-0.310	-0.211	-0.464	-0.245	-0.359	-0.320	-0.138	-0.246	-0.199	-0.171	-0.297	-0.815	-0.193	-0.337	-0.179	-0.063	1.000	0.704	-0.255
CaO	-0.304	-0.305	-0.289	-0.425	-0.132	-0.358	-0.269	-0.031	-0.015	-0.629	-0.393	-0.436	-0.334	-0.064	-0.408	-0.213	-0.112	-0.071	-0.896	-0.556	-0.663	-0.450	0.030	0.704	1.000	-0.439
Na2O	0.055	0.026	-0.035	0.264	-0.070	0.037	0.099	0.057	-0.086	0.390	0.201	0.280	0.086	-0.016	0.045	0.097	-0.113	-0.174	0.381	0.171	0.382	0.144	-0.092	-0.255	-0.439	1.000
K2O	-0.062	0.024	-0.099	0.403	-0.139	-0.082	0.906	0.050	-0.175	0.235	0.416	0.480	0.118	-0.041	0.051	0.415	0.224	-0.431	0.438	0.308	0.391	0.179	-0.017	-0.265	-0.424	0.263
P2O5	0.013	-0.007	0.041	0.023	-0.025	-0.045	-0.132	-0.051	0.938	0.391	0.067	-0.106	0.222	0.920	0.386	0.003	-0.077	0.054	-0.041	0.062	0.000	0.064	0.241	-0.081	0.053	-0.062
H2O-	0.265	-0.044	0.474	0.069	0.195	0.268	-0.091	-0.073	0.048	-0.016	0.095	0.048	0.113	0.099	0.251	0.071	-0.193	0.408	-0.021	0.131	-0.053	0.029	-0.001	-0.071	-0.087	-0.218
LOI	0.295	-0.055	0.282	-0.121	0.271	-0.389	-0.552	-0.027	-0.086	-0.511	-0.514	-0.077	-0.044	-0.178	-0.028	-0.245	-0.308	0.346	-0.796	-0.544	-0.725	-0.548	-0.346	0.545	0.687	-0.358

# Rb Vs K<sub>2</sub>O for the Merelani Lithologies

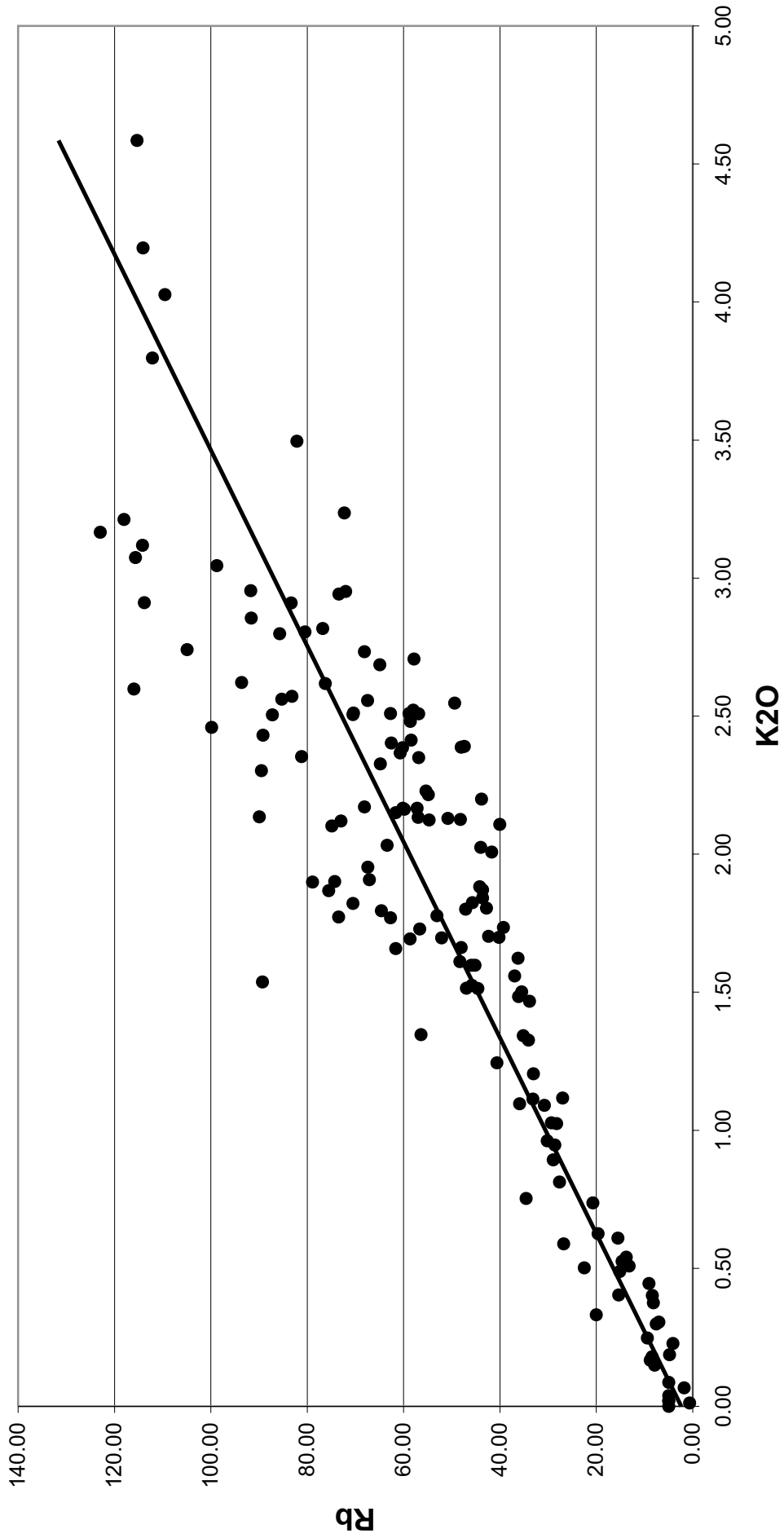


Fig.32 Scatterplot of Rb against K<sub>2</sub>O showing the excellent correlation between these two elements for the Merelani lithological units

It is well known by igneous petrologists and geochemists that apatite, which is present in the Merelani rocks, is an important sink for REE (Fleet and Pan, 1997, Rakovan and Reeder, 1996, Watson and Green, 1981). There are, however, two problems with the excellent correlations in the Merelani lithology data set. The first is fairly simple and relates to the amount of apatite in the rocks. Only three of the six zones of Merelani lithologies contain apatite and then only as an accessory. Fleet and Pan (1997) and Watson and Green (1981) published data on the ability of apatite to absorb REE from water-bearing phosphate fluoride melts and on the partition coefficients of REE between apatite and a liquid ( $D_{\text{REE}}^{\text{ap/liquid}}$ ) at temperatures of 700°C to 800°C and pressures of 0.10GPa to 0.15GPa. The partition coefficients in both these publications are in relatively good agreement and the data from Fleet and Pan (1997) will be used. Their partition coefficients are presented in Table 17.

<b>Rare Earth Element</b>	<b>Distribution Coefficient (D)</b>
La	5
Ce	7
Nd	8

The average values for La, Ce and Nd for the Merelani rocks are presented in Table 18.

<b>Rare Earth Element</b>	<b>Average Concentration</b>
La	23.32
Ce	38.50
Nd	25.50

Ce is taken as an example. For a total of 38.50ppm Ce with a  $D_{\text{Ce}}^{\text{ap/liquid}}$  of 7, a total of 33.69ppm Ce will theoretically partition into apatite with 4.81ppm remaining in the fluid. These values relate to a situation where apatite is the only primary REE absorbing mineral. Thus 12.5% of the Ce will either remain in the melt or be transported by supercritical (or hydrothermal) fluids and precipitate elsewhere such as in other

minerals. One thing that must be kept in mind is the linear correlation coefficient between Ce ( $r=0.560$ ) and  $P_2O_5$  and the even lower correlation coefficient between  $P_2O_5$  and the other REE. So even though the  $r_{Ce-P_2O_5}$  is significant, it may be that the correlation is due to other factors, such as possible mutual correlation with graphite, and not apatite. So, although an apatite Ce content of 33.69ppm is quite possible, it might be more likely that the REE were firstly absorbed onto organic carbon (Dissanayake et al., 1988) and then mobilised by progressive metamorphism and incorporated into apatite and various other minerals, hence the only significant correlation with each other and  $P_2O_5$ , which probably means that they (REE and  $P_2O_5$ ) moved together. Additional evidence for the aforementioned lies in the significant positive correlation between Ce and V in altered rocks. V is also thought to have been extracted from seawater by organic matter and mobilised during diagenesis and progressive metamorphism to be incorporated into silicate minerals (Breit and Wanty, 1991). It is not being implied that the apatite does not contain any REE, only that they are most probably primarily concentrated elsewhere and that the REE- $P_2O_5$  relationship can be explained by other factors.

The second problem with the REE- $P_2O_5$  correlation is that the values of  $r$  are classic examples of the influence of an outlier on the correlation coefficient (Fig.33). When Fig.35 is studied, it can be seen that an outlying sample plots to the right of all the rest. When this sample is removed, it can be seen that the correlation is reduced from 0.920 to 0.164 (Fig.35b). The significant correlation has been reduced from a status of significance to one of insignificance. The value of  $r$  is 82.17% less than when plotted with the outlier. This serves as additional evidence that it is not apatite that is the most significant drive in the Merelani REE chemistry. The sample was removed, because of its large effect on especially the REE- $P_2O_5$  correlations, rendering them unrepresentative. The sample must, however, not be excluded from the database and must be examined in more detail to discern the reason for the anomalous values.

Breit and Wanty (1991) highlights the significance of the V/Ni ratio, which is indicative of both the oxidation-state of the accumulation zone as well as the amount of S present. They state that:

*V accumulates relative to nickel (high V/Ni) in strongly reducing, H<sub>2</sub>S-rich environments.*

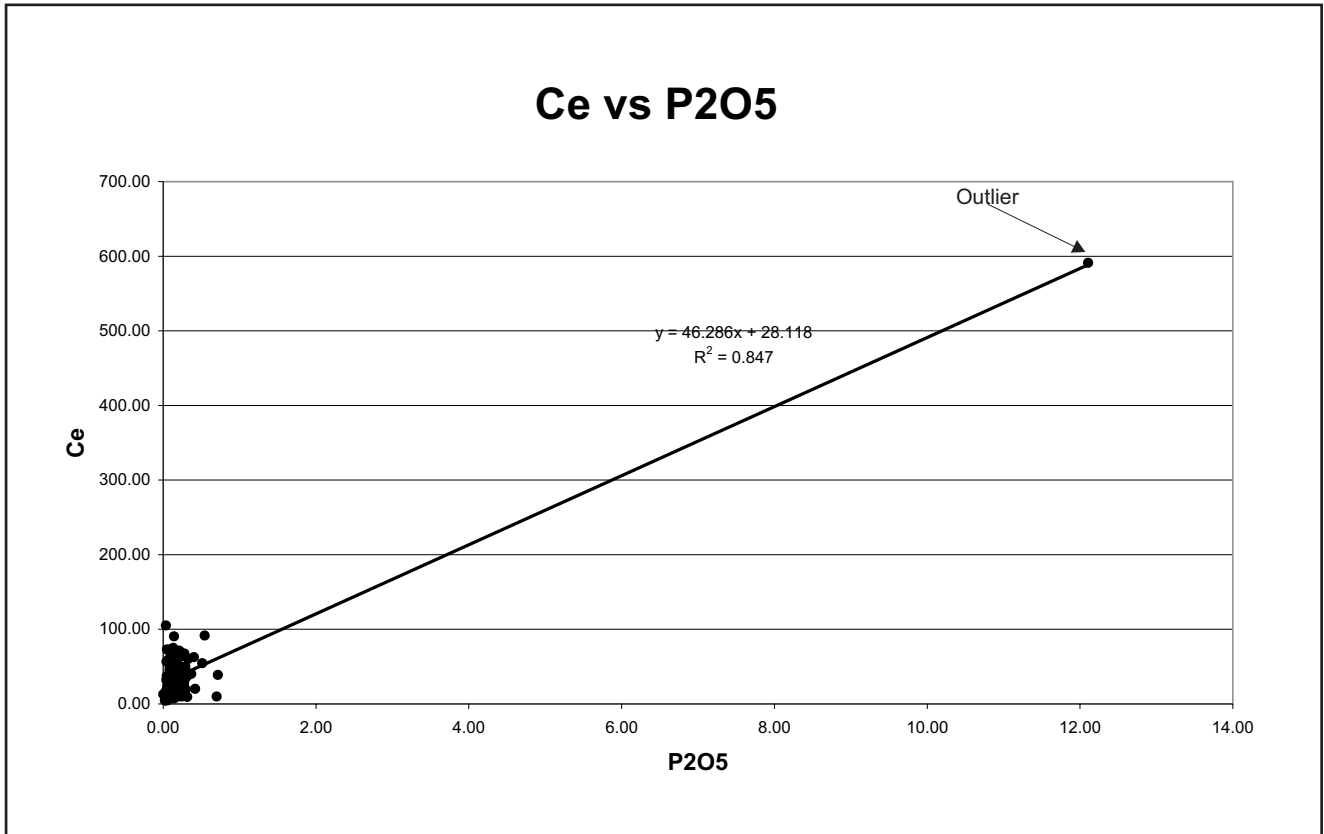


Fig.33a Ce vs P<sub>2</sub>O<sub>5</sub> plotted with outlier

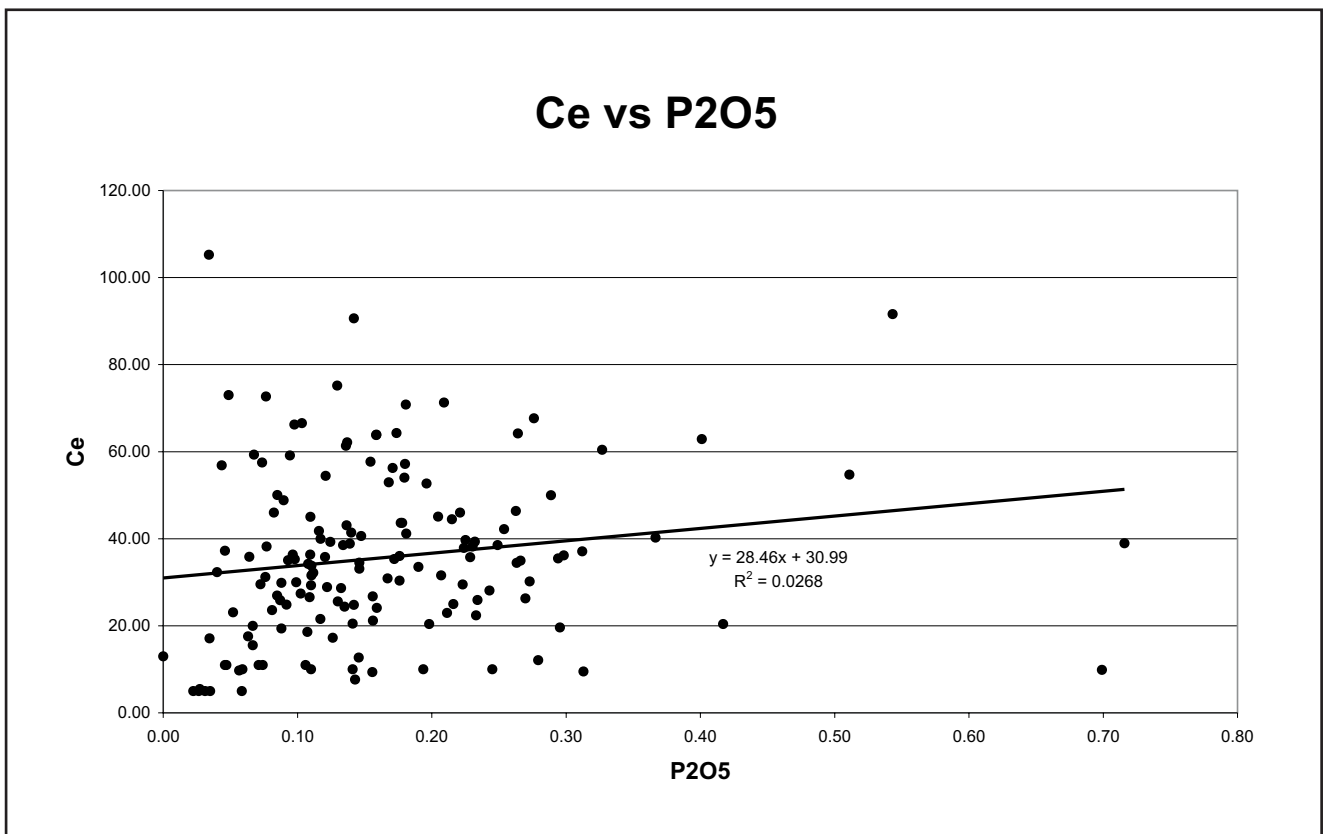


Fig.33b Ce vs P<sub>2</sub>O<sub>5</sub> plotted without outlier

Fig.33 Ce vs P<sub>2</sub>O<sub>5</sub> plot as an illustration of the influence an outlier can have on geochemical data

According to them, the larger the anoxia levels, the larger the V/Ni mole ratios in carbonaceous rocks (maximum ~5). Larger levels of anoxia also favour larger concentrations of both metals. They go on to state that V/Ni ratios are largest in S-rich petroleum. This, according to them, is because of the reduction of V by H<sub>2</sub>S and the immobilisation of Ni by NiS complexes. Deviations from the V/Ni values measured in bitumen is attributed by them to the incorporation of V in silicate minerals and Ni in sulphides.

In the Merelani lithologies observed H<sub>2</sub>S within the calcite in cavities (inferred from the yellow colour and characteristic H<sub>2</sub>S smell), as well as the presence of large pyrite crystals in the same cavities, is evidence of anoxic conditions. Analyses of various minerals are proof that V is indeed incorporated into silicate structures (Table 19). For example, one sample of tsavorite contains about 34 000ppm (~3,4%) of V! The V/Ni ratio ranges from 0.8 to 11.05 with an average of 3.35 for the total data set and an average of 3.18 for the altered zones, which is slightly lower and reflects the incorporation of V into silicate minerals, such as zoisite.

Dissanyake et al. (1988) studied trace elements from a vein graphite deposit in a high-grade metamorphic terrain, dominated by granulite facies rocks. The rocks are reported to be of Precambrian age, which makes an excellent chronological correlation with the neo-Proterozoic, high-grade metamorphic rocks of the Merelani area and its high graphite content (Davies et al., 1994).

They make the following important statement:

*Other elements such as V, Cr, Co, Ni, Cu and Zn though found in lesser concentrations (than Fe) at the parts per million (ppm) range show noteworthy accumulation in graphite.*

In addition they report a La-content of 4-10ppm and a Y-content of 0.5-2ppm, although this is in the order of ~10ppm less than the Merelani lithologies.

Table 19 Table of the averages of various silicate minerals sampled in the shafts by a Tanzanite One geologist, A Cunningham. The table also shows ppm values calculated on the right hand side.

	SiO2	Al2O3	MgO	Na2O	FeO	MnO	Cr2O3	CaO	TiO2	K2O	V2O3	Total	Cr	Ti	K	V
<b>Tanzanite (Zoisite)</b>																
Average	38.762	33.304	0.035	0.007	0.014	0.026	0.024	24.910	0.010	0.006	0.055	97.151	162.117	57.379	46.044	371.292
Std Deviation	0.607	1.819	0.069	0.013	0.016	0.068	0.025	1.888	0.047	0.009	0.109	1.191	170.514	284.073	75.535	742.498
Maximum	40.192	35.669	0.479	0.064	0.078	0.520	0.193	37.301	0.388	0.050	1.399	100.183	1320.120	2324.120	415.000	9513.200
Minimum	37.024	21.987	0.000	0.000	0.000	0.000	0.000	23.635	0.000	0.000	0.000	94.095	0.000	0.000	0.000	0.000
<b>Tsavorite (V-Garnet)</b>																
Average	38.995	21.874	0.510	0.007	0.053	0.426	0.034	36.827	0.234	0.005	0.236	99.201	231.199	1402.726	43.021	1605.904
Std Deviation	0.715	0.731	0.061	0.014	0.026	0.136	0.043	0.358	0.064	0.009	0.497	1.191	292.896	384.639	73.527	3376.674
Maximum	40.749	23.295	0.621	0.092	0.137	0.763	0.371	38.021	0.438	0.037	5.077	102.021	2537.640	2623.620	307.100	34523.600
Minimum	37.070	17.774	0.195	0.000	0.000	0.147	0.000	35.832	0.075	0.000	0.000	96.744	0.000	449.250	0.000	0.000
<b>Rhodolite (Spessartine Garnet)</b>																
Average	37.566	21.049	7.756	0.032	28.923	0.259	0.017	0.912	0.001	0.000	0.000	96.516	113.544	8.386	0.000	0.000
Std Deviation	0.528	0.466	0.458	0.034	1.095	0.061	0.016	0.266	0.004	0.000	0.000	1.244	108.883	26.577	0.000	0.000
Maximum	38.181	21.711	8.427	0.098	30.372	0.342	0.044	1.273	0.017	0.000	0.000	98.682	300.960	101.830	0.000	0.000
Minimum	36.494	20.267	7.108	0.000	27.385	0.168	0.000	0.533	0.000	0.000	0.000	94.533	0.000	0.000	0.000	0.000

Dissanyake et. al (1988) also report a significant correlation between Y and P ( $r = 0.907$ ) and La and P ( $r = 0.976$ ) in graphite. They infer a genetic relationship to explain the high correlation.

Thus it is reasonable to assume that the REE- $P_2O_5$  correlation in the Merelani Lower Horizon lithologies is not primarily due to apatite but to graphite. A possible explanation that the correlation is not as strong as that of Dissanyake et al's. (1988), is most probably because the REE are predominantly partitioned into graphite, while the  $P_2O_5$  is distributed between apatite and graphite. This possibility could certainly be important in certain specific lithologies, as reflected by the smaller correlation in these lithologies. The negative correlation between the REE and phosphate in a few lithological units points to an antipathetic correlation. This implies that the REE may be absent where phosphate is present and visa versa, although to a small degree as the negative correlations are weak, i.e. less than  $-0.500$ .

The final groups for the Merelani lithologies identified from the mutual correlations of trace and major elements and their inferred mineralogic hosts are shown in Table 20.



<b>Group</b>	<b>Elements</b>	<b>Associated mineral(s)</b>
1	V, Ni, Zn, U, Cu, Ba, Cr, Sr, Th	Graphite
2	Fe <sub>2</sub> O <sub>3</sub> T, MnO, Na <sub>2</sub> O, H <sub>2</sub> O <sup>-</sup>	Fe-Rich Minerals (Pyrite, Pyrrhotite, Garnet, Biotite, Ilmenite)
3	Zr, Nb, SiO <sub>2</sub> , TiO <sub>2</sub> , Al <sub>2</sub> O <sub>3</sub> , Ga	Heavy Minerals (especially, Zircon, Rutile, Ilmenite, Kyanite, Garnet)
4	Rb, Pb, K <sub>2</sub> O	Feldspars and Micas
5	CaO, MgO, LOI	Carbonates
6	REE, P <sub>2</sub> O <sub>5</sub>	Apatite, Allanite, Graphite

#### **5.4.2. Merelani Soil Trace Element Correlations**

The next phase was to calculate correlation coefficients for the A- and C-Horizons and the different size fractions of the Merelani trench soils. Groups of mutually correlating trace elements were identified and the average correlation coefficient of the different size fractions are presented in the tables. These groups were compared to the results obtained from the study of the mutual major and trace element correlations of the Merelani lithologies.

Table 21a shows the various trace elements and the elements with which they are correlated with in the A-Horizons. From the correlations two main groups were identified from mutual correlations (Table 21b). It must be said that a few elements, such as Cu, did not show any significant correlations and they were then placed in the group with which they shared the highest number of mutual correlations with the highest values of r.

Based on comparison with the study of the groups of mutually correlating trace elements and major element oxides and the minerals which these groups represent, the groups of mutually correlating trace elements of the soils were divided into the following groups: Group 1 of is taken to represent graphite, the clay minerals and the micas, while Group 2 is taken to represent the heavy minerals, based on the above study on the mutual correlations between the major and trace elements of the

<b>Table 21a Table of the A-Horizon trace element and the elements with which they are correlated</b>		
<b>Element</b>	<b>Correlated with</b>	<b>r</b>
<b>V</b>	Ni	0.901
	Zn	0.872
	Sr	0.868
	Y	0.647
	U	0.581
<b>Cr</b>	Ga	0.661
	Rb <a href="http://scholar.sun.ac.za/">http://scholar.sun.ac.za/</a>	0.707
	Zr	0.844
<b>Ni</b>	V	0.901
	Zn	0.967
	Sr	0.883
	Y	0.590
	Ba	0.661
<b>Cu</b>	Nb	0.396 <sup>1</sup>
<b>Zn</b>	V	0.872
	Ni	0.867
	Sr	0.817
	Ba	0.568
<b>Ga</b>	Cr	0.661
	Rb	0.686
	Zr	0.710
	Nb	0.568
	REE <sup>2</sup>	
<b>Rb</b>	Cr	0.707
	Ga	0.686
	Zr	0.754
<b>Sr</b>	V	0.868
	Ni	0.883
	Zn	0.817
	Y	0.640
	Ba	0.791
<b>Y</b>	V	0.647
	Ni	0.590
	Sr	0.640
	Ba	0.718
	U	0.650
<b>Zr</b>	Cr	0.844
	Ga	0.710
	Rb	0.754
	REE	
<b>Nb</b>	Ga	0.568
	REE	
<b>Ba</b>	V	0.798
	Ni	0.661
	Zn	0.568
	Sr	0.791
	Y	0.718
	U	0.567
<b>Ce</b>	Ga	0.682
	Zr	0.653
	Nb	0.802
	Th	0.664
	REE	
<b>Pb</b>	Y	0.358 <sup>3</sup>
<b>Th</b>	REE	
<b>U</b>	V	0.581
	Y	0.650
	Ba	0.567

<b>Table 21b Groups containing mutually correlating trace elements, extracted from the above relationships together with the minerals with which they are most probably associated</b>		
<b>Group</b>	<b>Elements</b>	<b>Proposed Minerals</b>
1	V, Ni, Zn, Sr, Y, U, Ba	Graphite, Clays, Micas
2	Zr, Cr, Ga, Rb, REE, Pb	Heavy Minerals

<sup>1</sup> Best correlation (i.e. highest r value)

<sup>2</sup> Correlations with all the REE were evaluated, therefore no single value

<sup>3</sup> Best correlation

Merelani lithologies in conjunction with published data on mineral chemistry (Klein and Hurlbut, 1993; Wederpohl, 1978).

A similar table was constructed for the C-Horizon (Table 22a). The table shows the four main groups which were identified (Table 22b). However, some elements in some groups showed significant correlations with other elements in other groups. These mutual correlations were examined and two main groups were identified (Table 22c).

Both groups in the A- and C-Horizons are virtually identical. The only difference is Pb. There is a very low concentration of Pb present in both soil horizons (average A-Horizon = 2.8ppm; average C-Horizon = 3.23ppm).

When the groups of mutually correlating trace elements from the soils are compared to the groups of mutually correlating trace elements and major element oxides of the lithologies, one thing is immediately apparent: The number of groups differ. This could either be due to the fact that the soil particles are slightly mobile or that some of the major elements in the soils are mobile, thereby causing a slightly different trace element variation pattern. However, some of the groups of mutual element correlations of the Merelani lithologies can be identified as grouped together in the groups of mutual correlations identified for the Merelani trench soil zones. Group 1 of the Merelani rocks have been divided into Groups 1, 2 and 4 in the C-Horizon samples of the soil, with the addition of Th to group 1 of the Merelani lithologies.

## **5.5. Discussion and Conclusions**

The following conclusions can be reached from the foregoing paragraphs:

- The study of the percentage change of the concentration of trace elements in the Merelani soils relative to their lithological counterparts have shown that the trace elements are mobile;
- The study of ICP relative to the XRF analyses of the trace element concentration in the Merelani trench soils has shown that the trace elements are not mobilised by hydromorphic means;

Element	Correlated with	r
V	Ni	0.543
	Y	0.548
	U	0.802
Cr	Ga	0.672
	Rb	0.577
	Zr	0.668
Ni	V <a href="http://scholar.sun.ac.za/">http://scholar.sun.ac.za/</a>	0.543
	Zn	0.703
	Y	0.673
	Ba	0.637
	U	0.510
Cu	Sr	0.530
Zn	Ni	0.703
	Ba	0.819
Ga	Cr	0.672
	Rb	0.723
	Zr	0.672
	Nb	0.541
Rb	Cr	0.577
	Ga	0.732
Sr Y	Cu	0.530
	V	0.548
	Ni	0.673
	Ce	0.523
	U	0.536
Zr	Cr	0.668
	Ga	0.672
	Nb	0.804
	REE	
	Th	0.708
Nb	Ga	0.541
	Zr	0.804
	REE	
	Th	0.643
Ba	Ni	0.637
	Zn	0.819
Ce	Y	0.523
	Zr	0.840
	Nb	0.821
	REE	
	Th	0.847
Th	Zr	0.708
	Nb	0.643
	REE	
U	V	0.802
	Ni	0.510
	Y	0.536

Group	Elements
1	V, Ni, Y, U
2	Ba, Ni, Zn, Pb
3	Cr, Ga, Rb, Zr, Nb, REE
4	Sr, Cu

Group	Elements	Proposed Minerals
1	V, Ni, Y, U, Ba, Ni, Zn, Pb, Sr, Cu	Graphite, Clay minerals, Micas
2	Cr, Ga, Rb, Zr, Nb, REE	Heavy Minerals

- Thus the trace elements are mobilised by physical means, such as soil creep on a sloping hill side or by flash floods in the rainy season. However, soil particle mobility is hindered, most probably by dense vegetation in the rainy season and the resultant trace element movement is low, as shown by the good correlation between profiles of individual trace elements of the soil and the lithologies;
- The trace element profiles of V, Ni, Cr and Zn in the Merelani soils, plotted over the trench, show the closest correlation to the profiles of these elements in the lithologies. Of the element profiles of the aforementioned elements, the profile of the fine and medium fractions of the C-Horizon of V showed the closest correlation between soils and lithologies over the trench.. This could be as a result of the fact that the medium fraction is a “best of both worlds scenario”, in other words, both the finer (e.g. graphite) and coarser (e.g. garnet) mineral particles are located in this fraction;
- The correlation coefficients show that the trace elements occur and move together in definite groups, which are attributed to the movement of individual mineral phases (Table 17).
- V, Ni, Cr, and to a lesser extent Zn, is concentrated in the fine fraction, as shown by the scatter plots of these elements against Th which is concentrated in the coarse fraction. The most probable, most important mineralogic host for V, Ni, Cr and Zn is graphite with the silicate minerals such as zoisite and garnet being of secondary importance in terms of element concentration. This is an indication that the panning of graphite and the subsequent geochemical analyses may be a viable exploration tool in the exploration for additional tanzanite deposits and may prove more effective than the whole-rock XRF and partial leach methods employed in this study.

Soil samples can therefore potentially be utilised in the search for tanzanite, using a whole-rock XRF method. The ICP-AE partial extraction method has proved to be

ineffective in exploring for additional tanzanite deposits, due to the low concentration of trace elements which can be extracted by this method.

It is not the tanzanite lithologies that are indicated by, for example, high V values, but rather the lithologies containing high contents of the chromophoric element, V that are illuminated. In addition to tanzanite, V has been shown to be most probably primarily concentrated in graphite. Thus it is these lithologies, such as the Graphitic Calc-Silicate schist units, which will be indicated when using V as a pathfinder. These units fortunately occur in close proximity to the JW-Zone, which is host to the tanzanite mineralisation and sandwiched between the Kyanite Gneiss units LK1 and LK2 (Olivier, 2006). Therefore, if a GCS-type unit is found, an altered zone might be in close proximity. Of all the trace elements, V shows the best results with the closest resemblance between lithologic and soil profile plots and it is this element which should therefore be utilised in the search for additional tanzanite-bearing lithologies, when using whole-rock XRF methods of analysis. Ni, Cr and Zn can be used in conjunction with the V values to lend additional potential credence to the identified V-anomalies. The highest values of Cr occur in the Garnet and Kyanite Gneiss units. The fine and medium fractions of the C-Horizon samples showed the best anomaly-background contrasts for V. Thus a fraction of smaller than 180 $\mu$ m of the C-Horizon should be sampled if soil sampling is to be used in an exploration programme.

## 6. Stream Sediments

### 6.1. Introduction

The trace elements contained within the stream sediments find themselves in a completely different geochemical environment relative to the same elements within the soil samples. Thus different data evaluation methods were used in the evaluation of the stream sediment data. These different geochemical environments are influenced by different geochemical parameters. One important parametrical difference is the velocity of fluid movement. In soils, fluids only start to flow laterally when precipitation, above freezing, exceeds the soil's speed of infiltration and/or capacity for fluid absorption. For the most part, elements are mobilised by soil solution and/or soil creep on hillsides. This implies that the soil fluids have a greater potential for chemical equilibration with the surrounding soil particles. When, however, soil is transported by surface runoff with the subsequent development of erosion channels, i.e. streams and rivers, the soil particles and their contained trace elements are mobilised physically. Some elements may go into solution due to changing physio-chemical conditions of river water. It follows that soils are associated mainly with chemical erosion, excluding arid climatic conditions, and rivers predominantly with physical erosion, depending on the climate and landscape topography (Foth, 1984).

Three streams were sampled (Fig.18, Chapter 3). The data analysis was done on the data for individual streams and then combined and analysed as a whole.

Elements are mobilised in rivers by three main mechanisms (Rose et al, 1979):

1. In mineral grains or rock particles on the river floor.
2. In suspension as fine mineral grains, adsorbed to clay and Fe and Mn oxy-hydroxides or on suspended organic matter.
3. In solution, either as complexes or as dissolved ions.

In the Merelani area, heavy rains fall in the months from March to May, causing flash floods. Due to the large amount of water available the heavy rains are accompanied by abundant vegetation growth, which subsequently choke the smaller rivers and streams in the area. The stream sediments, therefore, only have a small window of time in which to be significantly mobilised.

This chapter consists of three main parts. The first is the geochemical characterisation of the stream sediment data, followed by statistical data evaluation, and the conclusions drawn from it.

## **6.2. Stream Sediment Characterisation**

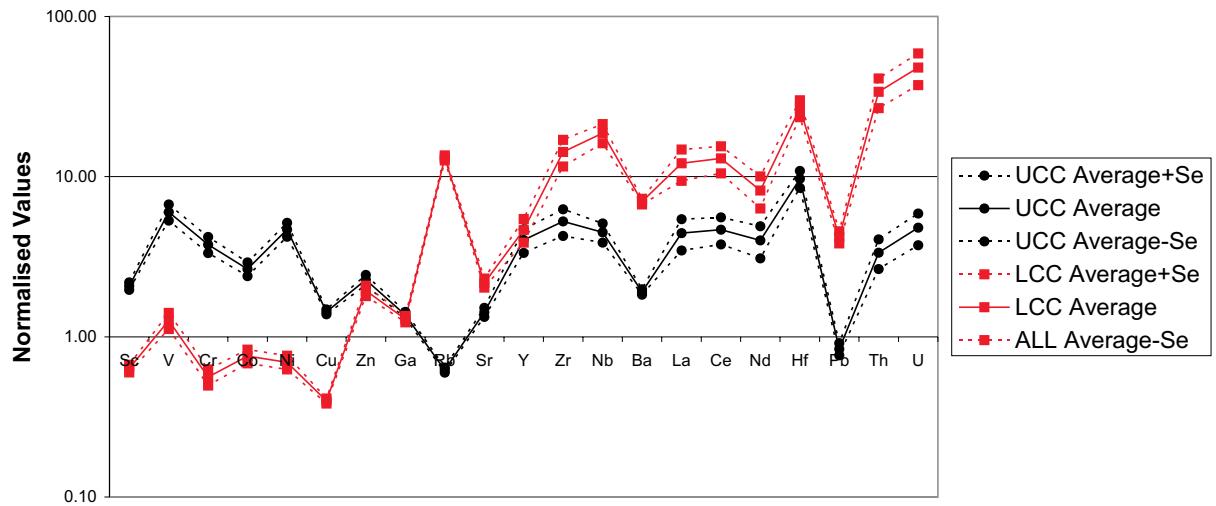
Parameters exist which can indicate whether stream sediments are derived from upper or lower continental crust (Vital and Stattegger, 2000). For this reason the trace element concentrations for both fractions were normalised to the Upper Continental Crust (UCC) and Lower Continental Crust (LCC) values of Taylor and McLennan (1995). The values were plotted as spider diagrams (Fig.34). This normalisation is a first approach to defining a geochemical signature for the Merelani stream sediment geochemical data as well as rendering the data comparable to that of similar studies, such as that of Vital and Stattegger (2000). No conclusions on genesis are derived for either the stream sediments or their parent lithologies from the above-mentioned normalisation plots.

The elements Sc, V, Cr, Ni, Cu, Zn and Ga seem to be relatively close to the values for the lower continental crust, while the values for the same elements are much higher relative to the upper continental crust (Fig.34). Rb shows high values relative to the Rb values for the lower continental crust while, relative to the UCC, the Merelani displays relatively lower Rb values. The heavier elements (Y to U), on the other hand, are enriched with an order of magnitude relative to the UCC. This enrichment is even more pronounced relative to the LCC values. This is an indication that the heavier trace elements in the Merelani stream sediments are enriched relative to the concentrations of the average continental crust.

V and Ni were both plotted against Th for the same reasons outlined for the Merelani soils (Fig.35a-b), namely that Th is associated with the coarser fraction. A slight vertical trend component towards enrichment of V in the medium fraction can be discerned, although it is weak. Slightly more significant, however, is the horizontal trend component indicating an enrichment in Th in the medium fraction, strengthening the view that Th is indeed associated with the coarser fractions in both the Merelani soils and stream sediments.



### UCC- and LCC-normalised Values of the Stream Sediment Trace Element Data - Fine Fraction



### UCC- and LCC-normalised Values of the Stream Sediment Trace Element Data - Medium Fraction

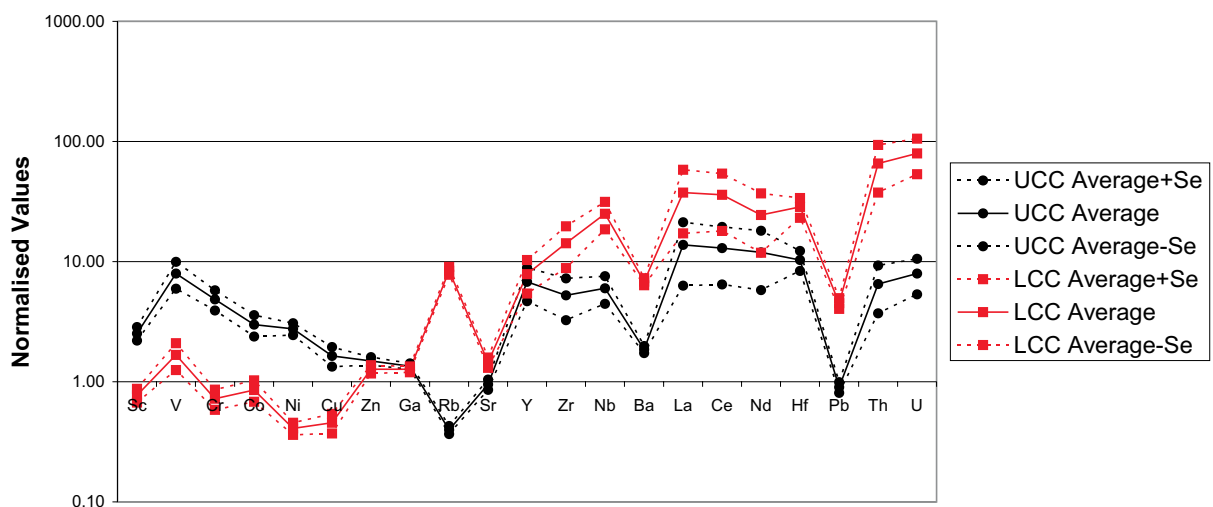


Fig.34 Merelani XRF fine and medium fraction stream sediment data normalised to the upper continental (UCC) and lower continental crust (LCC) values of Taylor and McLennan (1995)

### Evaluation of the Effect of Grain Size on the Geochemistry of V and Th

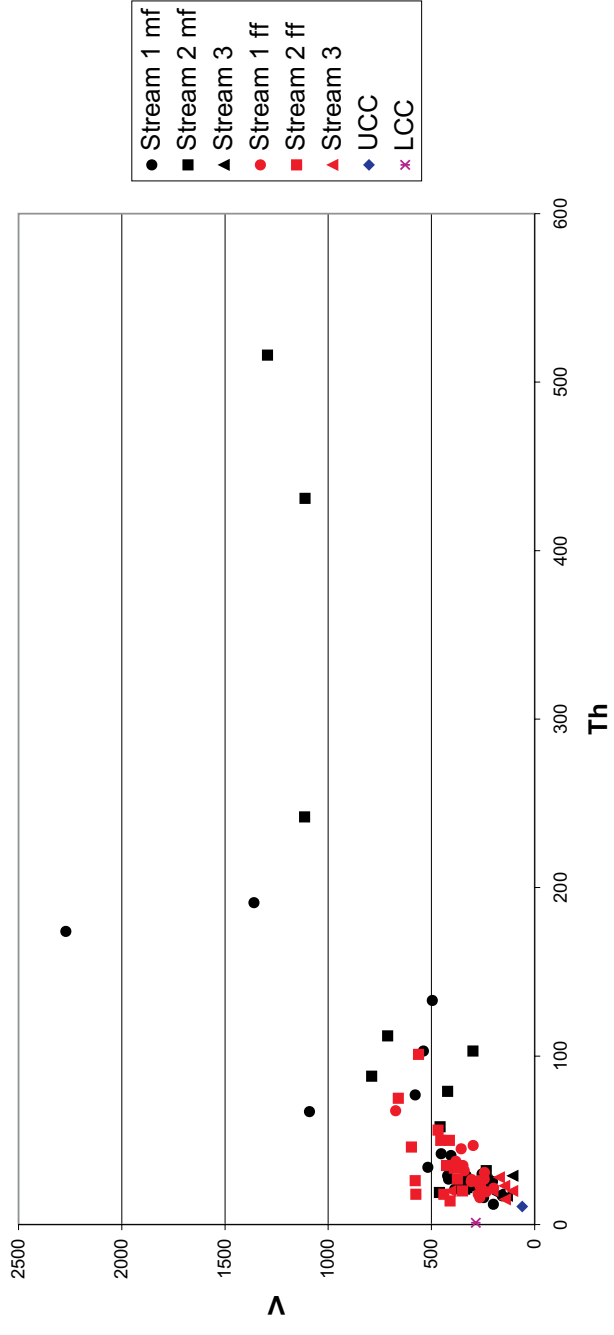
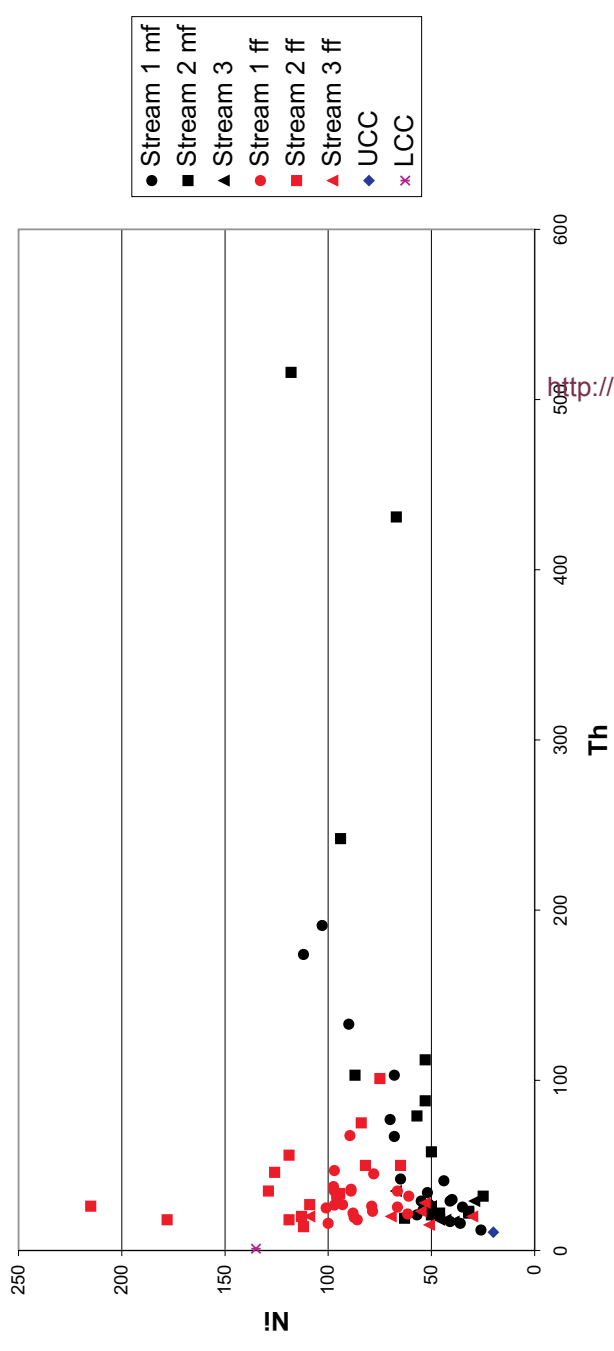


Fig.35a

### Evaluation of the Effect of Grain Size on the Geochemistry of Ni and Th



<http://scholar.sun.ac.za/>

Fig.35b

### Evaluation of the effect of Grain Size on the Geochemistry of La and Th

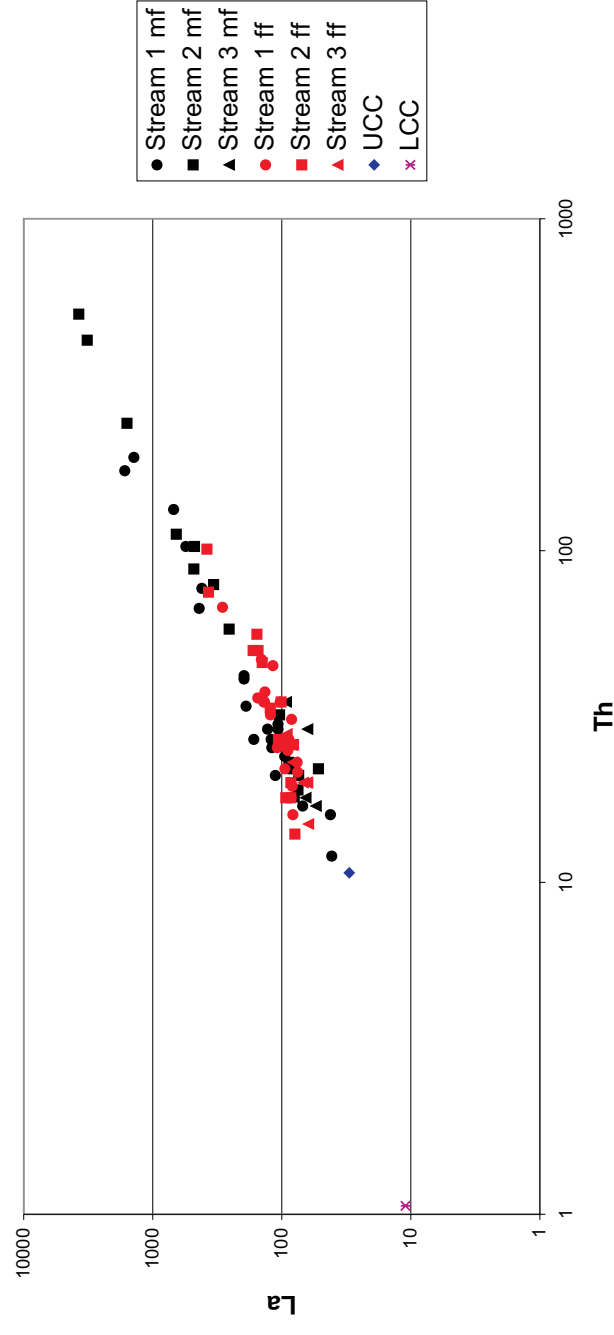


Fig.35c

### Evaluation of the Effect of Grain Size on the Geochemistry of U and Th

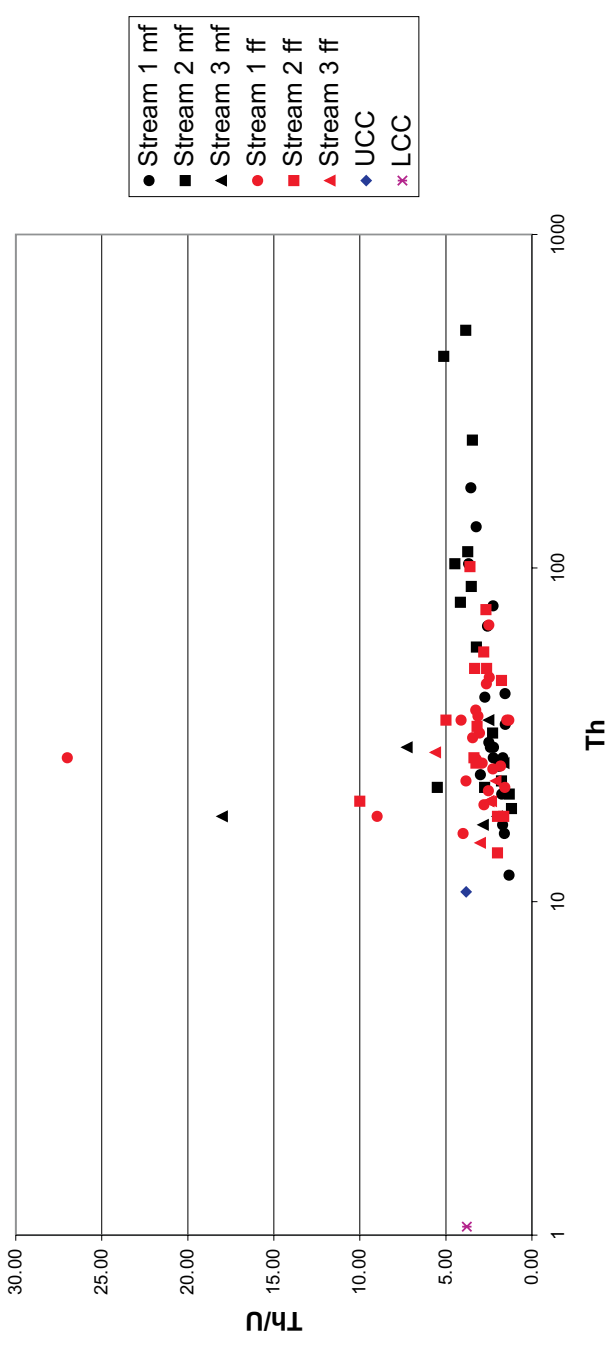


Fig.35d

Fig.35 Scatterplots for the fine and medium fractions of the Mereiani stream sediment data plotted with the upper and lower continental crust values to assess the influence of grain size on trace element distribution

### Evaluation of the Effect of Grain Size on the Geochemistry of Th, Zr and Sc

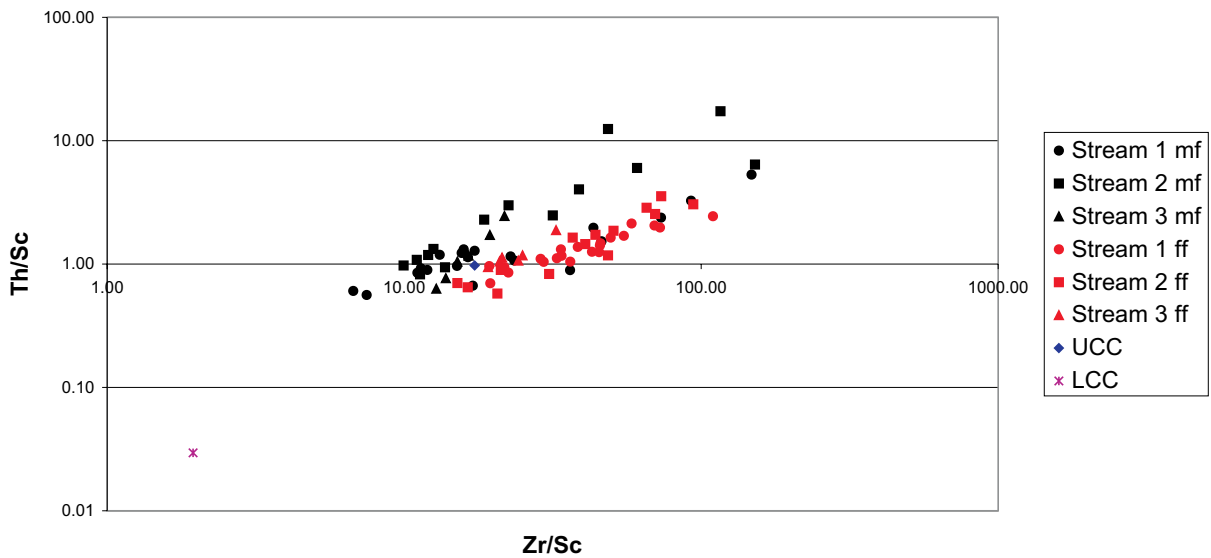


Fig.35e

### Evaluation of the Effect of Grain Size on the Geochemistry of Cr and Sc Relative to Th

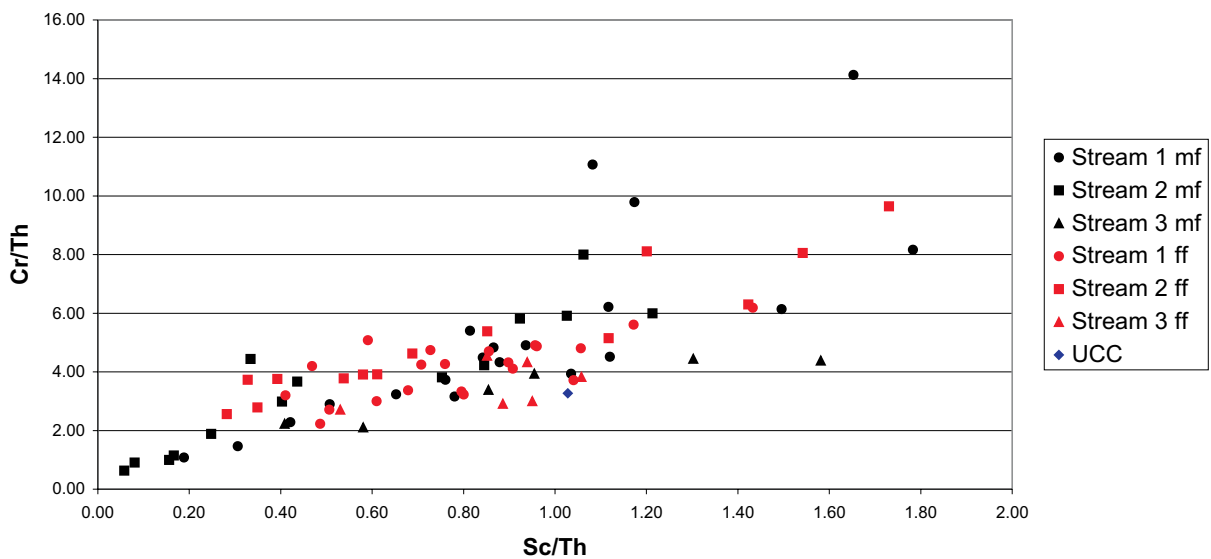


Fig.35f

Fig.35 ...continued

A much more obvious vertical trend component is visible in Fig.35b, indicating a strong tendency of Ni to be enriched in the finer fraction. The horizontal trend component is also present indicating, once again, the enrichment in Th in the medium fraction.

The La/Th plot in Fig.35c is a guide to provenance (Vital and Stattegger, 2000). The trend towards enrichment of both elements in the medium fraction is fairly conspicuous. A high La/Th ratio ( $3.6 \pm 0.4$ ) is an indication that sediments are related to Archaean sedimentary rocks (Vital and Stattegger, 2000). The average La-Th ratio for the medium fraction is 4.47 and 3.78 for the fine fraction. The most important observation, however, is that the values for the medium fraction are higher than the values for the fine fraction. The 95<sup>th</sup> percentile for the medium fraction is 7.30 and 5.08 for the fine fraction. The 65<sup>th</sup> percentile is 4.67 for the medium and 3.93 for the fine fraction. These values indicate that the values of the medium fraction constantly fall in a higher bracket than those of the fine fraction, indicating that both La and Th are enriched in the medium relative to the fine fractions.

The Th/U versus Th plot (Fig.35d) can be used to track weathering trends (Vital and Stattegger, 2000). During weathering there is a tendency for the elevation of Th-U ratios above upper continental crust values of 3.5 to 4.0. The values for the medium and fine fractions have average values of 3.36 and 3.58 respectively, well within the range for UCC values. When the scatterplot is examined, a slight trend towards Th enrichment relative to U can be seen in the fine fraction. This may be indicative of a larger influence of weathering conditions on the fine compared to the medium fractions. The trend towards Th enrichment in the medium fraction is once again recognisable. Overall the effects of weathering, and hence sediment mobilisation, seems to be at a minimum.

The Th/Sc versus Zr/Sc plot of Fig.35e is used to evaluate the influence of heavy mineral concentrations during sedimentary sorting (Vital and Stattegger, 2000). The Th/Sc ratio is sensitive to the provenance bulk composition, while Zr/Sc is a good indicator of Zr enrichment. There is a slight trend towards Zr enrichment in the fine fraction and a slightly larger trend towards Th enrichment in the medium fraction. There is an amount of overlap of medium and fine fraction data points, indicating a slight amount of mixing of stream sediments.

The Cr-Th ratio has been shown to be a provenance indicator largely due to its correlation with the Sc-Th ratio (Vital and Stattegger, 2000). When the scatterplot (Fig.35f) was studied, no apparent trend towards either enrichment or depletion towards the medium and/or fine fractions could be discerned. This implies that the sediments are most probably proximal to their source.

The values of the upper and lower continental crust were plotted on each of the scatterplots. It can be seen that although the LCC values plot close to the Merelani stream sediment data in some plots (e.g. Fig.35-b), they plot far away in other plots (e.g. Fig.35c-e). In fact the LCC values plot so far from the Merelani stream sediment data in Fig.35c that it had to be removed, due to it causing the data to clump in the bottom left-hand corner of the graph. The same can be said for the following ternary plots.

The ternary plot Th-Co-Zr/10 (Fig.36a) shows that, although the scaling factor was used to place the values in the centre of the graph, the stream sediment data still plots near to the Zr pole. A strong trend exists towards Th enrichment in the medium fraction, or Zr enrichment towards the fine fraction or a bit of both. Fig.36e has shown that a slight trend of Zr enrichment in the fine fraction does exist. Thus substantiating the latter view of both an enrichment in Th in the medium fraction and Zr in the fine fraction. No trend exists towards or away from the Co pole.

A significant trend towards Th enrichment in the medium fraction can be seen on Fig.36b. A slight trend exists towards enrichment of Hf in the fine fraction. This makes sense when taking into account that the linear correlation coefficient between Zr and Hf for the entire stream sediment data set is 0.718, indicating that Zr and Hf are significantly correlated. They are commonly correlated in nature (Wederpohl, 1978; Deer et al., 1966) and it is most likely that they are located within the same mineral, most likely zircon.

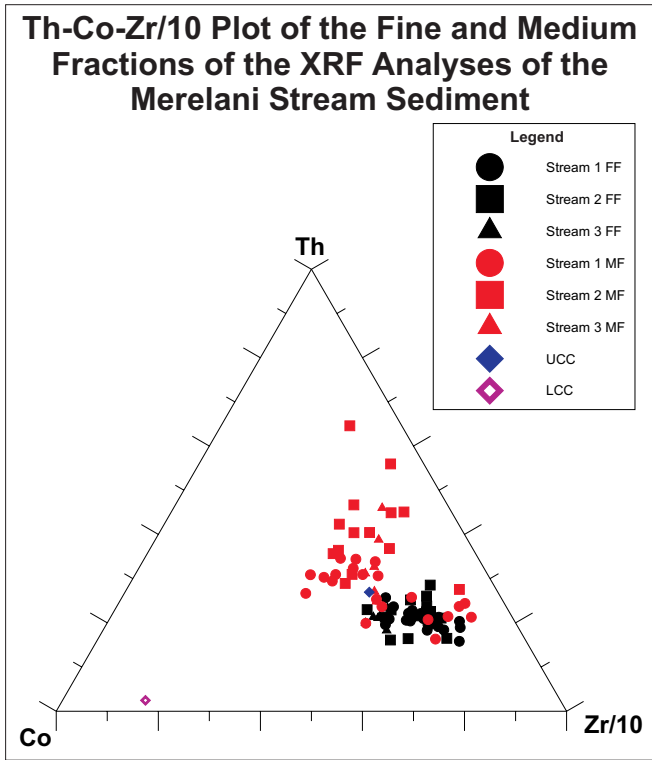


Fig.36a

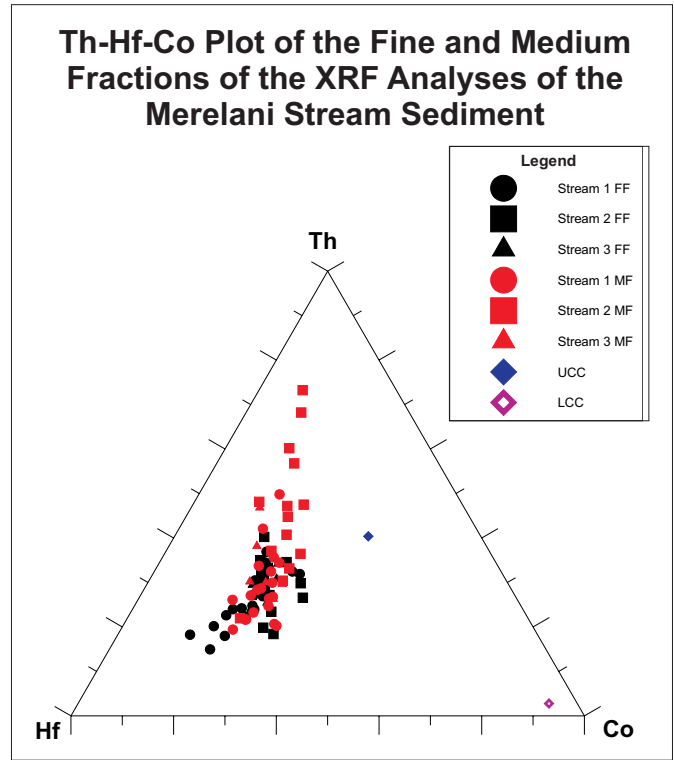


Fig.36b

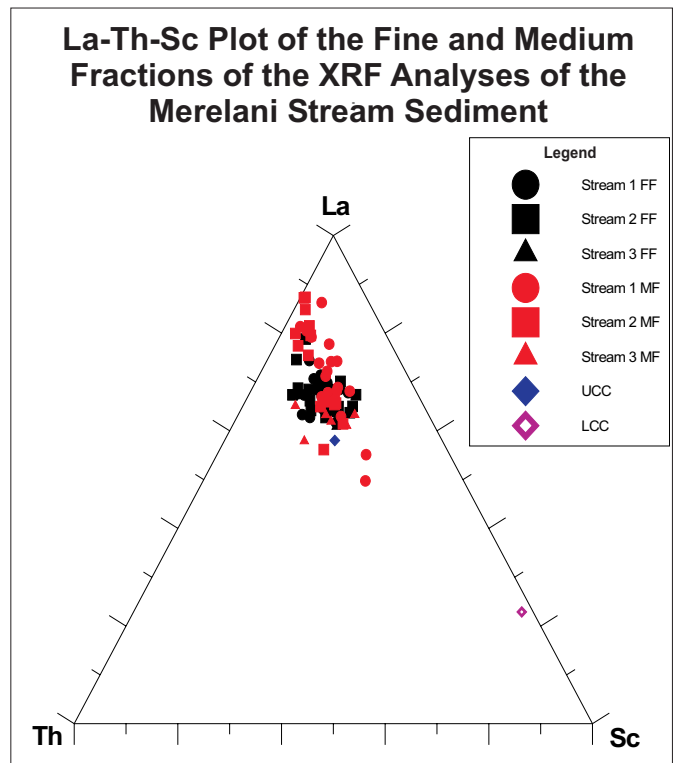


Fig.36c

Fig.36 Ternary scatterplots of the XRF data of the Merelani stream sediments

### 6.3. Factor Analyses

A detailed factor analysis was performed on the Merelani stream sediment data. The functionality of a factor analysis lies in the reduction of the amount of variables to a number of more manageable groups. If, as a purely hypothetical example, one has a data set of, say, five chemical variables: La, Ce, Nd, Ta, and Nb it would be theoretically possible that two factors would emerge from a factor analysis. Factor 1 would most probably be the REEs La, Ce and Nd and Factor 2 would be Ta and Nb, unless these elements were for some or other reason varying together, resulting in only one factor emerging. For the sake of the argument, say two factors emerged. It would then be necessary to assign names to them. Factor 1 could possibly be a REE-bearing mineral such as allanite or monazite, depending on the geochemical or petrological environment, and Factor 2 could be the minerals tantalite and/or columbite. The five variables would then be reduced to two and can be studied in two-dimensional space.

The factor analysis was done by utilisation of the computer software program Statistica®. It is true that a factor analysis contains an inherent amount of subjectivity due to the fact that the data is “rotated”. The law which is used to rotate the data is chosen by the observer. The data for n factors are plotted around a central point in n-dimensional space (Fig.37). The factors are calculated based on the angle between the vectors formed by connecting the central point of origin to the data point. The data for the different data points for each variable are simply the factor loadings, calculated as a function of the covariance in a data set between different variables and the angle between the data vectors. Each data point, which, in this case, are the chemical elements, will have a value for each of the factors called the factor loading.

The factor analyses were done for the fine and medium fractions of the Merelani stream sediment data.

Three factors were extracted for both the fine and medium fractions explaining 77.82% and 74.99% of the variability in the data respectively. The data was rotated using the Varimax Raw rotation law and the factors were extracted using the Maximum Likelihood extraction method.

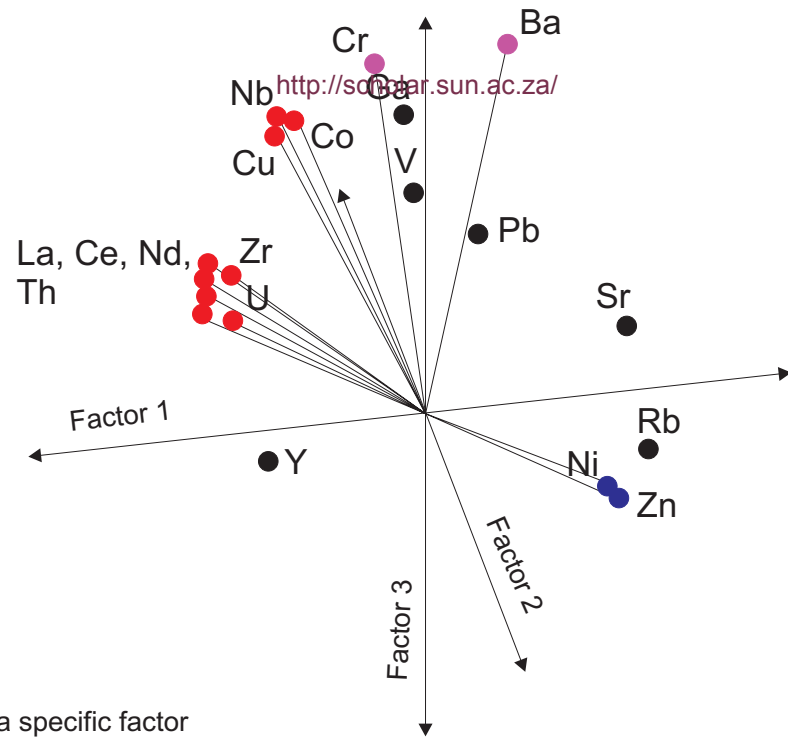


Fig.37a 3 Dimensional schematic diagram of the 3 factors of the fine fraction of the Merelani stream sediment samples, from a slightly different angle

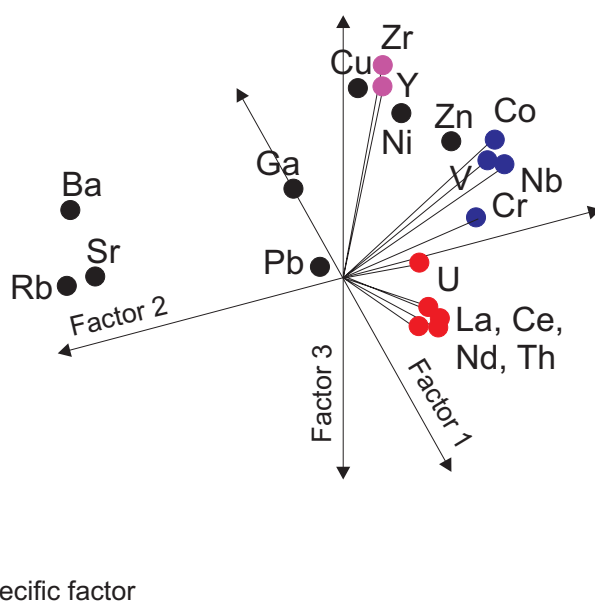


Fig.37b Schematic diagram of the distribution of data points of the medium fraction Merelani stream sediment sediments in three dimensions and the factors they represent as seen from a slightly different angle



The following factors were extracted for the fine fraction (Table 23):

<b>Table 23 The various Factors and the elements constituting them (cut-off loading: 0.7000) n = 46</b>	
<b>Factor</b>	<b>Elements Constituting the Factor</b>
1	Co, Cu, Y, Zr, Nb, La, Ce, Nd, Th, U
2	Ni, Zn
3	Cr, Ba

Factor 1 accounts for more than half (54.66%) of the variability in the data set and is by far the most important factor. Factor 2 and Factor 3 account for 13.03% and 10.12% of the data variability respectively. The cut-off loadings for each factor was chosen by the computer at 0.7000. It can be seen, however, that when the cut-off is reduced to 0.5000 the following factors are extracted (Table 24):

<b>Table 24 The various Factors of the Fine Fraction and the elements constituting them (cut-off loading: 0.5000) n = 46</b>	
<b>Factor</b>	<b>Elements Constituting the Factor</b>
1	Cr, Co, Cu, Y, Zr, Nb, La, Ce, Nd, Th, U
2	V, Ni, Zn
3	V, Cr, Co, Cu, Ga, Nb, Ba

When the correlation matrix (Table 25) is examined, it can be seen that the factors in Table 23 and 24 can be extracted by using mutual correlations. It is also apparent that only Rb, Sr and Pb do not mutually correlate with the other trace elements.

Seeing that these elements, especially Rb and Sr, partition into major mineral phases, such as the feldspars and micas (Icenhower and London, 1996), as shown for the Merelani soils, the above seems to imply that it is not the major mineral phases that dominate the stream sediment trace element chemistry, but rather the heavy mineral

Table 25 Correlation matrix of the medium fraction of the Merelani stream sediment sample data

V	Cr	Co	Ni	Cu	Zn	Ga	Rb	Sr	Y	Zr	Nb	Ba	La	Ce	Nd	Pb	Th	U
<b>1.000</b>	<b>0.876</b>	<b>0.796</b>	<b>0.593</b>	<b>0.694</b>	<b>0.567</b>	<b>0.563</b>	<b>-0.148</b>	<b>-0.412</b>	<b>0.444</b>	<b>0.670</b>	<b>0.680</b>	<b>0.645</b>	<b>0.676</b>	<b>0.690</b>	<b>0.652</b>	<b>0.309</b>	<b>0.652</b>	<b>0.630</b>
<b>0.876</b>	<b>1.000</b>	<b>0.935</b>	<b>0.204</b>	<b>0.843</b>	<b>0.172</b>	<b>0.731</b>	<b>-0.199</b>	<b>-0.302</b>	<b>0.321</b>	<b>0.698</b>	<b>0.859</b>	<b>0.737</b>	<b>0.745</b>	<b>0.760</b>	<b>0.686</b>	<b>0.387</b>	<b>0.697</b>	<b>0.607</b>
<b>0.796</b>	<b>0.935</b>	<b>1.000</b>	<b>0.113</b>	<b>0.939</b>	<b>0.076</b>	<b>0.744</b>	<b>-0.260</b>	<b>-0.360</b>	<b>0.556</b>	<b>0.852</b>	<b>0.937</b>	<b>0.630</b>	<b>0.864</b>	<b>0.888</b>	<b>0.841</b>	<b>0.401</b>	<b>0.830</b>	<b>0.761</b>
<b>0.593</b>	<b>0.204</b>	<b>0.113</b>	<b>1.000</b>	<b>-0.021</b>	<b>0.969</b>	<b>0.027</b>	<b>0.237</b>	<b>-0.349</b>	<b>0.304</b>	<b>0.146</b>	<b>-0.055</b>	<b>0.091</b>	<b>0.106</b>	<b>0.107</b>	<b>0.136</b>	<b>0.042</b>	<b>0.112</b>	<b>0.140</b>
<b>0.694</b>	<b>0.843</b>	<b>0.939</b>	<b>-0.021</b>	<b>1.000</b>	<b>-0.049</b>	<b>0.636</b>	<b>-0.521</b>	<b>-0.163</b>	<b>0.624</b>	<b>0.889</b>	<b>0.953</b>	<b>0.665</b>	<b>0.843</b>	<b>0.880</b>	<b>0.840</b>	<b>0.405</b>	<b>0.830</b>	<b>0.783</b>
<b>0.567</b>	<b>0.172</b>	<b>0.076</b>	<b>0.969</b>	<b>-0.049</b>	<b>1.000</b>	<b>-0.055</b>	<b>0.214</b>	<b>-0.355</b>	<b>0.265</b>	<b>0.090</b>	<b>-0.096</b>	<b>0.039</b>	<b>0.079</b>	<b>0.073</b>	<b>0.109</b>	<b>0.048</b>	<b>0.067</b>	<b>0.113</b>
<b>0.563</b>	<b>0.731</b>	<b>0.744</b>	<b>0.027</b>	<b>0.636</b>	<b>-0.055</b>	<b>1.000</b>	<b>-0.010</b>	<b>-0.324</b>	<b>0.302</b>	<b>0.571</b>	<b>0.632</b>	<b>0.594</b>	<b>0.553</b>	<b>0.576</b>	<b>0.537</b>	<b>0.368</b>	<b>0.551</b>	<b>0.476</b>
<b>-0.148</b>	<b>-0.199</b>	<b>-0.260</b>	<b>0.237</b>	<b>-0.521</b>	<b>0.214</b>	<b>-0.010</b>	<b>1.000</b>	<b>-0.444</b>	<b>-0.335</b>	<b>-0.335</b>	<b>-0.382</b>	<b>-0.435</b>	<b>-0.226</b>	<b>-0.270</b>	<b>-0.262</b>	<b>-0.140</b>	<b>-0.229</b>	<b>-0.264</b>
<b>-0.412</b>	<b>-0.302</b>	<b>-0.360</b>	<b>-0.349</b>	<b>-0.163</b>	<b>-0.355</b>	<b>-0.324</b>	<b>-0.444</b>	<b>1.000</b>	<b>-0.326</b>	<b>-0.322</b>	<b>-0.161</b>	<b>0.068</b>	<b>-0.341</b>	<b>-0.326</b>	<b>-0.373</b>	<b>-0.155</b>	<b>-0.351</b>	<b>-0.315</b>
<b>0.444</b>	<b>0.321</b>	<b>0.556</b>	<b>0.304</b>	<b>0.624</b>	<b>0.265</b>	<b>0.302</b>	<b>-0.335</b>	<b>-0.326</b>	<b>1.000</b>	<b>0.830</b>	<b>0.507</b>	<b>0.145</b>	<b>0.712</b>	<b>0.741</b>	<b>0.809</b>	<b>0.209</b>	<b>0.755</b>	<b>0.787</b>
<b>0.670</b>	<b>0.698</b>	<b>0.852</b>	<b>0.146</b>	<b>0.889</b>	<b>0.090</b>	<b>0.571</b>	<b>-0.335</b>	<b>-0.322</b>	<b>0.830</b>	<b>1.000</b>	<b>0.853</b>	<b>0.451</b>	<b>0.911</b>	<b>0.939</b>	<b>0.936</b>	<b>0.369</b>	<b>0.937</b>	<b>0.905</b>
<b>0.680</b>	<b>0.859</b>	<b>0.937</b>	<b>-0.055</b>	<b>0.953</b>	<b>-0.096</b>	<b>0.632</b>	<b>-0.382</b>	<b>-0.161</b>	<b>0.507</b>	<b>0.853</b>	<b>1.000</b>	<b>0.635</b>	<b>0.845</b>	<b>0.879</b>	<b>0.814</b>	<b>0.339</b>	<b>0.828</b>	<b>0.753</b>
<b>0.645</b>	<b>0.737</b>	<b>0.630</b>	<b>0.091</b>	<b>0.665</b>	<b>0.039</b>	<b>0.594</b>	<b>-0.435</b>	<b>0.068</b>	<b>0.145</b>	<b>0.451</b>	<b>0.635</b>	<b>1.000</b>	<b>0.337</b>	<b>0.390</b>	<b>0.307</b>	<b>0.366</b>	<b>0.345</b>	<b>0.354</b>
<b>0.676</b>	<b>0.745</b>	<b>0.864</b>	<b>0.106</b>	<b>0.843</b>	<b>0.079</b>	<b>0.553</b>	<b>-0.226</b>	<b>-0.341</b>	<b>0.712</b>	<b>0.911</b>	<b>0.845</b>	<b>0.337</b>	<b>1.000</b>	<b>0.993</b>	<b>0.985</b>	<b>0.287</b>	<b>0.970</b>	<b>0.881</b>
<b>0.690</b>	<b>0.760</b>	<b>0.888</b>	<b>0.107</b>	<b>0.880</b>	<b>0.073</b>	<b>0.576</b>	<b>-0.270</b>	<b>-0.326</b>	<b>0.741</b>	<b>0.939</b>	<b>0.879</b>	<b>0.390</b>	<b>0.993</b>	<b>1.000</b>	<b>0.988</b>	<b>0.303</b>	<b>0.976</b>	<b>0.899</b>
<b>0.652</b>	<b>0.686</b>	<b>0.841</b>	<b>0.136</b>	<b>0.840</b>	<b>0.109</b>	<b>0.537</b>	<b>-0.262</b>	<b>-0.373</b>	<b>0.809</b>	<b>0.936</b>	<b>0.814</b>	<b>0.307</b>	<b>0.985</b>	<b>0.988</b>	<b>1.000</b>	<b>0.274</b>	<b>0.971</b>	<b>0.908</b>
<b>0.309</b>	<b>0.387</b>	<b>0.401</b>	<b>0.042</b>	<b>0.405</b>	<b>0.048</b>	<b>0.368</b>	<b>-0.140</b>	<b>-0.155</b>	<b>0.209</b>	<b>0.369</b>	<b>0.339</b>	<b>0.366</b>	<b>0.287</b>	<b>0.303</b>	<b>0.274</b>	<b>1.000</b>	<b>0.304</b>	<b>0.253</b>
<b>0.652</b>	<b>0.697</b>	<b>0.830</b>	<b>0.112</b>	<b>0.830</b>	<b>0.067</b>	<b>0.551</b>	<b>-0.229</b>	<b>-0.351</b>	<b>0.755</b>	<b>0.937</b>	<b>0.828</b>	<b>0.345</b>	<b>0.970</b>	<b>0.976</b>	<b>0.971</b>	<b>0.304</b>	<b>1.000</b>	<b>0.903</b>
<b>0.630</b>	<b>0.607</b>	<b>0.761</b>	<b>0.140</b>	<b>0.783</b>	<b>0.113</b>	<b>0.476</b>	<b>-0.264</b>	<b>-0.315</b>	<b>0.787</b>	<b>0.905</b>	<b>0.753</b>	<b>0.354</b>	<b>0.881</b>	<b>0.899</b>	<b>0.908</b>	<b>0.253</b>	<b>0.903</b>	<b>1.000</b>

phase. This can be seen by the fact that the REEs and Zr, which are associated with heavy minerals such as monazite and zircon, occur in the first factor, which accounts for more than half the variability in the data set.

When the histograms of the various trace elements are examined, most display a positively skewed data distribution profile. The exceptions are V, Ga, Rb, Ba and Pb. Of these elements Ga, Rb and Pb display data distributions which are close to normal, as can be seen from their skewness (Table 26).

<b>Table. 26 Skewness and Kurtosis for the Merelani XRF Stream Sediment Data of the Medium and Fine Fractions</b>					
	n	Medium Fraction		Fine Fraction	
		Skewness	Kurtosis	Skewness	Kurtosis
V	46	2.533	7.794	0.579	-0.046
Cr	46	1.556	2.073	1.316	1.913
Co	46	2.253	6.755	1.461	2.292
Ni	46	1.291	1.539	1.481	4.730
Cu	46	5.795	36.564	1.298	1.604
Zn	46	2.003	6.437	1.966	6.399
Ga	46	0.014	-0.729	0.161	-0.259
Rb	46	-0.094	0.621	-0.746	0.028
Sr	46	1.519	6.440	2.787	10.175
Y	46	1.843	2.646	2.601	10.993
Zr	46	2.355	6.069	1.972	5.874
Nb	46	2.809	10.326	1.381	1.711
Ba	46	-1.640	7.475	0.582	0.536
La	46	3.249	10.958	3.286	12.517
Ce	46	3.170	10.452	3.074	11.503
Nd	46	3.169	10.800	3.373	14.495
Pb	46	0.538	-0.419	0.431	0.499
Th	46	3.213	11.089	3.093	12.363
U	46	2.847	9.363	2.461	9.321

The skewness is a statistical parameter which acts as a measure of the deviation of a data distribution from symmetry. If the skewness is clearly different from 0 the implication is that the data is distributed asymmetrically. Skewness is defined as:

$$\text{Skewness} = \frac{n \sum (x_i - \bar{x})^3}{(n-1)(n-2)\sigma^3}$$

with  $n$  the number of data points,  $\sigma$  the standard deviation,  $x_i$  the  $i^{\text{th}}$  data point for, in this case, a specific chemical element and  $\bar{x}$  the average for the same element.

Kurtosis, on the other hand, is a measure of the “peakedness” of a data distribution. Where the kurtosis is clearly different from 0, the data is either flatter or more peaked than the normal, or Gaussian, data distribution. Kurtosis is defined as:

$$\text{Kurtosis} = \frac{n(n-1)\sum(x_i - \bar{x})^4 - 3(\sum x_i - \bar{x})^2(\sum x_i - \bar{x})^2(n-1)}{(n-1)(n-2)(n-3)\sigma^4}$$

The only significant changes of skewness and kurtosis from the fine to the medium fraction are for the elements V and Ba (Table 26). When the total data set is considered, the skewness of V increases from 0,579 in the fine fraction to 2,533, i.e. positively skewed, in the medium fraction. The situation for Ba is exactly the reverse, with a value for skewness of 0,510 in the fine fraction to  $-1,262$ , i.e. negatively skewed, in the medium fraction. This implies that the data distribution increases to more data points with lower V concentrations from the fine to the medium fraction, i.e. material containing higher values of V is being removed. This is strong evidence for the graphite containing much of the V, since it is the soft graphite flakes that will be the first to be carried away by the flowing river water. The data distribution for Ba shows that the Ba data points are distributed over higher values in the medium relative to the fine fraction, i.e. material containing Ba is being concentrated in the streams. This is evidence that the feldspars which, as was shown for the soil data, is the most probable host to the Ba, are being concentrated in the streams and that the Ba is most predominantly associated with the feldspars and not the micas. This makes sense in terms of Merelani’s semi-arid climate in which the feldspars, which is resistant to physical weathering, would not be easily broken down and would therefore be associated with the heavier mineral fraction in the stream sediments. In addition, micas are light and will be swept away with the other light minerals, such as graphite. Thus if Ba was concentrated in the micas, the data distribution would mimic that of V.

When the data from the other streams are compared to the results from the overall data set they compare well. The only major difference is the data from Stream 3, with  $n = 6$ . Another important observation is that the change in Ba data distribution is more

pronounced than that of the V data distribution. This could either be an indication that the processes concentrating Ba in the stream sediments are more influential than those depleting V, or that the V is distributed more evenly between minerals with large and small specific densities (with grossular garnets as an example of the former and graphite as an example of the latter) than Ba, which could be concentrated in feldspar to a much larger extent than in, for example, mica.

Factor 1 of the fine fraction is taken to represent the bulk of the heavy mineral phase, due to it containing the REEs and Zr, most often associated with the heavy minerals such as zircon and/or apatite. Factor 2 is taken to represent the iron-rich minerals such as pyrite and pyrrhotite, which also seem to contain a sphalerite component. Factor 3 is taken to represent the major minerals such as feldspars and garnet. It can be seen from Table 27, however, that the factor loading for V in Factor 2 is 0,548, implying that other minerals such as V-rich zoisite and potentially graphite might also have a slight influence on this factor. It is noteworthy that Ni and Zn not only form an individual factor, but also that the correlation coefficient between these two elements is 0,969! This implies that these two elements are definitely mobilised together, either in the same mineral or as adsorbed onto clay particles or graphite, or both. The latter is attested to by the drop in Ni:Zn correlation coefficient to 0,820 in the medium fraction. It is still a significant correlation.

The scenario seems slightly different when examining the medium fraction (Table 28). Here the factors are as follows:

<b>Table 28 The various Factors of the Medium Fraction and the elements constituting them (cut-off loading: 0.7000)</b>	
<b>Factor</b>	<b>Elements Constituting the Factor</b>
1	La, Ce, Nd, Th, U
2	V, Cr, Co, Nb
3	Y, Zr

Factor 1 accounts for 50.02% of the variability in the data set and Factor 2 and Factor 3 account for 18.81% and 6.17% of the variability in the data set respectively.

**Table.27a Table of fine fraction factor loadings**

	<b>Factor 1</b>	<b>Factor 2</b>	<b>Factor 3</b>
<b>V</b>	0.476	0.548	0.661
<b>Cr</b>	0.503	0.142	<b>0.840</b>
<b>Co</b>	<b>0.701</b>	0.041	0.682
<b>Ni</b>	0.054	<b>0.979</b>	0.048
<b>Cu</b>	<b>0.727</b>	-0.088	<b>0.599</b>
<b>Zn</b>	0.028	<b>0.987</b>	0.021
<b>Ga</b>	0.392	-0.053	0.631
<b>Rb</b>	-0.231	0.240	-0.190
<b>Sr</b>	-0.300	-0.355	-0.098
<b>Y</b>	<b>0.817</b>	0.250	-0.110
<b>Zr</b>	<b>0.885</b>	0.069	0.312
<b>Nb</b>	<b>0.715</b>	-0.132	0.629
<b>Ba</b>	0.123	0.031	<b>0.819</b>
<b>La</b>	<b>0.944</b>	0.046	0.304
<b>Ce</b>	<b>0.932</b>	0.040	0.330
<b>Nd</b>	<b>0.961</b>	0.077	0.226
<b>Pb</b>	0.201	0.023	0.341
<b>Th</b>	<b>0.943</b>	0.044	0.259
<b>U</b>	<b>0.880</b>	0.090	0.202

- Factor Loadings (Verimax Raw)
- Extraction: Maximum Likelihood Factors
- Marked Loadings are > 0.700 (Values between 0.700 and 0.500 in italics)
- n = 46

**Table.27b Table of medium fraction factor loadings**

	<b>Factor 1</b>	<b>Factor 2</b>	<b>Factor 3</b>
<b>V</b>	0.4579	<b>0.7744</b>	0.3688
<b>Cr</b>	0.3968	<b>0.7545</b>	0.0978
<b>Co</b>	0.3957	<b>0.8267</b>	0.3863
<b>Ni</b>	<b>0.5033</b>	0.3837	<b>0.6687</b>
<b>Cu</b>	0.2032	0.3684	<b>0.5526</b>
<b>Zn</b>	0.3502	<b>0.6680</b>	0.3887
<b>Ga</b>	0.3312	0.0450	0.3422
<b>Rb</b>	-0.1941	-0.6614	-0.2770
<b>Sr</b>	-0.2910	-0.5129	-0.3458
<b>Y</b>	<b>0.5149</b>	0.2995	<b>0.7908</b>
<b>Zr</b>	0.4053	0.3705	<b>0.7753</b>
<b>Nb</b>	0.3296	<b>0.9043</b>	0.2353
<b>Ba</b>	-0.2277	-0.6185	0.0002
<b>La</b>	<b>0.9199</b>	0.3168	0.1831
<b>Ce</b>	<b>0.9129</b>	0.3201	0.2105
<b>Nd</b>	<b>0.9116</b>	0.2864	0.2592
<b>Pb</b>	0.2733	0.1620	-0.0578
<b>Th</b>	<b>0.9356</b>	0.2414	0.2158
<b>U</b>	<b>0.8580</b>	0.2635	0.3876

- Factor Loadings (Verimax Raw)
- Extraction: Maximum Likelihood Factors
- Marked Loadings are > 0.700 (Values between 0.700 and 0.500 in italics)
- n = 46

When 0.5000 is taken as the cut-off loading the factors are as follows:

<b>Table 29 The various Factors of the Medium Fraction and the elements constituting them (cut-off loading: 0.5000)</b>	
<b>Factor</b>	<b>Elements Constituting the Factor</b>
1	Ni, Y, La, Ce, Nd, Th, U
2	V, Cr, Co, Zn, Nb
3	Ni, Cu, Y, Zr

Rb, Sr, Ba and Pb stand alone, as with the fine fraction, which is substantiated by the examination of the correlation coefficients (Table 30). Factor 1 of the medium fraction is taken to represent the bulk of the heavy mineral phase, with the REE-bearing minerals having the major influence, which is the same for the fine fraction. Factor 2 is taken to be represented by predominantly the garnets and Factor 3 as the mineral zircon having the predominant influence.

The above scenario compares well with that for the fine fraction. All that has most probably occurred is that the influence of fine minerals in the medium fraction, such as the clay minerals and graphite, has been diminished and that of the heavy minerals has been increased. It can be seen that in both fractions, the first factor consists of elements which are commonly associated with heavy minerals.

Those elements, for the fine and medium fractions, that could not be grouped into a specific factor are most probably associated with major mineral phases such as mica or feldspar (e.g. Ba in the medium fraction). Ba has a negative loading count on all three factors, implying strongly that it does not seem to occur in the heavy mineral phase but rather in another phase, such as the micas or perhaps feldspars.

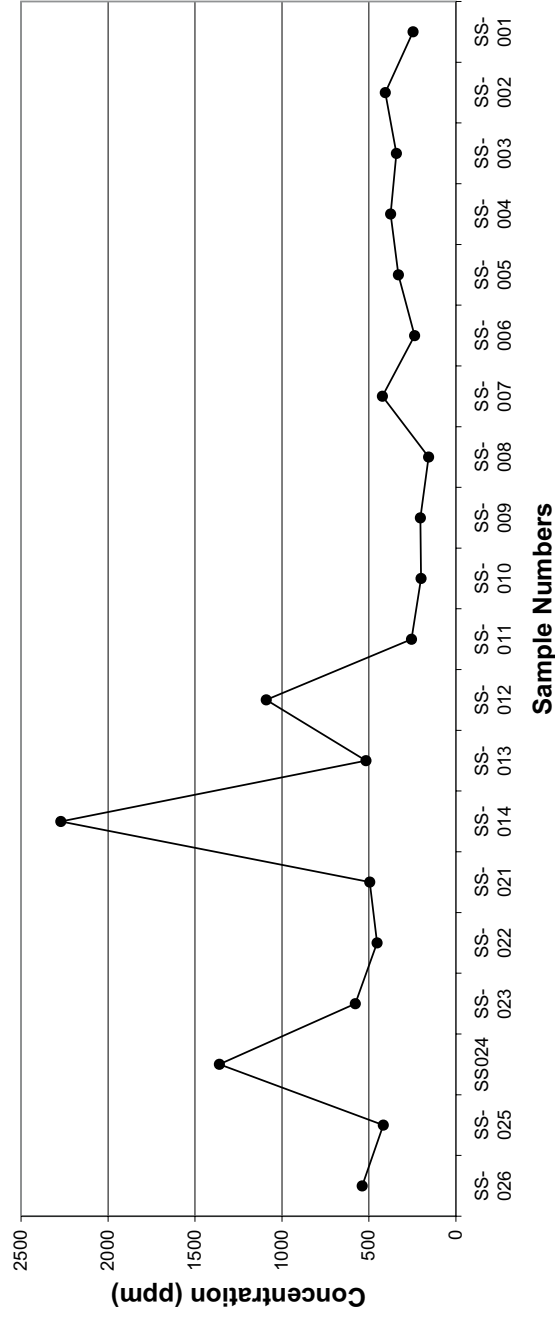
Five elements were chosen for the fine and medium fractions and their profiles were plotted for each stream sampled (Fig.38 and Fig.39). The choice of these elements was done on the basis of their respective differences and similarities in geochemical behaviour. V and Ni were chosen because of their similar profiles in the Merelani lithologies as well as their mobility in oxygenating conditions (Breit and Wanty, 1991). Cr was chosen because of its immobility and its abundance in the grossular garnets.

Table 30 Correlation matrix of the XRF Merelani stream sediment data of the medium fraction

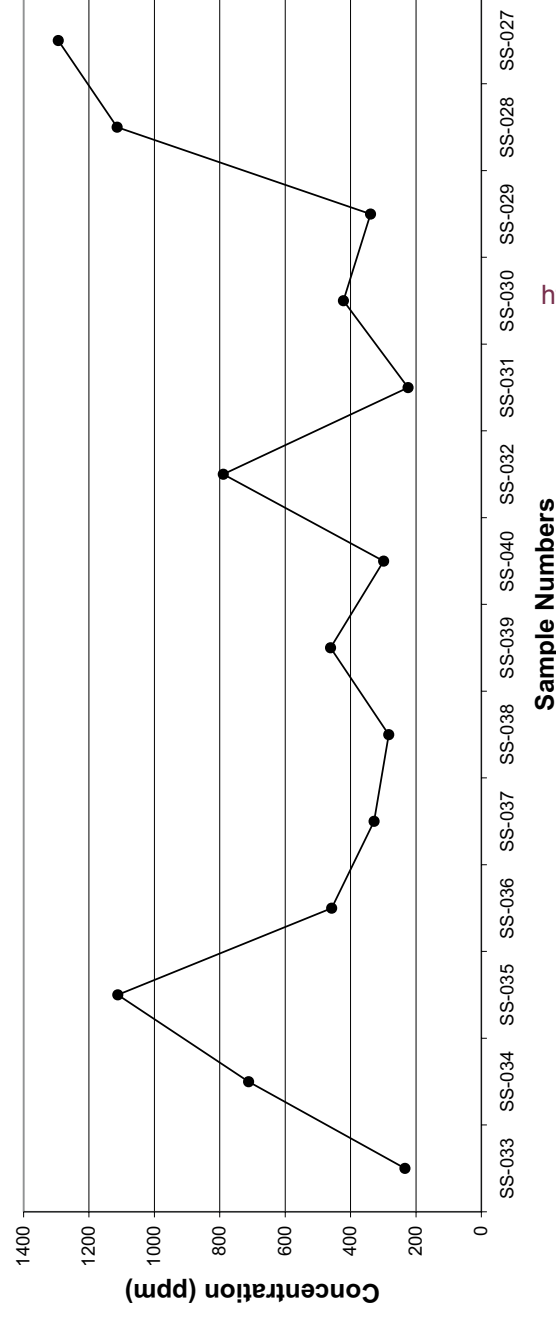
V	Cr	Co	Ni	Cu	Zn	Ga	Rb	Sr	Y	Zr	Nb	Ba	La	Ce	Nd	Pb	Th	U
1.000	0.814	0.962	0.795	0.593	0.887	0.297	-0.728	-0.664	0.759	0.741	0.943	-0.597	0.742	0.751	0.744	0.189	0.693	0.751
0.814	1.000	0.818	0.532	0.418	0.587	0.358	-0.750	-0.608	0.503	0.481	0.846	-0.403	0.628	0.630	0.613	0.210	0.595	0.609
0.962	0.818	1.000	0.767	0.594	0.839	0.317	-0.749	-0.687	0.761	0.765	0.974	-0.604	0.704	0.714	0.704	0.216	0.657	0.708
0.795	0.532	0.767	1.000	0.547	0.820	0.324	-0.476	-0.534	0.912	0.855	0.676	-0.301	0.714	0.729	0.749	0.192	0.714	0.795
0.593	0.418	0.594	0.547	1.000	0.478	0.236	-0.338	-0.372	0.640	0.788	0.534	-0.220	0.409	0.428	0.435	-0.111	0.385	0.530
0.887	0.587	0.839	0.820	0.478	1.000	0.094	-0.536	-0.538	0.687	0.658	0.811	-0.558	0.611	0.622	0.618	0.195	0.563	0.625
0.297	0.358	0.317	0.324	0.236	0.094	1.000	-0.436	-0.604	0.450	0.356	0.228	0.042	0.385	0.392	0.412	-0.109	0.434	0.462
-0.728	-0.750	-0.749	-0.476	-0.338	-0.536	-0.436	1.000	0.636	-0.518	-0.448	-0.723	0.333	-0.443	-0.452	-0.445	0.037	-0.418	-0.464
-0.664	-0.608	-0.687	-0.534	-0.372	-0.538	-0.604	0.636	1.000	-0.579	-0.520	-0.638	0.383	-0.499	-0.508	-0.508	-0.021	-0.490	-0.525
0.759	0.503	0.761	0.912	0.640	0.687	0.450	-0.518	-0.579	1.000	0.940	0.634	-0.322	0.724	0.743	0.771	0.148	0.732	0.826
0.741	0.481	0.765	0.855	0.788	0.658	0.356	-0.448	-0.520	0.940	1.000	0.658	-0.298	0.639	0.660	0.680	0.144	0.639	0.750
0.943	0.846	0.974	0.676	0.534	0.811	0.228	-0.723	-0.638	0.634	0.658	1.000	-0.636	0.643	0.650	0.630	0.236	0.585	0.616
-0.597	-0.403	-0.604	-0.301	-0.220	-0.558	0.042	0.333	0.383	-0.322	-0.298	-0.636	1.000	-0.410	-0.407	-0.388	-0.086	-0.344	-0.297
0.742	0.628	0.704	0.714	0.409	0.611	0.385	-0.443	-0.499	0.724	0.639	0.643	-0.410	1.000	0.999	0.996	0.295	0.992	0.953
0.751	0.630	0.714	0.729	0.428	0.622	0.392	-0.452	-0.508	0.743	0.660	0.650	-0.407	0.999	1.000	0.998	0.291	0.992	0.958
0.744	0.613	0.704	0.749	0.435	0.618	0.412	-0.445	-0.508	0.771	0.680	0.630	-0.388	0.996	0.998	1.000	0.286	0.993	0.969
0.189	0.210	0.216	0.192	-0.111	0.195	-0.109	0.037	-0.021	0.148	0.144	0.236	-0.086	0.295	0.291	0.286	1.000	0.292	0.216
0.693	0.595	0.657	0.714	0.385	0.563	0.434	-0.418	-0.490	0.732	0.639	0.585	-0.344	0.992	0.992	0.993	0.292	1.000	0.958
0.751	0.609	0.708	0.795	0.530	0.625	0.462	-0.464	-0.525	0.826	0.750	0.616	-0.297	0.953	0.958	0.969	0.216	0.958	1.000



### Profile of V XRF Values of the Medium Fraction of the Merelani Stream Sediments of Stream 1



### Profile of V XRF Values of the Medium Fraction of the Merelani Stream Sediments of Stream 2



### Profile of V XRF Values of the Medium Fraction of the Merelani Stream Sediments of Stream 3

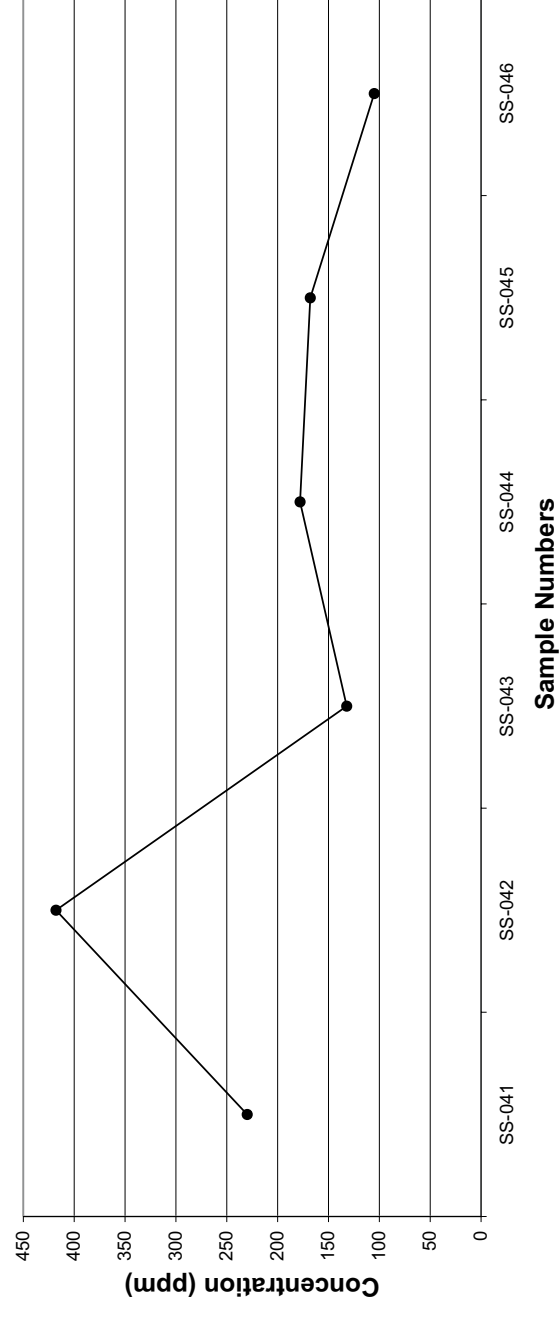
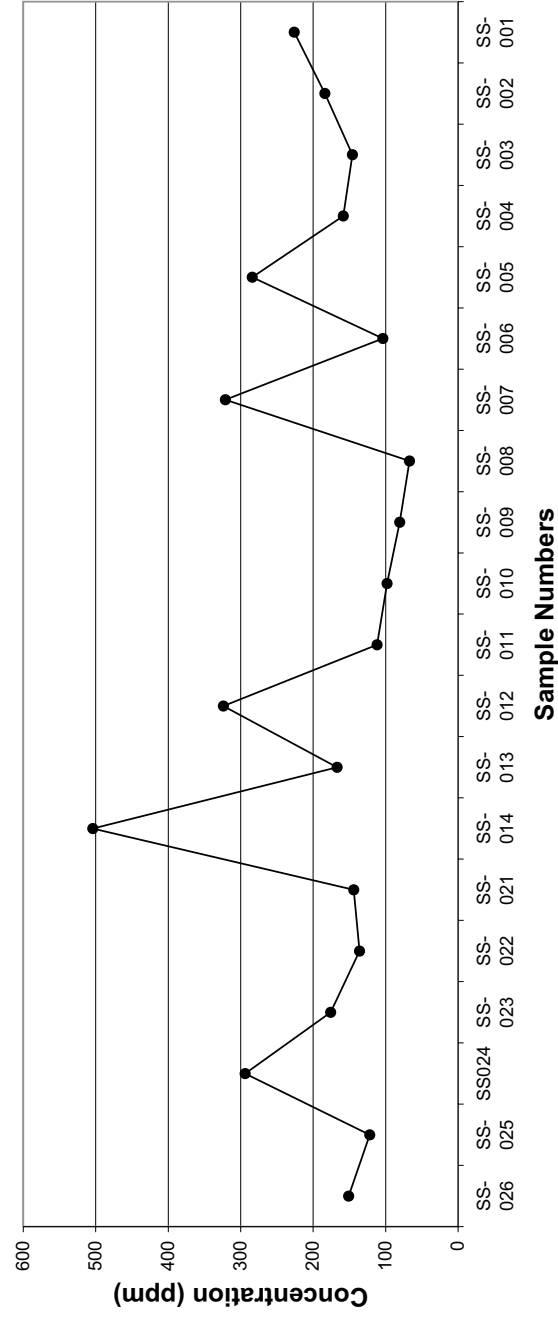
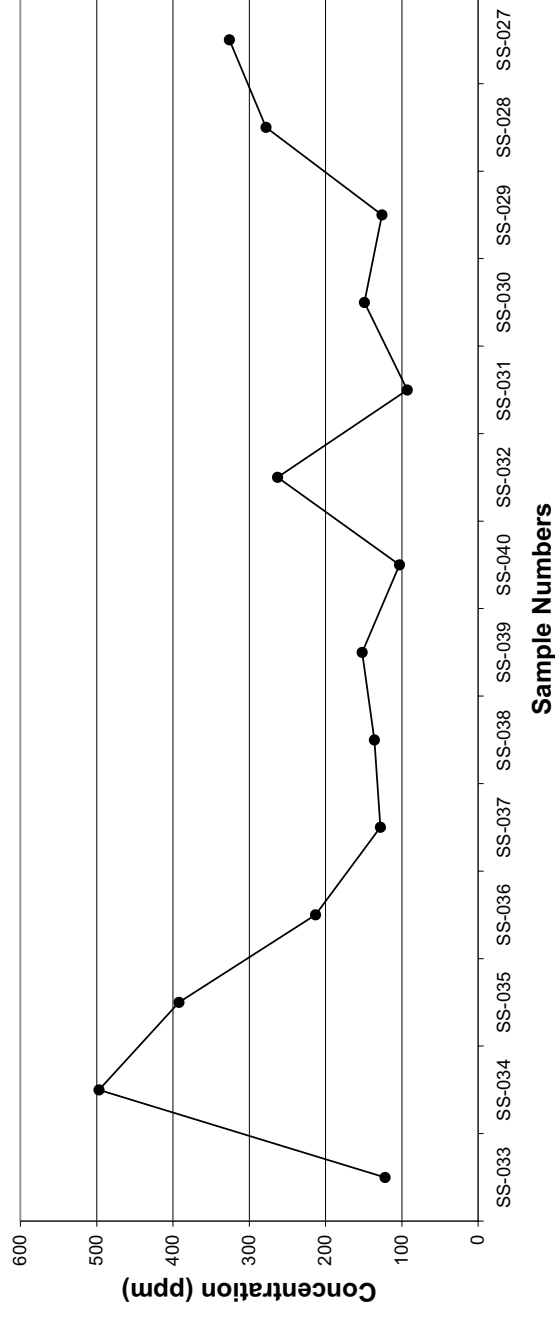


Fig.38 Profiles of XRF Merelani stream sediment data of the medium fraction over the three individual streams sampled

### Profile of Cr XRF Values of the Medium Fraction of the Merelani Stream Sediments of Stream 1



### Profile of XRF Cr Values of the Medium Fraction of the Merelani Stream Sediments of Stream 2



<http://scholar.sun.ac.za>

### Profile of Cr XRF Values of the Medium Fraction of the Merelani Stream Sediments of Stream 3

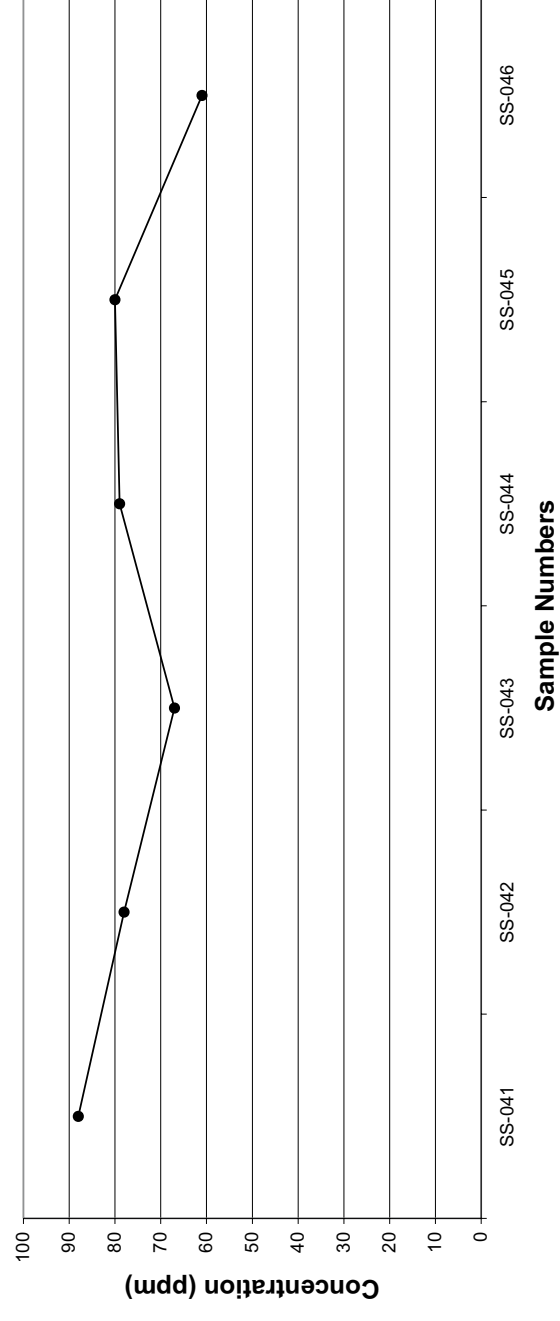
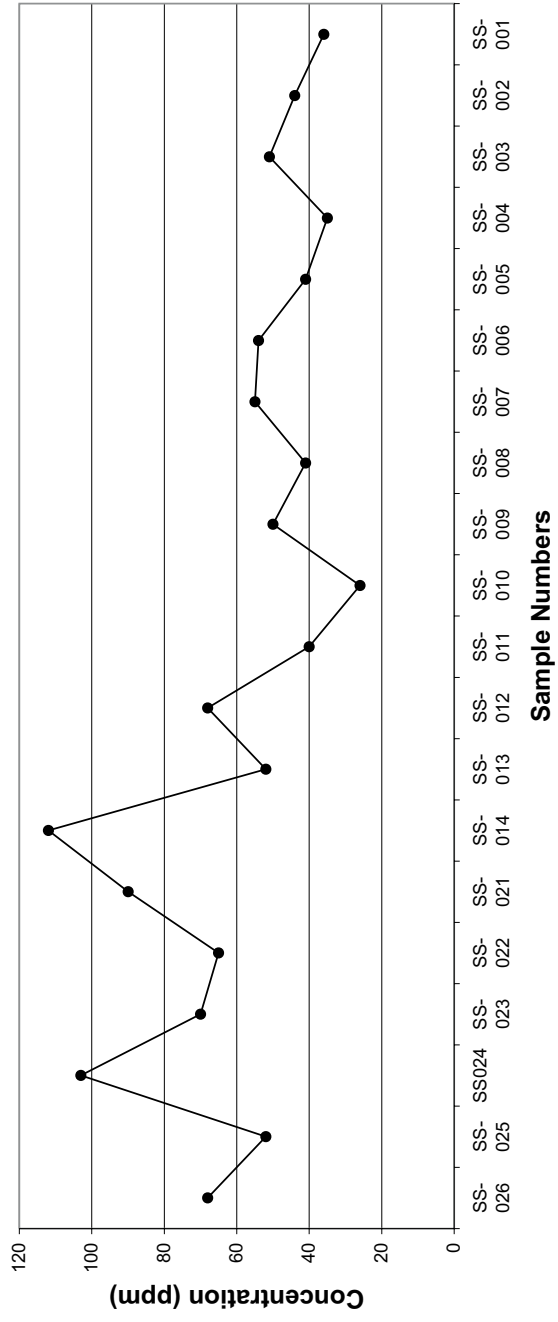
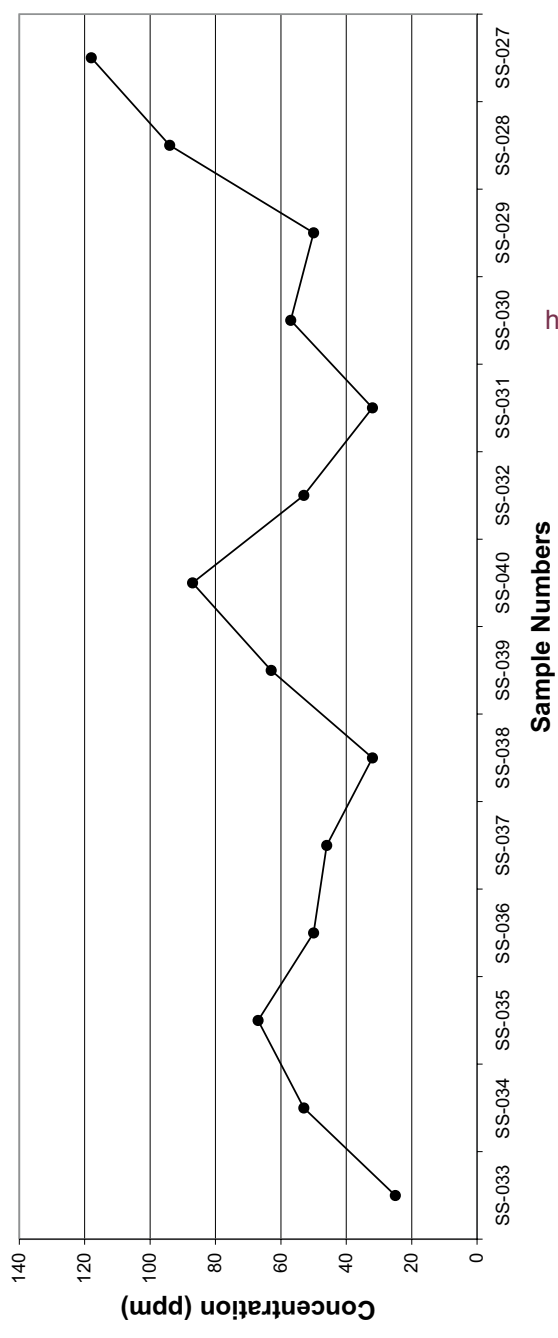


Fig.38 ...continued

### Profile of Ni XRF Values of the Medium Fraction of the Merelani Stream Sediments of Stream 1



### Profile of Ni XRF Values of the Medium Fraction of the Merelani Stream Sediments of Stream 2



<http://scholar.sun.ac.za/>

### Profile of Ni XRF Values of the Medium Fraction of the Merelani Stream Sediments of Stream 3

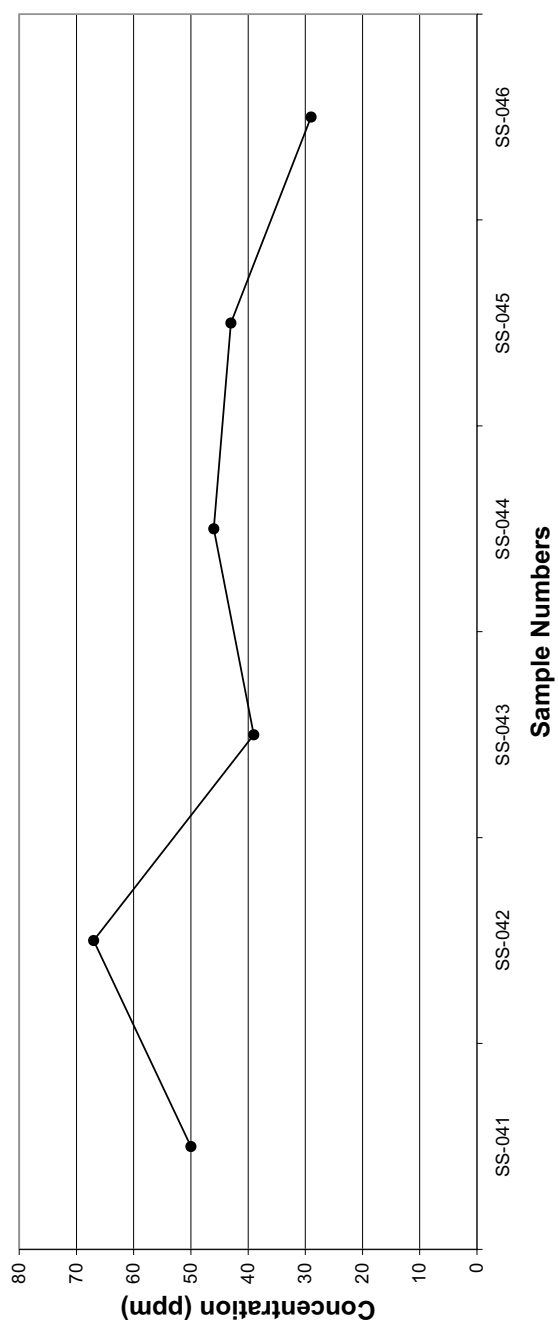
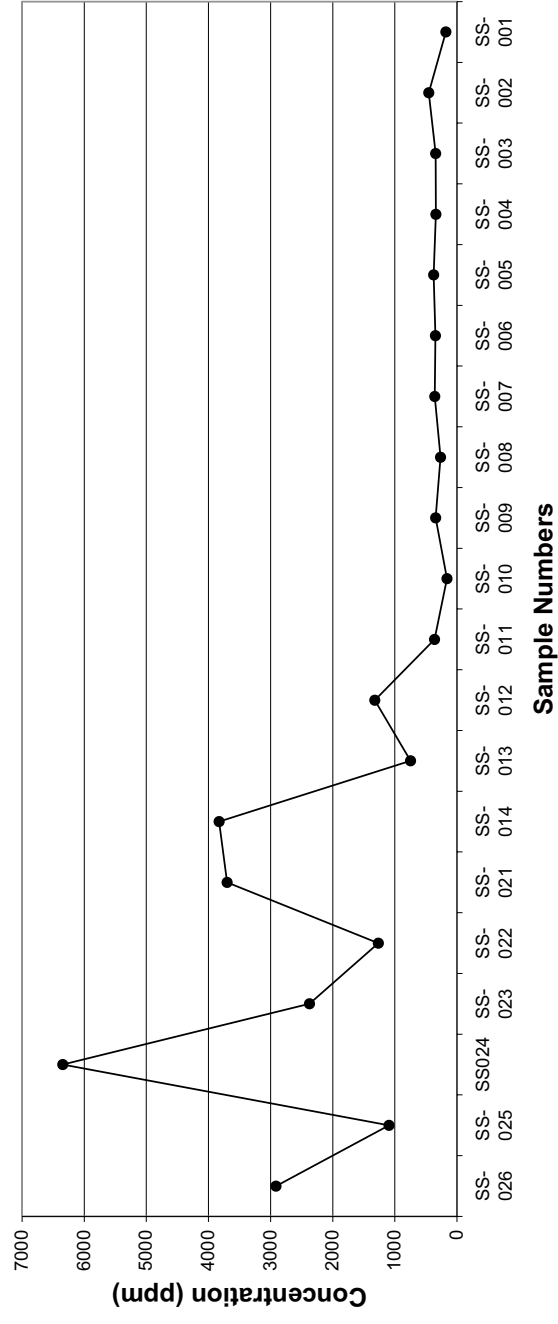
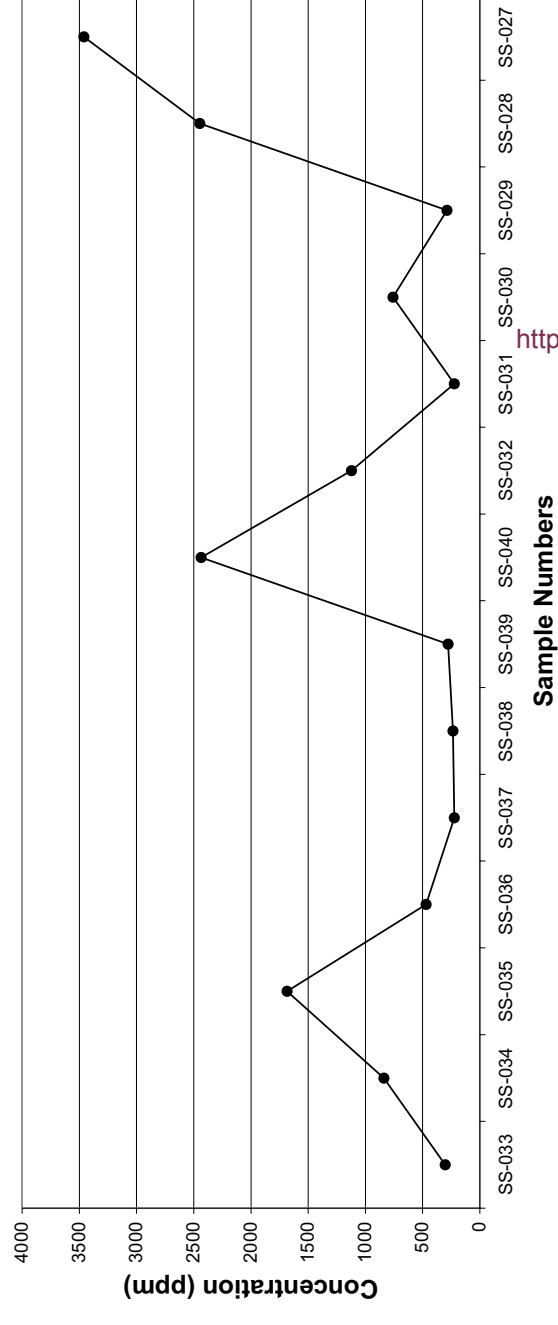


Fig.38 ...continued

### Profile of Zr XRF Values of the Medium Fraction of the Merelani Stream Sediments of Stream 1



### Profile of Zr XRF Values of the Medium Fraction of the Merelani Stream Sediments of Stream 2



<http://scholar.sun.ac.za/>

### Profile of Zr XRF Values of the Medium Fraction of the Merelani Stream Sediments of Stream 3

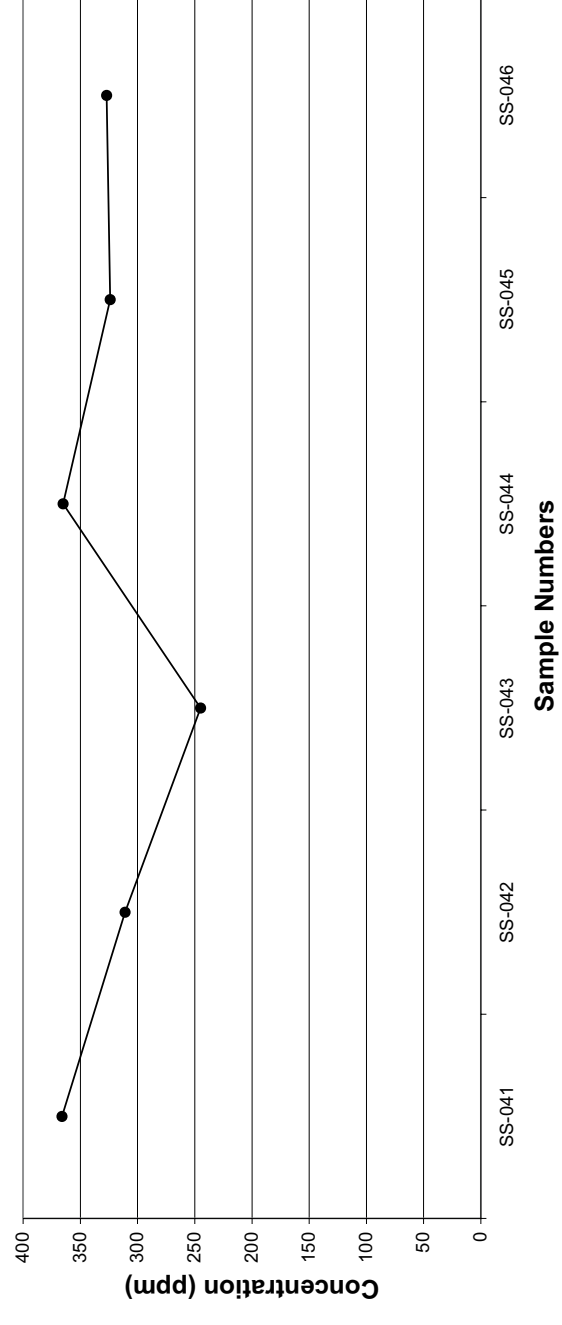
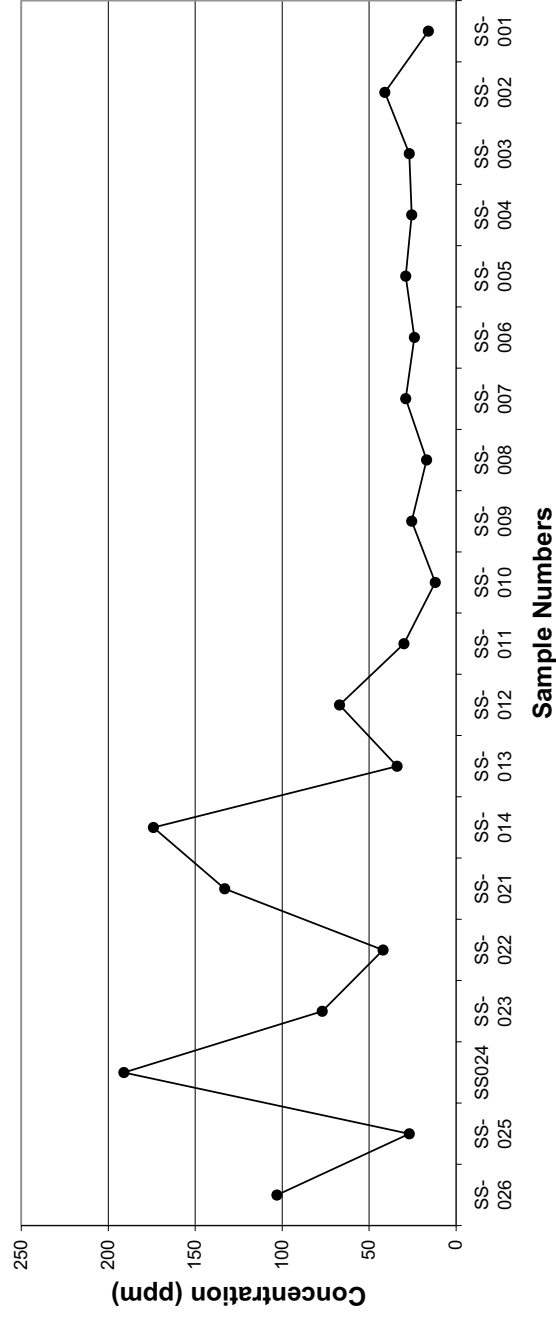
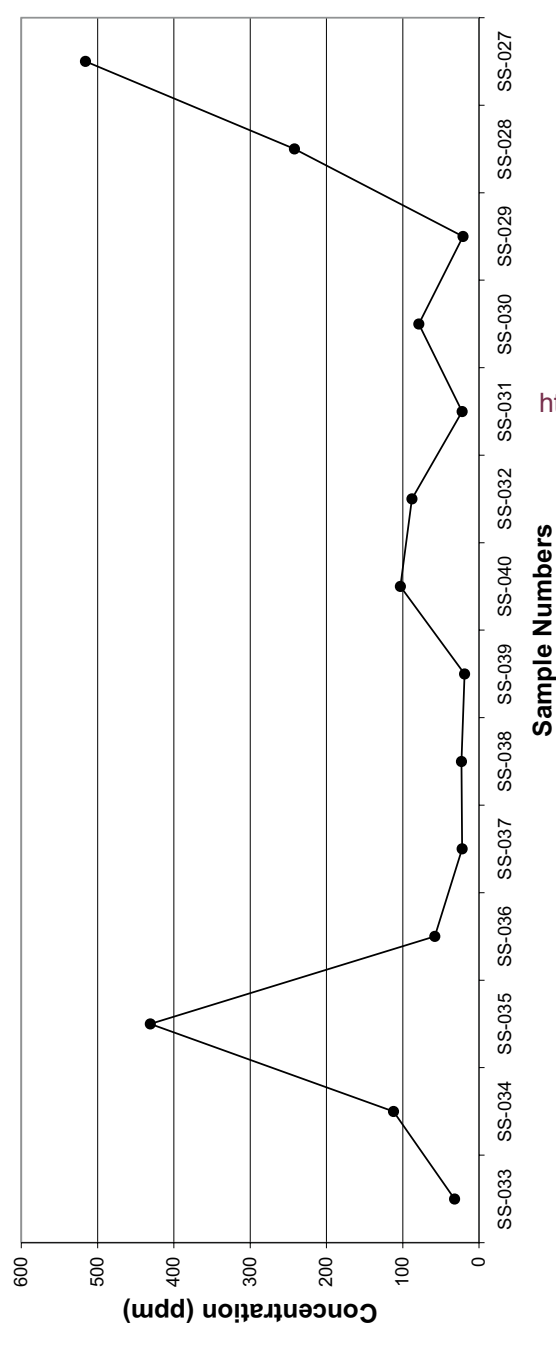


Fig.38 ...continued

### Profile of Th XRF Values of the Medium Fraction of the Merelani Stream Sediments of Stream 1



### Profile of Th XRF Values of the Medium Fraction of the Merelani Stream Sediments of Stream 2



<http://scholar.sun.ac.za/>

### Profile of Th XRF Values of the Medium Fraction of the Merelani Stream Sediments of Stream 3

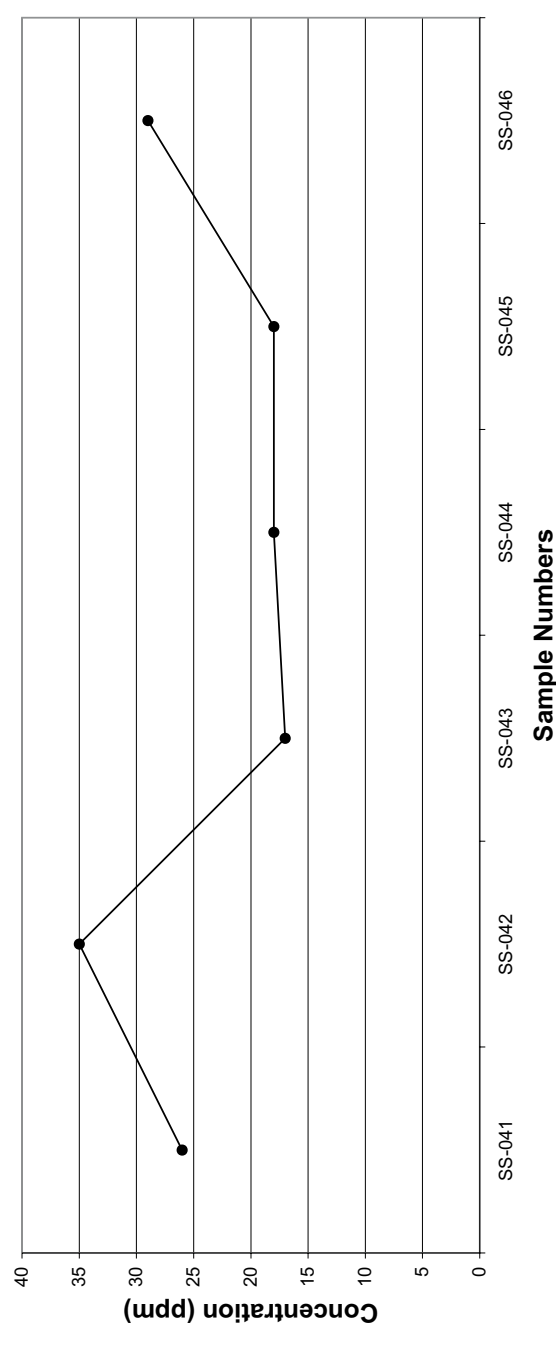
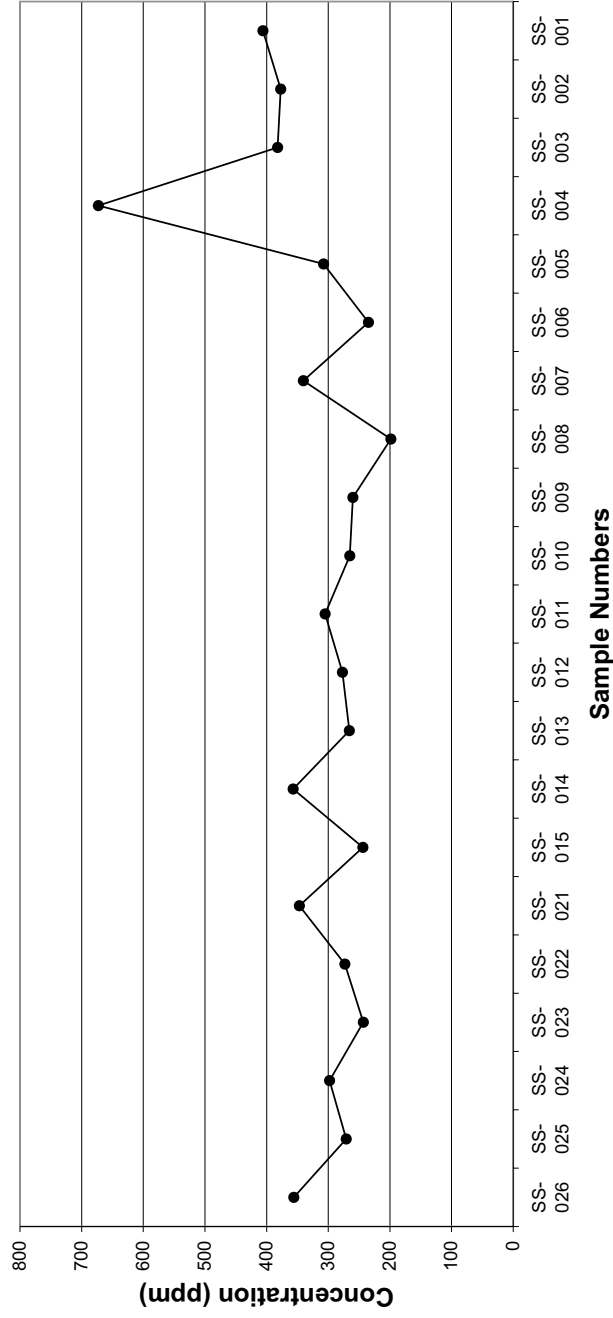
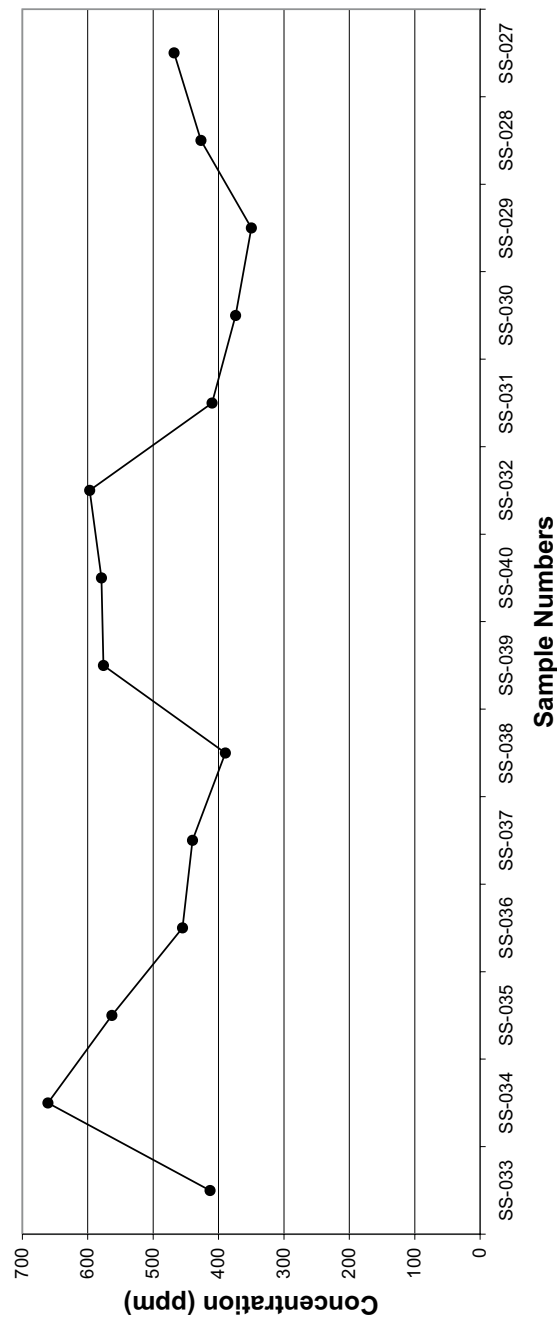


Fig.38 ...continued

### Profile of V XRF Values of the Fine Fraction of the Merelani Stream Sediments of Stream 1



### Profile of V XRF Values of the Medium Fraction of the Merelani Stream Sediments of Stream 2



<http://scholar.sun.ac.za/>

### Profile of V XRF Values of the Fine Fraction of the Merelani Stream Sediments of Stream 3

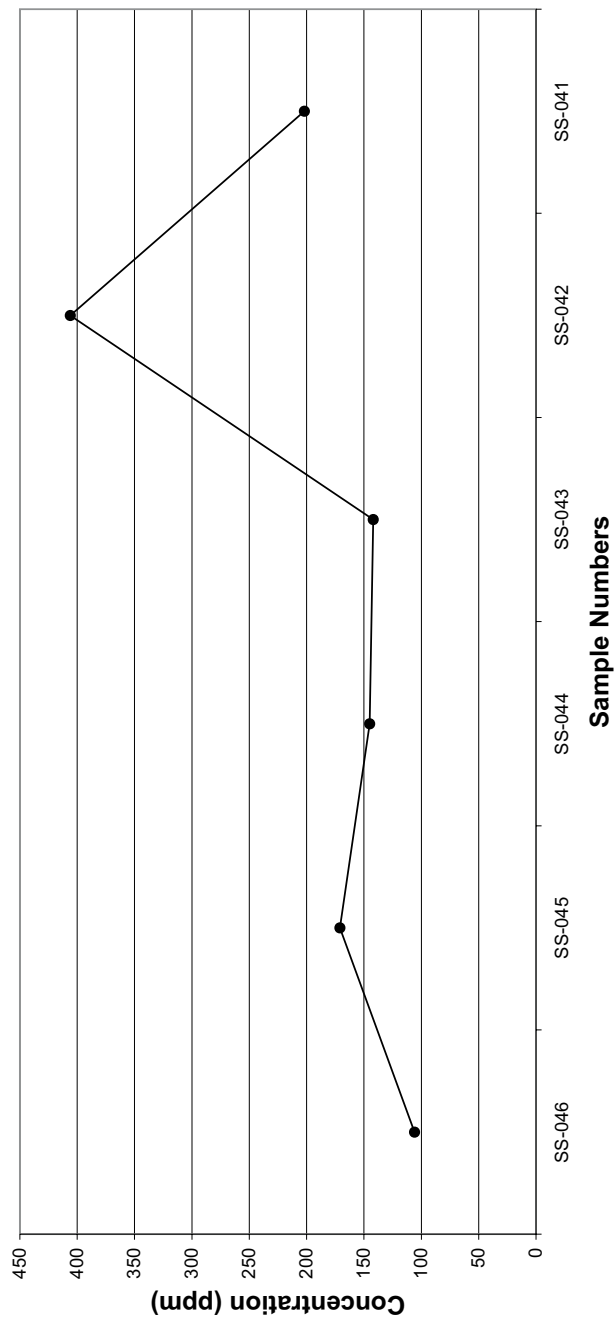
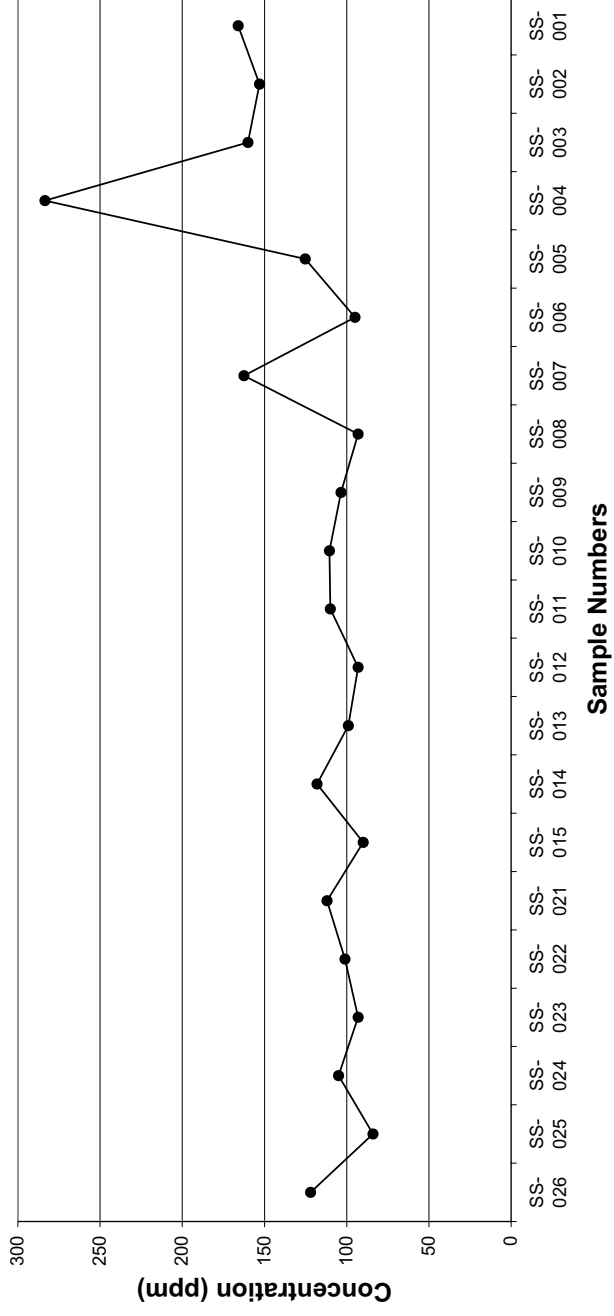
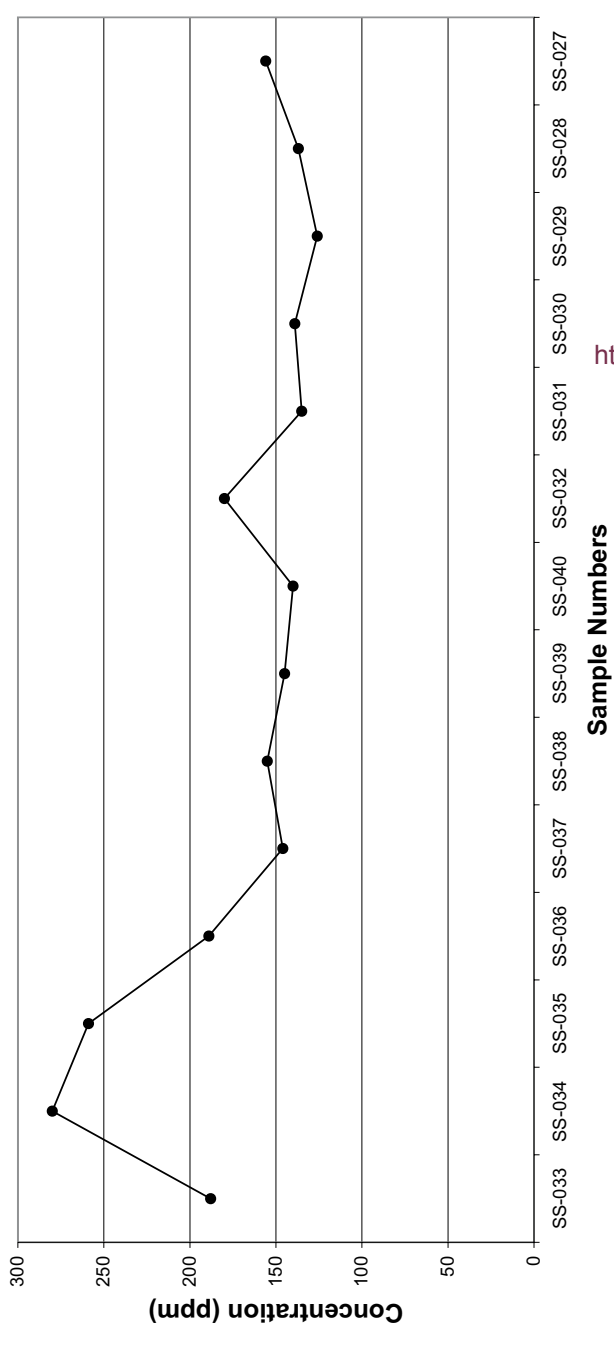


Fig.39 Profiles of the XRF Merelani stream sediment data of the fine fraction over the individual streams sampled

### Profile of Cr XRF Values of the Fine Fraction of the Merelani Stream Sediments of Stream 1



### Profile of Cr XRF Values of the Fine Fraction of the Merelani Stream Sediments of Stream 2



<http://scholar.sun.ac.za>

### Profile of XRF Values of the Fine Fraction of the Merelani Stream Sediments of Stream 3

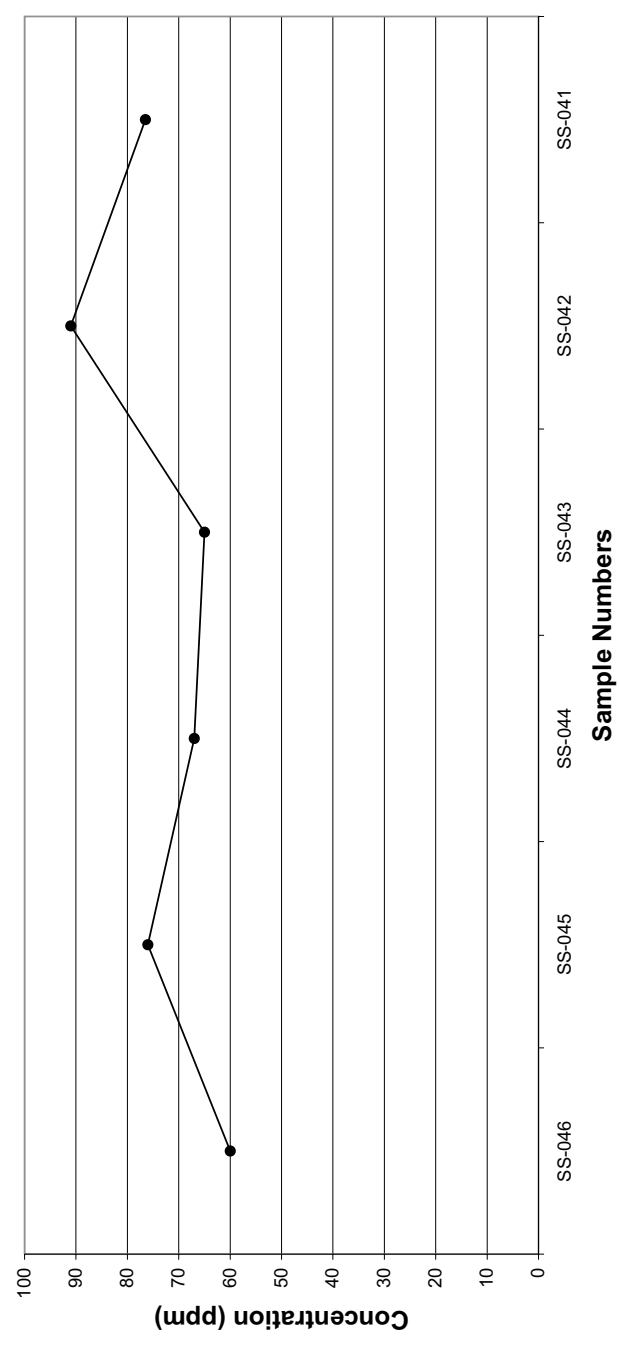
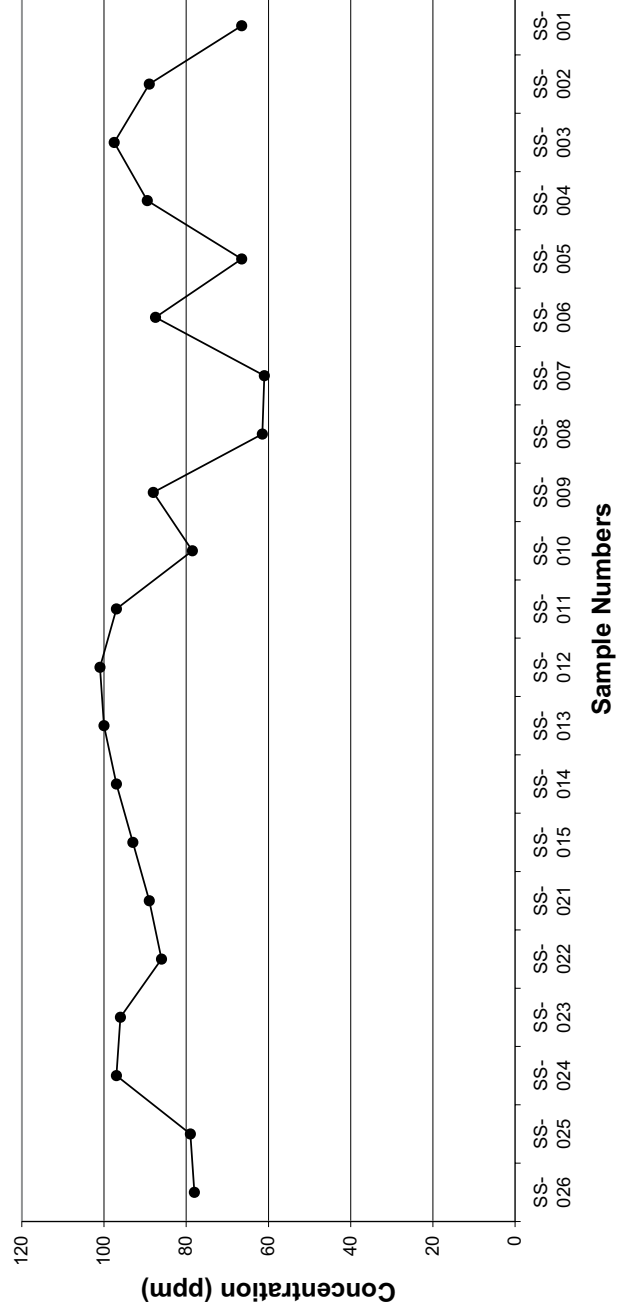
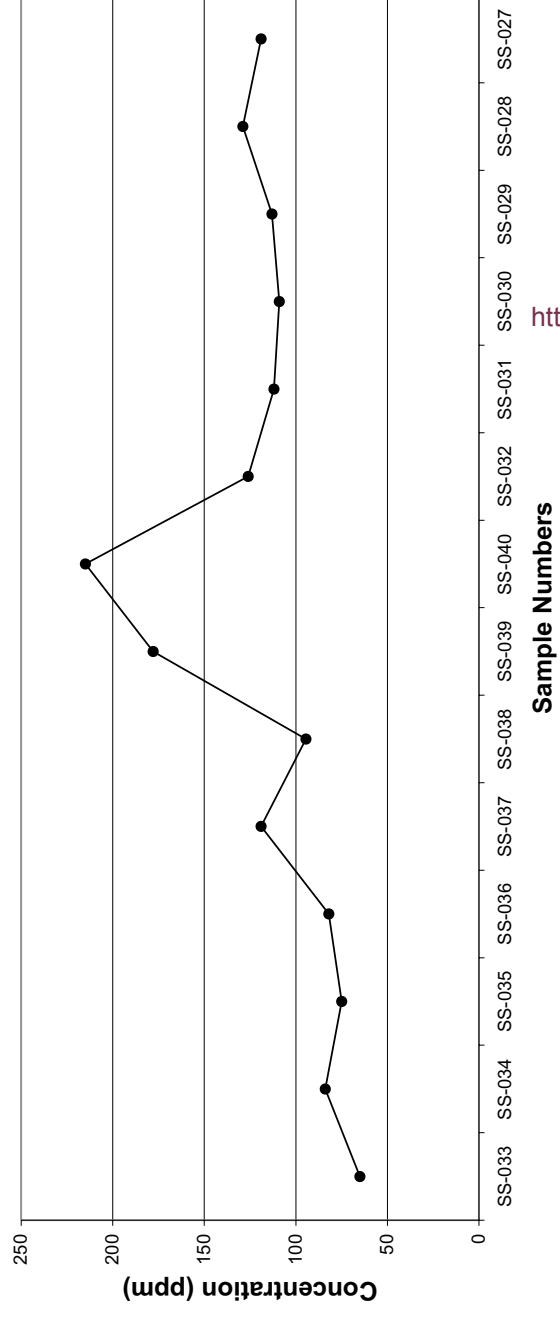


Fig.39 ...continued

### Profile of Ni XRF Values of the Fine Fraction of the Merelani Stream Sediments of Stream 1



### Profile of Ni XRF Values of the Fine Fraction of the Merelani Stream Sediments of Stream 2



<http://scholar.sun.ac.za/>

### Profile of Ni XRF Values of the Fine Fraction of the Merelani Stream Sediments of Stream 3

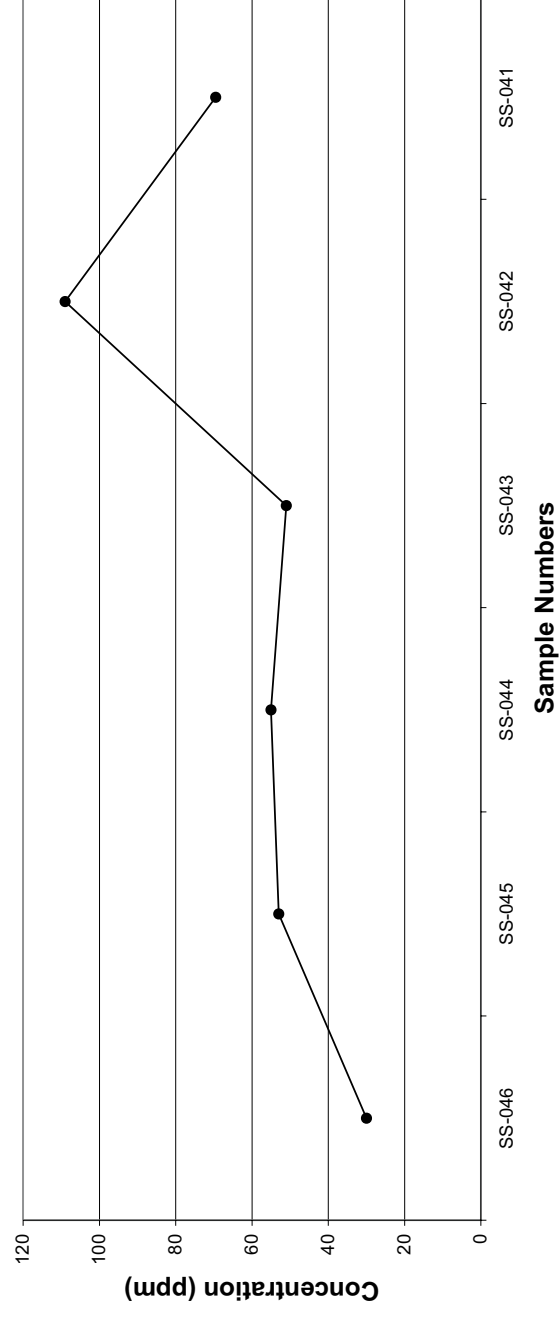
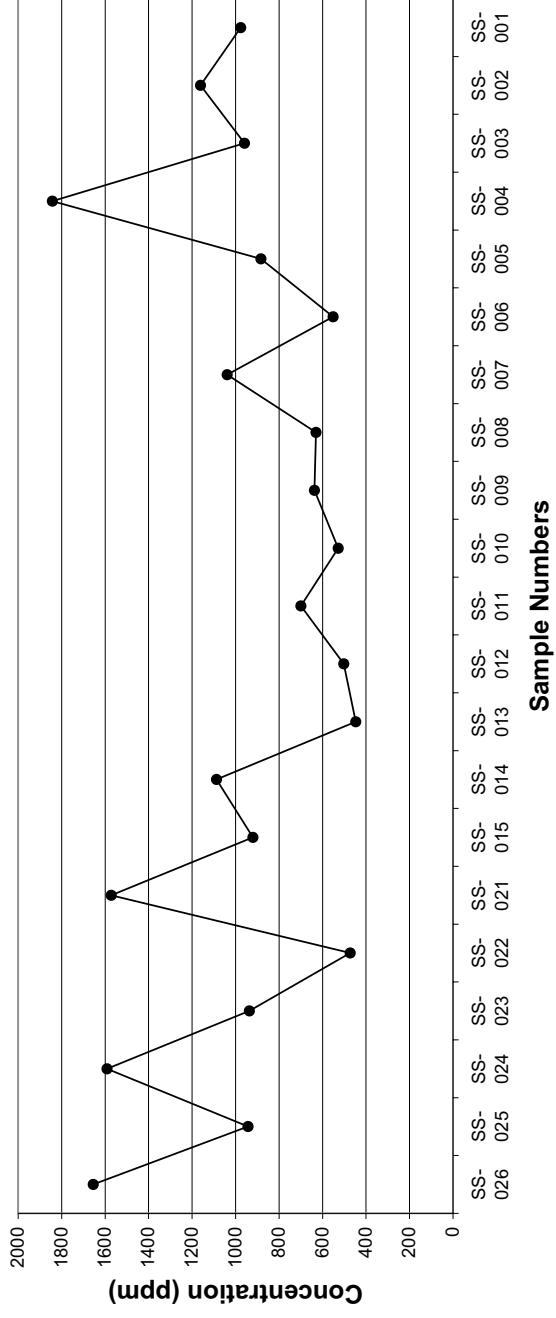


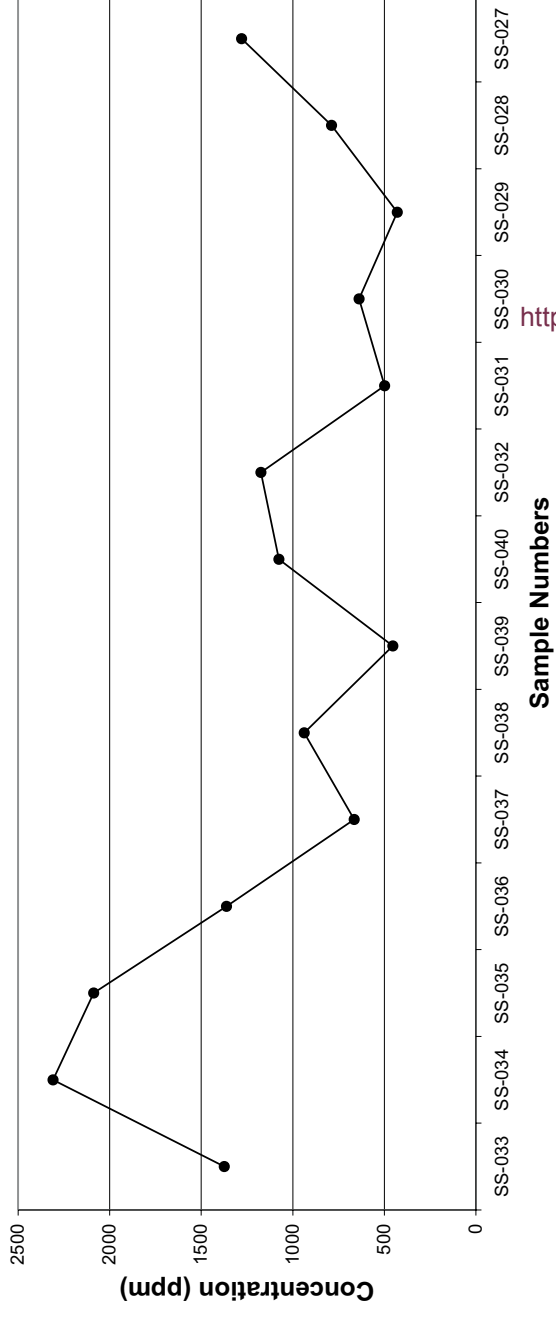
Fig.39 ...continued



**Profile of Zr XRF Values of the Fine Fraction of the Merelani Stream Sediments of Stream 1**



**Profile of Zr XRF Values of the Fine Fraction of the Merelani Stream Sediments of Stream 2**



<http://scholar.sun.ac.za/>

**Profile of Zr XRF Values of the Fine Fraction of the Merelani Stream Sediments of Stream 3**

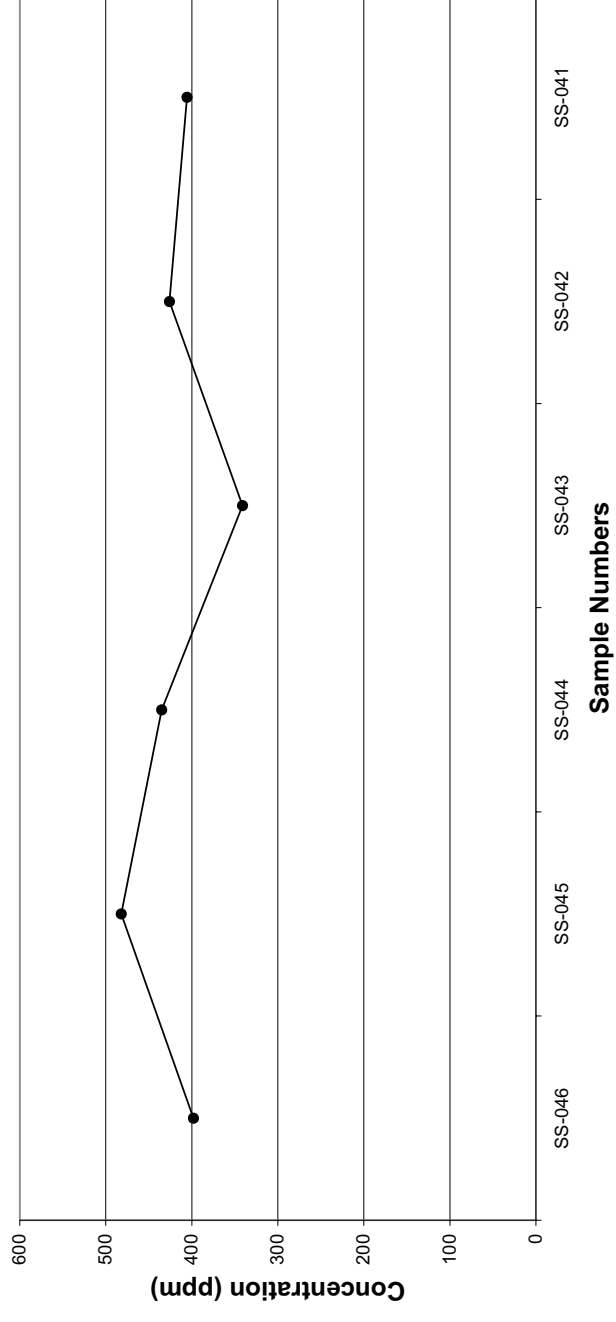
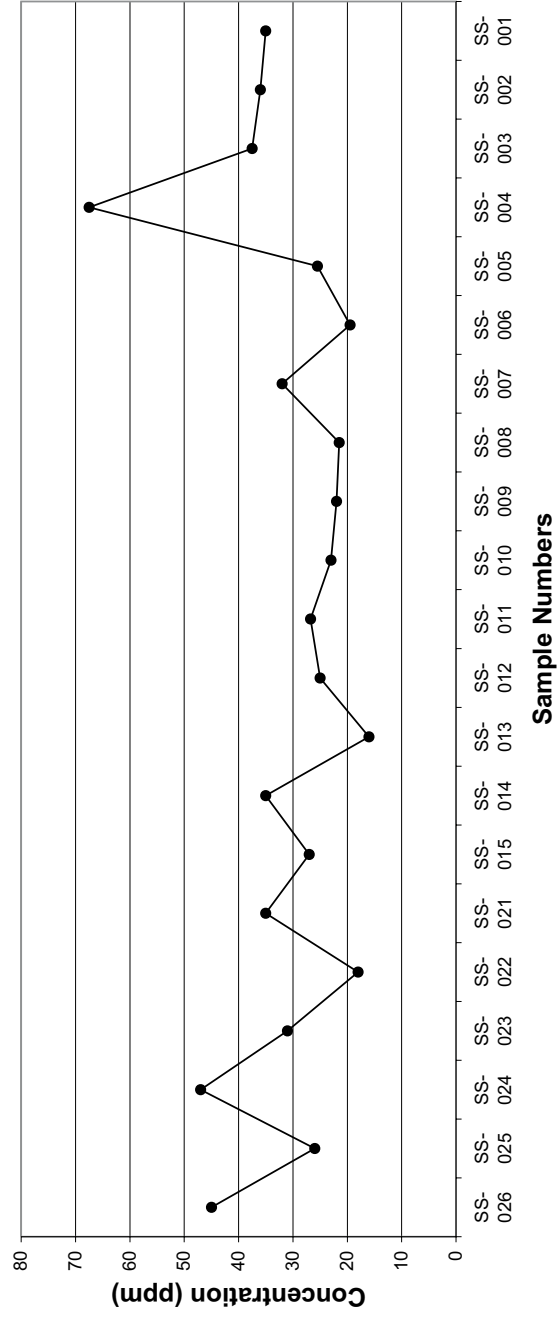
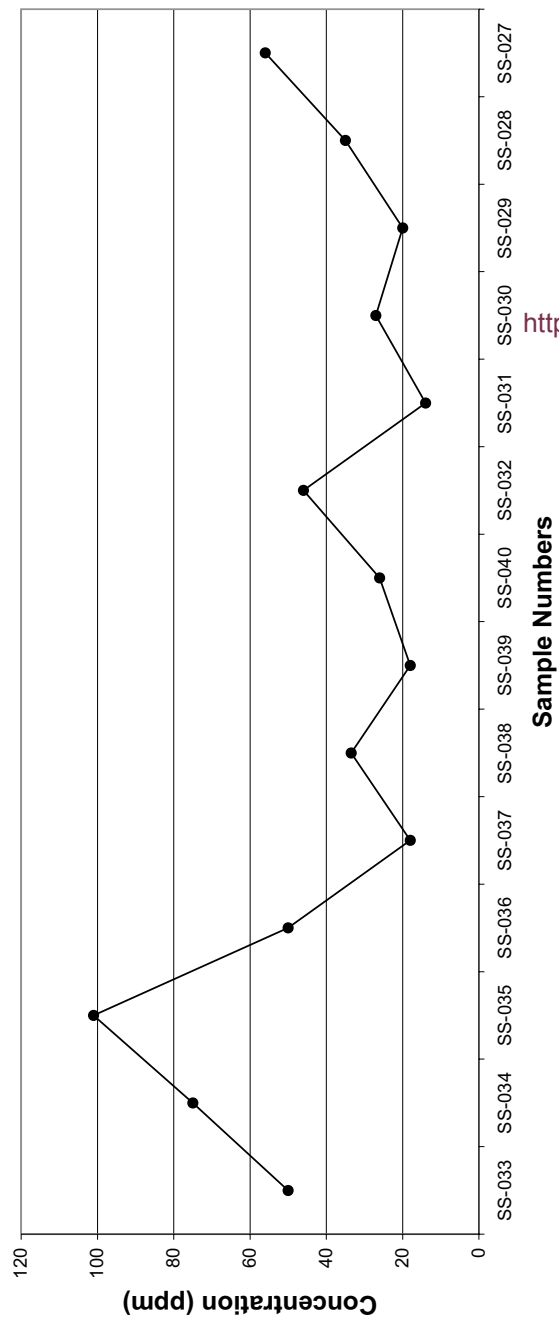


Fig.39 ...continued

### Profile of Th XRF Values of the Fine Fraction of the Merelani Stream Sediments of Stream 1



### Profile of Th XRF Values of the Fine Fraction of the Merelani Stream Sediments of Stream 2



<http://scholar.sun.ac.za/>

### Profile of Th XRF Values of the Fine Fraction of the Merelani Stream Sediments of Stream 3

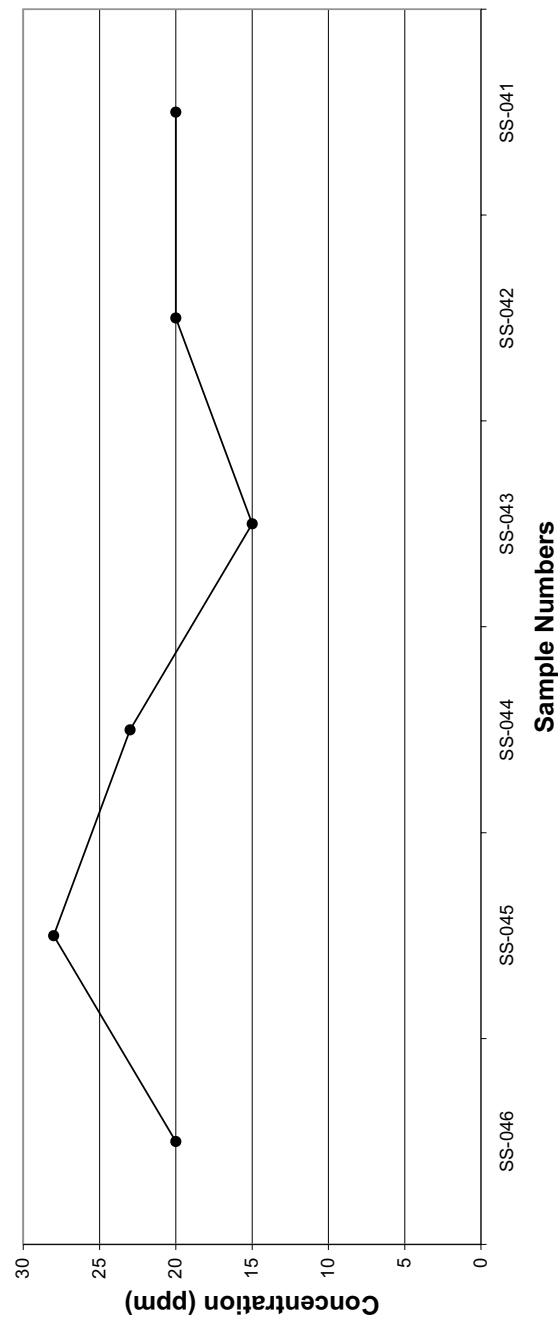


Fig.39 ...continued

Th and Zr were chosen because of their occurrence in the coarser fraction of the soils and stream sediments. The point where the y- and x-axes cross is the position furthest up-stream.

The most important observation when studying the profiles for all three streams is that for both size fractions no recognisable trend exists. There is neither a gradual increase or decrease in any of the profiles plotted.

What is interesting, however are the peaks, especially of V, which occur in the profiles. These peaks become extremely noteworthy when their spatial distribution is considered. When only the V peaks of the fine fraction are studied, the following samples are identified which have high (> 1000ppm) V values: SS-004, SS-020, SS-032, SS-034, SS-039 and SS-040. An old mine-working, where gem mining was once performed, is situated in close proximity to samples SS-032 and SS-034, which makes these samples very significant (Fig.40). If the general strike of 40° for the Merelani lithologies is taken into consideration the V peak over sample SS-020 also becomes significant in that it lies, more or less, on a line linking the high values of Stream 2. In terms of geologic mapping using geochemistry, the low values are also significant, but it would be much harder to discern their meaning as to which lithologic unit they may represent, if any at all.

The same V profile for the medium fraction (Fig.40) seems slightly different. Samples SS-032, SS-034 and SS-035 still display their V peaks. The peak over sample SS-004 is not present. What is exciting about the peaks over samples SS-012 and SS-014 is that a tsavorite (green, gem-quality, V-rich grossular garnet) mine, which is still operational, is situated near SS-012. When the 40° strike (Malisa, 1987) is taken into consideration the mine lies on a line more or less connecting it to SS-014. Though a peak does not occur over sample SS-020 one does occur over sample SS-024, which is just slightly off-set from SS-020. Samples SS-027 and SS-028 also show peaks and could possibly be due to a curvature of the lithologies, causing the peaks in SS-032, SS-034 and SS-035. The factor scores of both fractions were taken and plotted as scatterplots. This was done to see if any outliers and trends could be discerned.

When studying the fine fraction plots of the factors plotted against each other it can be seen that definite outliers and groups could be identified (Fig.41). It seems as if

V Peaks for the Fine Fraction  
V-Peaks for the Medium Fraction

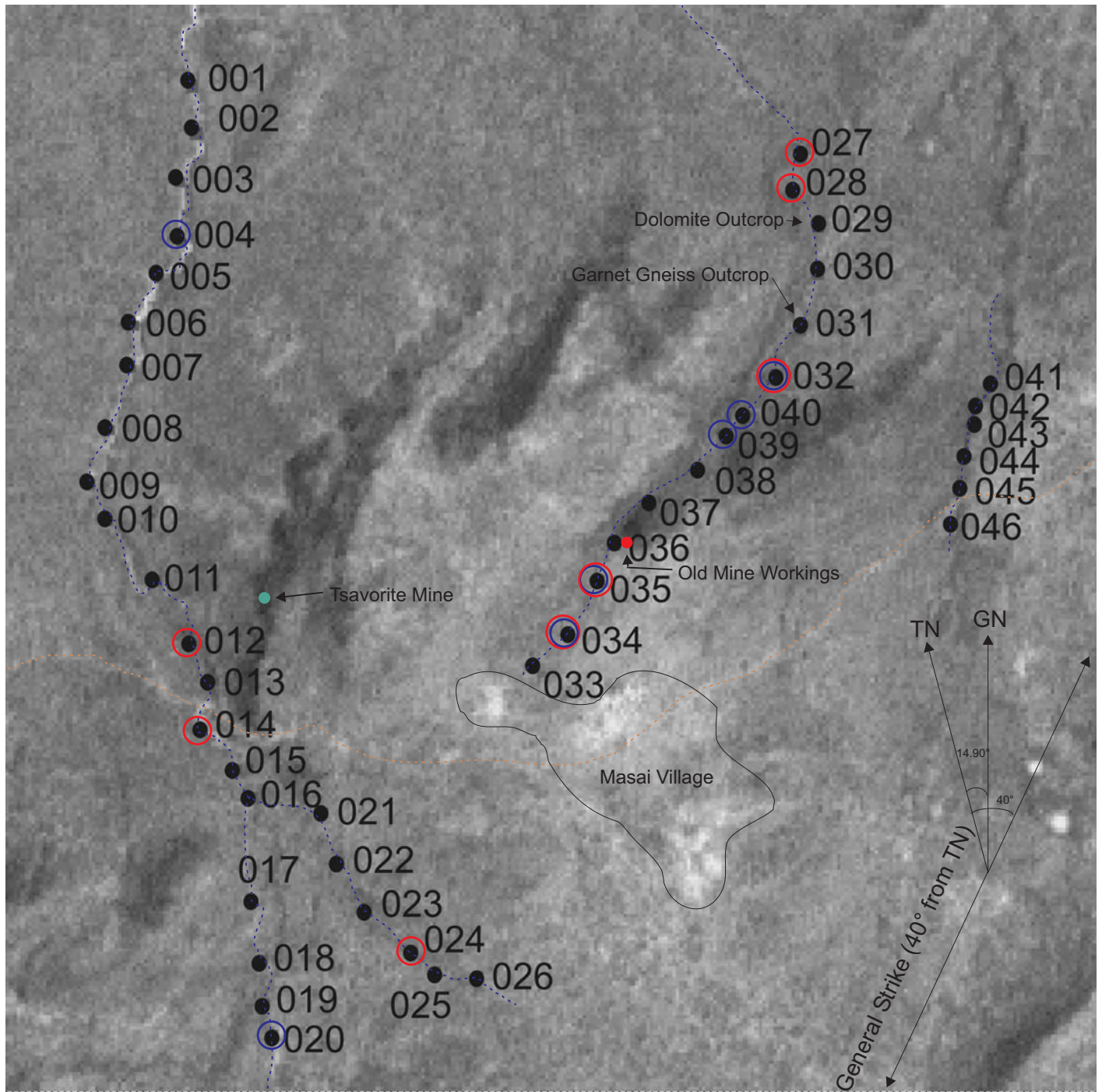
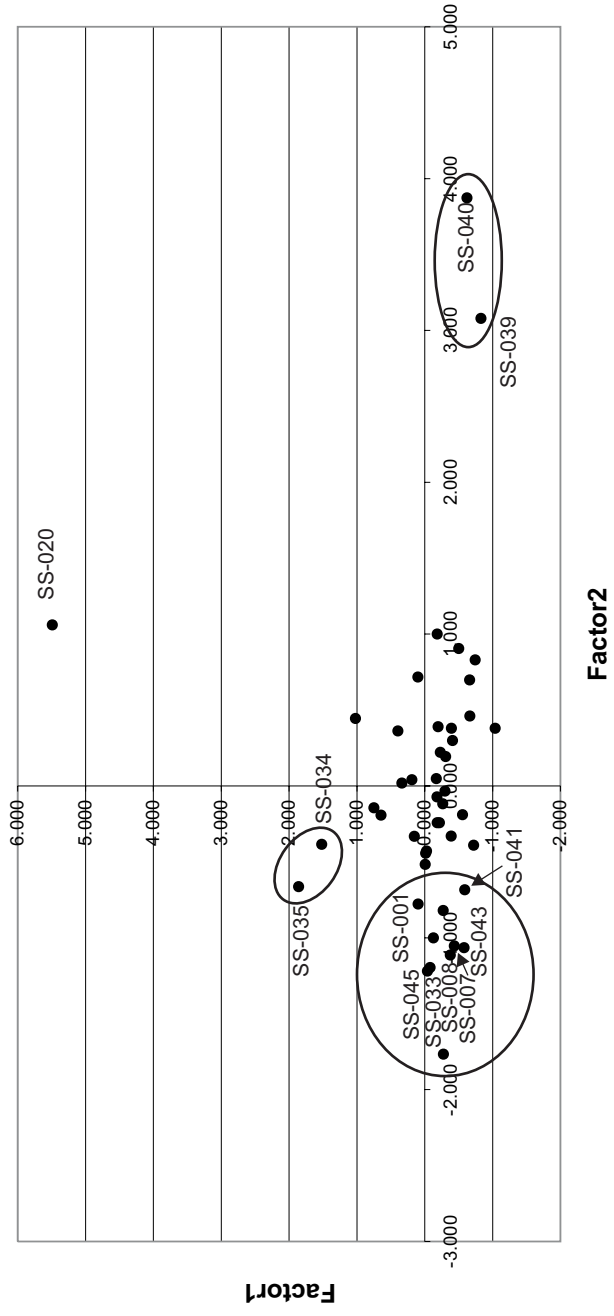
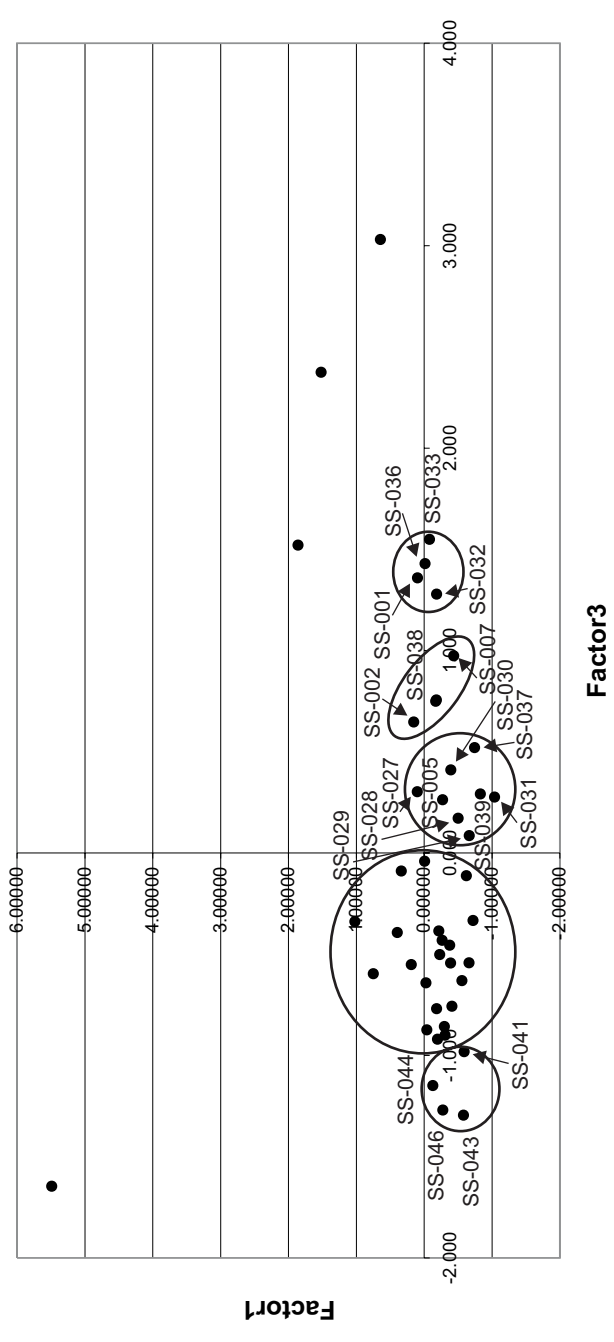


Fig.40 Satellite image containing the sampling sites. The samples representing high V values for the fine and medium fractions are indicated

### Factor 1 vs Factor 2 for the Stream Sediment Samples - Fine Fraction



### Factor 1 vs Factor 3 for the Stream Sediment Samples - Fine Fraction



<http://scholar.sun.ac.za>

### Factor 2 vs Factor 3 for the Stream Sediment Samples - Fine Fraction

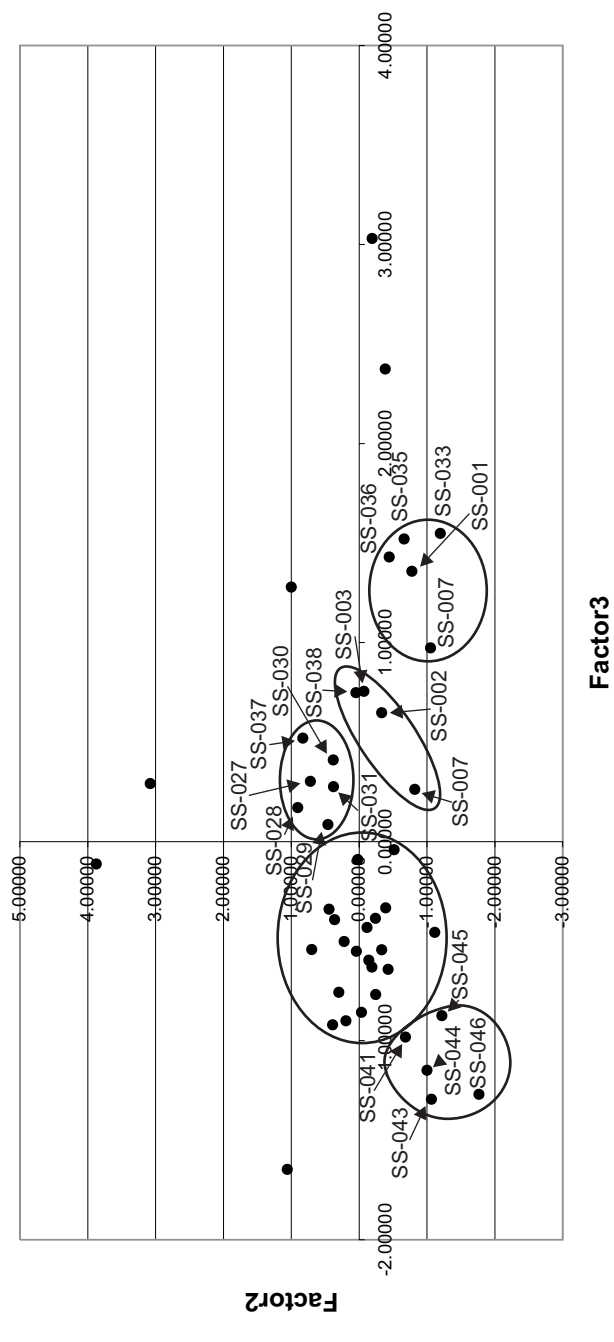


Fig.41 Scatterplots of the factor loadings of the fine fraction of the Merelani stream sediments

samples of more or less similar properties are grouped together. This is most conspicuous on the Factor 1 versus Factor 3 and Factor 2 versus Factor 3 graphs for the fine fraction. On the Factor 1 versus Factor 3 graph, which would essentially represent a plot of the heavy minerals and heavy major mineral phases, SS-035, SS-034 and SS-004 plot in a group. Most of the samples of Stream 3 also plot in a separate group. This is even more clearly seen on the Factor 2 versus Factor 3 plot where all the Stream 3 samples, with the exception of sample SS-042, are located. This is the same sample which displays a V peak on the V-profile, rendering this sample worthy of further scrutiny. The samples that plot as outliers are given in Table 31 below:

<b>Factors of which Scores were plotted</b>	<b>Outlying Samples</b>
F1/F2	SS-020, SS-040, SS-039, SS-035, SS-034
F1/F3	SS-020, SS-035, SS-034, SS-004
F2/F3	SS-020, SS-040, SS-039, SS-032, SS-034, SS-004

All the outlying samples correspond to the V peaks in the profile plots which, in turn, correspond to samples which occur near and on strike from currently exploited gem deposits.

When the factors of the medium fraction are examined the scenario seems, at first glance, slightly different. The fact that the medium fraction factors most probably represent a larger heavy mineral component, relative to the fine fraction, has already been discussed. This fact is evident simply by examining the elements which constitute the factors. The outlying samples of the factor ratio plots are given in Table 32 below.

<b>Factors of which Scores were plotted</b>	<b>Outlying Samples</b>
F1/F2	SS-027, SS-035, SS-028, SS-024, SS-034, SS-012, SS-014, SS-040
F1/F3	SS-035, SS-027, SS-028, SS-021, SS-024, SS-040, SS-034, SS-023, SS-026
F2/F3	SS-035, SS-034, SS-014, SS-012, SS-024, SS-021, SS-027, SS-040

As was previously mentioned, the samples with seemingly similar properties tend to cluster together. This is what makes the outlying samples so interesting because these samples will possess properties that are different, i.e. anomalous, to the rest. It is, once again, important to note that the outlying samples of the factor plots for the medium fraction correspond exactly with the V peaks for the same fraction.

Graphs were plotted for the fine and medium fractions of the individual factors (Fig.41 and Fig.42) as well as for the ratios (Fig.43 and Fig.44). It can be seen, by examining these graphs, that it is always the same samples over which the peaks occur. There are a few exceptions, but the sample that is different is always adjacent to samples which display peaks in other graphs. In other words, the peaks are always spatially distributed in the same general area. It is fairly obvious that no one graph contains all the peaks and that, to get a better view of what is happening in the data, it is necessary to study all these graphs together.

The samples which are most important and deserve further scrutiny with respect to correlation with geology and specifically with specific lithological units are as follows: SS-004, SS-012, SS-014, SS-020, SS-024, SS-027, SS-028, SS-034, SS-035, SS-039 and SS-040.

Of the above-mentioned samples SS-014, SS-020, SS-024, SS-034, SS-039 and SS-040 are deemed to be the most important, based on outlying character on the factor plots, on spatial distribution with regard to old and current mine workings as well as on

### Factor 1 vs Factor 2 for the Stream Sediment Samples - Medium Fraction

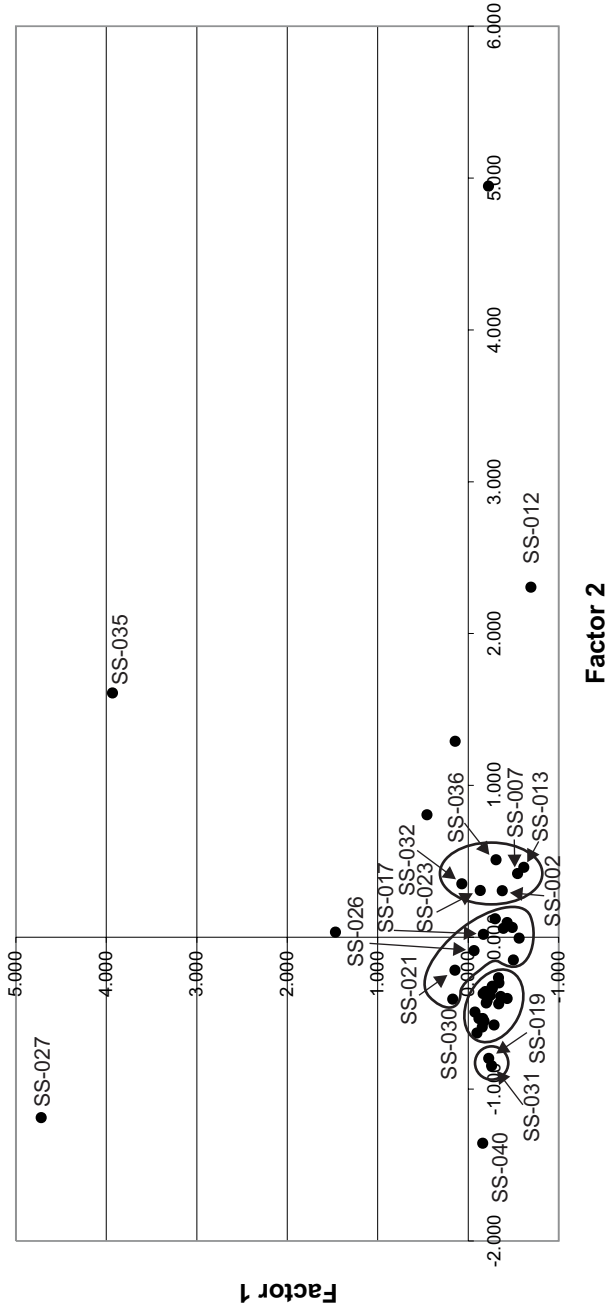
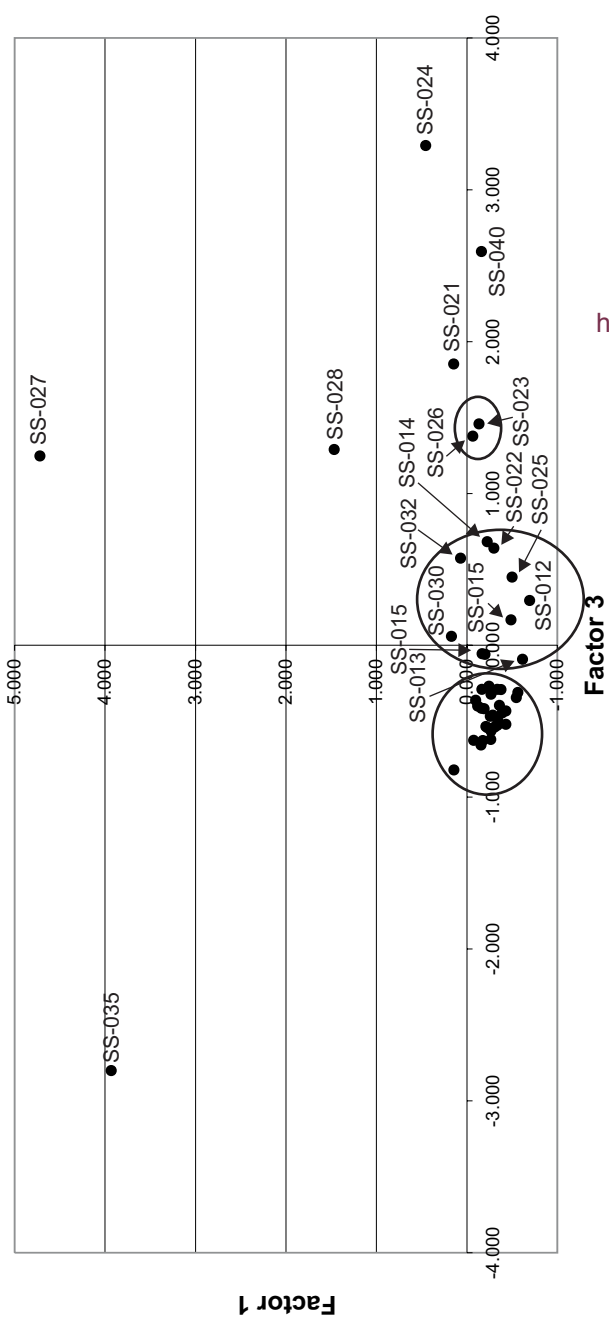


Fig.42a Factor 1 versus Factor 2

### Factor 1 vs Factor 3 of the Stream Sediment Samples - Medium Fraction



<http://scholar.sun.ac.za>

Fig.42b Factor 1 versus Factor 3

### Factor 2 vs Factor 3 of the Stream Sediment Samples - Medium Fraction

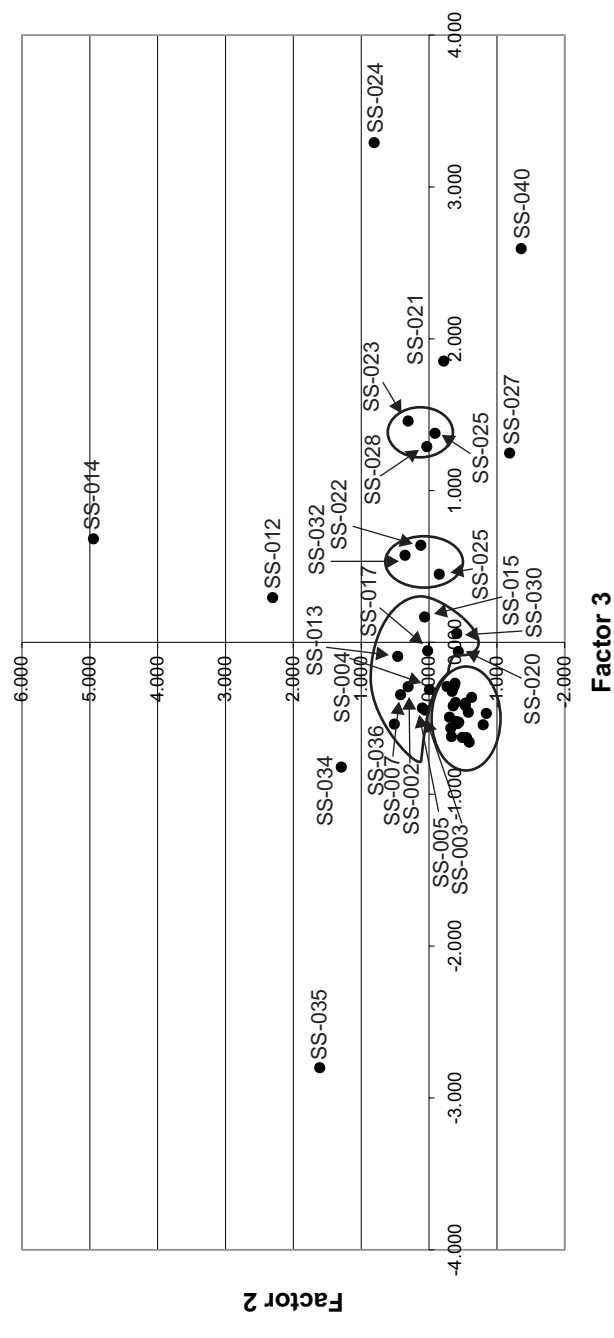
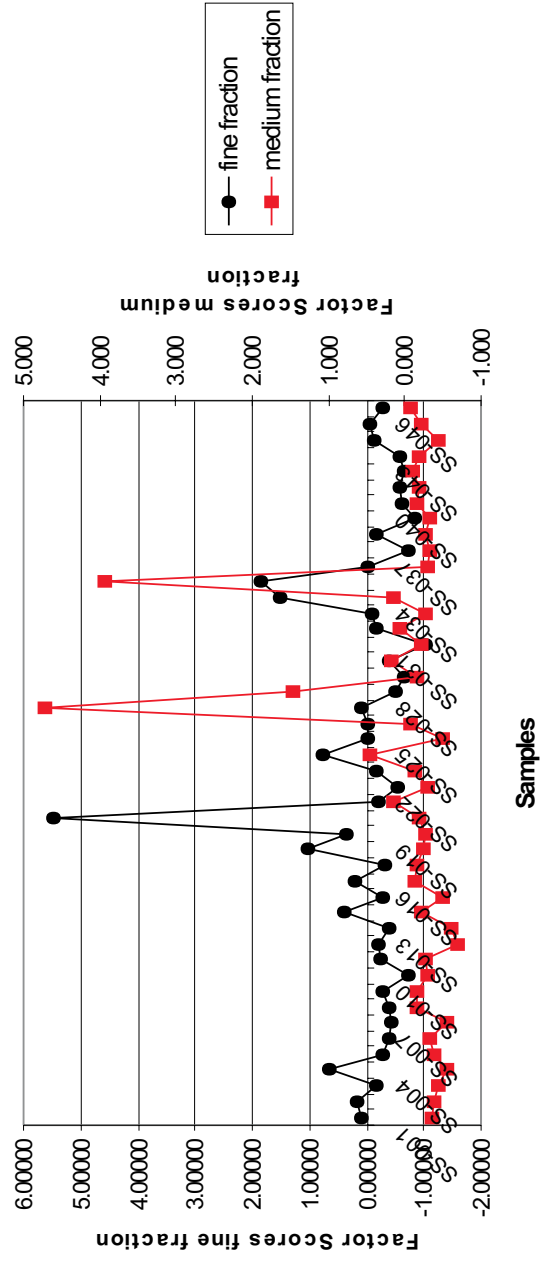


Fig.42 Scatterplots of the XRF data of the medium fraction of the Merelani stream sediments

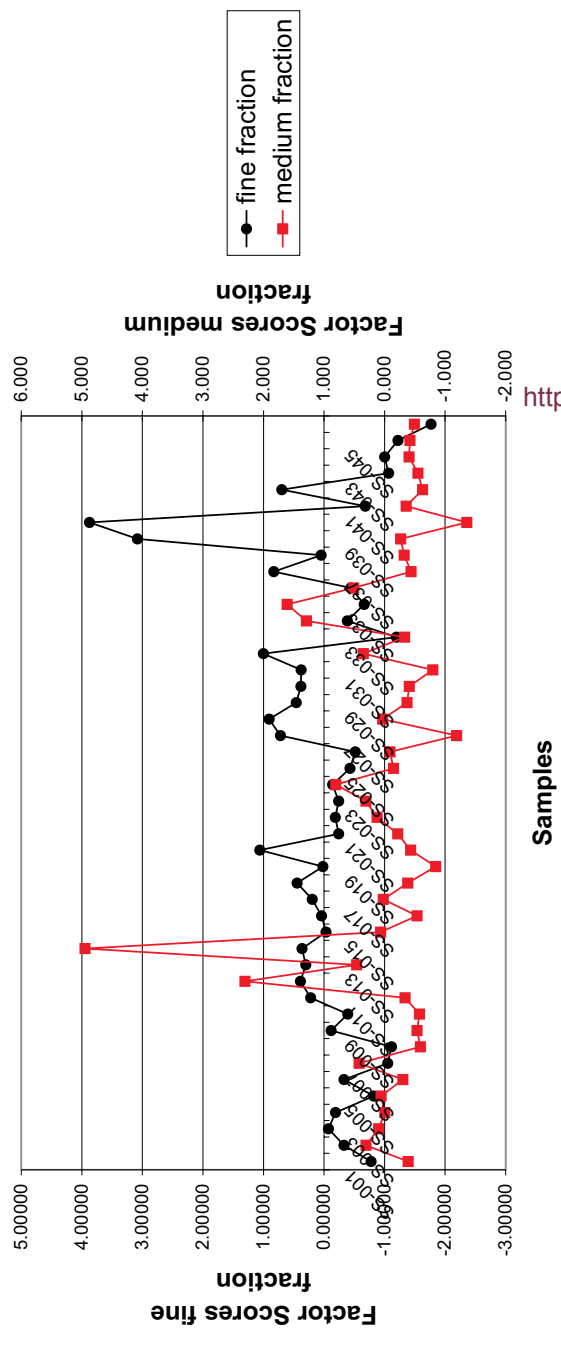
Fig.42c Factor 2 versus Factor 3



### Factor 1 Scores for the entire Stream sediment data set of the Fine and Medium Fractions



### Factor 2 Scores for the entire stream sediment data set of the Fine and Medium Fractions



### Factor 3 Scores for the entire stream sediment data set of the Fine and Medium Fractions

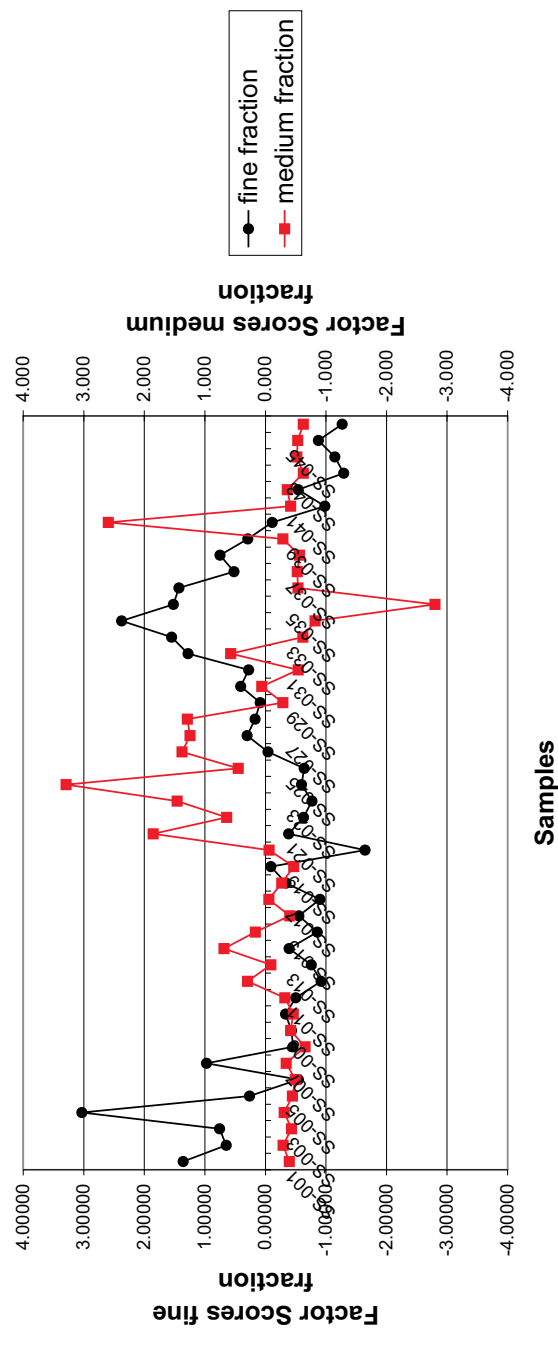
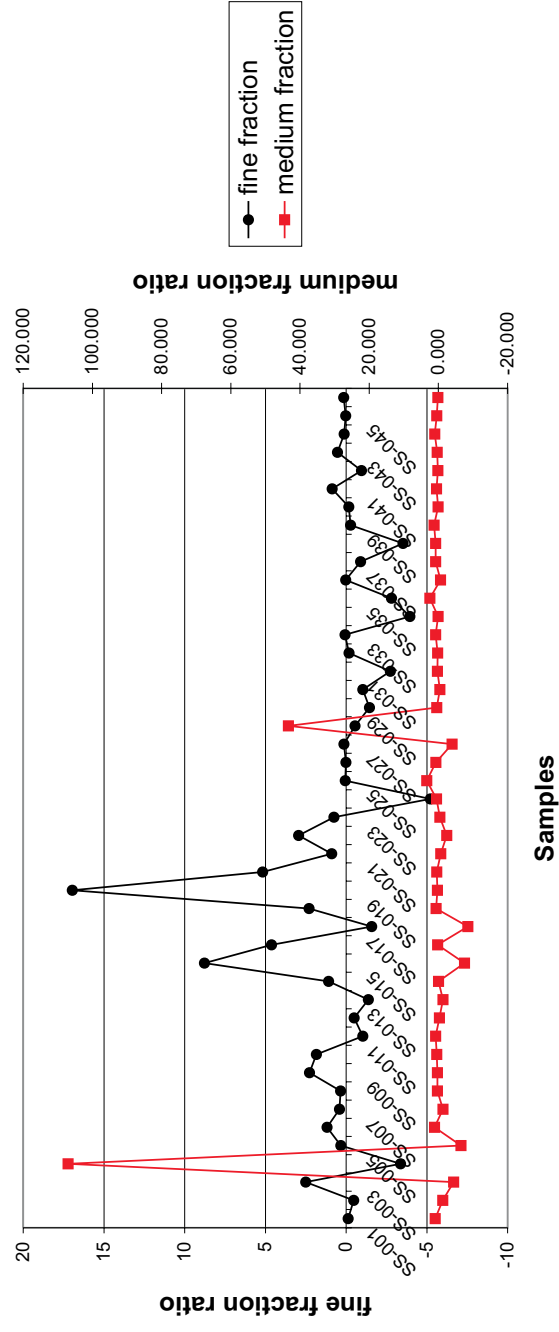
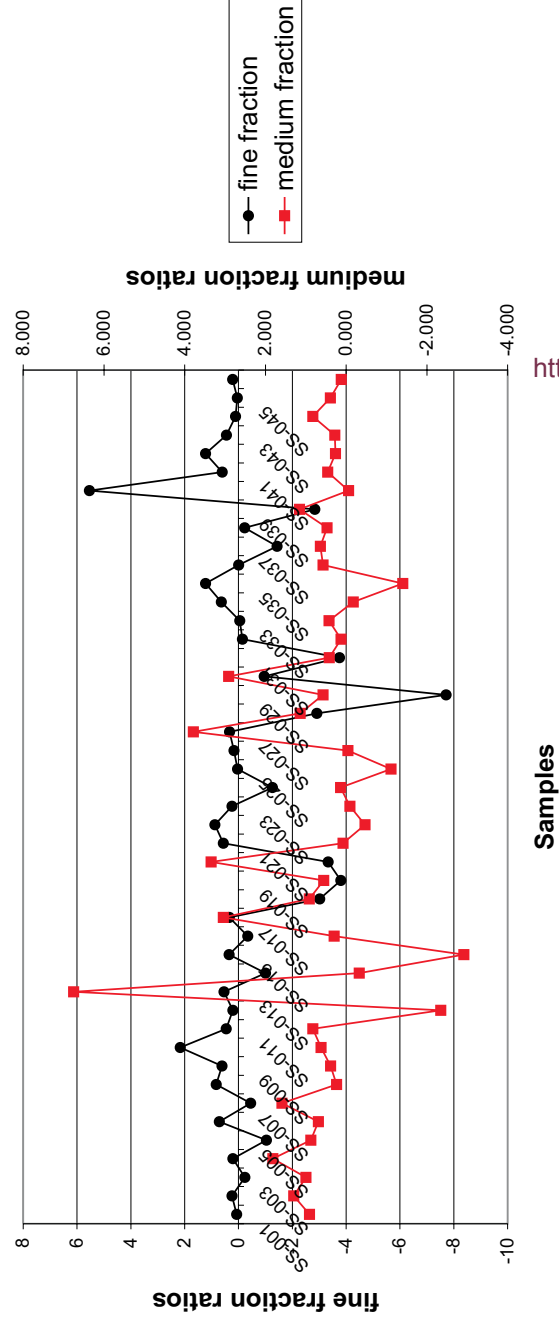


Fig. 43 Factor score plots for the fine and medium fractions of the Merelani stream sediment samples

### Factor1:Factor2 ratio of the entire stream sediment data set of the Fine and Medium Fractions



### Factor1:Factor3 Ratio for the entire stream sediment data set of the Fine and Medium Fractions



<http://scholar.sun.ac.za>

### Factor2:Factor3 Ratio of the entire stream sediment data set of the Fine and Medium Fractions

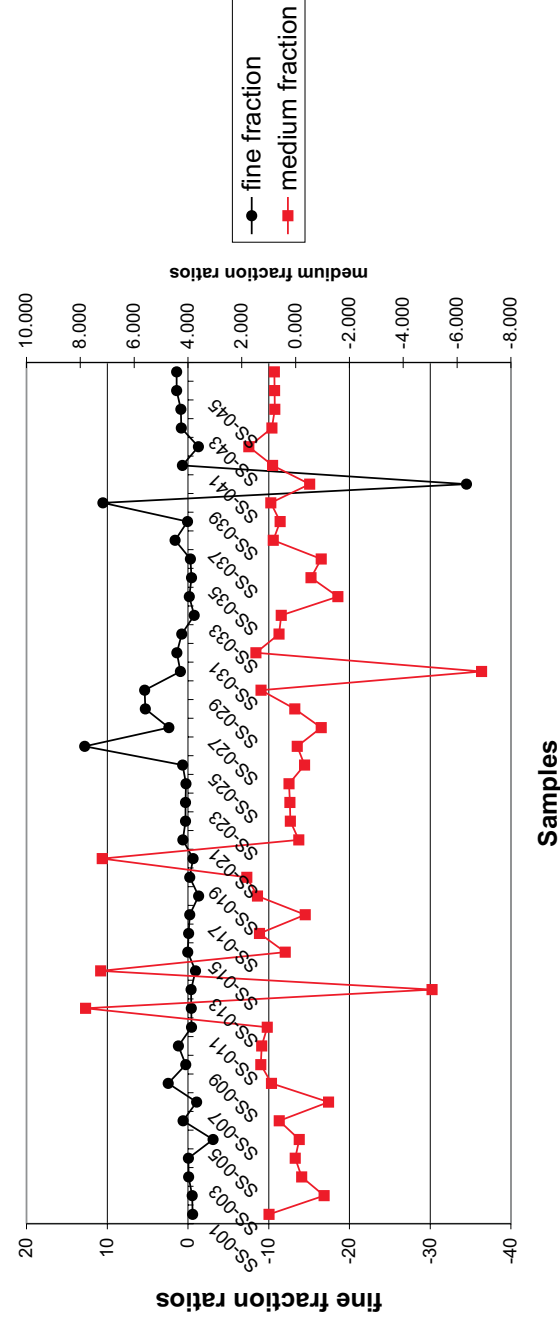


Fig. 44 Factor ratio plots for the fine and medium fractions of the Merelani stream sediment samples

their continued anomalous behaviour in all the plots for both fractions for the plotted elements, such as V as well as for the factors.

The samples containing V peaks as well as the samples represented by peaks on the factor plots and those that plot as outliers on the factor ratio plots are presented on the satellite image as a means of graphically presenting the spatial distribution of these anomalous samples (Fig.45 - Fig.48).

A detailed structural description of the area of study is beyond the scope of this thesis, as the primary focus is on the geochemistry. It is however necessary to make brief comments on the proposed structure, firstly, because minimal detailed regional structural work has been performed and, secondly, because the spatial orientation of the different lithological units will have a profound effect on the stream sediment composition because of the fact that the sediments are not extensively mobilised over great distances.

It has already been reported that boudinaging does occur within the relatively small scale of the tanzanite mine and that these boudins have very important implications for the tanzanite mineralization. When the satellite greyscale image with the stream sediment sampling points superimposed upon it is examined (Fig.49), two triangular shaped structures are seen in the centre slightly off-set towards the top right-hand corner. Other than that, it would also seem that there is a larger structure present, as delineated. When the image is zoomed out to display the major part of the western limb of the Lelatema anticline, the two smaller triangular structures can still clearly be seen. It would also appear that there is a larger block-like structure to the south-west of these two triangular structures. Furthermore, it can also be seen that there are a number of smaller oblate structures orientated with their long axes parallel to these two seemingly larger structures. Something else that is important is that the layers that form the Merelani lithologies, upper and lower horizons, seem to form "rolling" structures, i.e. they form structures which are convex towards the bottom of the image. It is therefore proposed, that the possibility exists that the small scale structures also occur on a larger scale and that the smaller structures in the mine just mimic the larger scale structures within the Lelatema anticline.

Factor 1 of Fine Fraction  
Factor 2 of Fine Fraction  
Factor 3 of Fine Fraction

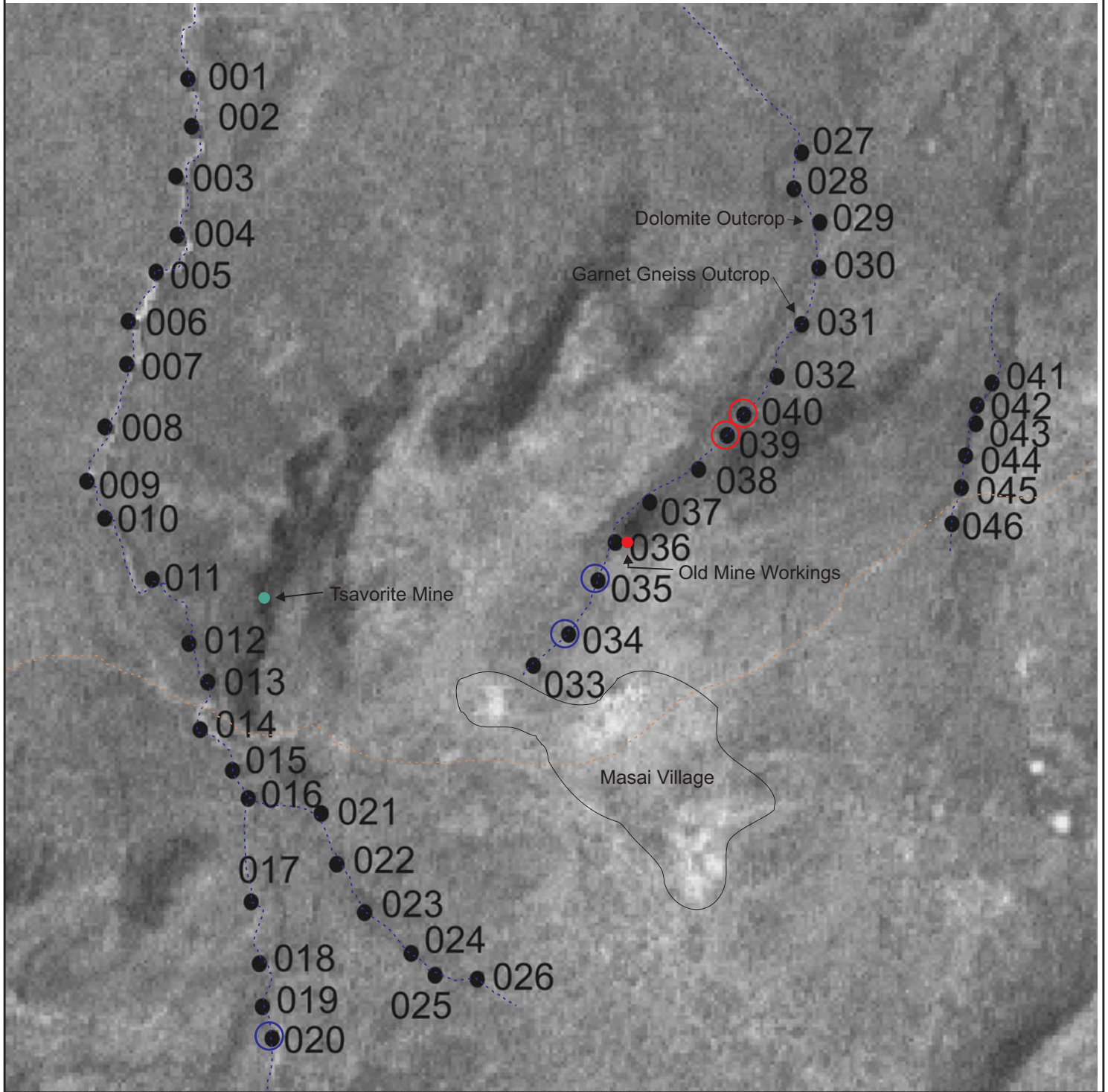


Fig.45 Samples with high factor scores are indicated for all three factors for the fine fraction

Factor 1 peaks of the Medium Fraction  
Factor 2 peaks of the Medium Fraction  
Factor 3 peaks of the Medium Fraction

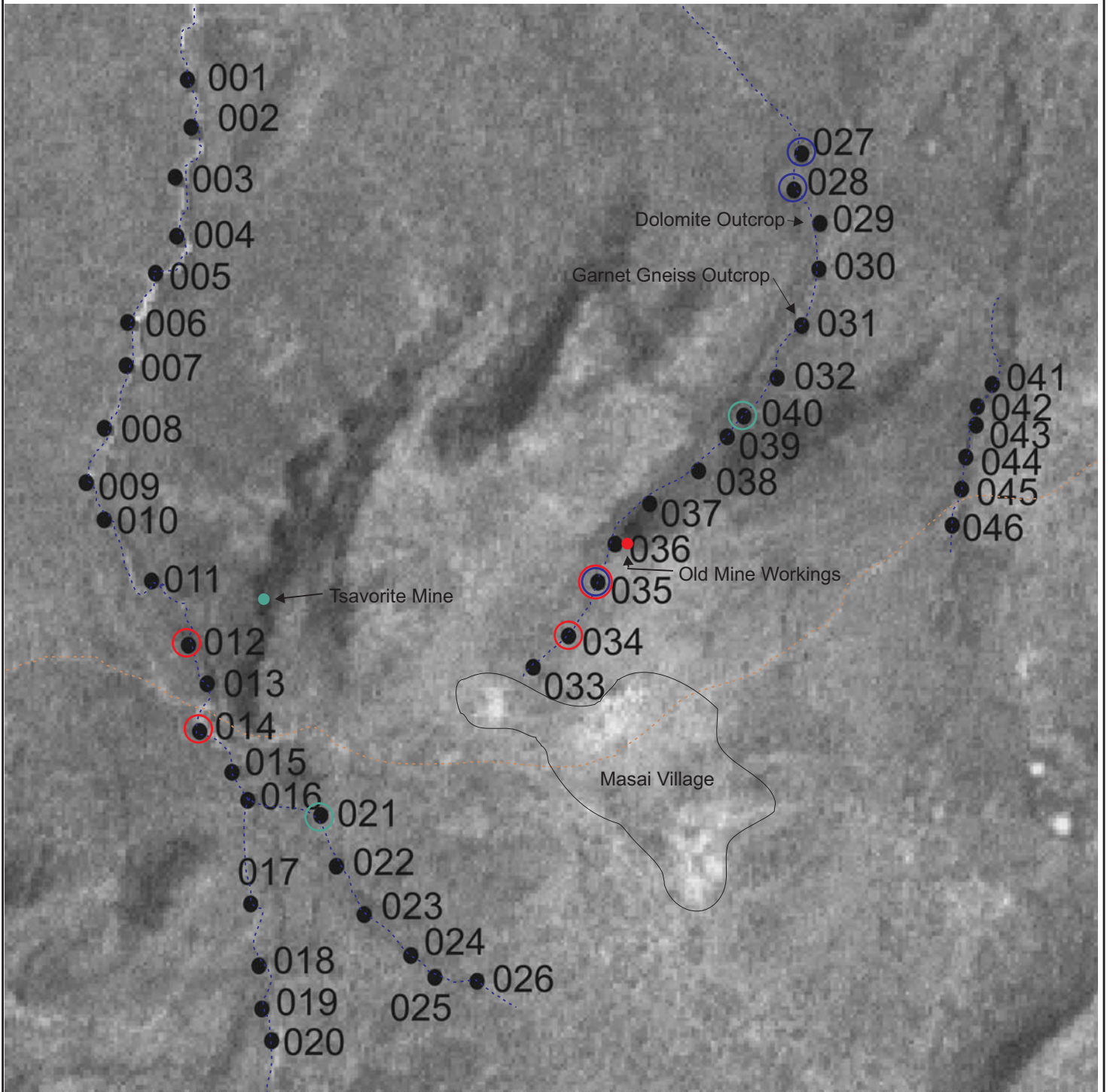


Fig.46 Samples with high factor scores are indicated for all three factors for the medium fraction

F1/F2 Outliers of the Fine Fraction  
F1/F3 Outliers of the Fine Fraction  
F2/F3 Outliers of the Fine Fraction

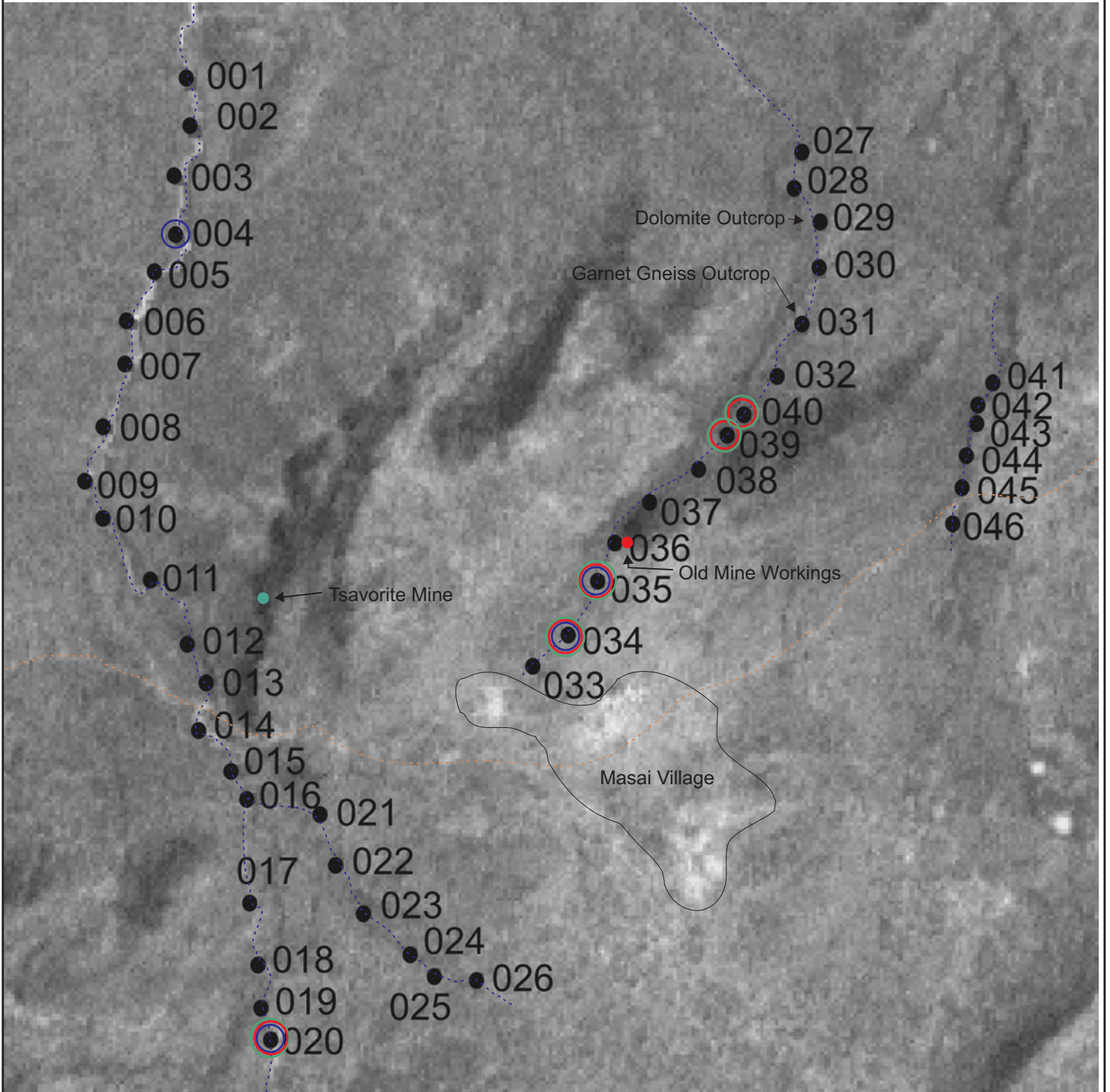


Fig.47 Factor ratio plot outliers indicated for all three factors plots of the fine fraction

F1/F2 Outliers of the Medium Fraction  
F1/F3 Outliers of the Medium Fraction  
F2/F3 Outliers of the Medium Fraction

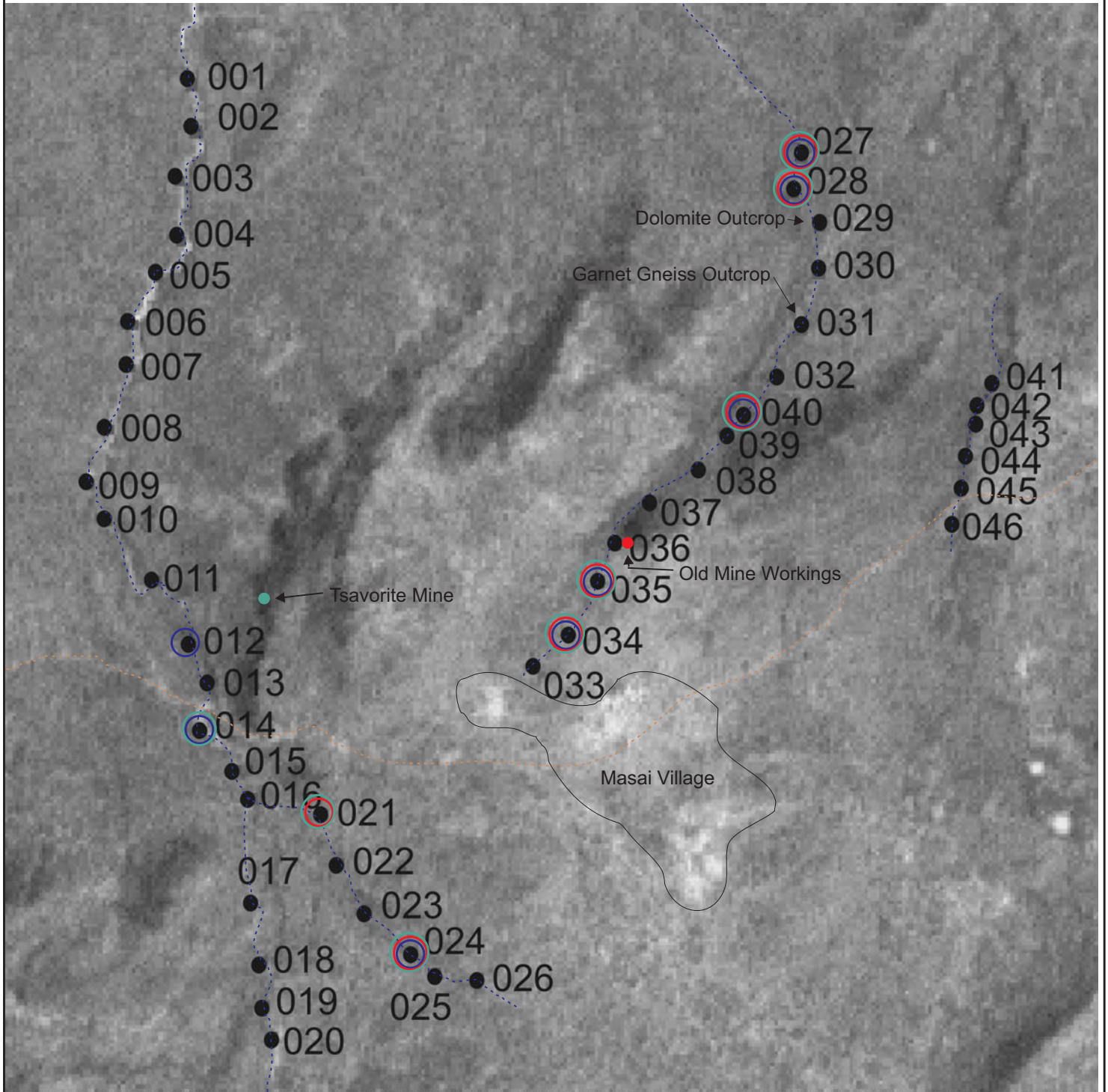
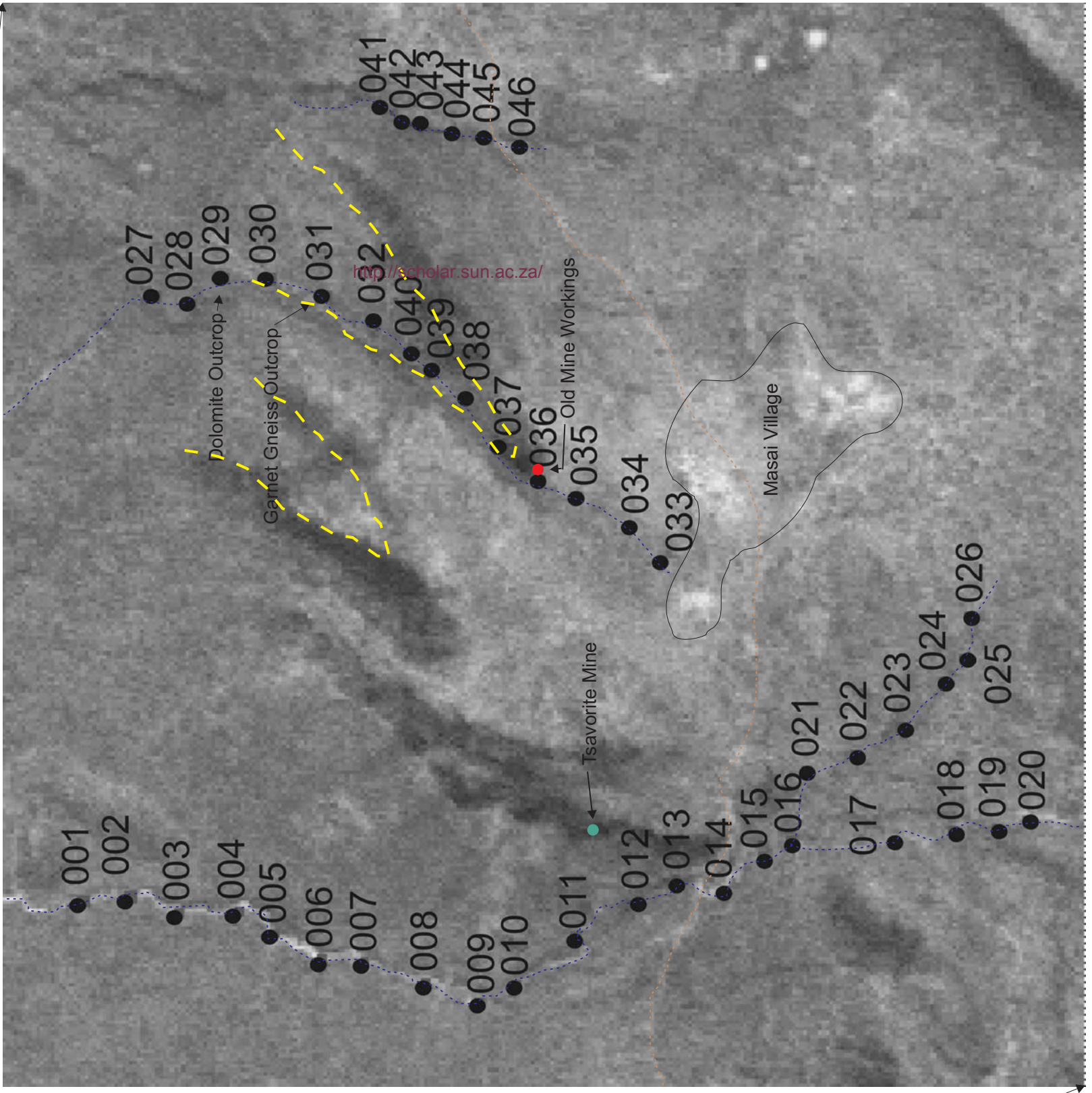
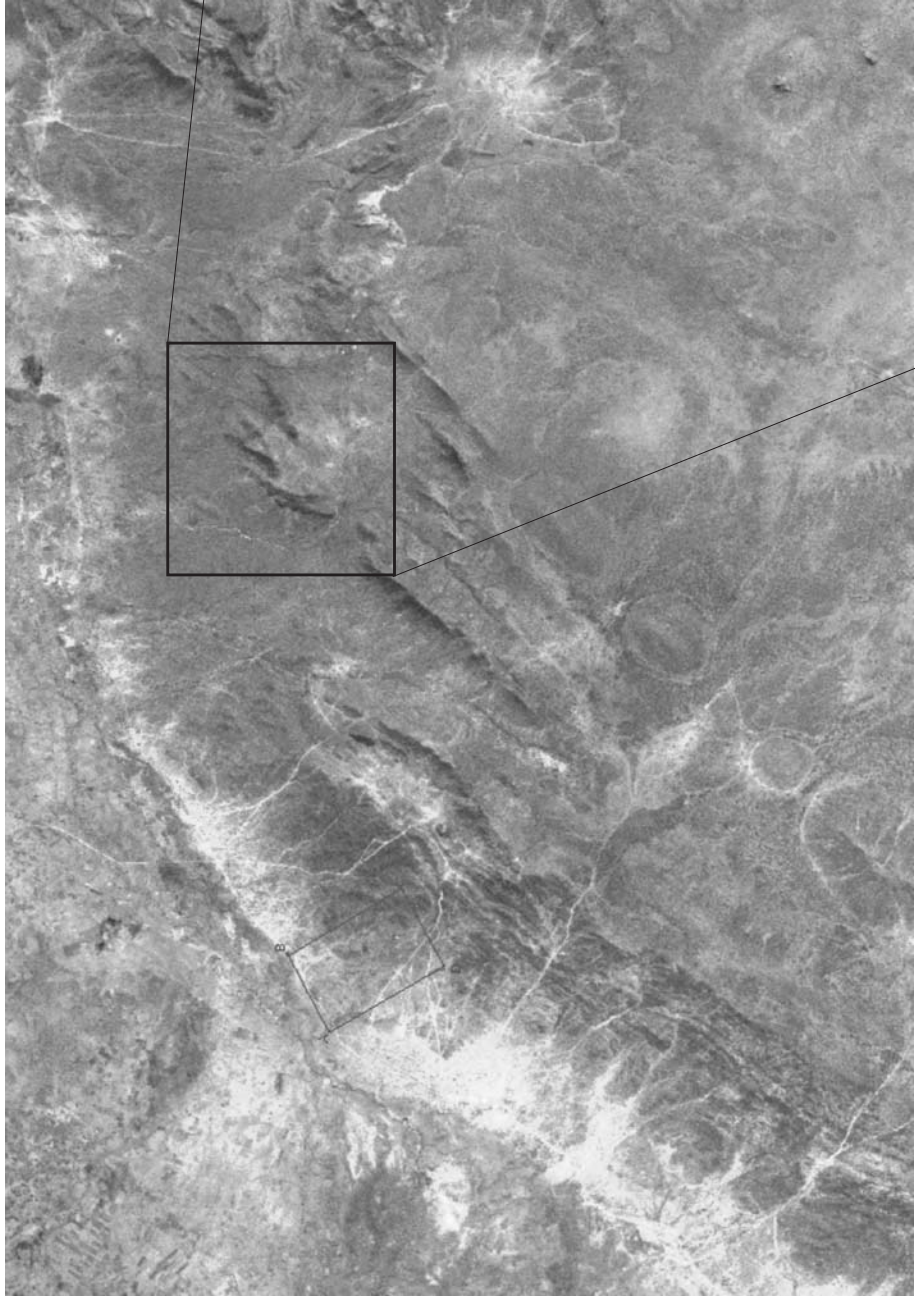


Fig.48 Factor ratio plot outliers indicated for all three factors plots of the medium fraction



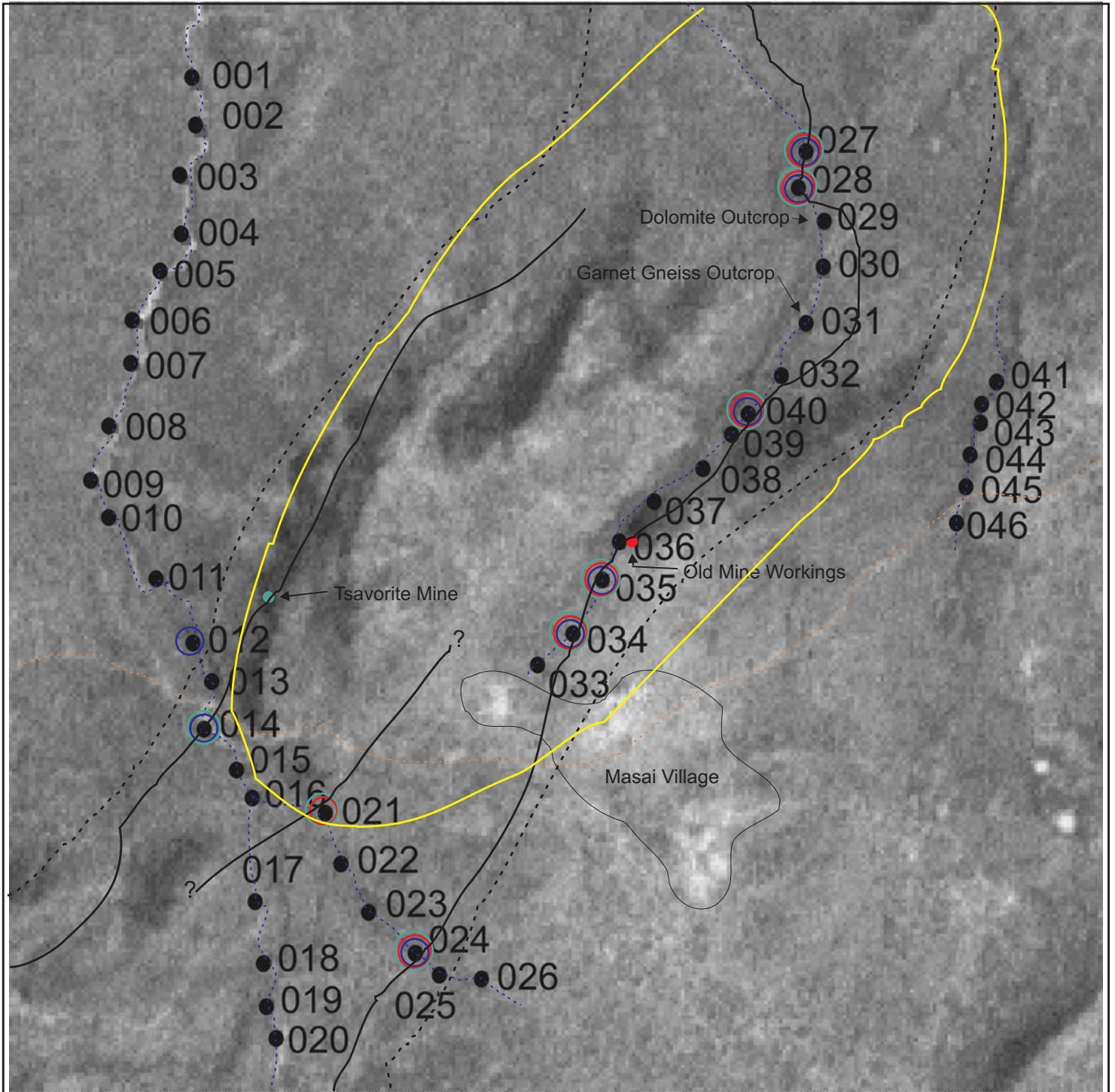
 Outline of triangular figures (see text for details)

Fig.49 Zoomed in satellite image with rivers sampled, the sampling points themselves, the "main" (dirt) road in the area as well as mines - current and worked out - superimposed upon the image.



The reason why this is so important can be seen on the satellite images marked by the anomalous V values identified in the plots of the various factors (Fig.42). The interpretation of these “anomalous” samples for the various factors is directly proportional to the spatial distribution of the lithological units and it is therefore vitally important that a profound attempt is made to map and understand the large-scale structures within the Lelatema anticline.

The image of the plot of the outliers for the factor ratios of the medium fraction will be used as an illustration (Fig.50) as to why detailed structural knowledge of the area is so important. Two possibilities are proposed to explain the anomalous sample distribution, all three of which are heavily dependent on the structure of the underlying lithological units. The first possibility is a straight line, sub-parallel to strike, following the general outcropping rocks on the image, connecting the anomalous samples. A second possibility is that the anomalous samples represent different parts of the same folded JWZ-, or graphitic calc-silicate type zones, occurring in a larger structure such as a boudinaged stratigraphic package, as demarcated on the image. The third possibility is much like the second: the large scale structure is just seen as a large boudinaged package with either linear or folded packages within the larger boudin. That the “anomalous” factor samples represent a lithological unit, albeit altered or a GCS type unit, is fairly certain and if indeed the altered zones in the rest of the Merelani structure occur in such a close proximity as in the JWZ-GCS1 case in the Merelani Lower Horizon it wouldn't matter which of these two units are being delineated. The general strike is known and the general dip is known, which implies that one or two strategically placed drill holes should illuminate the location of the altered zones. As mentioned before, detailed geological mapping preceding any drilling will further elucidate the structure of the Merelani area and will substantially raise the level of certainty of what exactly it is that we are dealing with in terms of structure and type of lithology.



F1/F2 Outliers of the Medium Fraction  
F1/F3 Outliers of the Medium Fraction  
F2/F3 Outliers of the Medium Fraction

Possibility 1    ———  
Possibility 2    ———

Fig.50 Different possibilities for the structural interpretation of observed features. Possibility 1 is where the solid lines are a stratigraphic package (between the dashed lines) similar to the Merelani Lower Horizon in which the samples represent altered zones. If this is the case, then it would explain the river channels, because the altered rock is less competent than the surrounding lithologies. Possibility 2 is a stratigraphic package occurring in a mega-boudin.

## 6.4. Discussion and Conclusions

The following conclusions are derived from the foregoing chapter:

- The UCC values constantly plot in the vicinity of the Merelani stream sediment data, which could indicate that the Merelani sediments are possibly derived from upper continental crustal rocks. This can easily be verified by a study on the protoliths of the various Merelani metamorphic rocks.
- Ni-Th and V-Th scatterplots confirm that V and Ni are concentrated in the fine fraction and that Ni is concentrated to a larger degree than V. This indicates that V is distributed between minerals which are concentrated in the fine fraction, such as graphite, and minerals which concentrate in coarser fractions, such as grossular garnet and zoisite. This is substantiated by the study of the change in skewness of the V data distribution from the fine to the medium fraction. The same skewness study performed on the distribution of Ba data suggests that the Ba is predominantly concentrated in the feldspars;
- Factor analysis and the scatterplots indicate that the heavy minerals dominate the trace element chemistry;
- Lack of trends in the trace element profile plots over the three stream sampled suggests that the mineral particles in which the trace elements find themselves are not appreciably mobilised and that the stream sediment trace element geochemistry is a good indication of proximal geology which could immensely aid geological mapping;
- High V values, factor loading and factor ratio plots indicate samples which lie close to presently and historically mined gemstone deposits and these plots can therefore be employed as a tool in the search for hidden gemstone deposits.

## **7. Conceptual Geochemical Model**

### **7.1. Introduction**

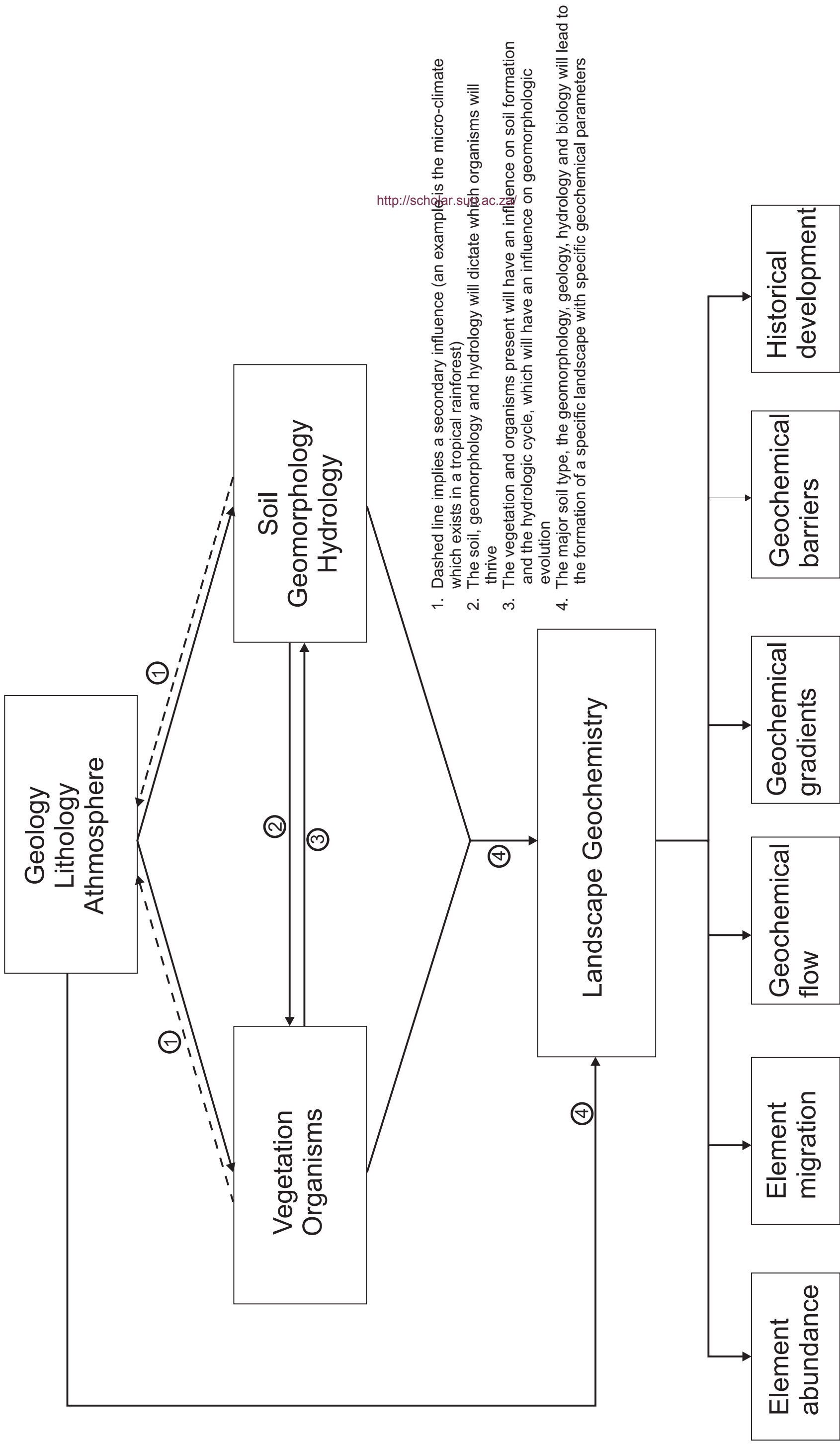
Hoffman and Thomson (1987) describe a landscape as:

*a dynamic system involving the relationship between vegetation, soils, underlying rocks, the atmosphere, surface and ground waters, geomorphology and geology.*

Fletcher et al. (1987) list six fundamental concepts in landscape geochemistry. The relationship between these concepts and the definition of a landscape, as given in the above paragraph, is presented graphically in Fig.51. A landscape starts off with a specific geology and therefore lithologic composition under a specific prevailing atmosphere. These parameters will lead to the formation of a specific set of soils and geomorphology and hydrology, which in turn will have an influence on the type of vegetation and organisms which will thrive. The vegetation and organisms will in turn have an influence on the hydrologic cycle as well as soil formation. All these parameters will define each of the six fundamental concepts in landscape geochemistry (Fig.51).

### **7.2. Conceptual Geochemical Model for Soils**

The Merelani area in north-eastern Tanzania has a semi-arid climate although heavy rains fall during the months of March to May. The landscape is hilly and is densely vegetated by Acacia trees and various shrubs. The rocks in the area are mostly garnet and kyanite gneisses, graphite-rich schists and dolomitic marbles. The dolomitic marbles weather positively and form prominent ridges. Vegetation growth and density reaches a maximum in the rainy season. Ti- and Zr-normalised trace element values show that the soils on the slopes of the Merelani hills are mobile. The good correlation between the profiles of specific trace element concentrations plotted over the Lower Horizon stratigraphy and the profiles for the same elements plotted in the soils covering the lower horizon stratigraphic units indicate that the soil particles are mobilised on a small scale of a few tens of centimetres to a few metres. Analysis of acid leachate from the Merelani soils shows that the trace elements are not primarily mobilised by



<http://scholar.sun.ac.za/>

Fig.51 Adapted from Hoffiman and Thompson (1987) and Fletcher et. al. (1987)

hydromorphic means. The trace element concentration in the acid leachate, although very small, increases with distance down slope, as shown on the profile plots of the ICP-analysed values (Fig.38, Fig.39). This implies that soil solution movement is dictated by the landscape topography.

There is a sharp drop in element concentration in Zone 8 soil. The landscape over which the trench was dug has two primary slope directions: One toward the east, the hill slope, and one toward the south (Fig.52).

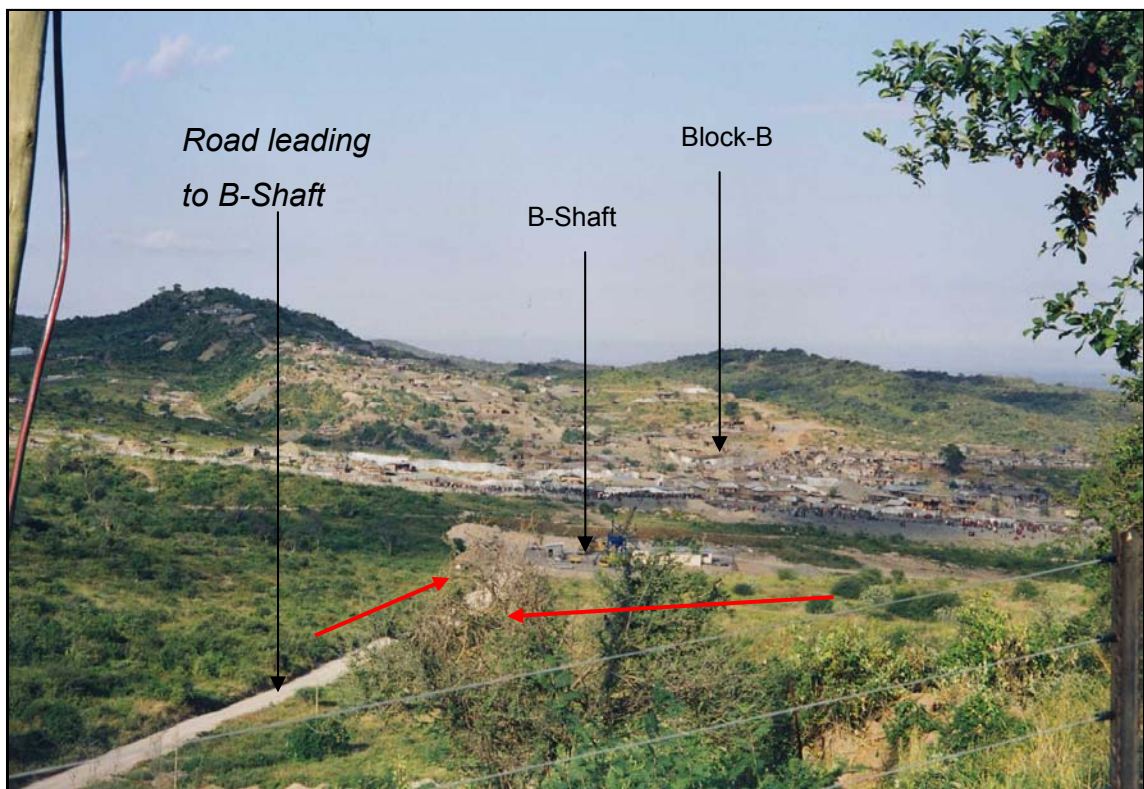


Fig.52 The two slopes (shown in red) most important for the mobility of the Merelani soils in the vicinity of the trench. The trench is obscured by the shrubs in the foreground, but the slope of the hill is similar to the slope of the ridges in the background. The road leading down to B-Shaft is representative of the second slope and the direction of sediment and fluid movement. Block-B, which is mined by local miners, can be seen in the background. The view is to the south.

The slope of the hill is significantly larger than the slope towards the south. Therefore it is expected that the largest component of soil fluid migration would be in the direction of the road and then down the secondary slope towards the south. The same components are proposed for soil particle movement due to gravity sliding. The movement of trace elements in the Merelani soils by hydromorphic means was shown to be very low. Thus the movement of soil particles can be equated to the movement of the trace elements, as in placers. The abundance of vegetation, however, is most

probably the main force in restricting soil particle movement, resulting in short dispersion trails in the order of a few tens of centimetres to a few metres.

A graphic representation of the model is shown in Fig.53.

### **7.3. Conceptual Geochemical Model for Stream Sediments**

The scenario for trace element mobility in the Merelani streams is very similar to that of the trace elements in the soils. The binary and ternary scatterplots, as well as the lack of visible trends in trace element profiles along stream length, shows that the stream sediments are not significantly mobilised for particle sizes of  $>90\mu\text{m}$ . This implies that the stream sediments are therefore proximal to their source lithologies. The skewness and kurtosis of V and Ba data distribution show that it is only the fine fraction that is mobilised to any significant degree. A statistical factor analysis has indicated that the majority of the trace elements are represented by three factors for both size fractions. The first and largest factor accounts for more than half the variability of the data in both fractions and can be ascribed to a fraction containing the heavy minerals. The aforementioned is based on the elements which constitute the fraction (e.g. Zr, Y and the rare earth elements) and a literature study on element distribution (Deer et al., 1966; Wederpohl, 1978; Klein and Hurlbut, 1993). This indicates that the heavy mineral fraction is the most important “carrier” of the trace elements in the Merelani area. Thus the movements of the heavy minerals will control the movement of the trace elements. Some anomalous values of factor scores and factor score ratios for specific samples plot close to currently and historically mined coloured gemstone deposits, indicating proximity to the source.

Most of the streams have shallow slopes and are choked by vegetation. These two facts are seen as the major forces inhibiting stream sediment and therefore trace element mobility. Thus geochemical dispersion occurs physically due to the flash floods from March to May relative to the abundant vegetation which chokes the streams and subsequently inhibits particle mobility.

The above is summarised in Fig.54.

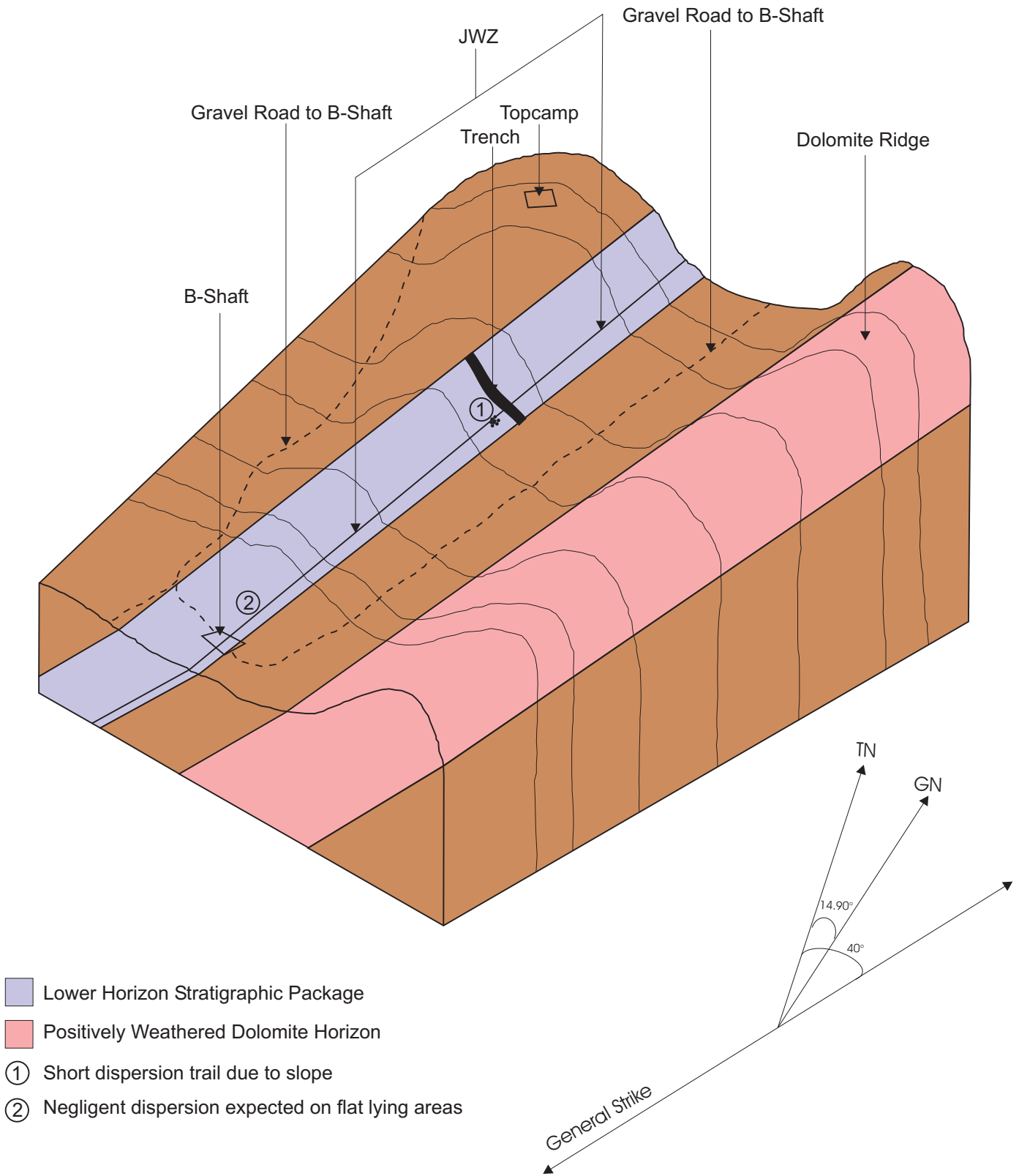


Fig.53 Graphic representation of the geochemical model for the Merelani soils as described in the text



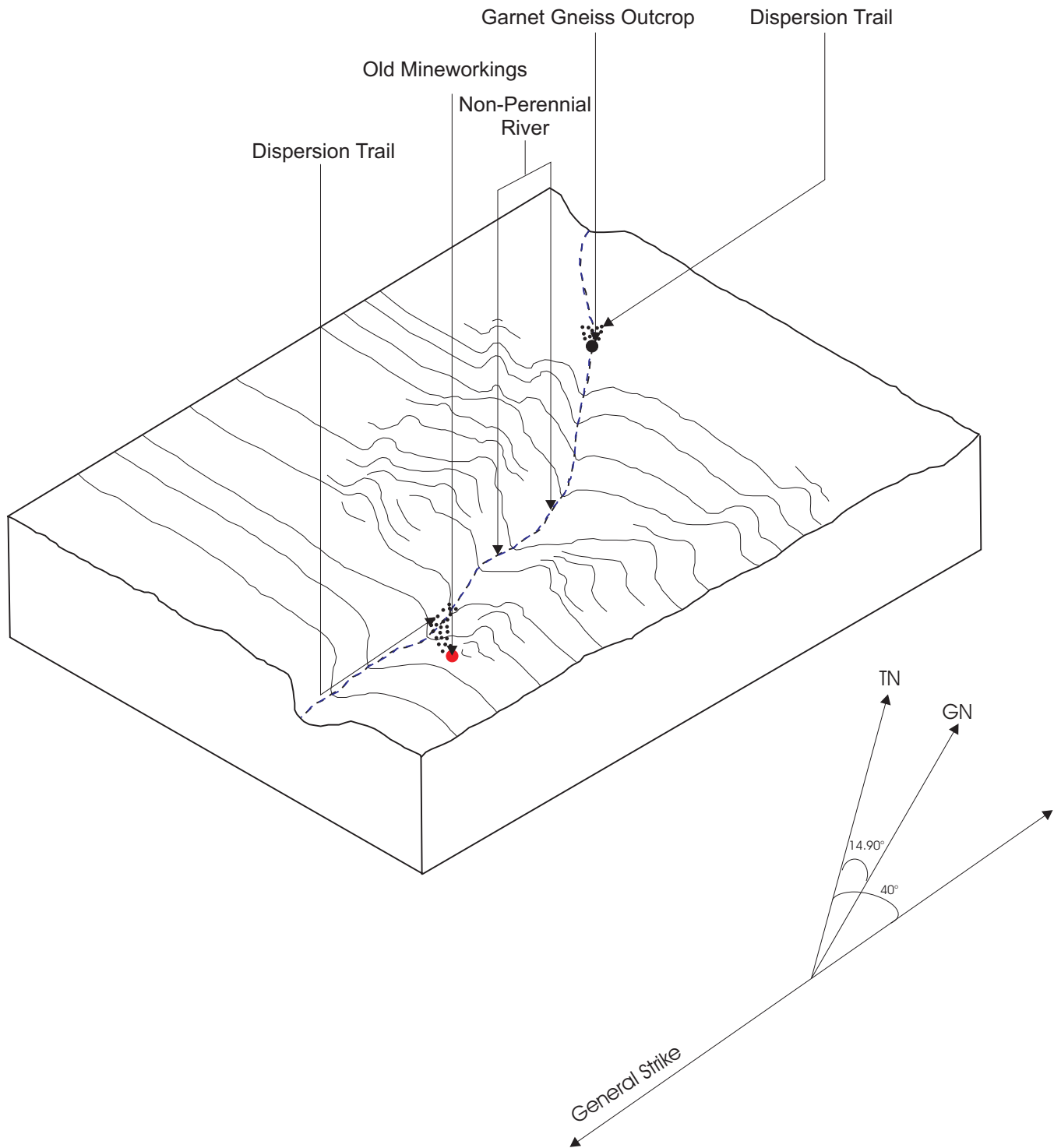


Fig.54 Graphic representation of the geochemical model for the stream sediments as described in the text

#### **7.4. Discussion Final Conclusions and Recommendations**

The study has shown that soil and stream sediment sampling followed by whole-rock XRF analysis is a viable method of exploring for tanzanite.

The study has also shown that the trace elements are only mobilised to a small degree in both the soils and stream sediments and that trace elements are located in soluble phases. Therefore partial extraction methods have proven to be inadequate in tanzanite exploration. The best results were obtained by whole-rock XRF methods. In the soils the fine and medium fractions of the C-horizon showed the closest correlation between soil and bedrock. In the stream sediments it was also the fine and medium fractions which provided the largest V anomaly-background contrasts. Samples containing V anomalies occurred close to the existing and abandoned tsavorite mines in the area selected. Thus the study has shown that V is indeed the vital element to geochemical exploration for additional tanzanite deposits.

The study on the soil samples has revealed that the Graphitic Calc-Silicate Schist 1 and 2 units are indicated by V-anomalies. The GCS 1 unit occurs adjacent to the Kyanite Gneiss 1 and 2 units, which host the tanzanite mineralisation located in the JW zone. Thus whole-rock geochemical exploration on soil samples has provided an indirect method in exploring for tanzanite.

The study on the stream sediment samples has shown that by grouping the trace elements into factors using factor analysis and by subsequently using calculated factor ratios and factor scores in conjunction with anomalous V-values, samples could be identified, which occur close to abandoned and operating tsavorite mines in the selected area. Thus a potentially viable method for exploring for as yet unknown tanzanite and tsavorite deposits is provided by the whole-rock geochemical analyses of stream sediments.

Although the study of both soil samples and stream sediments via a whole-rock XRF method has proven useful, other methods may prove more effective. This would include a heavy-mineral exploration technique on both the soils and stream sediments as well as a technique involving the panning of graphite. Further studies on both these techniques is therefore warranted and could provide a geochemical exploration

technique, which could prove most effective in searching for additional tanzanite deposits. To further refine and constrain any geochemical exploration method, further research is also required to quantify the length of trace element dispersion trails in the soil and stream sediments. This will ensure more accurate estimates on the location of the graphitic calc-silicate units as well as the position of planned exploration drilling points. In addition, further research into the soil and stream sediment formation since the last eruption of Neogene lavas (~1,2Ma) is required to better understand trace element dispersion patterns surrounding the tanzanite deposit.

The conclusions reached in this study are thus:

- Whole-rock XRF geochemical techniques are best suited for tanzanite exploration;
- Partial leach ICP methods have proven that the trace elements are not mobilised hydromorphically. In addition it has also proven that partial leach methods will prove to be ineffective in exploring for tanzanite;
- V is the key in the geochemical exploration for tanzanite in both the soils and stream sediments;
- In terms of the soils it was the GCS units which displayed the largest V-anomalies;
- In conjunction with the V-anomalies in the stream sediments, the factor scores and factor ratios have shown that abandoned and existing gemstone mines can be detected and that the anomalous samples not associated with any known gemstone mining activities should be investigated further;
- This study has also shown that although whole-rock geochemical exploration techniques have proven successful in identifying tanzanite and other gemstone deposits, exploration methods involving heavy minerals and perhaps graphic may prove to be more effective in exploring for tanzanite deposits.

Recommendations for further research are:

- A study of the mineral geochemistry and parameters governing the dispersion of heavy minerals in the soil and stream sediments as a possible alternative exploration tool for tanzanite;

- A study of the geochemistry and parameters governing the dispersion of graphite in the soil and stream sediments as a possible alternative exploration tool for tanzanite;
- A detailed study of the parameters governing the formation of soils, calcrete and stream sediments in the Merelani area since the last eruption of neogene lavas (~1,2Ma) to the present with the aim of better understanding geochemical dispersion patterns;
- A study to quantify the exact trace element dispersion distance in soil solutions as well as of the soil and stream sediment particles.

## 8. References

- Anand, R.R., Phang, C., Wildman, J.E., Lintern, M.J. (1997) Genesis of some Calcretes in the Southern Yilgarn Craton, Western Australia: Implications for Mineral Exploration. *Australian Journal of Earth Sciences* **44**, 87-103
- Bonavia, F.F., Chorowicz, J. (1992) Northward Expulsion of the Pan-African of Northeast Africa Guided by a Reentrant Zone of the Tanzania Craton. *Geology*, **20**, 1023-1026
- Breit, G.N., Wanty, R.B. (1991) Vanadium Accumulation in Carbonaceous Rocks: A Review of Geochemical Controls during Deposition and Diagenesis. *Chemical Geology* **91**, 83-97
- Brookfield, M.E. (1993) The Himalayan Passive Margin from Precambrian to Cretaceous Times. *Sedimentary Geology*, **84**, 1-35
- Bridges E.M. (1997) World Soils. *Cambridge University Press*, 170p
- Chandrajith, Dissanayake, C.B., R., Tobschall, H.J (2001) Enrichment of High Field Strength Elements in Stream Sediments of a Granulite Terrain in Sri Lanka – Evidence for a Mineralized Belt, *Chemical Geology* **175**, 259-271
- Chesley, J.T., Rudnick, R.L., Lee, C.T. (1999) Re-Os Systematics of Mantle Xenoliths from the East African Rift: Age, Structure and History of the Tanzanian Craton. *Geochimica et Cosmochimica Acta*, **63**, 1203-1217
- Colin F., Alarçon C., Vieillard P. (1993) Zircon: an immobile index in soils? *Chemical Geology* **107**, 273-276
- Dahl, P.S., When, D.C., Feldman, S.G. (1993) The Systematics of Trace-Element Partitioning between coexisting Muscovite and Biotite in Metamorphic Rocks from the Black Hills, South Dakota, USA. *Geochimica et Cosmochimica Acta* **57**, 2487-2505
- Davies, C., Chase, R.C. (1994) The Merelani Graphite-Tanzanite Deposit, Tanzania: An Exploration Case History. *Exploration, Mining Geology* **3**, 371-382

Dawson, J.B. (1997) Neogene-Recent Rifting and Volcanism in Northern Tanzania: Relevance for Comparisons between the Garadar Province and the East African Rift Valley. *Mineralogical Magazine* **61**, 543-548

Dawson, J.B. (1992) Neogene Tectonics and Volcanicity in the North Tanzanian Sector of the Gregory Rift Valley. Contrasts with the Kenyan Sector. *Tectonophysics* **204**, 81-92

Deer, W.A., Howie, R.A., Zussman, J. (1966) An Introduction to the Rock Forming Minerals. *Longmans, Green and Co. Ltd.*, 528p

Dill, H.G. (1998) A Review of Heavy Minerals in Clastic Sediments with Case Studies from the alluvial fan through the near-shore marine environments. *Earth Science Reviews* **45**, 103-132

Dissanayake, C.B., Gunawardena, R.P., Dinalankara, D.M.S.K. (1988) Trace Elements in Vein Graphite of Sri Lanka; *Chemical Geology* **68**, 121-128

Fleet, M.E., Pan, Y. (1997) Rare Earth Elements in Apatite: Uptake from H<sub>2</sub>O-bearing Phosphate-Fluoride Melts and the Role of Volatile Components. *Geochimica et Cosmochimica Acta* **61**, 4745-4760

Fletcher, W.K., Hoffman, S.J., Mehrtens, M.B., Sinclair, A.J., Thomson, I. (1987) Exploration Geochemistry: Design and Interpretation of Soil. *Reviews in Economic Geology* **3**, 180p

Foth, H.D. (1984) Fundamentals of Soil Science. *John Wiley and Sons*, 251-285

Fritsch, E., Rossman, G.R. (1987) An Update on Colour in Gems. Part 1: Introduction and Colours caused by Dispersed Metal Ions. *Gems & Gemology* **Fall 1987**, 127-139

Fritsch, E., Rossman, G.R. A (1988) An Update in Gems. Part 2: Colours Involving Multiple Atoms and Colour Centres. *Gems & Gemology* **Spring 1988**, 3-15

Fritsch, E., Rossman, G.R. A (1988) An Update in Gems. Part 3: Colours caused by Band Gaps and Physical Phenomena. *Gems & Gemology* **Summer 1988**, 81-102

Garver, J.I., Smick, T.A. (1996) Chromium and Nickel in Shale of the Taconic Foreland: A Case Study for the Provenance of Fine-Grained Sediments with an Ultramafic Source. *Journal of Sedimentary Research* **66**, 100-106

Gobba, J.M. (1974) The Geology and Geochemical Prospecting of Part of the Pangani River Escarpment. *M.Sc. Thesis, University of Nairobi (Kenya)*

Gurney, J.J., Zweistra, P. (1995) The Interpretation of the Major Element Compositions of Mantle Minerals in Diamond Exploration. *Journal of Geochemical Exploration*; **53**, 293-309

Hall, G.E.M. (1998) Analytical Perspective on Trace Element Species of Interest in Exploration. *Journal of Geochemical Exploration*; **61**, 1-19

Hoffman, P.F. (1989) Speculations on Laurentia's First Gigayear (2.0 to 1.0Ga). *Geology* **17**, 135-138

Hoffman, S.J., Thomson, I. (1987) Models, Interpretation and Follow-up. *Reviews in Economic Geology* **3**, 117-128

Icenhower, J., London, D. (1996) Experimental Partitioning of Rb, Cs, Sr and Ba between Alkali Feldspar and Peraluminous Melt. *American Mineralogist*; **81**, 719-734

Jennings, C.M.H. (1995) The Exploration Context for Diamonds. *Journal of Geochemical Exploration* **53**, 113-124

Kabata-Pendias, A., Pendias, H. (1986) Trace Elements in Soils and Plants. *CRC Press, Inc.* 315p

Komov, I.L., Lukashev, A.N., Koplus, A.V. (1987) Geochemical Methods of Prospecting for Non-Metallic Minerals. *VNU Science Press, Utrecht, The Netherlands*, 241p

Klein, C., Hurlbut, C.S. (1993) *Manual of Mineralogy*. John Wiley & Sons, Inc., 681p

Kröner, A., Pallister, J.S., Fleck, R.J. (1992) Age of Oceanic Magmatism in the Late Proterozoic Arabian Shield. *Geology* **20**, 803-806

Kröner, A., Sacchi, R., Jaeckel, P., Costa, M. (1997) Kibaran Magmatism and Pan-African Granulite Metamorphism in Northern Mozambique: Single Zircon Ages and Regional Implications. *Journal of African Earth Sciences* **25**, 467-484

Kröner, A., Willner, A.P., Hegner, E., Jaeckel, P., Nemchin, A. (2001) Single Zircon Ages, PT Evolution and Nd Isotopic Systematics of High-Grade Gneisses in Southern Malawi and their bearing on the Evolution of the Mozambique belt in Southeast Africa *Precambrian Research* **109**, 257-291

Levinson, A.A. (1974) *Introduction to Exploration Geochemistry*. Alcraft Printing Co. Ltd, Calgary, Alberta, 614p

Levitski, A.G., Sims, D.H.R (1997) Surface Geochemical Techniques in Gemstone Exploration at the Rockland Ruby Mine, Mangare Area, SE Kenya. *Journal of Geochemical Exploration* **59**, 87-98

Maboko, M.A.H. (1995) Neodymium Isotopic Constraints on the Protolith Ages of Rocks Involved in Pan-African Tectonism in the Mozambique Belt of Tanzania; *Journal of the Geological Society of London* **152**, 911-916

Maboko, M.A.H. (2000) Nd and Sr Isotopic Investigation of the Archean-Proterozoic Boundary in North Eastern Tanzania: Constraints on the Nature of Neoproterozoic Tectonism in the Mozambique Belt. *Precambrian Research* **102**, 87-98

Maboko, M.A.H., Nakamura, E. (1995) Sm-Nd garnet ages from the Uluguru Granulite Complex of Eastern Tanzania: Further Evidence for Post-Metamorphic Slow Cooling in the Mozambique Belt. *Precambrian Research* **74**, 195-202



Maboko, M.A.H., Nakamura, E. (2002) Isotopic Dating of Neoproterozoic Crustal Growth in the Usambara Mountains of Northeastern Tanzania: Evidence for Coeval Crust Formation in the Mozambique Belt and the Arabian-Nubian Shield. *Precambrian Research* **113**, 227-242

Malisa, E. (1987) Geology of the Tanzanite Gemstone Deposits in the Lelatema Area, NE Tanzania. *Annales Academiae Scientiarum Fennicae, Series A, III Geologica-Geographica* **146**, 160p

Malisa, E., Muhongo, S. (1990) Tectonic Setting of Gemstone Mineralization in the Proterozoic Metamorphic Terrane of the Mozambique Belt in Tanzania. *Precambrian Research* **46**, 167-176

Malisa, E., Koljonen, T. (1989) Geological Process Leading to Gemstone Formation in Lelatema Mountains, Northeast Tanzania; *28<sup>th</sup> International Geological Congress, Washington DC, July 9-19, Abstracts*, 356-357

Malisa, E., Koljonen, T. (1989) Geological Processes Leading to Gemstone Formation in Lelatema Mountains, Northeast Tanzania. *Pangea* **15/16**, 41-42

Marshall, T.R., Baxter-Brown, R. (1995) Basic Principles of Alluvial Diamond Exploration. *Journal of Geochemical Exploration* **53**, 277-292

Middelburg, J.J., Van der Weijden, C.H., Woittiez, J.R.W. (1988) Chemical Processes Affecting the Mobility of Major, Minor and Trace Elements During Weathering of Granitic Rocks. *Chemical Geology* **68**, 253-273

Möller, A., Appel, P., Mezger, K., Schenk, V. (1995) Evidence for a 2Ga Subduction Aone: Eclogites in the Usagaran Belt of Tanzania. *Geology* **23**, 1067-1070

Möller, A., Mezger, K., Schenk, V. (1998) Crustal Age Domains and the Evolution of the Continental Crust in the Mozambique Belt of Tanzania: Combined Sm-Nd, Rb-Sr and Pb-Pb Isotopic Evidence. *Journal of Petrology* **39**, 749-783

- Muhongo, S., Kröner, A., Nemchin, A.A. (2001) Single Zircon Evaporation and SHRIMP Ages for Granulite-Facies Rocks in the Mozambique Belt of Tanzania. *Journal of Geology* **109**, 171-189
- Muhongo, S., Lenoir, J.L. (1994) Pan-African Granulite-Facies Metamorphism in the Mozambique Belt of Tanzania: U-Pb Zircon Geochronology. *Journal of the Geological Society of London* **151**, 343-347
- Muhongo, M., Tuisku, P., Mtoni, Y. (1999) Pan-African Pressure-Temperature Evolution of the Merelani Area in the Mozambique Belt in Northeast Tanzania. *Journal of African Earth Sciences* **29**, 353-365
- Nesbitt H.W. (1979) Mobility and Fractionation of Rare Elements During Weathering of a Granodiorite. *Nature* **279**, 206-210
- Noble, W.P., Foster, D.A., Gleadow, A.J.W. (1997) The Post-Pan-African Thermal and Extensional History of Crystalline Basement Rocks in Eastern Tanzania. *Tectonophysics* **275**, 331-350
- Olivier, B. (2006) The Geology and Petrology of the Merelani Tanzanite Deposit in NE Tanzania. *PhD Thesis, University of Stellenbosch*, 434p
- Rakovan, J., Reeder, R.J., (1996) Intracrystalline Rare Earth Element Distributions in apatite: Surface Structural Influences on Incorporation During Growth. *Geochimica et Cosmochimica Acta* **60**, 4435-4445
- Ranasinghe P.N., Dissanayake C.B., Rupasinghe M.S. (2005) Application of geochemical ratios for delineating gem-bearing areas in high grade metamorphic terrains. *Applied Geochemistry* **20**, 1489 - 1495
- Rombouts, M. (2003) Assessing the Diamond Potential of Kimberlites from Discovery to Evaluation Bulk Sampling. *Mineralium Deposita* **38**, 496-504
- Rose, A.W., Hawkes, H.E., Webb, J.S. (1979) *Geochemistry in Mineral Exploration (Second Edition)*; Academic Press Inc (London) Ltd

Rutuhundurwa, F. (1995) Geologic map of the Merelani graphite-tanzanite deposit. (Mine map – Afgem, Tanzania)

Scheepers R. and A.F.M. Kisters(2000). The Geology of the Merelani tanzanite deposit. *Internal technical report to Afgem*. 37p

Scheepers, R., Rozendaal, A. (1993) Redistribution of U, Th, and rare-earth elements during weathering of subalkaline granites in SW Cape Province, South Africa. *Journal of African Earth Sciences* **17**, 41-50

Stern, R.J. (1994) Arc Assembly and Continental Collision in the Neoproterozoic East African Orogen: Implications for the Consolidation of Gondwanaland. *Annual Review of Earth and Planetary Sciences* **22**, 319-351

Stern, R.J. (2002) Crustal Evolution in the East African Orogen: A Neodymium Isotopic Perspective. *Journal of African Earth Sciences* **34**, 109-117

Taylor, S.R., McLennan, S.M. (1995) The Geochemical Evolution of the Continental Crust. *Reviews of Geophysics* **33**, 241-265

Vital, H., Statterger, K. (2000) Major and Trace Elements of Stream Sediments from the Lowermost Amazon River. *Chemical Geology* **168**, 151-168

Watson, E.B., Green, T.H. (1981) Apatite/Liquid Partition Coefficients for the Rare Earth Elements and Strontium. *Earth and Planetary Science Letters* **56**, 405-421

Wedepohl, K.H. (1978) Handbook of Geochemistry. *Springer-Verlag Berlin, Heidelberg*